Locating Zones and Quantify the Submarine Groundwater Discharge into the Eastern Shores of the Dead Sea - Jordan

Dissertation
zur Erlangung des Doktorgrades
der Mathematisch-Naturwissenschaftlichen Fakultäten
der Georg-August-Universität zu Göttingen

vorgelegt von

Emad Akawwi

MSc.
Master of science in geotechnical engineering

aus Al Fuhais-Jordanien

Göttingen 2006

Dedication

To my Parents who supported me and light up my life

To my brothers

&

To my sisters

Emad

Abstract

This study aims to locate the zones of groundwater discharge into the eastern shores of the Dead Sea and to estimate its quantity. The evaluation of inflow was accomplished by different ways of approach: the first one to use the electrical conductivity-temperature with a depth, the second to use a chemical tracer (Radon-222), the third to use thermal infrared imagery and the last is to use electromagnetic radiation techniques in addition to the schematic geological and hydrogeological models of the study area.

The Dead Sea divides into two layers relating to the electrical conductivity and temperature with depth. The upper layer subdivides into two members. The upper member extends from the sea surface down to a depth of 15-25 m. The lower member extends from a depth of 15-25 m to 40 m and it characterized with high TDS and low EC. The second layer extends from a depth of 40 m to the end of profiles. Laboratory experiments carried out to find a relationship between the EC at a specific T and the TDS. These experiments indicate that the EC reachs its maximal 202 mS/cm at a salinity of about 267 g/l from where it starts decreasing with the increase of the TDS and it reachs about 175 mS/cm at a salinity of 404 g/l. The minimal of TDS was observed at about 460 g/l at EC about 156 mS/cm.

The submarine groundwater discharged into the Dead Sea in the upper 16 m in Sweimah area. It is discharged in the upper 25 m in Zarka Ma'in area, in the upper 15 m in Zara and it is discharged in the upper 18 m in Mujeb.

The reason why the lower member has the highest TDS was explained. It is due to the very high T at the Dead Sea area in summer and very high evaporation. The density of the upper layer becomes higher than that of the layer underneath. Therefore this denser upper layer sinks beneath the layer which has lower density at the layer where the groundwater discharged into the Dead Sea and this last layer upwelling to the surface.

The chemical tracer radon-222 technique shows that the highest radon concentrations were found at the area close to the shoreline. This means that the largest amount of groundwater discharge is close to the shoreline. As well the highest radon-222 concentrations were found at a depth of 12 m in the three stations while it was at a depth of 7 m in the Zarka Ma'in station. It shows also that the groundwater dischargs into the Dead Sea in the upper 20 m. This is coinciding with the finding from the EC and T survey. The submarine groundwater discharge is estimated using Radon-222 as 135.7 million m^3/y in Sweimah area, about 128.5 million m^3/y at Zarka Main area, about 33.7 million m^3/y in Zara area and it is about 90.3 million m^3/y in Mujeb area. The total quantity of submarine groundwater discharge into the eastern shoreline of the Dead Sea is 388.2 million m^3/y. The quatity of groundwater discharge is estimated by using mixing of TDS about 181 MCM/y, and it is estimated about 59 MCM/y by using Darcys' law. The results of SGD estimations from different methods compared with the discharge from water balance 480 MCM/y. The results showed that the discharge might be between 200 and 300 MCM/y.

The thermal infrared imagery (TIR) was used to identify thermal anomalies along the eastern shoreline of the Dead Sea, thereby to determine the exact locations of submarine groundwater discharge. As well as, the locations of springs onshore surround the area. Many submarine groundwater discharge zones were identified. The main zones were in Zarka Ma'in, Zara and Mujeb areas. The highest differences in temperature between the groundwater discharge and the sea surface water were observed at the Zarka Ma'in and Zara areas, because these areas have a hot springs flow into the Dead Sea. The TIR imagery showed that the extent of the discharge was between 350 m and about 750 m away from the shoreline.

The electromagnetic radiation (EMR) identifies the energy anomalies, thereby determining the active faults and fractures as well as the sinkholes along the eastern shoreline of the Dead Sea. These features are considered zones of weakness for the submarine groundwater discharge. The maximum radiation was observed in Sweimah area. Many major faults and non-opened sinkholes were found along this area at different locations. This proves the finding from chemical tracers that showed that the maximum discharge is in this area. As well few major fault and non-opened sinkholes were observed in Zara-Zarka Ma'in and Mujeb areas.

The geological and hydrogeological models showed that the direction of the groundwater flow is to the west and northwest directions toward the Dead Sea.

Keywords: submarine groundwater discharge, Jordan, Dead Sea, electrical conductivity, thermal infrared, electromagnetic radiation, radon.

Kurzfassung

Ziel der vorliegenden Studie war es, die Grundwasser-Austrittszonen entlang des östlichen Randes des Toten Meeres zu lokalisieren und die austretenden Mengen zu bestimmen. Die Studie basiert auf der Anwendung verschiedener Techniken: erstens der Temperatur- und Tiefen-Abhängigkeit der elektrischen Leitfähigkeit; zweitens Verfolgung eines natürlichen chemischen Tracers (Radon 222); drittens thermische Abbildung durch Infrarot-Aufnahmen und letztens der elektromagnetischen Strahlungsmessung. Zusätzlich wurden schematische geologische und hydrogeologische Modelle des Untersuchungsgebietes berücksichtigt.

Der Wasserkörper des Toten Meeres teilt sich in zwei Schichten entsprechend der elektrischen Leitfähigkeit (EC) und dem Temperatur-Verlauf mit der Tiefe. Die obere Schicht wird unterteilt in zwei Glieder. Das obere erstreckt sich von der Wasseroberfläche bis in eine Tiefe von 15 bis 25 m. Das untere Glied reicht von dieser Grenze bis in eine Tiefe von 40 m ; es is charakterisiert durch hohen TDS - Gehalt und niedrige EC. Die untere Schicht wurde von 40 m Tiefe bis zur Endtiefe der Beprobung (ca 100 m) beobachtet. Laborexperimente wurden ausgeführt, um die Beziehung zwischen EC bei gegebener Temperatur und den ungewöhnlich hohen TDS -Gehalten des Toten Meeres zu bestimmen. Die Experimente zeigen, daß die EC ihren Maximalwert von 202 mS/cm bei einer Salinität von etwa 267 g/l erreicht, von wo aus die EC mit weiter steigendem TDS wieder sinkt und bei 404 g/l etwa 175 mS/cm beträgt. Der niedrigste EC - Wert von 156 mS/cm wurde bei einem TDS von etwa 460 g/l beobachtet.

Im Suweimah - Gebiet strömt das Grundwasser in den oberen 16 m des Toten Meeres ein. Im Zarka Ma'in - Gebiet geschieht das in den obersten 25 m, und im Mujeb-Gebiet in den oberen 18 m.
Als Grund für den höchsten TDS-Gehalt im unteren Schichtglied der oberen Wasserschicht wird die sehr hohe Evaporation durch sehr hohe Sommer-Temperaturen am Toten Meer angesehen. Dadurch steigt die Dichte der obersten Wasserschicht über die der darunterliegenden. Darauf sinkt Wasser dieser dichtesten obersten Zone unter die Zone, die auf Grund des einströmenden Grundwassers leichter ist und daher zum Aufsteigen tendiert.

Die Messung des natürlichen Tracers Radon 222 zeigt, daß die höchsten Radon-Konzentrationen in Gebieten nahe der Küste vorliegen. Das bedeutet, daß der größte Grundwasserzustrom nahe der Küstenlinie stattfindet. Weiterhin wurden die höchsten Radon-222-Konzentrationen in Zarqa Ma'in in einer Tiefe von 7 m gefunden, in den übrigen 3 Stationen wurden sie in einer Tiefe von 12 m beobachtet. Auch das zeigt, daß die Grundwasser-Eintritte in den oberen 20 m des Toten Meeres liegen in Übereinstimmung mit den EC- und Temperatur-Befunden. Die Menge des eindringenden Grundwassers wurde mit Hilfe des Radon-222 - tracers zu 135,7 million m[3]/Jahr für das Suweimah-Gebiet, zu etwa 128,5 Millionen m[3]/Jahr für das Zarqa Ma'in-Gebiet, zu etwa 33,7 Million m[3]/Jahr für das Zara - Gebiet und zu etwa 90,3 Million m[3]/Jahr für das Mujeb-Gebiet geschätzt. Die Gesamtmenge des über dei östliche Küstenlinie des Toten Meeres eintretenden Grundwassers beträgt damit 388,2 Millionen m[3]/Jahr. Zusaetzlich wurde der

submarine Grundwasser-Zustrom zu 181 MCM/jahr abgeschaetzt, basierend auf der mischung der TDS- Gehatter, und mittels Darcy's Gesetz ist 57 MCM/jahr. Zusammenfassend liegt der submarine Grundwasser- Zustrom wohl zwischen 200 und 300 MCM/jahr.

Thermische Infrarot-Abbildung (TIR) wurde benutzt, um thermische Anomalien entlang der Ostküste zu identifizieren und so die exakten Grundwassereintritte zu lokalisieren. Das Verfahren zeigt auch die landseitig benachbarten Quellen. Eine Vielzahl von untermeerischen Grundwasseraustritten wurde identifiziert, wobei die hauptsächlichen Zonen die Zarqa Ma'in - Zara - und Mujeg -Gebiete sind. Die höchsten Temperatur-Differenzen zwischen Grundwasser und Oberflächenwasser des Toten Meeres wurde in Zarqa Ma'in und Zara Gebieten gefunden, da dort heiße Quellwässer in das Tote Meer fließen. Die TIR-Abbildungen zeigen, daß der Grundwassereintritt bis zu zwischen 350 und 750 m von der Küstenlinie entfernt liegt.

Die elektromagnetische Strahlung (EMR) identifiziert durch Energie-Anomalien aktive Störungen und Brüche und auch Lösungshohlräume (Erdfälle) landseitig entlang der Ostküste. Diese Elemente werden als Schwächezonen für die subaquatischen Grundwasserzutritte betrachtet. Die höchste EMR wurde in dem Suweimah- Gebiet beobachtet, wo viele größere Störungen und nicht-durchgebrochene Lösungshohlräume identifiziert wurden. Das unterstützt die Befunde mittels des chemischen Tracers, die die höchsten Grundwasserzutritte in diesem Gebiet anzeigen. Aber auch in den Zara-, Zarqa- und Mujeb-Gebieten wurden einige größere Störungen und nicht- durchgebrochene Lösungshohlräume beobachtet.

Die geologischen und hydrogelogischen Modelle zeigen, daß die Hauptfließrichtung des Grundwassers westwärts und nordwestwärts in Richtung Totes Meer verläuft.

Schüsselworte: untermeerische Grundwasseraustritte, Jordanien, Totes Meer, elektrische Leitfähigkeit, thermische Infrarot-Abbildung, elektromagnetische Starhlung, Radon-222

Acknowledgements

Table of Contents

List of figures

List of Tables

1. INTRODUCTION

The Dead Sea is a hypersaline terminal lake with a surface area in 2004 is approximately 634 km^2 and its border is approximately 148 km (Rishmawi et al. 2005). It located in the central part of the Jordan Rift Valley, which extends from Lake Tiberias in the north to the Gulf of Aqaba at the south, and includes the Jordan River in the north, the Dead Sea region in the middle and the southern Ghors (Haditha, Mazra, Safi), Wadi Araba and the Gulf of Aqaba in the south. Geologically, the Dead Sea "lake" is situated within the large Dead Sea basin, which is one of the pullapart basins that formed along the Dead Sea Rift (Quennell, 1959) and it is located in the southern sector of the Dead Sea Transform (DST), which separates the arabian and African plates (Capaccioni et al. 2003) as shown in (Fig. 1-1A). The Dead Sea can be traced in terms of plate tectonics to the movement of the great plates into which the lithosphere is divided (Steinhorn and Gat, 1983). The Dead Sea is subdivided into two basins, the southern shallow basin, and the deep northern basin. The investigated area covers the eastern coast of the Dead Sea region, which extends from northern part of the Dead Sea in Sweimah to the southern part of the Dead Sea in Ghor Haditha (Fig.1-1B). This study is trying to find the answering for the questions: How much is the quantity of the groundwater discharge into the Dead Sea? Where are the discharge zones located?
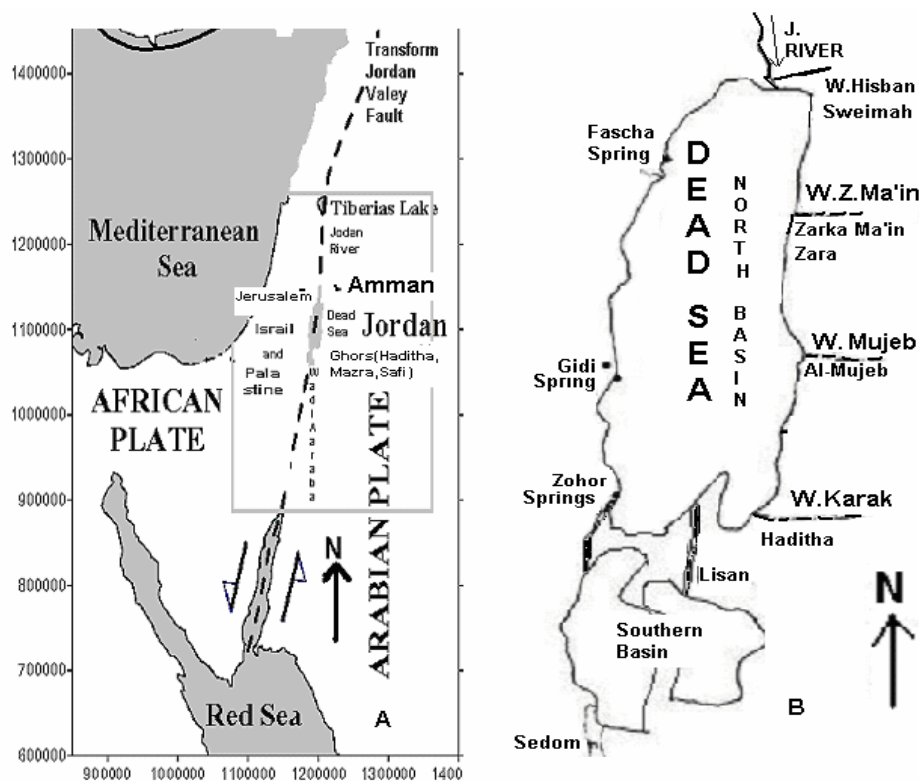
Figure (1-1): A: Location map of the Dead Sea, B: The study area.

1.1. Motivation and Problem

Jordan is one of the Middle East Countries. It located in arid and semi arid climatic zones. Only the highlands, with a width about 30 km and a length of about 300 km are considered as of Mediterranean climate. As water is considered to be one of the most important resources, so its presence is essential for achieving the overall economic and social development in the country.

Jordan is water stressed country and lacks for enough water resources. Therefore the deficit in the water supply was estimated at 238 MCM in 2005. This deficit is expected to rise to about 408 MCM in the year of 2020. This is because of the water demand in the country is much higher than the water supply (i.e. the water supply don't satisfy the country needs) from which emerge areal problem must be solved.

Groundwater is considered to be the major water resources for many regions, and the only resource in other regions-in Jordan. It supplies more than 80% of the total quantity of water in the Jordanian areas and plays an important role in urban industrial and agricultural water supply. High and continually increasing demands for groundwater for domestic, industrial and agricultural and other needs due to high population growth rates (around 2.9%/year), the continual upgrading in living standard and the existing degradation in groundwater quality because of pollution and salinization are putting more pressure on the groundwater resources of the country. Therefore the groundwater management and planing are required. Concluding that, the groundwater is a valuable and an important natural resource in Jordan. So the priority of all strategies is to preserve water quatity and purity to use clear fresh water.

Groundwater is the major source of fresh water in the Dead Sea region which issuing from the surrounding highlands. The high demand for fresh water occurred in the Dead Sea area due to the major industries established at the area as Potash Company and other sub-companies, and the irrigation.

However the countries (Jordan, Syria, Palestine and Israel) controlling the fresh watershed of the Dead Sea. They began to consume these waters intensively (Salameh and Khawaj, 1984). As well Israel and Jordan are using the Dead Sea water for potash and other minerals production, which contributes to the depletion of water (Gavrieli, 1997). Also the evaporation from the Dead Sea exceede the rain and runoff into it. As a result, the inflow of fresh waters into the Dead Sea has diminished significantly.

This drop of the Dead Sea level will have an effect on groundwater by increasing the head differences between the Dead Sea and the groundwater levels in the surrounding areas. Then the groundwater drainage is expected to increase toward the Dead Sea (Salameh and Khawej, 1984, Yechieli et al., 1996, Salameh and El-Nasir 2000a,). The decline in the Dead Sea level also accelerates the discharge of

groundwater into the Dead Sea (Salameh & Naser 1999, 2000b). Around 423 MCM of the groundwater discharge to the Dead Sea for every meter drop in the level of the Dead Sea for the period between 1994 and 1998. This amount of fresh water discharging to the Dead Sea decreased to 370 MCM in 2000 as a result of exploitation mismanagement of water, which formerly fed the Dead Sea. The area underlying the coastal aquifers already occupy by the Dead Sea water. They become gradually flushed and occupied by freshwater. This freshwater become saline due to the residuals of the Dead Sea water in the aquifer matrix (Salameh and El-Nasser, 2000b).

The shoreline of the Dead Sea also has retreated during the last four decades by an average of 2 Km. The newly exposed shoreline along the eastern side of the DS has not been studied with respect to hydrogeology and hydrochemistry. Their water resources altogether with the older coast resources are not yet understood.

A large parts of the Dead Sea area characterize as a highly karstic and fractured rock formations that are genetically connected with faults and karstic routes extending from the land into the sea, and the prevailing seaward-sloping rock strata. A steep escarpment along the Eastern shoreline of the Dead Sea controls the morphology of the Dead Sea area. The difference in the elevation between the Dead Sea level and the highlands to the East is more than 1210 m over a horizontal distance of 15 km. These might be a reason for the submarine groundwater discharge (SGD) into the Dead Sea. The quantity of freshwater input into the Dead Sea occurred due to surface water runoff in winter season or due to submarine groundwater discharge.

The drop of Dead Sea level is accompanied by a retreat of the shoreline and in reduction in the size of the surface area, accompanied by change in the location of existing springs, and in the appearance of new springs along shoreline. Then its need to understand and evaluate newly exposed of the eastern shoreline along the the Dead Sea in respect of hydrogeology.

Several subsidence and sinkholes (i.e. circular depressions in a karst area of subterranean drainage) rose in the cultivated area of Ghor Haditha and Lisan Penesula in the end southern part of the Dead Sea. Due to inflow of the fresh groundwater into the Dead Sea, These phenomena cause a serious danger to residences and farmers at these areas. It may be possible to reduce the scale of these subsidence by reduce the rate of dissolution of the layer by removing the waters undersaturated with respect to salt or by controuling the groundwater discharge into the Dead Sea.

1.2. Objectives

This study expected to assist several major objectives in terms of the submarine groundwater discharge, which are very useful for controlling the discharge to the Dead Sea and they are related to the problems mentioned above.

1- To locate and evaluate the areas of submarine ground-water discharge along the eastern coast of the Dead Sea.

2- To test the ability of the electrical conductivity and temperature techniques for delineating the fresh water flow into very high saline Dead Sea water.

3- To establish a quantitative relationship between the flow of submarine groundwater discharge and the inventory of water column radon-222 and then estimating the quantity of the groundwater discharges into the eastern shoreline of the Dead Sea.

4- To investigate and evaluate if method of thermal infrared imagery data collection and analyses have the potential for detecting groundwater discharge to the Dead Sea.

5- To develop a geological model of the study area

6- To scheme a conceptual hydro-geological model of the studied area that describes the groundwater horizontal and vertical movements.

7- To determine the availability of exploitable water resources that can be abstracted to assist in the water supply along the shores of the Dead Sea in order to provide the basis for future development e.g. tourism in that unique geologic area.

1.3. General Approach

An appropriate approach and procedures were followed in order to examine groundwater discharge into the Dead Sea and to achieve the other objectives related to this study.

The geological and topographic map sheets of scale 1:50,000 that cover the investigated area were collected. These maps sheets are the southern part of Karameh, Ma'in and Ar-Rabba. The wadies and the main faults were defined by using these maps. These faults and wadies were used as prospective indicators for the submarine groundwater discharge locations as springs, seepages and other points of discharges in the investigated area. Also different geological cross-

sections were constructed by using these maps. Then a geological model for the study area was created depending on these geological cross-sections.

The methods and techniques for localizing and quantifying the submarine groundwater discharge (SGD) were determined in relation to the temperature, the salinity, and other geochemical fingerprints of the seawater and fresh water.

Due to the highly contrast of the salinity and the electrical conductivity between the sea water and fresh water the electrical conductivity was selected to locate the submarine groundwater discharge into the Dead Sea. An inductive (electrodeless) electrical conductivity device type 871EC-BW sensor manufactured by Invensys FOXBORO was used for carrying out the electrical conductivity, temperature measurements. Because of the electrode sensor is not suitable for the very high saline Dead Sea water (more than 340 g/l). The sensor was calibrated relating to temperature compensation at 25°C.

The other technique that used for quantifying submarine groundwater discharge into the Dead Sea is the chemical tracer technique (Radon-222).

The chemical tracer Radon-222 (^{222}Rn) was chosen as one of techniques for quantifying a submarine groundwater discharge into the Dead Sea, because it is 3-4 orders of magnitude more concentrated in groundwater than that typical surface water and seawater, and the half-life decay rate is known and short (3.82 day). RAD7 radon device manufactured by (Durridge Co. Inc.) was used for analyzing the ^{222}Rn samples. An under sea surface soils samples were collected and analyzed for determining the radon diffusion from the sediments. As well samples from the springs and seepages surrounding the Dead Sea were collected and analyzed by using the same device. After one month the sea samples were analysed again for determining the radon ingrowths. As well the porosity and wet bulk density of the Dead Sea sediments were determined. The electrical conductivity and radon-222 measurements were carried out between July and August-2005 by using small engine boat.

The promising places for the electrical conductivity and radon-222 measurements and sampling were determined using the geological maps and field investigations according to the lithological and geological formations of the Dead Sea area, and the distribution of the springs and seepages.

The other technique is the thermal infrared (TIR) imagery. It was used in this study in order to delineate the zones of submarine groundwater discharge occurring at the eastern coast of the Dead Sea. This method of the thermal fingerprint is based on a pronounced thermal gradient between the groundwater and ambient surface conditions. The thermal infrared images were carried out in the end of December 2005 using a small commercial plane with the assistance of the Federal Geological Survey of Germany (BGR). The plane was developed especially for this purpose. The thermal infrared camera (FLIR System 8-13 μm) was fixed at the bottom of the

plane (Appendix I) after calibrating relating the air temperature and the humidity for the area. The plane with a camera was flight over the eastern coast of the Dead Sea and the over the Dead Sea itself. The images were taken from an elevation between 1300 and 1600 meter above standard sea level. The flight direction was from the south to the north and vice versa. The length of each strip was about 25 km of the eastern coast of the Dead Sea. Four strips were carried out with different coordinates. GPS data were taken by using fixed GPS stations. One GPS station was fixed inside the plane and the other station in the ground at the airport.

The electromagnetic radiation (EMR) is the other technique was used in this study. The principle of this method is the energy release from the fault and fractured activities. This method was used to localise the active faults, fractured zones and the non-opened sinkholes along the Dead Sea shoreline. These are considered as zones of weakness of the groundwater discharge at the Dead Sea area.

The data that used for estimating the groundwater discharge into the Dead Sea by using the water budget technique were collected from the previous study of (Salameh and El-Naser, 1999). This result was compared with the results that were obtained by using the chemical tracers (^{222}Rn) technique.

Finally a hydrogeological conceptual model for the groundwater movement in the study area was developed based on the geological maps, the geological model, the structural patterns and the aquifers properties in the study area.

1.4. Concepts of Submarine Groundwater Discharge (SGD)

The direct discharge of groundwater into the coastal zone has received increased attention in the last few years as it is now recognized that this process may represent a potentially important pathway for material transport. Understanding SGD is important for both a component of the general water cycle and potential resource as well as to coastal environmental management where undesirable contaminants in groundwater can be discharged into the near-shore marine environment. Generally almost all coastal zones are subject to flow of groundwater either as submarine springs or propagated seepage. The same can be happened in some deep aquifer if has fractures or other breaches in the overlying, confining layers, allowing groundwater to flow into the sea. The groundwater might flow directly to the sea wherever a coastal aquifer is connected to the sea. In addition to fresh groundwater from land, also the re-circulated seawater is driven through bottom sediments by a number of processes might discharge into the sea (Fig. 1-2).

The groundwater seepage near shorelines comes out from hydraulic gradients on land and this seepage may contribute to flow further out on the shelf from confined aquifers (Burnett et al. 2003). In other words groundwater may enter coastal

surface waters as dispersive seepage along shorelines, as point source seepage due to a breach in the confining layer of an underlying aquifer, and as spring discharge (Moore, 1999). However Groundwater will seep into the marine environment along any coastline where the water table and underlying aquifers slope toward the sea or when weaknesses in confining layers generate springs. Submarine groundwater discharge (SGD) in general occurs everywhere through permeable sediments where the hydraulic head of aquifers is above sea level, and sometimes includes a re-circulated seawater component (Burnett et al. 2001, Charette et al. 2003).

As a result aquifers lose or gain water to lakes, streams and coastal waters by several natural mechanisms set up by the hydraulic gradient between the aquifer and these standing bodies of water (Cable et al. 1997). Changes in groundwater discharge from an aquifer can vary overtime periods. The rapid fluctuations in groundwater seepage might occur over time due to changes in lake level and barometric pressure (McBride and Pfannkuch, 1975).
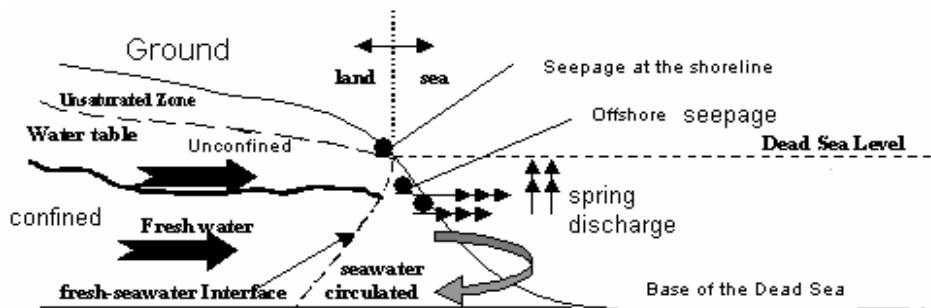
Figure (1-2): Schematic diagram showing the submarine discharge from seepages and springs.

The term SGD has been used in different ways over the years. Zektser et al. (1983) defined SGD to be the net groundwater discharge to the ocean, which comes essentially from recharge. Church (1996) defined SGD to be direct groundwater outflow across the ocean-land interface into the ocean, which would include re-circulated seawater. Li et al. (1999) Considered SGD to be the sum of net groundwater discharge, outflow due to wave-setup-induced groundwater circulation, and outflow due to tidal driven oscillating flow.

Total water, in the coastal environment, discharge into the ocean consists of surface water discharge and SGD. Submarine pore water exchange occurs across the seabed by SGD and submarine groundwater recharge. The water depth, the groundwater hydraulics and the geometry of the flow domain are the main parameters for controlling submarine groundwater discharge

There are three measurement units applied commonly to SGD: (1) volume per unit time (m^3 day^{-1}, 1 s^{-1}); (2) volume per unit time per unit length of shoreline (m^3 day^{-1} (m shoreline)$^{-1}$, m^3 year^{-1} (km shoreline)$^{-1}$); and (3) volume per unit time per unit area which is Darcy's flux (cm^3 cm^{-2} s^{-1}, cm s^{-1}, m year^{-1}) (Taniguchi et al. 2002).

2.   PREVIOUS STUDIES AND BACKGROUND INFORMATION

2.1. Previous Studies in General

Despite its importance, Submarine groundwater discharge (SGD) remains difficult in most places because it is diffuse and miscellaneous and occurs below the ground surface usually unseen and the measurement and direct observation are difficult (Bokuniewicz et al. 2003, Crusius et al. 2005). SGD has been measured at only about a hundred sites worldwide and most of them are along the east coast of the United States, Europe, around Mediterranean Sea and in Japan (Taniguchi et al. 2002). Fewer studies have been done on the west coast of the United State of America and Hawaii, and wide areas of the world as South America, Africa, and southern Asia have little to no SGD assessments at all.

SGD may affect both water quality and biogeochemical cyclic (Capone and Bautista, 1985).

SGD can be estimated by several geological and hydro-geological methods. These methods are divided into two groups: methods based on investigation of the coastal drainage area (hydrodynamic, combined hydro-geological, average long-term water balance method, modelling of groundwater discharge method), and methods based on hydro-geological investigation of the estuary as (remote-sensing method, geophysical methods, measurement of anomalies of sea water electrical conductivity, temperature distribution, and chemical composition) (Mulligan and Charette, 2006).

The following are some of these methods: -

-   Geochemical tracers techniques investigate excesses of the tracers Radium isotopes (Ra-226, 228, 223 and Ra-224), Radon (Rn-222, 220), Methane (CH4), Hydrogen (H3), Helium (He3, He$_4$), Carbon (C1$_4$) (Moore, 2003). The present of the above isotopes with high concentrations in the open water are often indicative of groundwater sources.

-   Seepage meters (flow chambers vented to plastic bags accompanied by volume and salinity measurements), or ultrasonic seepage meters.

- Geophysical/Hydrology, salinity, and conductivity. If the discharges of freshwater are great enough, the depression of salinity in the overlying water alone may pinpoint the source of SGD.

- By using airborne thermal infrared imaging 'characterize groundwater – surface water interactions between the sea and the shallow aquifers. It based in measurable physics parameters such as sea surface temperature

- Can be calculated directly in terrestrial water budgets (water balance), hydro-geological model.

- As well total SGD might be calculated by using piezo-meters and application of Darcy's law at a particular spot if the vertical hydraulic gradient is measured of the sediment-water interface along with measurements of the vertical permeability of the sediments.

- Or can be determined also by using mathematical models, either analytical or numerical techniques.

The difficulty of quantifying SGD is because of the methods are often indirect and pressing a many of assumptions (Oberdorfer, 2003).

2.1.1. Previous Studies on Chemical Tracers

Several studies have employed to use the natural uranium decay-series nuclide (Chemical Tracers) Ra-226 and Rn-222 as well as Methane to estimate and evaluate groundwater inputs to the Seas.

Radium isotopes as tracers were reporting on the quantity and effects of SGD off the coast of southeastern U.S. (Moore, 1984, Moore, et al. 1985, Moore, 1996; Rama and Moore 1996; Moore and Shaw, 1998, Moore, 2000, Moore, 2003). Radium isotopes were used by (Krest and Harvey, 2003, Charette et al. 2001; Kelly and Moran, 2002; Charette et al. 2003) in order to study SGD and coastal residence times. Radon-222 was used by scientist such as (Burnett et al. 1996;Cable et al. 1996b; Burnett et al. 2001; Burnett et al., 2002; Lambert and Burnett, 2003; Burnet and Dulaiova, 2003) to investigate SGD into the Gulf of Mexico in U.S.A. (Chanton et al. 2003; Corbett et al. 1997; Corbett et al. 1999, Corbett et al. 2000) used radon-222 in Florida Bay.

Methane was used for investigating groundwater input into the Gulf of Mexico (Bugna et al. 1996), in Florida Bay (Corbett et al., 1999; Schwartz, 2003), in West Neck Bay, U.S.A. (Dulaiova et al. 2004) and in Korea (Kim and Hwang, 2002).

According to D'Elia et al. (1981) many researchers have recognized the biogeochemical importance of groundwater discharge through coastal sediments. Such fluids may be an important source of nutrients for the coral reefs

Cable et al. (1996b) used the radon-222 as grab sample to estimate the submarine groundwater discharge into the Gulf of Mexico. They constructed a mass balance for Rn-222 for one layer. They did not intrest with the radon transport to or from adjacent coast areas under normal flow conditions.

Corbett et al. (1997) used the standard hydrologic budget in addition to natural tracer (Rn-222) approach for estimating groundwater input. The results show that helping to constrain estimated groundwater flow into surface reservoirs.

Corbet et al. (1999) used radon-222 and methane (CH4) to evaluate the patterns and assessment of groundwater discharge. They used a grab samples method, and the samples were collected both from the wells and from the seawater. They obtained good comparative results between two methods.

Burnett et al. (2001) Burnett and Dulaiova (2003); Lambert and Burnett (2003) used the continuous monitor of Radon-222 for estimating the groundwater input into the coastal ocean. They demonstrated an automated system that can determine the radon activity in coastal ocean water. They used the RAD7 device for the radon-in-air monitor because it is very sensitive.

Swarzenski et al. (2001) investigated the fluxes of radium in order to estimate the submarine groundwater discharge to the Indian River Lagoon. They used three independent methods (lagoon budget, benthic flux chamber, and pore-water modelling).

Taniguchi et al. (2002) used the term SGD to represent the direct discharge of subsurface fluids across the land-ocean interface (i.e. SGD rate is the sum of submarine fresh groundwater discharge and the re-circulated saline groundwater discharge). They made the comparison between the SGD and water depth. They found that the discharge estimates tend to decrease fairly systematically with increasing water depth over about three orders of magnitude.

Lambert and Burnett (2003) found that the comparison between the submarine groundwater measurements using grab sampling and the continuous monitor shows excellent agreement and there are few samples not in agreements due to handling, loss of radon during sampling, or analysis of the grab samples.

Schwartz (2003) used and assessed a multiple radon fluxes to determine the source of the Torally persistent and spatially fixed the excess radon at a maximum value. The assessed radon fluxes included diffusive input for sediment, surface water advection, air-sea evasion, groundwater input, and radioactive decay of radon

Abraham et al. (2003) attend to overcome the limitations of poor understanding of the distribution of radium and radon isotopes in coastal groundwater. They mapped the distribution of Rn-222 and Ra-226 across a groundwater salinity gradient, and deployed a new in situ Rn-222 analyzer to study time dependence of SGD in Waquoit Bay. They used a drive-point piezometer, in order to collect four depth profiles of groundwater Ra-226 and Rn-222 along a transect perpendicular to the shore at the head of Waquoit Bay. They created a vertical section of each isotope at the groundwater-seawater interface. According to Abraham et al. (2003) Rn-222 displayed an increase in activity with increasing salinity, depth and distance from the beach. The distribution of Rn-222 throughout the aquifer should be uniform, and not affected by changes in salinity, because Rn-222 is a noble gas. They quantify SGD to Waquoit Bay applying a non-steady-state mass balance model to them time series Rn-222 record which collected over 3 days at the head of the Bay.

Burnett and Dulaiova (2003) compared the results of the ground water discharge, which they obtained by using the continuous measurement of radon-222 for estimating groundwater discharge into the coastal zone with results of other studies in the same area using methods such as radium isotopes (Ra-223, Ra-224), and the automated seepage meters. They found that the results were comparable for the three approaches in the august readings. But in October the radon measurements indicate similar but slightly higher rates of flow than those calculated from the automated seepage meter. The estimate based on radium isotopes indicates a flow about a factor of two greater.

Charette et al. (2001) measured the activities of radium isotopes (Ra-223, Ra-224, Ra-226, and Ra-228) to estimate the submarine groundwater discharge. They compared the data, which they obtained with the other, which obtained from previous years. Then they estimate the groundwater discharge by calculating the excess radium flux in the sea.

Charette et al. (2003) made an interpretation of two decades of unique set of radium isotopes data spanning in order to quantify submarine groundwater discharge in Great Sppewissett Marsh. They measured the activities of four radium isotopes (Ra-226, Ra-228, Ra-223 and Ra-224) at the marsh in 1999 and 2001. They compared the results, which they obtained with radium activities measured at the same location in 1983 and 1985. They found that the long-lived radium isotopes (Ra-226 and Ra-228) activities were two times higher and 1.5 time higher for the short-lived isotopes (Ra-223 and Ra-224) in 1999 than that during the other three time periods. They estimated the total groundwater discharge to the marsh, which include both freshwater and re-circulated seawater. They compared the results of SGD, which they obtained, with the other results, which obtained from previous studies. Some differences were found between them results and the previous results, which obtained from other researchers who used other different approaches.

Moore (2003) used radium isotopes (Ra-223, Ra-224 and Ra-226, Ra-228) to determine and estimate sources and fluxes of submarine groundwater discharge (SGD). He collected the radium isotopes samples by using seepage meters, piezometers and surface and deep ocean waters. He found that all samples are unusually enriched in all four radium isotopes (Ra-223, Ra-224, Ra-226, and Ra-228). He supposed that this high radium concentration in the Gulf Water came from the groundwater because there is no surface water flow into his study area. He compared the results of radium concentration for the samples, which collected by the different ways. He found that the samples which colleted by seepage meters were about a factor of 2-3 higher in radium activity compared to the overlying waters and the samples which collected by piezometers (1-4 meter below sea-bed) were 1-2 orders of magnitude higher than surface waters.

Charette and Buesseler (2004) investigated the submarine groundwater discharge to evaluate the nutrients and copper to the Elizabeth River estuary. They used an approach based on radium isotopes. They found that radium activities in the groundwater were 10 times more enriched relative to surface waters.

Dulaiova et al. (2004) investigated the groundwater discharge into west Neck Bay in USA by using the chemical tracers.

2.1.2. Previous Studies on Seepage Meters

Seepage meters provide point measurements of submarine groundwater discharge (SGD) or, when arrayed in transects offshore, can give an integrated value of SGD per unit length of shoreline (Burnett et al. 2002).

Manual Lee-type seepage meters have been used for many years to measure specific groundwater discharge and then the total discharge (volume per time into a designated area or volume per unit width of shoreline per unit time). It can be calculated by integrating the measured seepage over space and time (Lee, 1977). This method only yields an average discharge rate spanning the small area of measurements (typically area less than 1 square meter). Then many seepage meters are needed to yield discharge estimates representative of a large area (Crusius et al. 2005).

Cable et al. (1997) used the direct seepage measurements in order to focus on groundwater flow through near-shore sediment. They made extensive measurements of flow to document the spatial patterns of groundwater seepage in a small area of the northeastrn Gulf of Mexico. They found that variations in sediment hydraulic conductivity and the presence of impermeable clay layers within a sediment column can cause the channelling of groundwater flow through the aquifers to seepage points in lakes and the coastal ocean. As well they found

that there is a general decrease in groundwater discharge with increasing distance from shore.

Taniguchi et al. (2002) compiled data from the previous published articles that reported both the measured rate and water depth in order to examine the relationship between direct measurements of submarine groundwater discharge and the water depth. They found that discharge estimates decrease with increasing water depth with about three orders of magnitude.

Taniguchi et al. (2003) measured the submarine groundwater discharge using a different types of automated seepage meters. They measured it also using standard Lee-type manual operated meters. They compared the rate of submarine groundwater discharge obtained from the various automated seepage meters (the continuous heat-type automated seepage meter, the heat pulse-type automated seepage meter and the ultrasonic-type automated seepage meter) with the results obtained from Lee-type manual seepage meters. They found that the groundwater discharge rates measured by the various types of automated seepage meters relatively well with the results measured by Lee-type manual seepage meters.

Schneider et al. (2005) used seepage meters with associated controls in order to quantify rates and directions of groundwater flow along a 120 m stretch of shoreline of Oneida Lake in New York. They reported that flow changes were highly synchronous among stations but increased in intensity or spikiness both positive and negative, with increasing distance from shoreline, out to a distance of 100 m.

2.1.3. Previous Studies on Remote Sensing (TIR)

Rundquist et al. (1985) pioneered the idea of using the thermal infrared remote sensing for quantitative analysis of hydrology of flow-through lakes. They obtained the data from thermal infrared multi spectral (TIMS) airborne scanner in 8.2-12.2 micron range, from NASA National Space Technology Laboratory (NSTL). They selected four lakes in the Sand Hills with greater potential for inference of the zones on intensive groundwater seepage. They detected also the thermal variability and possible groundwater discharge zones to these locations.

Baskin (1990) used the Thermal Infrared Multispectral Scanner (TIMS) for locating the groundwater discharge zones, in the non-mixed motionless environment of the Great Salt Lake. The enhanced Thermal Imaging Multispectral Scanner (TIMS) showed tonal differences associated with variations in surface Temperature. He found that a sharp decrease in digital value as compared to the digital values of surrounding pixels were the initially suspected of being groundwater inflow locations. He mentioned that the size of the thermal anomaly would vary with the volume of water, which is flowing into the lake. This study illustrated the utility of

the thermal imagery for identifying the density stratification of fresh water over saltwater much like what occurs in coastal systems.

Mckena et al. (2001) mapped the groundwater discharge locations in Rehnoboth River and Indian River bays by using ground aerial thermal infrared and satellite image thermal bands from LANDSAT7 image (60 meter resolutions).

Tcherepanov et al. (2002) evaluated thermal-infrared imaging as a tool for characterizing groundwater – surface water interactions between the lakes and shallow aquifer of the Nebraska Sand Hills. They identify zones of active groundwater-surface water and their orientation with respect to the regional flow by using thermal infrared imaging technique. As well they collect data on the distribution of lake surface temperatures using ground methods (digital thermometer). They compare the results, which they obtained from the surface Temperatures using ground methods with that which they obtained by using satellite (Landsat) image thermal infrared band. They found that the thermal infrared remote sensing has a potential for identification of the groundwater discharge zones in the shallow groundwater.

Ballestero et al. (2004) used field verifications of thermal infrared imagery method and topographic maps to identify the groundwater discharge zones. They mentioned that the field investigations typically involved characterizing the size of the discharge area, confirming an upward groundwater gradient, and quantifying the flow per unit area.

Erica et al. (2005) used high-resolution airborne thermal infrared imagery to locate mine pools and discharges in Kettle Creek watershed-Pennsylvania.

The emitted thermal infrared radiation (TIR) was used to measuring surface water temperatures by Kay et al. (2005). These methods were used to evaluate the accuracy of stream and lake radiant Temperatures derived from airborne (MASTER, 5 to 15 m) and satellite (ASTER 90 m, Landsat ETM+ 60 m resolution) TIR images. They found that agreement between images temperatures and ground Temperatures does not always imply that accurate temperatures have been recovered from TIR images. They concluded that an assessment of thermal stratification should be made in any field area before TIR images are use to measure water temperatures.

Shaban et al. (2005) applied airborne thermal infrared to recognize groundwater discharge along coastal stretch of Lebanon and to compare the results which they got with the results which got by Food and Agriculture Organization (FAO) for the same area and using the same technique. They recognized twenty-seven major SGDs. As well they did a correlation between SGDs and geologic controls on the land after doing interpretation of the satellite images.

2.1.4. Previous Studies on Resistivity and Electrical Conductivity

Salinity anomalies have been used by (Valiela et al. 1990) to identify sub sea freshwater seeps at a variety of scales from regional water budgets to vertical profiles at specific locations.

Manheim et al. (2001) used a streamer resistivity survey 'dipole-dipole' system for defining groundwater discharge into coastal bays of the Delmarva Peninsula. They found that many freshwater anomalies limit to a few hundred meters from the shore at some places and 1 km or more for some other places.

Crusius et al. (2005) quantified submarine groundwater discharge to the salt pond in USA, using radon and salinity measurements within a channel. They measured the salinity, temperature and depth of the water in the channel every 5 minutes. They measured the radon continuously at the pond. From the temperature and salinity measurements they observed that the channel was well mixed and the changes in channel temperatures were less consistent than changes in salinity and radon values. As well they found that the surface water salinity was demonstrably lower than deep-water salinity during only one profiles due to high tide. After low tide they found that a consistently a minimum in salinity and maximum in radon activity, which suggest inflow of low salinity groundwater. As well they used the salt balance calculations to constraint on the discharge of fresh groundwater to the pond. They assume that fresh groundwater is the only source of fresh water inters the system and they ignore the evaporation.

2.1.5. Previous Studies on Water Budget and Hydrogeological Model

A water budget is one of the methods that always done on a regional scale, including when applied to estimate submarine groundwater discharge. Water budget calculates the freshwater inputs and outtakes from the groundwater system.

This method is based on the conceptual model of dynamics of groundwater flow or is based on the examination of sea-side watersheds include the analysis of the geological and hydrogeological conditions in the coastal part of the sea and incorporate hydrodynamic calculations of flow rates (analytically or through simulation), hydrological-hydrogeological method, and the method of normal annual water balance for groundwater recharge zones.

In general saying a water balance (water budget) of a standing body of water is viewed as the equilibrium between water inflow components, outflow components, and the change in the water volume over a particular time interval (Feruson, 1981). Smith and Nield, (2003) and Smith and Zawadzki, (2003) used the water budget and hydrogeological methods for estimating the submarine groundwater discharge in western Australia and in Florida respectively.

Pluhowski and Kantrowitz (1964) estimated the submarine outflow in Babylon-Islip area, Suffolk County and Long Island, New York. They used both the water balance equation of the groundwater reservoir and Darcy's formula. They calculated the groundwater discharge by using water balance is about (68,000 m^3/day), and the quantity is about (72,000 m^3/ day) by using Darcy's formula. The difference in both estimates was explained by the inaccuracy of values of permeability and hydraulic gradients, which were used in Darcy's formula computations.

Mower (1968) also estimated the confined groundwater discharged directly into Great Salt Lake by applying Darcy's formula. Burdon and Papakis (1961), investigate the groundwater discharge through inland and coastal springs in Gulf of Corinth, Greece by using water balance.

Borisenko (2001) discussed the structural hydrogeological model based on the assumption of the leading role of faults in groundwater distribution. He found that groundwater drained by a streak-strip faults and discharge into the sea through this fault.

Elhatip (2003) estimated the discharge volume from the submarine springs on the Mediterranean coast of Turkey by using hydrogeological studies. He carried out some field measurements of Cl contents and electrical conductivity for outlet points and in several sections against depth of seawater. In order to determine the ratio of freshwater per unit volume of saline water discharge from the submarine springs. As well he used the water budget for a period of 10 years to calculate the recharge and the discharge of that submarine springs.

Vsevolozhskii and Kochetkova (2003) mentioned that the combination of the climate, relief, landscape and geomorphological conditions, geological structure, and hydrogeological conditions are controlling the values of specific characteristics of groundwater runoff, as well as their distribution and the contribution to the formation of water budget

Destouni and Prieto (2003) simulated large-scale dynamics and resulting of submarine groundwater discharge SGD in three different coastal aquifers on the Mediterranean Sea. They used the water budget techniques for their study.

2.2.   Specific Previous Studies on the Dead Sea

Neev and Emery (1967) studied the layering of the Dead Sea water. They mentioned that the shallow water layer of the Dead Sea the upper 40 meters undergo seasonal variations in both density and salinity. They found that a sharp increase of both density and salinity occurs at 40 m. The deeper layer, which is below 100 m depth the density, and salinity remain nearly uniform as a function of depth. They found also that the temperature, density, and salinity of the water, indicate that there are two main layers of water are present in the North Basin.

These two layers (the upper water mass and the lower water mass) are divided by a clear and sharp boundary at about 40 m depth. They divided the upper water mass into two members, which are surface member, and beneath surface member. The first member is varying seasonally in thickness and properties. It affected by runoff, evaporating, solar heating and currents. These properties of this member are uniform from top to the bottom of the member. The depth of this member is about 15 m in spring and about 40 m in early winter.

Stiller and Chung (1984) measured the radium-226 in the meromictic Dead Sea during 1963-1978 for three profiles along the western shoreline of the Dead Sea for a depth of about 300 m. They found that the radium activities in the upper water mass for the depth between 0 and 160 m were higher than that in the lower water mass. On the other hand they mentioned that the radium inventory for the three profiles were similar. They tried also to find the geological origin of radium in the Dead Sea. They mentioned that the origin of radium at the Dead Sea is not from neither the salt domes nor from igneous and sedimentary source beneath the deep part of the Dead Sea, because the radium concentrations in the upper water layer was much higher than that at the lower one. They suggested that the Dead Sea pore water, which migrates landwards, then flushed back by meteoric waters, could be a source of radium for some of its shoreline springs. They mentioned also that the lower water mass was a layer of fossil water that had been isolated at least for several centuries.

Steinhorn (1985) described the overturn process on a seasonal scale, and the reason for the destruction of the long-term stratification of the Dead Sea. He mentioned that the surface layers were cool in autumn and depth of mixed layer increases. As well the lake was cooled in winter and warmed up in spring, the salinity of its surface layers decreases due to the higher inflow rate from October to May. The surface layers (0 - 5 m or 10 m) are usually colder in winter and warmer in spring than the layers underneath. He found that the temperatures in October 1975 was sharp thermocline at about 25-m depth and the salinities at region from 65 to 75 m consisted of water layers with alternating low and high temperatures and also salinity. He found also that the surface Temperatures in July 1977 were high, 32°-37°C, with temperature gradient, accompanied by a reversed salinity gradient, in the upper 20-30 m. In February 1979 the water column of the Dead Sea was homogeneous in physical properties; except for relatively small diurnal variations in the upper 10 m. in august 1978 he found that the surface layers had higher salinity values than did the bottom layers. The mixolimnion 'the middle circulating layer' of the lake became deeper from about 80 m in 1975 to 110 m in 1976, 150 m in 1977, and 180 m in 1978. As well he evaluates the density, salinity and temperature of the Dead Sea water column.

Salameh and Rimawi (1988) studied the hydrochemical and the groundwater system of Zara-Zarqa Ma'in thermal field. They found that the salinity of the thermal springs in the region is high. They connected this high salinity of Zarqa

Ma'in thermal water to a possible mixing with the Dead Sea saline water. This is might be due to the Dead Sea water connected with the submarine aquifers and circulation of the Dead Sea water.

Gavrieli et al. (1989) found that the Dead Sea is presently saturated to oversaturate with respect to aragonite ($CaCo_3$), anhydrite ($CaSO_4$), and halite (NaCl).

Beyth et al. (1993) computed the quasi-salinity the Dead Sea water. They found that the quasi salinity of the surface layer of the Dead Sea saline water reached a maximum of 236 $kg.m^{-3}$ during the summer of 1991. But it dropped to 164 $kg.m^{-3}$ during the following winter due to heavily rainy season and rain flooded to the Dead Sea surface layer.

Abu-Jaber and Wafa (1996) investigate the hydrochemistry of the groundwater in the alluvial and deep sandstone aquifer in Safi and Haditha fields. They found that there is no obvious long-term degradation in the water quality can be identified. On the other hand there is degradation in the water quality with time within the distal portions of the alluvial fan due to the dissolution of the Lisan Marl.

Jiries and El-Alali (1996) studied the mechanism of salt Reef growth in the southern basin of the Dead Sea. They found that Reef growth at this area is due to common ion effect of chloride ions, from mixing of two different type of water, namely the artisan water issuing from groundwater flow, and the saltpan brine Dead Sea water.

Yiechieli et al. (1996) studied the source and age of the groundwater brines in the Dead Sea area using Cl^{36} and Cl^{14}. They found that the groundwater brines in the Dead Sea area are the results of direct infiltration of brines from precursor Dead Sea Lake.

Gavrieli (1997) modeled the effect of evaporation and the consequent concentration increases on the saturation index of the Dead Sea surface brine. He found that a 1% increase in concentration equivalent to about 1% volume evaporation, increase the saturation index of the 1959-1960 lower water mass from 1.01 at 25°C to 1.06, even though a 2% volume evaporation increase the index to 1.11. As well a 1% evaporation of the 1979 surface brine increases its saturation index from 1.11 to 1.16 and 2% evaporation increasing the index from 1.11 to 1.22. He mentioned also that for 35°C undersaturated 1990 (Ω_{halite} =0.94) surface brine, evaporation of 3.3% was required to reach a saturation index of 1.11. He defined the halite saturation index as:

Ω_{halite}= a_{Na} * a_{Cl} **/** K_h. where a_{Na} is the activity of Na, a_{Cl} is the activity of Cl and K_h is the thermodynamic solubility constant of halite.

Krumgalz (1997) applied the Pitzer system of equations to Dead Sea water as natural hyper-saline brines. He found that the degree of gypsum over-saturation in the Dead Sea water is less than 1.7, then he expected that the mixing of the Dead Sea water with rainwater and water coming from the springs surrounding the Dead Sea might be changed the gypsum precipitation-dissolution equilibrium. As well he mentioned that mixtures of the Dead Sea water with more than 10% wt. of freshwater became under-saturated with respect to gypsum. He determined also the degree of saturation of the different minerals in the Dead Sea water as the Degree of saturation of aragonite; calcite, dolomite, anhydrite, sulfite, maginesite and halite were 3.2, 4.92, 421, 2.23, 0.16, 12.3 and 0.94 respectively, but they did not mention are the saturation of these mineral at the Dead Sea surface water or at the deeper water layers.

Niemi and Ben-Avrahm (1997) analyzed the 3.5 kHz seismic reflection along the east to west trending of En Gadi fault which mapped by Neev and Hall (1976, 1979). They characterized a complex region of faults, channels and escarpments of uncertain origin. The date indicates a crosscutting relationship between the fault systems, with the northeast-trending faults. From the interpretation of these trends an interesting feature was observed at the fault intersection of the Ein Gedi fault and the northeast-trending intrabasinal fault is an expected a site of hydrothermal activity, which possibly is a hot springs on the floor of the Dead Sea.

Anati (1998) divided the Dead Sea water column into two water bodies; the deep water layer extending to 326 m below sea surface constituting most of the sea volume, and a shallow upper layer a few meters thick (between 5 and 20 m). The lower layer effected with a little vertical variation, while the upper layer is depending on the season and the regime. The salinity of the seawater increases continuously out of the rainy season (December to March), and decreases by the same amount in a balance year during the short rainy season (December to March). Anati found that the salinity of the upper layer water type in spring of 1980 increased by 5 times faster than in the spring of 1985. In spite of a similar evaporation rate and similar surface salinity in the two stages, and occurred during a season with no inflowing fresh water. According to Anati (1998) the deep water layer of the Dead Sea is isolated from the outside influenced during a complete seasonal cycle and consequently remain constant in all their properties during the 1979-1982 meromictic regime. She mentioned that the deep water attains its highest temperature in December and its lowest salinity in June, July or August.

Salameh and El-Naser (1999) estimated the water discharge to the Dead Sea by using water balance calculations. They compared the water balance before (predevelopment) and after water resources development. They found that the amount of water that used to flow into the Dead Sea before development was 1980 MM^3/y and after development (present day) is about 617 MM^3/y for the total catchments area of the Dead Sea.

Asmar and Ergenzinger (1999) estimated the evaporation from the Dead Sea over a range of salinity between 0 and 500 g/l. They used two methods approach for that. One is the modified penman method and the other is the modified Dalton-type formula. They found that the evaporation from the Dead Sea will drop to Zero at the salinity of 486.2 g/l by using Penman method and it will drop to zero at salinity of 483.55 g/l by using Delton method.

Krumgalz et al. (2000) issued a model for predicting the evaporation from the Dead Sea related to the Dead Sea level. They found that the evaporation from the Dead Sea would reach a balance, which will protect the further reduction of its level. This is expected to occur when the Dead Sea level drop to about –550 m below mean sea level.

Salameh and El-Naser (2000a), studied the saltwater – freshwater interface and transition zone in the groundwater flow system of Dead Sea in Zarka Ma'in area in detailed. They mentioned that the saltwater–freshwater interface starts at the shores of the Dead Sea with very steep gradient of inclination and gradually events out landward where it tends to become horizontal at an aquiclude. By using Ghyben - Herzberg formulas, which consider the density of the Dead Sea water (taken as 1.235 $g.cm^{-3}$), density of fresh water (1 $g.cm^{-3}$) and height of the groundwater level for a known point relative to the Dead Sea. They found that the depth of the interface between the fresh water and Dead Sea water is 4.255 m deeper for one meter increasing in groundwater level. Figure (2-1) shows the relationship between the groundwater level and the interface between the fresh water and seawater. Z1 is the depth of interface at groundwater level h1 and z2 is the interface depth at h2 groundwater level.
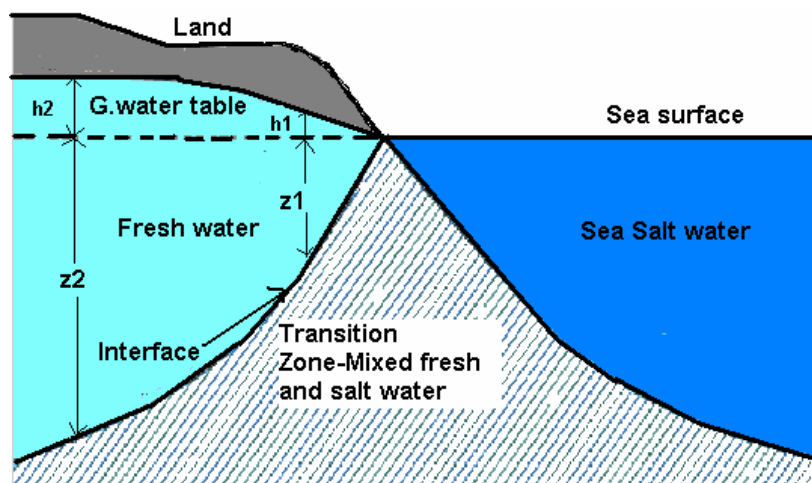
Figure (2-1): Schematic diagram showing the relationship between groundwater level and depth of the interface.

Salameh and El-Naser (2000b) reported that the interface seaward migration resulted in a groundwater discharge estimated at approximately 400 MM^3 per

meter drop in the level of the Dead Sea during the period between 1994 and 1998. They also mentioned that at the present day the loss of fresh water to the Dead Sea through the interface readjustment mechanism is calculated 370 MM^3/year as a result of over exploitation of waters that formerly fed the Dead Sea.

Getman and Hecht (2002) studied the hydrograph of the Dead Sea at the period from 1992 to 2000. The study area, which they considered, was at middle off the Dead Sea with about 12 Km and 5 Km from the west shoreline of the Dead Sea. They mentioned that the surface level of the Dead Sea has been lowered by an average rate of about 0.60 m/year since 1977 and for the period from 1998 to 2000, the lowering rate has reached about 1 m/year. They reported that the upper layer salinity of the Dead Sea has been increased and the gravitational stability of the water body diminished due to the runoff reduction. They did some evaluation of water temperature and quasi salinity at 1 and 30 m depth. They found that during summer, the seasonal thermocline is constantly above the 30 m level, while during the autumn; the thermocline deepens below 30 m. As a result the intensification of thermal fluctuation during this period shows the intermittent character of the mixing processes. After end of March, evaporation induces a salt concentration increase in the layer above the thermocline. They mentioned that the thickness of the upper layer during July and August is about 25-28 m. They considered two cooling process phases in the holomictic period. The upper layer of the Dead Sea water that is above the seasonal thermocline was affected by the first phase with cooling rate of about 0.1°C.day^{-1}. When the thermocline got beneath the 30 m depth, then about 30 days is necessary to entirely mix the Dead Sea volume. They donated that the salinity of the meromictic upper layer increased dramatically and in the summer of 1995, it overshot the salinity of the deep water.

Gavrieli and Oren (2004) studied the stratification of the Dead Sea. They observed that the stratification is maintained by a stabilizing thermocline (between 25 m and 30 m) during the summer months. They found that the surface water temperatures might reach 35-36°C, while the temperature of the water mass below the thermocline remains stable between 22-23°C. They mentioned that this stabilizing thermocline is sufficient to balance the destabilizing halocline that is formed during the summer months as a result of increased evaporation. As well they found that the over turn occurs following the autumn cooling of the upper water column and the increase in its density. They found also that the Kinetic factors which dominant over thermodynamic considerations indicate that gypsum ($CaSO_4.2H_2O$), rather than anhydrite is the actual Ca-sulphate mineral that precipitate from the Dead Sea brine. The Na/Cl ratio has slightly decreased over the years due to precipitation of halite from the Dead Sea brine.

2.3. Background Information

2.3.1. Geology of the Dead Sea Area

The Dead Sea area lies at the north margin of the Arabian Shield. From the plate tectonic point of view it is located at the western margin of the Arabian plate, which is separated from the Palestine Sinai plate by the Dead Sea Rift with horizontall displacement to the north relative to the Palestine Plate (Freund et al. 1970).

According to Bender (1968) the Dead Sea area has been controlled through the geological history by two factors, namely:

- The Tithys Ocean, which invaded the region several times, depositing the marine successions.

- The presence of the neighbouring Arabian Shield in the south, which displayed an important source for sediments.

2.3.2. Stratigraphy of the Study Area

Cretaceous rocks cover the eastern part of the investigated area, while westwards; the oldest formations are of middle Cambrian age. Close to the eastern shoreline of the Dead Sea, Triassic and Lower Cretaceous rock crop out. Volcanic eruptions occur in many places of the area but mostly in the western part along the Dead Sea coast. The stratigraphical lowest outcropping member is the Cambrian; Umm Ishrin formation, which consists of sandstone followed up by Triassic Zarka Ma'in group consisting of sandstones, limestone and shale, followed up by the Lower Cretaceous Kurnub sandstone and the Upper Cretaceous Ajlun group being mainly a carbonate-dominated sequence. Belqa group Upper Cretaceous - Tertiary follows it. This group is missing in the end northern part of the study area. The youngest geological units are the Quaternary Lisan marl of Pleistocene age (Bender, 1974) and the basalt flows dated 0.6 Ma BP (Duffield et al. 1987). Figure (2-2) shows the geological and structural map of the area surrounding the Dead Sea.

The sequence of the lithological units of the Dead Sea area is shown in table (2-1). The detailed of these units are described in the geological maps Ma'in, Ar-Raba and the southern part of Al-Karameh sheet in scale 1:50,000, which were produced by the Geological Mapping Division in NRA. The details are described as the following:

2.3.2.1.Ram Sandstone Group

This group has named by Quennell (1951) and Burdon (1959). It is concedered one of the lower aquifer in the area. This group divided into two formations in the study area as following:

- Burj Dolomite-shale Formation (BDS)

Only the uppermost part of the carbonate sequence of this formation is exposed in Wadi Zarka Ma'in area. The outcrop extends about 1 km to the north along the eastern shoreline of the Dead Sea. This formation had defined by Quennel (1951). It consists of dolomitic limestone, dolomite and sandy dolomite. The age of this formation is Lower to Middle Camprian.

- Um Ishrin Sandstone Formation (IN)

This formation has named by Lloyd (1969). It is equivalent to Quwiera sandstone as Quennel (1951) and Burdon (1959). It crops out at the in the west along the Dead Sea escarpment north of Wadi Al Hasa and at the eastern part of the Dead Sea at Wadi Al-Hidan. It is steeping rugged cliffs and deep Wadies to the south. It consists of brown, red-brown, yellowish, and red-violet colored, medium to coarse grained, massive weathered sandstone. The thickness of Umm-Ishrin formation is about 300-350m. The age of this formation is Lower to Middle Cambrian (Freund et al., 1975).

2.3.2.2.Zarka Ma'in Group (MK-MN)

Blake (1936) described the Triassic Rocks near the mouth of Wadi Huni and Wadi Zarka Ma'in 25 km of south Wadi Hisban. It was divided into six Formations as following:

- Umm Irna Sandstone Formation

The outcrop of this formation is restricted to cliffs adjacent to the Dead Sea shorelines. It consists of lower thin-bedded clastics unit and upper thick bedded clastic unit. It consists of sandstone upward fining sequences. It is from Permo-Triassic age (Bandel and Khouri 1981).

- Ma'in Sandstone Formation

It consists of fine to coarse-grained sandstone, siltstone, and clay intercalated with carbonate rocks. It crops out along the Dead Sea shorelines and in deep Wadis between Wadi Mukheiris to the north and Al Mamaleh to the south. It is from a Scythian age.

- Dardour Formation

This formation is from an Anisian–Carnian age. It consists of cream, yellowish, black and dark green marl, shale, dolomitic limestone with cross-bedded sandstone and dolomitic sandstone. It crops out along the Dead Sea shorelines between Wadi Abu Khusheiba to the south and Wadi Mukheiris to the north.

- Ain Musa Formation

It consists of massive glauconitic sandstone intercalated with siltstone, clay beds, marl and fossiliferous limestone. It crops out between Wadi Manshala to the south and Wadi Mukheiris to the north along the eastern shoreline of Dead Sea. It is age from Anisian (Bandel and Khoury, 1981).

- Hisban Limestone Formation

It consists of massive dolomitized limestone. Its age is early Anisian (Parnes, 1975).

- Mukheiris formation

It crops out in Wadi Mukheiris directly at the shore of the Dead Sea in Wadi Mukheiris and Wadi Dardur. It consists of calcareous sandstone intercalated with sand and clay (Bandel and Khoury 1981). Its age is from early Ladinian.

2.3.2.3. Kurnub Sandstone Group (KS)

Kurnub sandstone is locally cropping out along the eastern heights of Jordan Valley along the rift margins along the eastern shoreline of the Dead Sea. It forms accessible cliffs above the steep escarpment of the harder Umm Ishrin Sandstone. Kurnub sandstone is composed mainly of red, violet, purple, and brown sandstone with varying proportion of clay and siltstone beds. The upper part of this unit is characterized by the increase in the presence silty shale and marl and characterized by cross bedding. Its thickness in Zarka-Ma'in is around 330 m (Bender 1974). The age of this group is Neocommian to Cenomanian from Mesozoic Era. It is one of the deep aquifers in the area.

2.3.2.4. Ajlun Group

Ajlun group discomformably overlays the Kurnub sandstone group. It has been subdivided into five formations as follows:

- Na'ur Limestone Formation (A_1-A_2)

It consists of succession of limestone, dolomite and marl (Powell, 1989). Its age is from Lower Cenomanian. It crops out in the deep Wadies in the central parts of the Ma'in sheet east of the Dead Sea. It is one of the minor aquifers in Jordan.

- Fuhays Formation (A_3)

It is equivalent to A_3 and the middle part of the Nodular limestone of Bender (1974). It is consisted of yellow grey calcareous siltstone, marl and marly limestone, nodular limestone and fossiliferous limestone. It exposes along the deep Wadies north of Wadi Abu khusheiba and road cuts between Ma'in village and Ma'in hot springs. The age of this formation is Cenomanian.

- Hummer Formation (A_4)

It is equivalent to A_4 and to the echinoidal limestone of Bender (1974). It consists mainly of grey limestone, dolomitic limestone and dolomite. The age of this formation is Cenomanian. It is crops out north of Wadi Abu Khusheiba along the Dead Sea shoreline. It is a minor aquifer in the area.

- Shuayb Formation (A_5-A_6)

It is equivalent to A_5 and A_6. It consists of red green buff calcareous siltstone with gypsum viens and thin limestone beds with orange algallaminated dolomite and mudstone. It crops out in north of Wadi Abu Khusheiba along the Dead Sea shoreline. Its age is Early Turonian.

- Wadi Es-Sir Limestone Formation (A_7)

It comprises the upper most part of Ajlun group (A_7) (Mackdonaled et al. 1965). It consists of limestones, dolomitic limestones, marly sandstone, chert. The upper part consists of thick-bedded fossiliferous limestone alternating of thin chert bands. Its thickness is about 100 m in Wadi Abu Khusheiba and 85 m north of Wadi Zarqa Ma'in. It crops out at the middle part of the Dead Sea along the shoreline.

2.3.2.5.Belqa Group

The age of this group ranges from Coniacian to Eocene. It had divided lithologically by Paker (1970) into four formations as the follows:

- Wadi Umm Ghudran Formation (B_1)

It is equivalent to B_1 (Mackdonald et al. 1965), and equivalent to upper part of massive limestone (Bender, 1974). This formation is well exposed above the prominent cliff, which is formed Wadi Es-Sir (A7) formation at the north and south of Zarka Ma'in fault. It consists of white or buff chalk with bed of grey chert, phosphatic sandstone and phosphatic siltstone (Bender, 1974 and Powell, 1988). The age of this formation is Coniancian–Campanian (Powell, 1988).

- Amman Silicified Limestone Formation (B_2)

This formation consists of limestone, dolomite intercalation with chert and lamians of chalk.

It crops out in the deeply incised Wadi Al-Hidan and south of Wadi Mujeb. The age of this formation is Campanian. This formation compined with B_2 formation is considering a main upper aquifer (B_2/A_7) in the area.

- Al Hisa Phosphorite Formation (B_3)

It consists of calcareous, silicified, argiallaceous phosphorites beds, limestone, chert, marl, and oyster lumlachella (coquina) beds. It crops out at the east of the southern part of the Dead Sea between Wadi Mujeb and Wadi Al Hidan and south of Wadi Mujeb (Wadi Al Hasa). The age of this formation is Campanian to Maastrichtian-Danian (Powell, 1988).

- Muwaqar Formation (B_4)

It poorly crops out at the southern part of the Dead Sea at south and north of Siwaqa fault. It is covering with soil in the south and north of Wadi Mujeb. It consists of soft marl and white yellowish chalk. The age of this formation is Upper Maastrichtian.

- Um Rijam Formation (B_5)

The outcrops of this formation are restricted to the Adh Dhira Monocline south of Wadi Al Karak. It consists of chalk, chalky limestone, and phosphatic limestone with laminas of chert. Its age is Early Palaeocene to Eocene.

2.3.2.6. Dana Conglomerate (DC)

It crops out at the end southern part of the Dead Sea at the Adh Dhira area at Wadi Al Karak. It consists of marl, and sandy marl, layers and nodules of conglomerate. Its age is Oligocene.

2.3.2.7. Lisan Marl Formation (LMg)

It presents adjacent to the Dead Sea unconformable on strata. It is ranging in age from Cambrian to Neogene (Bender, 1974).

2.3.2.8. Superficial Deposits

- Fluviatile and Lacustrine Gravel (PL)

It consists of coarse-grained sand and gravels. The latter composed of sub-angular pebbles and cobbles. Clasts are chert, limestone, dolomitic limestone, sandstone and basalt.

- Alluvial Fans

It consists of sand and gravel with soil covered developed in Holocene to present.

- Travertine

It is a carbonate rock resulting from the precipitation of limestone from hot waters and its age is Pleistocene (Bender, 1974).

2.3.2.9. Volcanic Rocks

Basalts crops out between Siwaqa fault and Wadi Ash Shaqiq. It is recorded of 10 m basalt on the flanks of Wadi Mujeb (Barberi, et al. 1980). It crops out along Zarka Ma'in fault and at some locations to the east of the Dead Sea.

Table (2-1): Chronological sequence of the lithological units   in the Dead Sea area (Internal reports, NRA)

Period	Age	Group	Unit	Lithology
Quaternary	Recent		River,Terrace	Gravel, Clay, Sand
	Pleistocene	Jordan Valley	Lisan	Marl, Gravel, Clay, Gypsum, Sand
Tertiary	Pliocene		Undifferentiated	Conglomerate, Marl
	Miocene			
	Oligocene			
	Eocene	Belqa	Wadi Shallala(B5)	No data at Dead Sea area
	Paleocene		Umm Rijam(B4)	Limestone,Chert
Upper Cretaceous	Maestrichtian		Muwaqqar(B3)	Chalky Marl
	Companian		Al Hasa(B2a) Amman(B2b)	Phosphate Silic. Limestone
	Santonian		W. Ghudran(B1)	Chalky Marl, Chalk
	Turonian	Ajlun	Wadi Es Sir(A7)	Limestone
			Shueib(A5-6)	Marly Limestone
			Hummar(A4)	Dolomatic Limestone
			Fuheis(A3)	Marl
			Na'ur(A1-2)	Marly Limestone
Lower Cretaceous	Albian	Kurbub	Kurnub Sandstone	White Sand Stone
	Aptian			Varicolored Sandstone
	Neocomian			Lst.,Shale, marl, dolomite.
Permo Triassic		Zarqa-Ma;in	Dardur	Sandstone, Marl, Shale
			Ma'in	Sandstone, Siltstone,Clay
			Umm Irna	Sandstone, Siltst., Shale
Silurian	No Strata	Present i	n The Dead	Sea Area
Ordovician	No Strata	Present in	The Dead	Sea Area.
		Ram	Umm Sahm	No strata at the Dead Sea
			Disi	No Strata at the Dead Sea
Camprian			Umm Ishrin	Sandstone, Siltstone
			Burj	Dolomite,Shale,Sandst.
			Salib	Sandstone, Siltstone
Pre-Camprian		Safi	Not presented	In the Dead Sea Area

2.3.3. Structural Settings in the Dead Sea Area

Most of the structural features in the study area are parts of and influenced by the prominent outstanding structural feature affecting the whole are along Jordan Graben.

The Dead Sea Transform in Jordan is composed of three morphotectonic segments; Wadi Araba at the south, Dead Sea at the middle and Jordan Valley at the north. Together they form morphological depression that extends from the Gulf of Aqaba to Lake Tiberias about 360 km long (Bender, 1974). It is a part of the east African-South Turkey rift system that has a total length of 6000 km (Bender, 1974). The Wadi Araba segment trends 15° east of N with length about 200 km while the Dead Sea –Jordan Valley Rift segments trends with 5° NE with about 160 km length (Burdon, 1959, Bender, 1974).

In addition to the Dead Sea transform fault system, which is the major active strike – slip fault system, there are many other structural features in the area between the northern end of the Dead Sea and the northern part of Wadi Araba. These are:

- Zarka Ma'in Fault

This fault commences at the Dead Sea and continues eastwards. The downthrown of this fault is about 250 m near the Dead Sea. The downthrown decreases eastwards and turns over in a flexture. On the southern part of this fault basaltic eruption occurred at the downthrown block, while hot springs issue on the northern block from Lower Cretaceous Kurnub Sandstone (Wiesemann, 1969). It trends E–W.

- Wadi Atun Fault

This fault trends E–W. It extends from the Dead Sea shore to Wadi Wala. It is sub-parallel to Zarka Ma'in Fault. It divides Zara area into north and south Zara.

- El-Maslubia Fault

It starts at Wadi Kashem Jiwan basalt (in the northwest) and extends for about 5 km eastwards (north of Ma'in village). It trends E–W.

- Humrat Ma'in Fault

It is parallel to the Dead Sea coast in the southern part between Wadi Zarqa Ma'in and Wadi Manshala. It appears 2 km east of the Dead Sea coast at its southern part and 4 km distance from the Dead Sea at its northern end (Atalla 1981). It trends NE–SW and the downthrown is the NW block.

- Zara Fault

It trends N–S. It commences north of Wadi Mujeb and runs along the eastern escarpment of the Dead Sea. The hot springs in Zara area are related to this fault (Wiesemann, 1969).

- Wadi er Rashsha Fault

This fault extends from upper Wadi Zerka Ma'in to about 1 km south of Ma'in village. It is trending NE–SW and the downthrown is towards the SE.

- The Karak Al-Fiha Fault zone

 It rends NW-SE and extendsabout 300km.

- The Siwaqa Structure

It is a normal fault, which strikes between NNE and ENE. It has a northern downthrown, while the eastern main fault has a southern downthrown. The faults trend NE-SW, while it trends NW-SE in the northern part of the area (Atalla 1981).

- Amman-Halabat Structure- NE-SW trending

- Wadi Zarka Ma'in Syncline

It passes gradually through a graben and pluges westwards. Its axis is almost along the Wadi and parallel to the Zarka Ma'in fault. Both the graben and the syncline are asymmetric.

- Wadi Um Ghureiba Anticline

It is exposed east of the Dead Sea at Um Ghureiba north of Wadi Mujeb with a NE axial strike. The extension of this anticline is about 8 km.

- Quallat Et Taweiyil Anticline

It extends for about 3 km in a NNE–SSW direction along the road to Zarka Ma'in hot springs.

- Hammrat Ma'in Anticline

It is an asymmetrical anticline NNE trending. It starts near Wadi Durdur and extends to about 3 km to the SSW.

- The Haditha Syncline: it trends NNE-SSW and plunges NNE

- According to Bender (1968), there are many flexures east of the Dead Sea dipping to the west as (Karak flexure, Wadi Mujeb and Wadi Hisban).
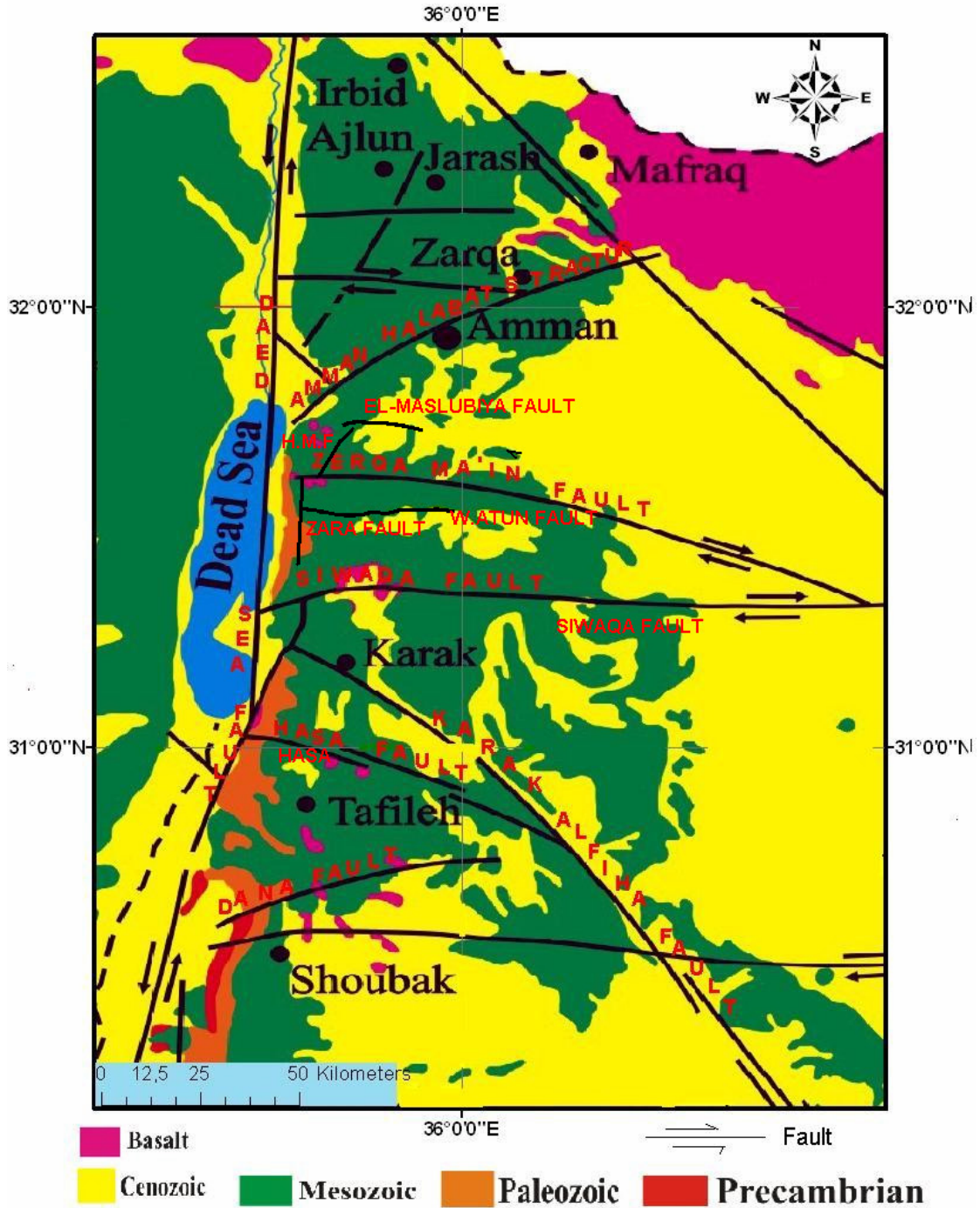
Figure (2-2): Simplified geologic and structural map of the area surrounding the Dead Sea

2.3.4. Water Balance

A water budget is generally carried on a regional scale, including when applied to estimating submarine groundwater discharge. It calculates the freshwater inputs and outtakes from the groundwater system for a long-term average annual submarine discharge (Loaiciga and Zektser, 2003). This kind of approach deals with the water inputs to the groundwater system and assumes that what goes into a coastal aquifer must discharge into the coast.

Because the Dead Sea is an enclosed system and has no underneath water outflow the only losses from the Dead Sea system are only due to evaporation from its surface (Salameh and El-Nasser, 1999). Groundwaters feeding the Dead Sea evaporate when emerging as seepages to the groundsurface and by extraction by the Potash Companies on the both sides of the Dead Sea to produce different kind of salts. Then by accounting for these amounts the hydrological budget can be estimated using the following equation:

$$\Delta V = P_t + S + G_n - E - K \tag{1}$$

Where ΔV is the change in the Dead Sea volume, P_t is precipitation over the Dead Sea itself (m^3/y), G_n is net groundwater flow (inflow-outflow) (m^3/y), S is the surface water flow into the Dead Sea (m^3/y), E is evaporation (m^3/y), and K is the amount extracted by Potash Company (m^3/y). Each parameter was calculated and substituted into the equation. The balance was calculated as an average for a long time period.

An important part of the water balance is the estimation of the surface area and volume of the Dead Sea, since the size of the Dead Sea changes dramatically with time. The surface area and the volume were taken as given in (Salameh and El-Nasser, 1999). This water budget was calculated for a long period of time from 1950s until the year 1994/1995 when the Dead Sea level was – 410 m below mean sea level.

2.3.4.1. Surface Water Flows into the Dead Sea

The surface water discharges into the Dead Sea come from Jordan River and other Wadies surrounding the Dead Sea from the eastern (S_e) and western sides (S_w) and from Wadi araba (S_a), then the total amount of surface water discharging into the Dead Sea equal the sum of these amounts:

$$S = S_r + S_e + S_w + S_a \tag{2}$$

The total surface water inflow from the Jordan River and its surrounding Wadies is equal to about 142 MCM/y (40 MCM/y from Tiberias + 10 MCM/y from west side of

Jordan River + 50 MCM/y from Yarmouk River + 42 MCM/y from the eastern side of the Jordan River).

The inflow into the Dead Sea from the western side Wadies of the Dead Sea is equal to about 13 MCM/y, and from the eastern side Wadies is equal to about 147 MCM/y (Zerka Ma'in, Mujeb, Karak, Ibn Hammad, Udheimi Wadies, and from Zara hot thermal springs). Inflows of surface water from the western side of Wadi Araba equal 10 MCM, and from the eastern side of the Wadi Araba equal 10 MCM/y (Salameh and El-Naser, 1999). Then the total amount of the surface water (S) inflow into the Dead Sea from all surface water sources from all sides of the Dead Sea equal about 322 MCM/y.

2.3.4.2.Groundwater Flow into the Dead Sea

The quantity of groundwater discharge into the Dead Sea from the western side equals about 50 MCM/y (Salameh and El-Naser, 1999), and the flow from the eastern side 90 MCM/y. As well there is about 85 MCM/y of return flow from irrigation and subsurface flows and saltwater diversions into the Jordan River (Salameh and El-Naser, 1999). Then the total amount of groundwater inflow into the Dead Sea equals to 225 MCM/y.

2.3.4.3.Precipitation

Precipitation (P_t) over the Dead Sea area is simply the total sum of precipitation multiplied by the surface area of the lake. The precipitation is measured by rain gauges spread in the area.

The average precipitation over the Dead Sea is about 92 mm/y. This average was calculated for a time between 1937 and 1994 (MWI, 1997). The total area of the Dead Sea surface is about 667 km^2 (Salameh and El-Nasser, 1999). Then the total precipitation over the whole Dead Sea (P_t) equals:

$$P_t \ (m^3/y) = P \ (m/y) * A \ (m^2) \hspace{3cm} (3)$$

$$P_t \ (m^3/y) = 92 * 10^{-3} * 667 * 10^6 = 61364 * 10^3 \ m^3/ \ y \ (61 \ MCM/in \ the \ year \ 1995).$$

2.3.4.4.Extractions of the Potash Companies

Water from the Dead Sea is extracted by the Potash Companies at the Eastern and Western sides of the Dead Sea. The total abstraction rate is about 490

MCM/y. About 200 MCM/y of which return to the Dead Sea as brine return flows. That means that the two companies consume about 290 MCM/y from the Dead Sea water (i.e. K= 490-200= 290 MCM).

2.3.4.5. Evaporation

In the past only evaporation losses balance the incoming amounts of water into the Dead Sea. But after the potash companies have been established at the both sides of the Dead Sea, water has been extracted and exposed to evaporation in saltpans to extract different kind of salts. Then the net of amount of water remaing in the Dead Sea equals the total amount of incoming water from all sources minus the amount extracted by the Potash Companies. According to (Salameh and El-Naser, 1999) the evaporation is 1334 m^3/y at when the Dead Sea surface area (667 km^2)

2.3.4.6. Final Balance Calculation

After substituting all incoming and losses amounts in the equation (1) above as following:

ΔV = 61 + 322 + 225 - 1334 – 290

ΔV = -1016 MCM/y

If this amount is dividing by the surface area of the Dead Sea 667 km^2 (-1016 MCM/667 km^2), then the result will be -152 cm drop in the Dead Sea level. But the actual drop of the Dead Sea level during last decade averaged only -80 cm (Salameh and El-Naser 1999). Then the difference of 72cm/y drops in Dead Sea level, is considered due to additional groundwater discharge into the Dead Sea. The quantity of this additional groundwater flow is equal (0.72 m/y * 667 km^2) = -480.2 MCM/y

According to Salameh and El Nasser (2000) the loss of freshwater into the coastal line of the Dead Sea was -370 MCM/y with 0.8 m dropping in the Dead Sea level for the period of 1994 to 1998.

2.3.5. Hydrology and Chemical Aspects of the Dead Sea (DS)

- One of the main features of the Dead Sea is its very high salinity (more than 340 g/l). While the water salinity in the Atlantic Ocean is 35 g/l and it is about 230 g/l in the Great Salt Lake in USA. This means that the water

salanity of the Dead Sea is more nine times than that of other oceans. The density of the water of the Dead Sea is more than 1.237 g/cm^3 (Gavrieli et al., 2005). That is mean no lakes in the world posses such a high salinity and high density as the Dead Sea.

- The salinity of the Dead Sea increases as a result of evaporation with very limited interaction between fresh water and rocks, sand and soils. The fresh water flows into the Dead Sea through the Jordan valley carrying light burden of salts, which is produce from interaction and leaching process. As well there are no out flow and high evaporation process, the inflowing water evaporate leaving salts concentrate in the Dead Sea (Steinhorn and Gat, 1983).

- The water level of the Dead Sea oscillated significantly due to throughout. It is indicated with the historical records (Klein, 1961), Getman and Hetch (2002), Gavrieli and Oren, (2004), Anati and Shasha (1989) and open report APC). The level of the Dead Sea has been continuously dropping since 1860 from 395 to 417.8 in 2005 below sea level as seen in (Fig. 2-3). Figure (2-3) shows that in some years as in 1883, 1895, 1945, 1975, 1980 and 1991-1992 the elevation increased due the high rain.
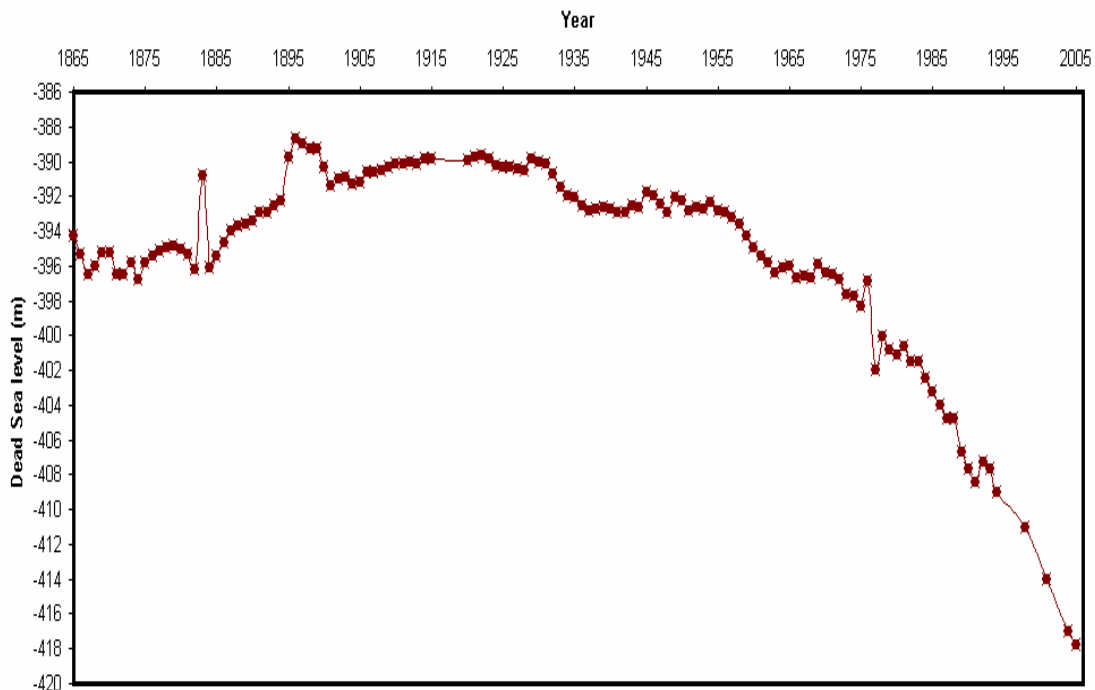
Figure (2-3): Long term changes in the surface level of the Dead Sea 1862-2005 (after Klein, (1961), Getman and Hetch (2002), Gavrieli and Oren (2004) and data from Arab Potash company).

During the winter of 1980 the surface level rose by almost 1.5 m, and in 1991-1992 the surface level rose nearly 2 m, due to a large amount (~ 1500 MCM) of fresh water entered the lake, causing a dilution of the upper 5 m of the water column to about 70 % of their previous salinity (Beyth et al., 1993). Generally if we exclude the above years the surface level of the Dead Sea has been lowered by an average rate of about 60 cm/year since 1977 and for the period from 1998 to 2005 the lowering rate has reached about 100 cm/year.

- The length of the Dead Sea decreased from 80 km (1978) to about 50 km now a days, its maximum depth has diminished from 328 m in 1978 to 316 m (Getman and Hetch, 2002) its surface area was 815 km^2 (Neev and Hall 1979) dimensioned to about 643 km^2 in 2004 (Rishmawi et al., 2005).

- As well the decreasing in volume of the Dead Sea is naturally followed by an increase in salinity (Gavrieli et al. 1989).

- The separation and gradual drying of the southern basin of the Dead Sea is the most visible impact of declining the Dead Sea level (Asmar and Ergenzinger, 1999).

- The halite began to precipitate from the Dead Sea in 1979 (Steinhorn, 1983). A decrease in halite precipitation rate was observed in the years 1992 to 1995. This was because of the stratification at these years, which diluted the upper water body and isolated the lower water body (Anati et al., 1995).

2.3.6. Hydrology of Jordan and the Dead Sea Area

The highlands in Jordan generally have a semi-arid Mediterranean climate, characterized by cold, wet winter and moderate dry summer. The Temperature in winter reach a few degrees below zero, but in summer the temperature raised to more than 32°C with relative humidity of 15-30%. On the other hand climate in the Dead Sea classified as arid climate with hot summer and warm winter. The temperature in summer (June-August) is as high as 45°C, while in the winter (December- February) the temperature is around 20°C during the day and it is fall down to about 5°C at night and may reach to zero at some nights in January. The annual average of temperature at the Dead Sea area is about 24°C.

The precipitation is confined to the winter season and it falls in the form of rainfall. Snow falls two to three times a year over the highlands. The precipitation ranges from about 600 mm in the northwestern highlands at Ajlun and at the middle part of Jordan decreases gradually to the south to less than 30 mm in the southeast part and at the Dead Sea. Figure (2-4) shows the annual rainfall distribution at the Dead Sea and the surrounding area. According to Salameh and Bannayan (1993) the

precipitation is less than 100mm over the 80.6% of the area of Jordan, 12.5% between 100-200 mm, 3.8% between 200 and 300, 1.8% between 300 and 500mm and 1.3% more than 500mm annually.

According to Salameh (1996) the average annual amount of precipitation all over Jordan is about 7200 MCM. Figure (2-5) shows the rainfall percentages in Jordan. This precipitation amount is flow down to the Dead Sea and Jordan Valley areas through the Wadies adjacent to these areas. Some of it also infiltrate through the fractures and porosity into the upper aquifers (B2/A7) and Jordan Valley conglomerate deposit which contain a meteoric water flow to the Dead Sea under hydrostatic head. Part of this surface water which flow toward the Dead Sea and Jordan River are collected by dams which established in these areas as Shueib, Kafrain, Al Waleh, Mujeb and Al Karameh before reaching the Dead Sea and Jordan River. The rest of the precipitation drains to the Dead Sea and Jordan River. The deep Aquifers (Kurnub) contain fossil water in the Jordan. These aquifers In the Dead Sea area exposed and receive amount of the precipitation through faults, fractures. Then the meteoric water and fossils water are mixing in the Dead Sea area and seep to the Dead Sea under hydrostatic head.

The Potential evaporation ranges from 2000mm/year at the most northwestern edge of the country, to more than 4000mm/year in the Aqaba at the south and Azraq at the East of Jordan. It rates about 2500 mm / year at the Dead Sea (Salameh and Bannayan 1993).
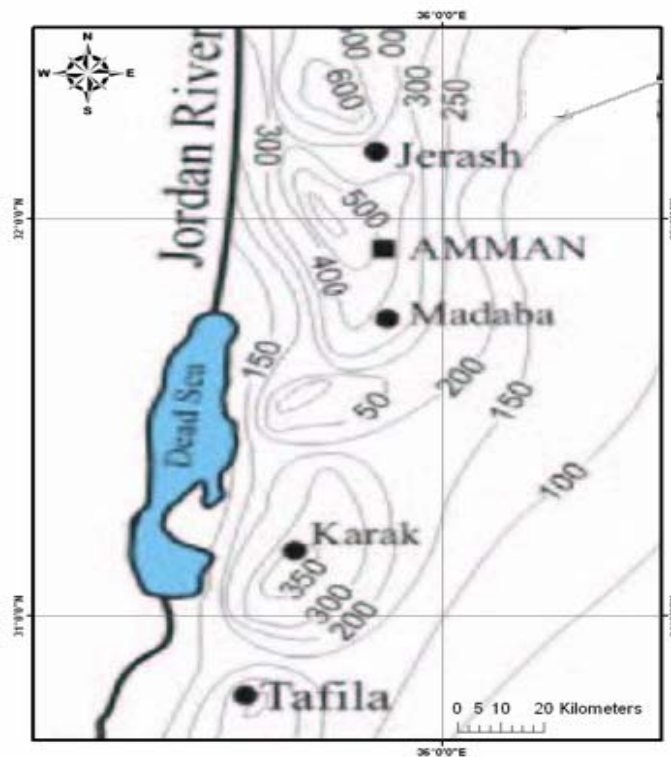
Figure (2-4): Average rainfall annual distribution
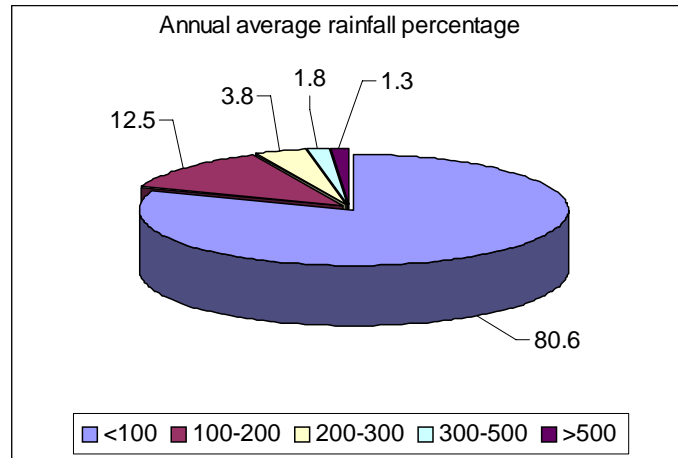
Figure (2-5): Annual average rainfall in percentage

The floodwater from the rainfall and snowfall at the eastern highlands during wintertime and the base flow springs around the area are the main recharge source for the groundwater of the shallow aquifers in the study area. It flows through the Wadies passing adjacent the Dead Sea area.

2.3.7. Morphology of the Dead Sea Area

A steep escarpment along the eastern shoreline of the Dead Sea controls the morphology of the Dead Sea area. The difference in the elevation between the Dead Sea Surface and the highlands surrounding the Dead Sea is between 1210 and 1600 m within of 15 Km horizontal distance to the East of the Dead Sea (Fig. 2-6).
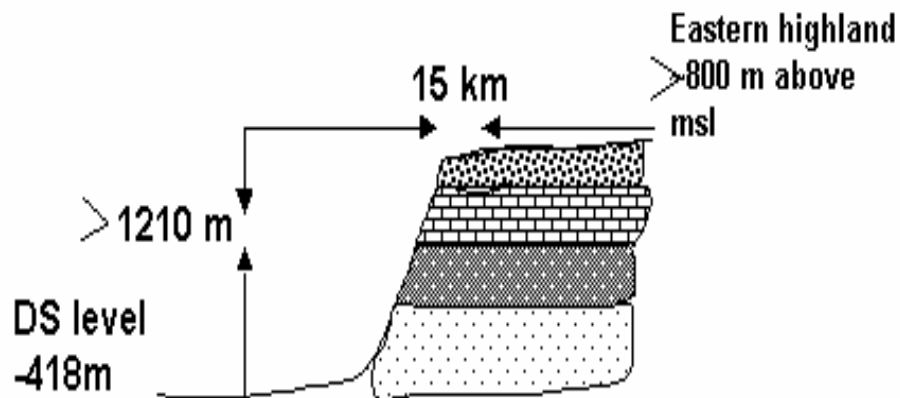
Figure (2-6): Difference of elevations between Dead Sea and the eastern highlands

2.3.8. Springs Surrounding the Dead Sea

There are many springs discharging into the Dead Sea located at the eastern side of the Dead Sea. Some of these springs occurring to the west of the Edhira Monocline and south of the Siwaqa fault. They emerge from Pleistocene and Recent gravels. Among these is Ayn Al Merweh in Ghor Haditha. There are many springs emerge from F/H/S (Fuheis, undifferentiated formation of Hummer Shuaib) as Al Ayn al Bayda, Ayn al Maliha, Ayn Umm Wa'il southern flank of Wadi Mujeb, Ayn Arafat, Ayn Maqbula. There are some springs emerge from Wadi Es Sir (A_7) formation as Buwayra, Ayn al Mughaysil. Some springs issue from Kurnub Sandstone as Ayn Hammam al Hamra in Wadi Ibn Hammad (thermal spring).

All the previous springs locate at the south and east of Wadi Mujeb at the coordinate 1073-1097 N and 200-220 E (Palestine Grid). There are some springs which locate at the north and east of Wadi Mujeb at the coordinate 1098–1128 N and 203–220 E (Palestine Grid) as: Ez-Zarqa, El-Qattar, El-Mnya, Ujeirman, Edardor and Ed-Dhib. The temperature of these springs range from 18 to 21°C. These springs are discharging from the Kurnub (KS) and Ajlun groups along the escarpment area. There are also about 109 thermal springs located in this area. According to Abu Ajamieh, (1980) the temperature of these springs ranges from 34°C to 62°C. Sixty four of these springs located at the northern part of the Wadi Zarka Ma'in. Forty-five springs located at north-south trend in Zara area on the eastern shore of the Dead Sea. All thermal springs in this area issue from upper part of the Kurnub sandstone group (Cretaceous age) (NRA reports) (Fig. 2-7).
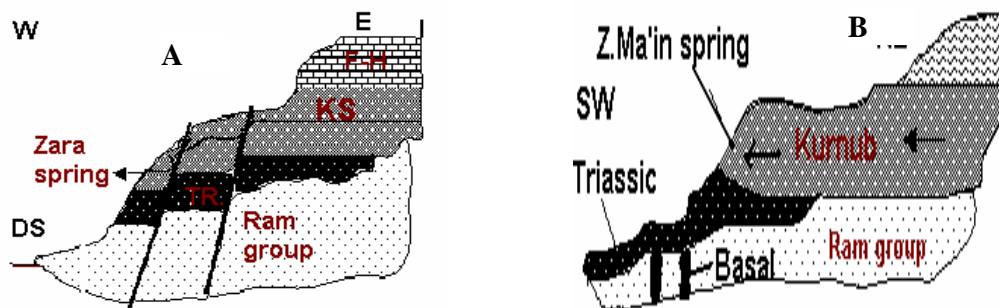
Figure (2-7): Schematic geological cross section of springs in Zara area (A): Zarka Ma'in area (B)

2.3.9. Sinkholes

Sinkholes are circular depressions developing in a karst area. They are natural phenomena, which occur in certain geological environments associated with surface, subsurface processes.

The occurrence of sinkholes and subsidence in Ghor Haditha and Lisan Peninsula areas at the southern Dead Sea basin dates back to about 15 years. The new generations of subsidence in Ghor Haditha and Lisan areas are attributed to the lowering of the Dead Sea level. Tens of collapsed sinkholes formed along the Dead Sea coast. The first opening sinkhole in these areas collapsed during winter 1985, and many others sinkholes followed. The diameter of sinkholes in these areas ranges from a few meters to 20 meters in deepth, and between 1 and 25 meter in diameter. Figure (2-8) shows one of the sinkholes located in the Lisan Peninsula at the eastern coast of the Dead Sea (Jordan side). They present danger to both life and property and they affect fields, houses, roads and salt evaporation ponds. These sinkholes are not randomly scattered on the Dead Sea shores, but tend to occur in clusters (Itamar and Rezmann, 2000). The sinkholes in Ghor Haditha and Lisan are located on the edge of an alluvial fan consisting of coarse clasting sediments and gravels and clay.
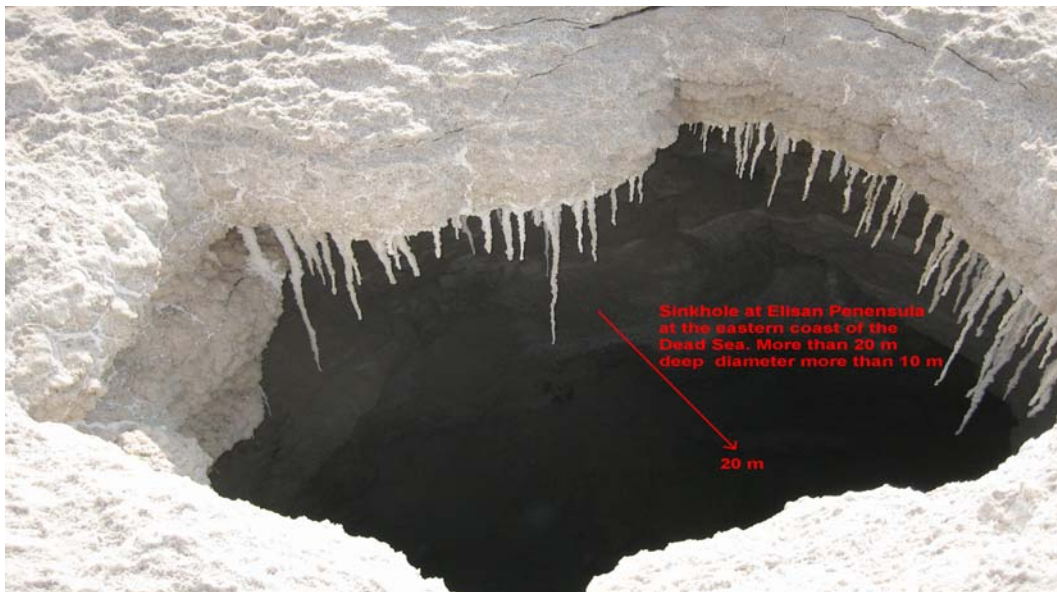
Figure (2-8): One of the sinkholes located in the Lisan Peninsula at eastern coast of the Dead Sea.

The development of the sinkholes is effected by underground mass mobilization; mass transport is cultivated by alluvial. The most generally result from upward sub-vertical movement of cavities that developed because of the dissolution of underlying layers (Taqieddin et al. 2000). As a consequence of the Dead Sea falling, the interface between the Dead Sea water and the groundwater also is falling. Thus the salt layers surrounded by saturated water in the past in respect to salt, are now exposure to aggressive dissolution by unsaturated groundwater water, which flows to the coast of the Dead Sea through the faults or the joints (Salameh and El-Naser, 2000a, Closson et al. 2005). Then Chemical and physical erosion takes place along the fault and the flow line. Underground voids start to form, creating holes and cavities. As a result numerous sinkholes and subsidences

appeared in many places along the Dead Sea shoreline. In other words the drop in levels of the Dead Sea and surrounding water table cause decrease of pore pressure and vertical equilibrium of sediments in the vadose zone. These factors are triggering these phenomena (Closson, 2005).

The comparison of the fresh water's conductivity at the apex and tip of the most affected place showed that the concentration of salt increased to 40 g/l which confirm the existence of soluble deposits in the underground (Clossen, 2005).

3. METHODOLOGY

3.1. Electrical Conductivity-Temperature with Depth Method

Electrical conductivity is the ability of a medium to support the flow of an electrical current. It is a measure of the movement of mobile charge carriers to the influence of an electrical field.

Measurement of seawater electrical conductivity is based on the relationship between the ions concentration and the electrical conductivity of seawater. Electrical conductivity device measures the conductivity and temperature. The electrical conductivity anomalies and the temperature distribution are indicators of fresh groundwater discharge. The conductivity in seawater is due to the charged solute ions of dissolved salts in seawater. Thus the electrical conductivity is a property of seawater that varies predictably with both temperature and total ionic concentration (salinity).

Electrical conductivity might be a useful indicator of total dissolved solids because the conduction of current in an electrolyte solution dependent on the ionic concentration. Electrical conductivity-temperature with the depth was used in this study to examine the mixing of the fresh groundwater with Dead Sea water.

Four stations were considered in this study for the electrical conductivity-temperature with depth measurements, along the eastern shoreline of the Dead Sea. These stations were chosen depending on the geology, the structures and the expecting discharge areas which were determined by using the geological, topographical maps and the field trips which were done before starting the measurements. The profiles were carried out for a different depth and chosen relating to the distance away from the eastern shoreline of the Dead Sea.

The air temperature during the measurements was between 40-46°C at the Dead Sea area, while the temperature at night decreased to about 30°C. The inductive

electrical conductivity sensor (Fig. 3-1) with a cable 100 m length was used for carrying out the electrical conductivity, temperature and depth measurments.

The electrical conductivity and the temperature were measured continuously by using an electrochemical transmitter, which is connected with the sensor and with a portable computer. The depths were measured manually by marking every one-meter of the 100 m cable length. The sensor was connected tightly with the cable to not loss the sensor in the sea under a pressure at deep-sea water. As well some weight from lead was added in the top of the sensor to keep the sensor diving vertically or with very low deviation to get an exact depth. The electrical conductivity was compensated to 25°C. The sensor was checked for temperature compensated at 25°C by using a standard solution of MgCl2, CaCl2, NaCl, KBr salts as a same of the Dead Sea water composition and a same concentration of the Dead Sea water. The solution was put into a water bath. The temperature was heated up to about 40°C and Then it cold back down to about 19°C. The temperature readings were taken every two degrees. The compensated and noncompensated electrical conductivity reading was found the same at the temperature of 25°C, which means that the sensor work properly with a temperature compensated. Then the curve of the temperature versus electrical conductivity was issued.
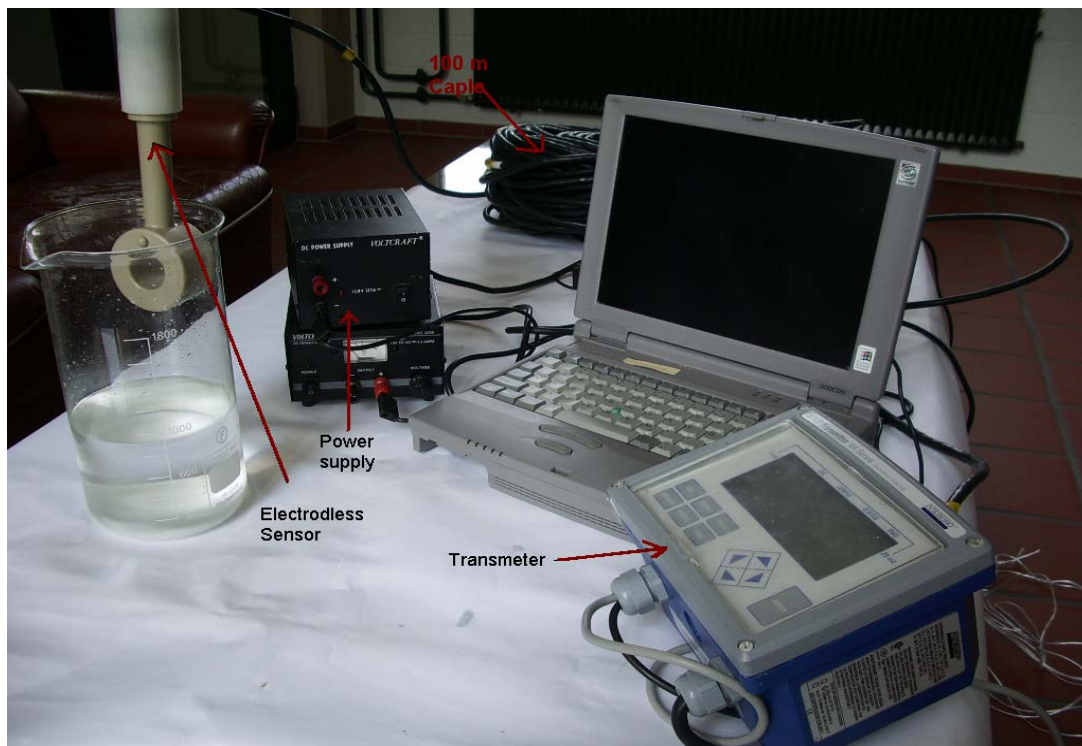
Figure (3-1): Inductive electrical conductivity sensor and its connections

The samples, which were collected from the different depths and different station into 250 ml plastic containers (section 4.1), were diluted by distilled water as a 1:1 ratio because of salt precipitation at the bottom of the containers were observed after some days. Then the TDS were calculated for these samples using a traditional technique (gravimetric technique).

Gravimetric TDS is defined as the weight of the residue in a known volume of water sample after evaporating all the water from the samples. A 100 ml of well-mixed samples were transferred into pre-weighed 200 ml beakers and evaporated to dryness in an oven at a specific temperature until a constant weight is obtained or until change less than 4% of previous weight. Then the residual salts were weighed for each sample and the weight result multiply by 2 to get the value of the TDS for each sample.

TDS (g/l) = {((A – B) *1000)/ sample volume (ml)} * 2

A = weight of dried residue + beaker

B = weight of empty beaker

The values, which obtained by using gravimetric technique, were compared with the results of the TDS, which were calculating by using equations, related to the electrical conductivity.

The samples were collected from Mujeb area (section 4), were analyzed to determine the anions and cations concentrations in the Dead Sea water. A standard salts contain $MgCl_2.6H_2O$, $CaCl_2.2H_2O$, NaCl, KBr, with a similar ration of the Dead Sea water were mixed with distilled water to get 6 litter salt solution with TDS of 380 g/l. Two litters of this solution were transferred into a five litters glass container. This solution were used both to calibrate the inductive electrical conductivity sensor, which used in the field and to create a relationship curve between the electrical conductivity and total dissolved solids especially for the Dead Sea and for highly saline solutions. The solution was diluted gradually with adding 25 ml of distilled water to the solution and stirred it for about 15 minutes. The final solution was stirred for about 15 minutes until got a homogeneous solution. Then the electrical conductivity and temperature were measured by using the inductivity conductivity sensor, which used in the filed and the total dissolved solids was calculated.

TDS_f (g/l) = TDS_i * F

Where TDS_f is the final total dissolved solids after adding 25 ml of distilled water; TDS_i is the initial total dissolved solids (380 g/l); and F is the factor {equal volume after adding distilled water / initial volume (2000 ml)}.

These procedures were repeated for one hundred and thirty times. Then an electrical conductivity versus total solid dissolved curve was created. This curve was used for the electrical conductivity results interpretations- and for calculating the TDS for the Dead Sea water.

Three liters of the previous standard salts solution (380 g/l) were transferred into three 2000 ml beakers. Every one letter of the standard solution was transferred to a 2000 ml beaker. These beakers, which include the standard solution, were used for testing the behaviour of the electrical conductivity of these solutions when some more salt adding.

The first beaker was tested for adding different amounts of $MgCl_2$, the second beaker was tested for adding different amounts of $CaCl_2.2H_2O$ and the third beaker was tested for adding different amounts of NaCl. All the beakers and the solutions after every adding were heated to 40°C and stirred until all the salt was completely dissolved, then they were put in a water bath thermostat until reach a temperature of 25°C then the electrical conductivity was measured at each salt adding. The amounts of $MgCl_2$ salts adding were 10, 15, 20 and 25 grams. The amounts of $CaCl_2$ salts adding were 10, 20, 30, 40, 50 and 60 grams. The amounts of NaCl salts added to the third beaker were 5, 10, 15 and 20 grams. The density for the final three solutions of three salts and the density of the initial solution were measured using pincometer technique by taking a known volume from the solutions and weighed them. Then a relationship between the densities and the total dissolved solids of each salt were plotted.

3.2. Chemical Tracer (Radon-222) Method

Standard sampling and analysis techniques may apply measurement of radon concentrations in the water column. A special care must be taken for measurement radon-222 (Broecker et al. 1968, Mathieu et al. 1988).

Radon-222 is a useful geochemical tracer for analyzing groundwater discharge due to facts that are radon-222 is greatly enriched in groundwater relatively to seawater by three or four order. It can be measured at very low concentration (Cable, 1996, Lambert and Burnett, 2003,).

The hydrographic characteristics were obtained from the previous section (3.1) conductivity, temperature, and depth readings at each water collection station. Water samples for [222]Rn analysis were collected in 50 ml evacuated gas bubbler (Fig. 3-2) using a small submersible pump and a rubber hose that drew water from depth directly into the bubblers.

Radon-222 gas was extracted and counted using RAD-7 device manufactured by (Durridge Co. Inc) (Fig. 3-2b).

The sample was spurge by air pumped in by the RAD7 internal pump. The out-flowing gas was dried with a drier before entering the RAD7 device in order to keep the humidity into the device always less than 10 %, which is required to obtain an optimum radon-222 concentration result, then the radon start for counting.
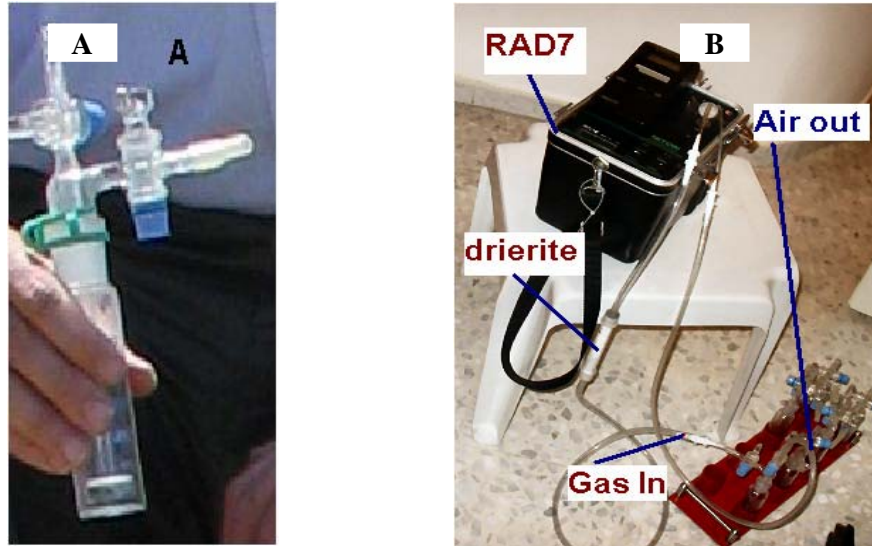
Figure (3-2): (A) Photo of the gas bubbler   (B): Photo of the RAD7 device

The starting counting time was written down for each sample. This time was used latter for the decay-corrected back to the time of sampling.

Each sample was purging for about 40 minutes to account all the radon gas in the samples.

Then the reading of radon-222, obtained from the Device and the volume of water in the radon bubbler were written down.

The radon-222 concentrations values were decay-corrected back to the time of sampling in order to assess the in situ radon concentrations. They were calculated for all the samples by using the following formula:

F= 1/exp (-2.097 *10^{-6} * Δt).

Where F is the radon decay corrected-back factor, Δt is the difference of time between the analysis time and sampling time (in second).

The factor of volume was calculated for each sample by using the formula

55

V_F = 900/ V_I. Where V_F is the volume correction factor, V_I (in ml) is the initial volume of the sample in the gas bubbler (between 30 and 35 ml), and 900 ml is the constant number storage in the RAD7 device.

The actual radon concentration for each sample was calculated by using the following equation:

^{222}Rn= (Rn $_{(RAD7)}$* F * V_F)/1000. Where Rn $_{(RAD7)}$ is the radon reading got direct from RAD7 device.

As well many sample were taken from the springs and seepage at the surrounding the Dead Sea area. The ^{222}Rn concentrations were measured and calculated for each sample using the same procedures and equations that mentioned above.

The diffusion of radon from bottom sea sediments was measured by using technique that described by (Corbett et al., 1998). About 80 g of sediment and about 200 ml of water was but in the flasks and sealed very well for about 30 days. After the thirty days equilibration period the radon-222 was measured for each sample.

The temperature at the sea surface was measured by using the FOXPORO device, which was used for the electrical conductivity measurements. The radon concentration at the atmosphere was estimated.

The porosity was calculated and the Bulk density was measured for some samples. The results were used for estimating the radon diffusion from the sediments.

The radon-222 inventory, atmospheric evasion, and diffusive flux from the sediments, radon-222 productions were calculated by using different equations (details in section 5.2).

After measurments were completed the approach of (Burnett and Dulaiova, 2003 and Lambert and Burnett, 2003) was followed as the following concepts:

- Calculate the ^{222}Rn inventory for the water column by integrating the ^{222}Rn concentration with depth in the water column.

- Using a radon budget approach for estimating and accounting of any ^{222}Rn inputs and outputs to the investigate area by other processes "such as loss to atmosphere, inputs from sediments, Ingrowths from ^{226}Ra dissolved in water column)" (Fig. 3-3).

- Calculate the total input flux of ^{222}Rn to balance the measured inventories.

- Measure the ^{222}Rn concentration in the groundwater around the investigate area.

- Estimate advection rate by dividing the radon flux by the radon activity in the groundwater.
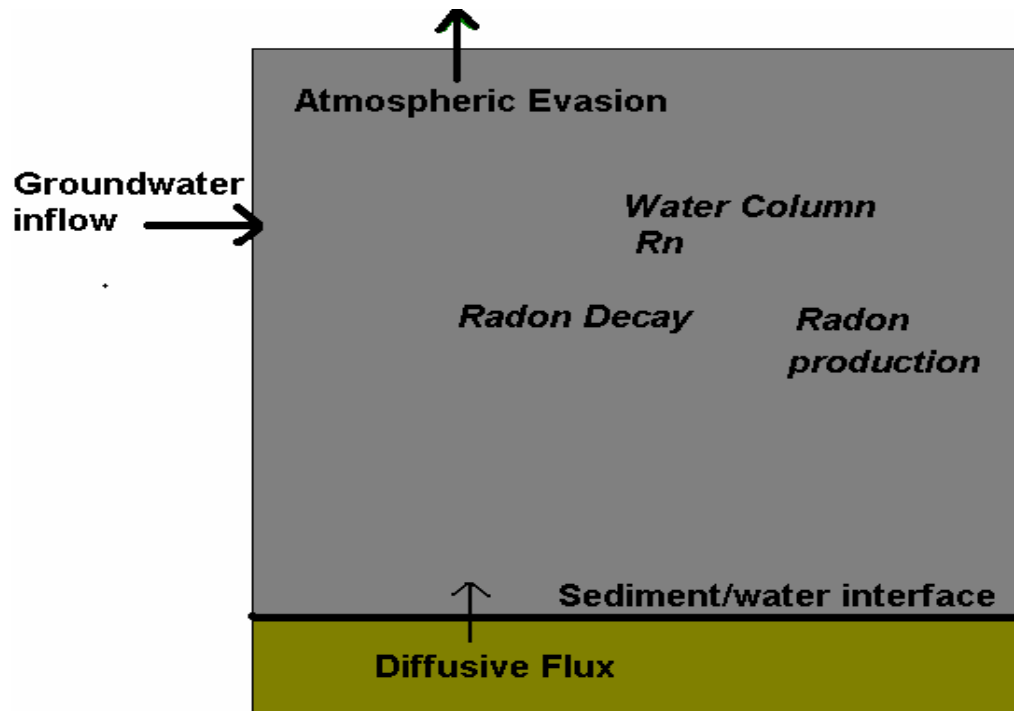
Figure (3-3): One-dimensional model of sources and losses of ^{222}Rn in a well-mixed coastal environment.

3.3. Thermal Infrared Imagery (TIR) Method

The base of the thermal fingerprint is based on a pronounced thermal gradient between the groundwater and ambient surface conditions. The thermal infrared Imagery is an effective method to quickly assess large-scale areas and acquire information about specific locations of groundwater discharge.

This study exploited an idea of using temperature differences between groundwater and surface water in the Dead Sea to delineate zones of comprehensive groundwater-sea surface water exchanges. The groundwater temperature is relatively stable and it is as an average temperature of the area, while the temperatures of the surface water are changeable with changing the seasons. Thermal infrared only measures surface temperatures so its application is limited to the intertidal zones and above (Ballestero et al., 2004).

The thermal infrared imagery was carried out as the following procedures:

- The flight paths were drawn down on a geo-referenced Land7 satellite image to determine the coordinates for each flight line at the office.

- The optimal flight elevation from the standard sea level was determined in order to obtain the require resolution, the overlapping percentage and the ground coverage of the images.

- An initial site characterization was performed and the study area was reviewed for existing land use and irrigation areas.

- The thermal camera was prepared and calibrated for the sky temperature, the humidity and the sharpness.

- Finally the thermal camera was fixed at the bottom of the plane and the GBSs stations were also fixed.

After carrying out the Imagery many steps for interpretation and processing were carried out.

(a) Identification and cataloguing of discharge zones by thermal Imagery,

(b) Geological field investigations based on the identification of potential groundwater discharge zones, e.g. fractured zones, lineaments,

(c) Each images strip was calibrated relatate to flight elevation, water temperature, atmospheric temperature at flight height and relative humidity by using the camera software as shown in (Fig. 3-5).

Strip one images no.1 – 53

Strip two images no.55-101

Strip three images no. 102-153
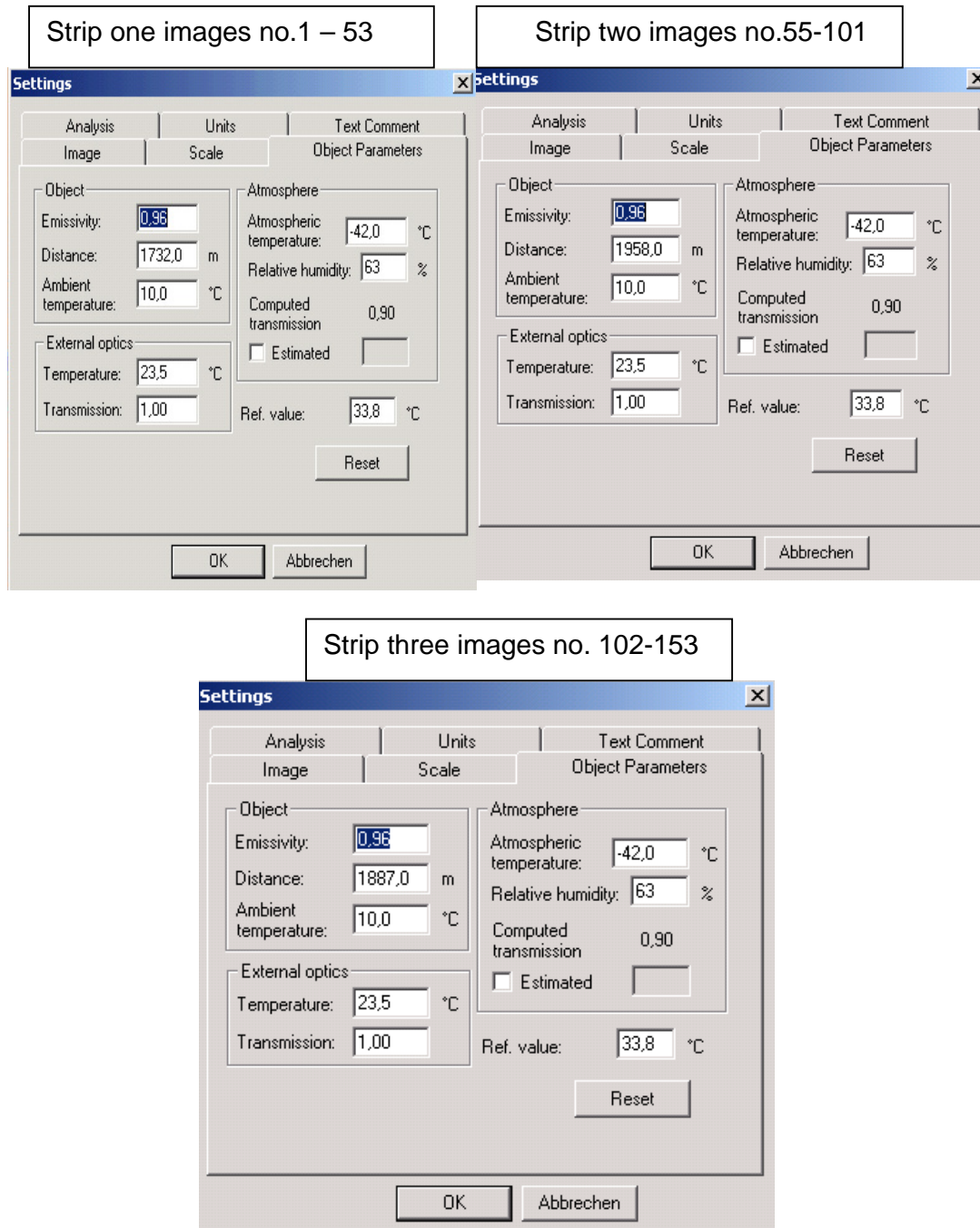
Figure (3-4): Settings in ThermaCamResearcher for flight lines

3.4. Electromagnetic Radiation (EMR) Method

This method is depending on the measurement of natural pulsed low frequency electromagnetic radiation (EMR) signals. Generally in geoscience the detection and analysing of these signals can assist to conceive and understand deformation

processes. The electromagnetic radiation starts during crystal deformation superior to and at the same time of the nucleation phase of nanocracks. Where the more fractures are formed the more electromagnetic Pulses are emitted. The emission and radiaton direction is normal to the fracture surfaces because of the polarization (Obermeyer, Personal commencation). The instrument, which will use for performing these measurements named Cerescope (Fig.3-5). The Cerescope is a scientific instrument for detection and registration of transient pulses of electromagnetic radiation (EMR), which produced by nanofractrures, and by piezoelectric, turboelectric or pyroelectric effects (Bahat et al. 2005).

This method was used to identify the underground active faults and fractured zone along the Dead Sea. These faults and joints consider as a zones of weekness for the groundwater discharge along the shoreline. As well the sinkholes could be identifying by using this method.

Figure (3-5): Electromagnetic radiation sensor (Cerescope)

3.5. Geological Model of the Dead Sea Area

The geology of the Dead Sea is quite complicated. It includes both unconsolidated superficial geological formations and bedrock outcrops. The area is highly faulted and folded with axes extending NE-SW. The bedrock is typically highly fractured at the surface extending in the subsurface for many meters.

Different geologic cross sections were constructed parallel to the Dead Sea shores direction N-S and others E-W and NE–SW. Figure (3-6) shows the locations of these cross sections exposed on the geological map. That is expected to assist in understanding the hydrological and hydrogeological aspects of the area adjacent to the Dead Sea.

Symbols and coordinates of the geological cross sections are given in table (3-1).

Table (3-1): Symbols and coordinates of the geological cross sections.

Section symbol	East	North	Section symol	East	North	Section symbol	East	North
A-A′ A A′	35° 34′30″ 35° 45′00″	31° 37′30″ 31° 38′30″	D-D′ D D′	35° 34′58″ 35° 45′00″	31° 28′40″ 31° 29′57″	G-F′ G F′	35° 33′30″ 35° 45′00″	31° 33′30″ 31° 42′42″
B-B′-B″-B‴ B B′ B″ B‴	35° 31′30″ 35° 32′56″ 35° 34′30″ 35° 44′48″	31° 17′10″ 31° 16′00″ 31° 15′22″ 31° 15′30″	F-F′ F F′	35° 35′00″ 35° 45′00″	31° 42′30″ 31° 42′42″	M-D′ M D′	35° 33′00″ 35° 45′00″	31° 20′28″ 31° 29′57″
C-C′ C C′	35° 33′00″ 35° 36′30″	31° 15′00″ 31° 30′00″	G-G′ G G′	35° 33′30″ 35° 45′00″	31° 33′30″ 31° 33′31″	C′-C″ C′ C″	35° 36′30″ 35° 38′00″	31° 30′00″ 31° 46′00″

Geologic cross sections cover a large extends of the Dead Sea area, which is divided in three parts. The first one extends from the northern end of the Dead Sea in Sweimah area to Zarka Ma'in fault line. The second part extends between Zarka Ma'in fault line and Siwaqa fault and the third one extends from the Siwaqa fault to end southern of the Dead Sea.
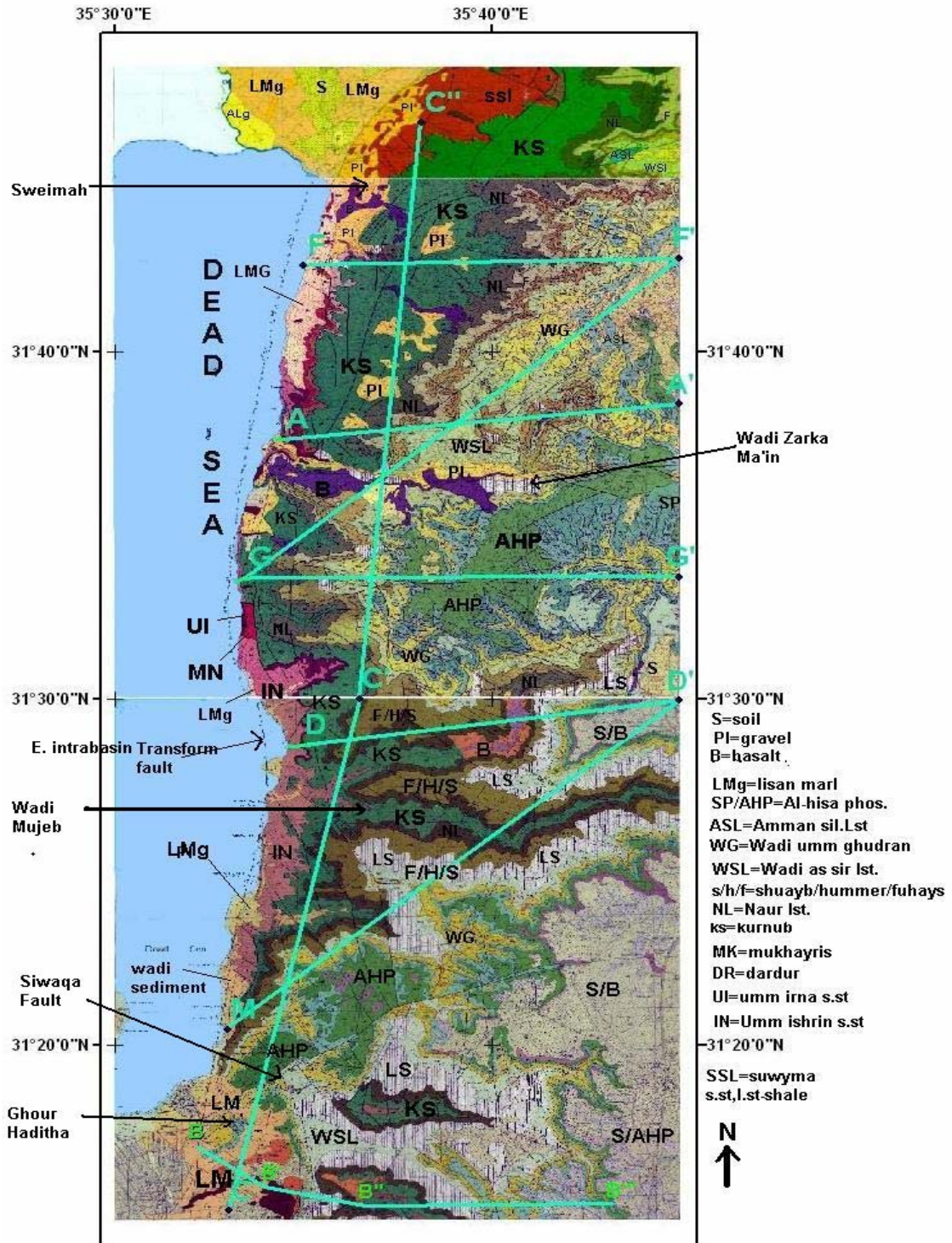
Figure (3-6): Locations of geologic cross-sections exposed on the geological map.
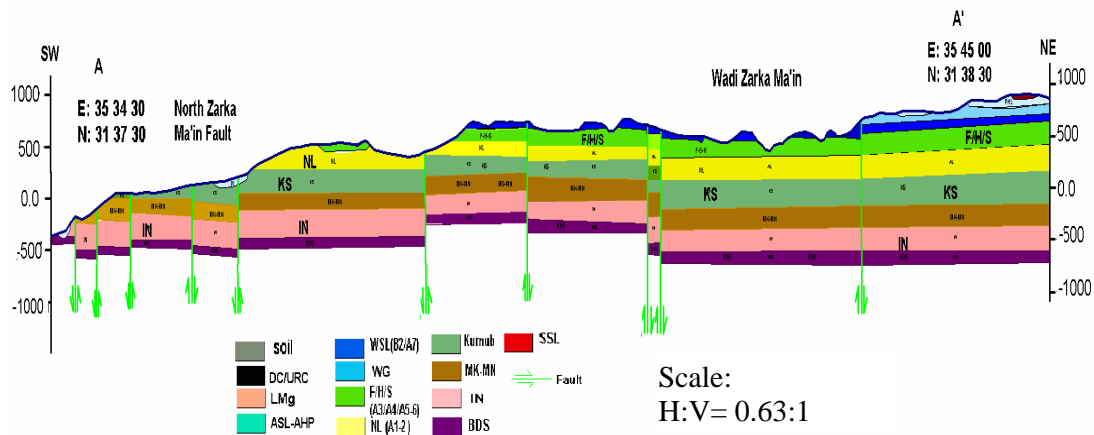
Figure (3-7): Geological cross section A-A′ in north of Zarka Ma'in fault

The geological cross section A-A′ is located at the north of Zarks Ma'in fault. The direction of this section is SW-NE (Fig. 3-7). The section shows that the layers slope gently toward Wadi Zarka Ma'in. Kurnub sandstone aquifer (KS) cropps out at the SW part of the section north of Zarka Ma'in fault. The upper aquifer (B_2/A_7) is cropping out along the section and missing farther to the SW direction. The expected groundwater flow direction is from NE toward Wadi Zarka Ma'in and it continues to the SW toward the Dead Sea.
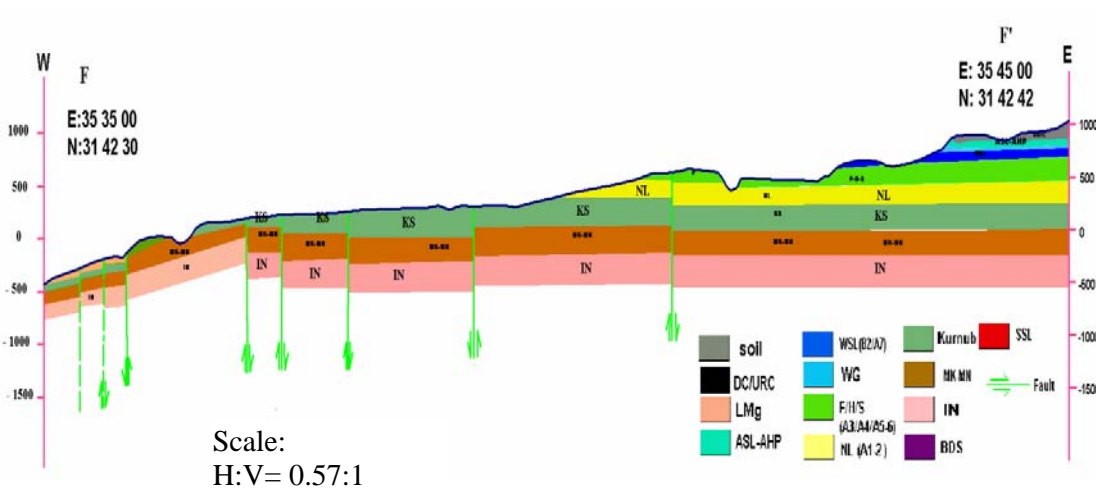
Figure (3-8): Geological cross section F-F` in Sweimah area

The geology of Sweimah area is described by using the geological cross section F-F` which is located at this area with direction W-E (Fig. 3-8). The cross section shows that the geological strata of Sweimah area dipps gently from east to west, but they are dipping with high increased slope at the west end of the cross section toward the Dead Sea. The cross section shows that the lower aquifer (KS) is cropping out in the west of the cross section. The groundwater might be flowing from the east to the west toward the Dead Sea relating to the dip direction of the layers.

The geology of the area, which is located between Wadi Mujeb and Zarka Ma'in, is represented by the geological cross sections D-D` and G-G` (Fig. 3-9), and (Fig. 3-10) respectively. The direction of the geological cross section D-D` is SW-NE. It represents the geology of the area located to the north of Wadi Mujeb. The cross section shows that the eastern part of the section is highland with horizontal geological layers covered with a layer of soil. Then the layers are sharply removed by erosion toward the Wadi Hidan to the west of the section. The upper aquifers (B_2/A_7) are missing and the lower aquifer (KS) is cropping out at Wadi Hidan and Wadi An Nimer. The lower aquifer Umm Ishrin (IN) is cropping out southwest of Wadi An Nimer adjacent to the Dead Sea. The groundwater direction is from NE to SW to Wadi Hidan and Wadi An Nimer then toward the Dead Sea.
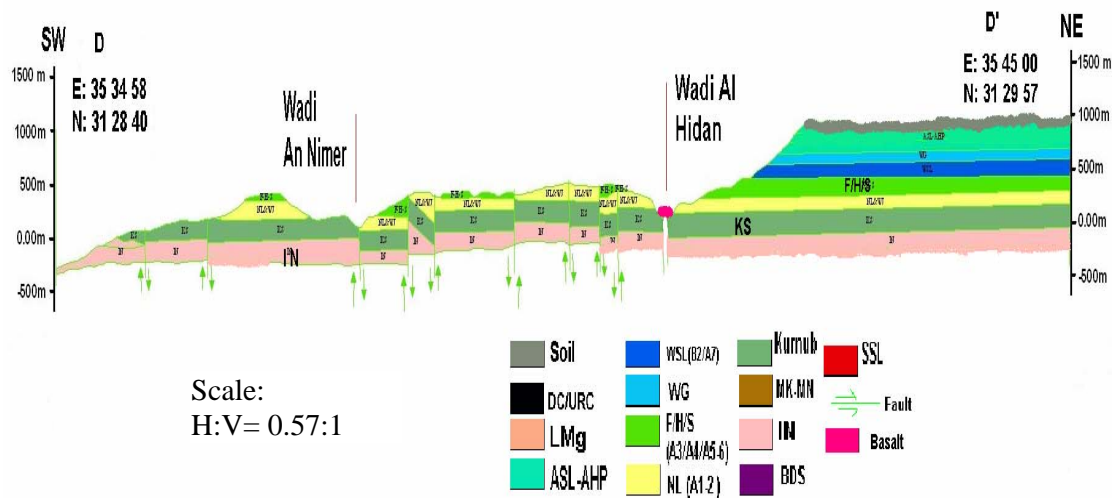
Figure (3-9): Geological cross section D-D` located north of Mujeb

The direction of the cross section G-G` is W-E and it shows that strata dip toward Wadi Arya and Wadi Hidan to the west of the section. They are uplifted again to the west of these Wadies and so the upper aquifer is cropping out and then missing farther to the west. Thereafter the upper layers are eroded and the lower aquifer is cropping out adjacent to the Dead Sea. The expected groundwater flow direction is from the eastern highland toward Wadi Arya and Wadi Hidan then continues toward the Dead Sea at the west of the section.
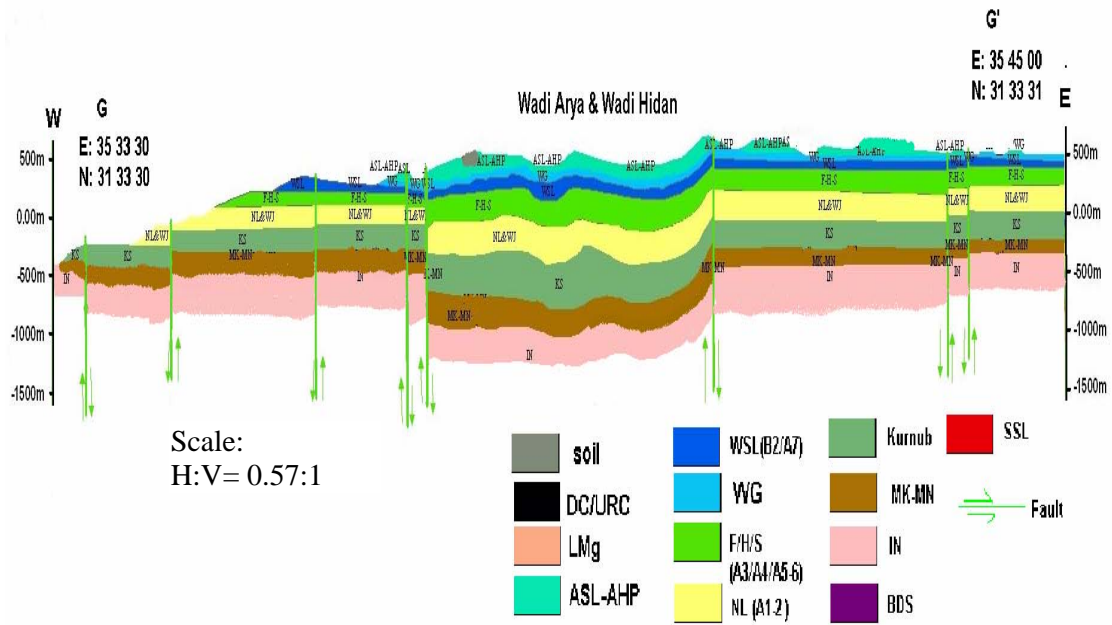
Figure (3-10): Geological cross section G-G` located in north Wadi Mujeb
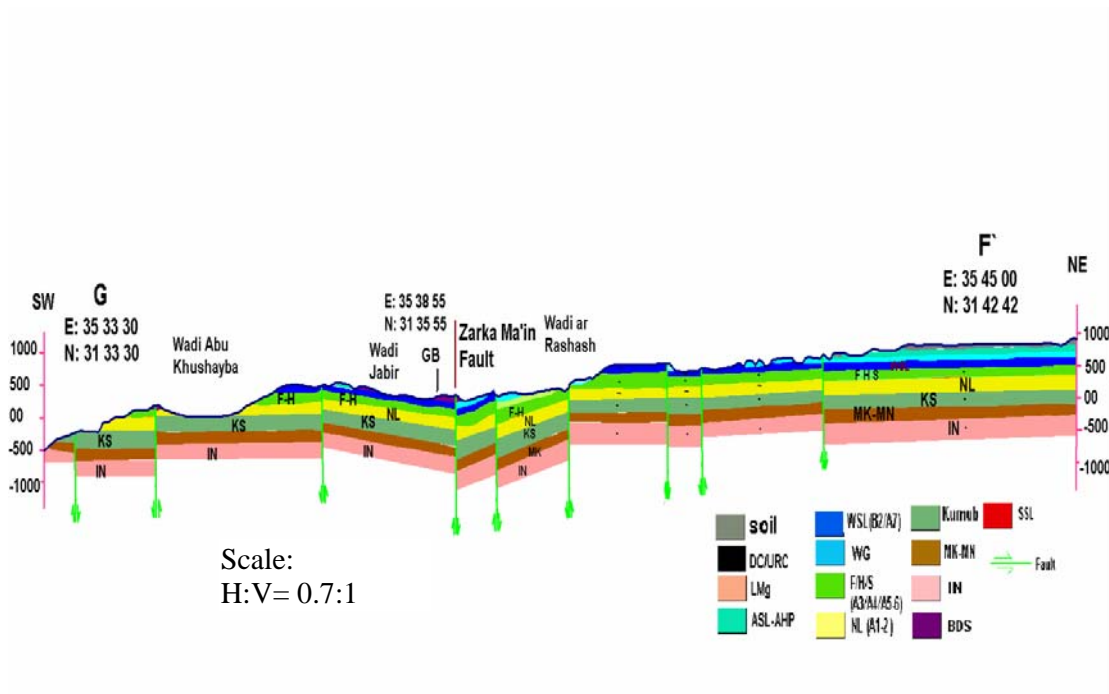
Figure (3-11): Geological cross section G-F` crossed Wadi Zarka Ma'in

To understand the effect of Wadi Zarka Ma'in Fault on the geology in the area surrounding this fault the geology cross section G-F` (Fig. 3-11) was contructed in the SW-NE direction crossing this fault. The cross section shows that the layers are dipping toward Wadi Zarka Ma'in from both NE and SW directions. The groundwater might be flowing from NE and SW toward the Wadi Ar Rashash and Wadi Jaber which are located to both sides of Wadi Zarka Ma'in fault. From there it might be flowing to Wadi Zarka Ma'in then it continues to the west toward the Dead Sea. Also, a surface and groundwater might be flowing to Wadi Abu Khushiba at the southwest of the cross section and then might be discharging into the Dead Sea to the west.
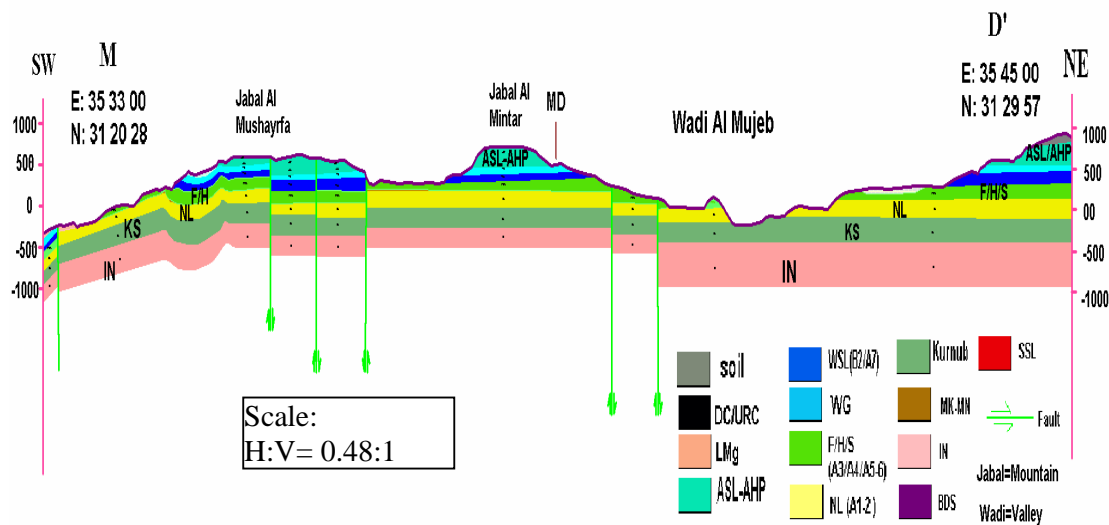
Figure (3-12): Geological cross section M-D` crossed Wadi Mujeb

The geological cross section M-D` (Fig. 3-12) was drawn to understand the geology of Wadi Mujeb. This cross section is SW-NE direction crossing Wadi Mujeb. The cross section shows that the geological strata are eroded and the topography dipps toward Wadi Mujeb from both NE and SW directions. At the uplifted western side of the cross section the layers are dipping to SW direction. The lower aquifer (KS) crops out in Wadi Mujeb. The surface and groundwater might be flowing toward Wadi Mujeb. At the uplifted side of the cross section the groundwater might flowing in SW direction toward the Dead Sea.
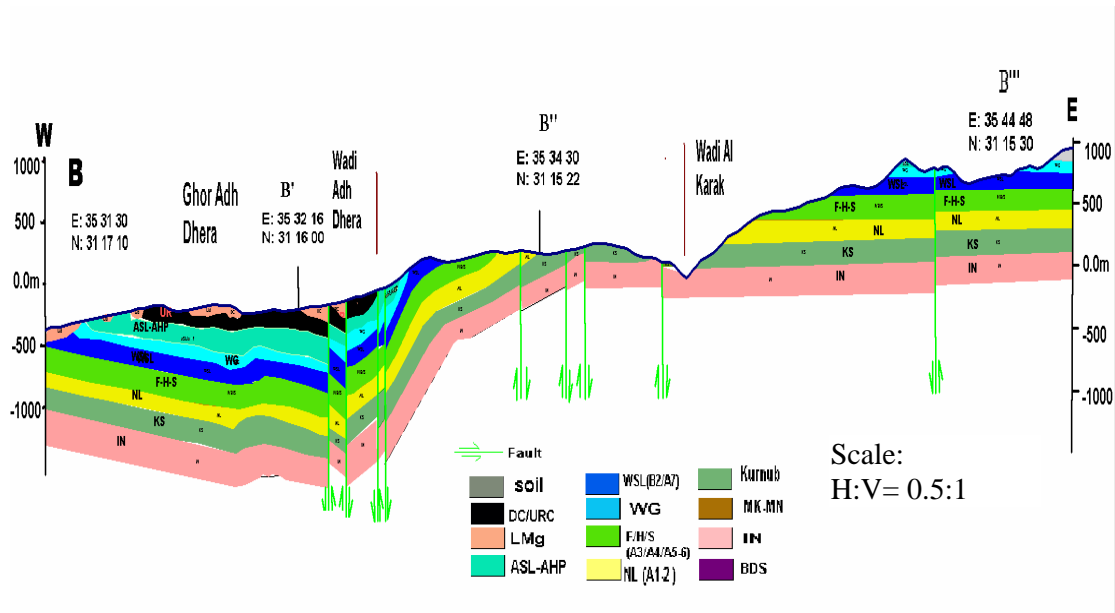
Figure (3-13): Geological cross section B-B′-B″-B‴ in Ghor Haditha.

The cross section B-B′-B″-B‴ is located in the southern of the study area at Gohr Haditha (Fig. 3-13) close to the southern basin of the Dead Sea. The direction of this section is W-E. The section shows that the layers in the eastern part are quite horizontal and the topography is high. The topography slopes toward the west direction and the layers dip sharply to the west and then become horizontal with very small dip angle. The deep aquifers Umm Ishrin sandstone (IN) and Kurnub sandstone (KS) are outcropping in Wadi Al Karak. As well the upper aquifer crops out at east of Wadi Al karak and at Wadi Adh Dhera. The surface water and groundwater are expected to flow toward the Wadi Al Karak from the eastern mountains. The groundwater might be flowing from the east toward Wadi Adh Dhera.
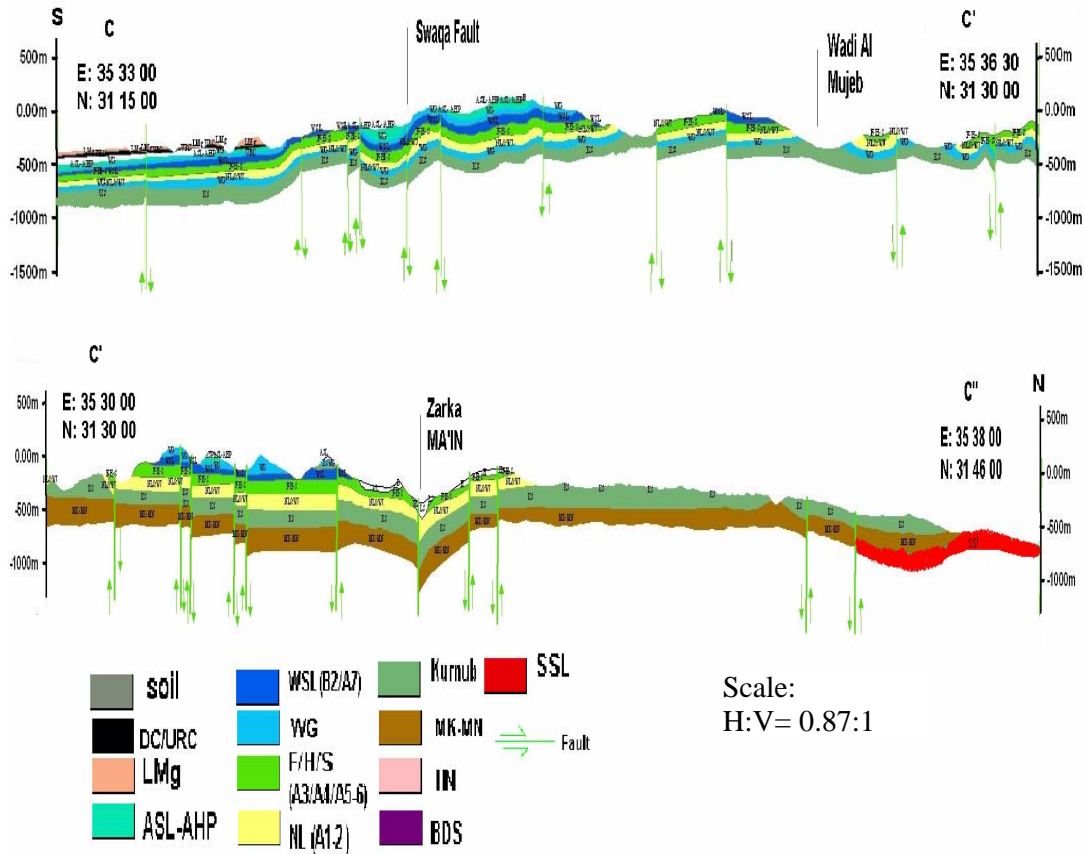
Figure (3-14): Geological cross section C-C`-C`` parallel to the Dead Sea

One cross section (C-C`-C``) was constructed parallel to the Dead Sea in a S - N direction. It extends from Ghor Hadetha, southern part of the Dead Sea, to Sweimah, northern part of the Dead Sea (Fig. 3-14). The figure shows that the Siwaqa fault intersects the section. South of Siwaqa fault, the layers dip to the south while in the north of Siwaqa fault the layers dip to the north (apparent dip). The lower aquifer (Kurnub sandstones) crops out at the northern part while they are overlying with the younger strata at the southern part. Considering the 3-D situation the groundwater is expected flows west with a southerly component of Siwaqa. As well considering the northerly components of Siwaqa the groundwater might be flowing to the north to Wadi Mujeb then it continues to the west toward the Dead Sea. The groundwater at the area located between Wadi Mujeb and Wadi Zarka Ma'in might be flowing toward Wadi Mujeb and Wadi Zarka Ma'in then it continues toward the Dead Sea at the west. Also, considering the northerly components north of Wadi Zarka Ma'in the groundwater might be flowing to the

north direction parallel to the Dead Sea then it continues to the west toward the Dead Sea.

3.6. Integration of Techniques

The integration of techniques is one key to element a successful study. While each technique by itself can offer a partial view of the discharge, a suitable and correct integration between the methods provides proper focus about the research. In this section of the research the integration among the different methods, geological model and structural features, electrical conductivity (EC) and temperature (T) with the depth, chemical tracer (radon-222), thermal infrared imagery, electromagnetic radiation and water budget were applied to get a better view and results to locate and to estimate the submarine groundwater discharge into the eastern shores of the Dead Sea.

The geological and the topographical maps of scale 1:50,000 covering the study area were used to produce a geological model, and to determine the geological characteristics of the area. Using the results obtained from the geological model, the study area can be subdivided into three sub areas (stations) related to their different geological setup. Using the results obtained from the geological and topographic maps localized the expected locations of the groundwater discharge. These findings are combined with the finding of the electromagnetic radiation, which supported the findings resulting obtained from the geological interpretation and the geological model.

The data obtained from the methods, mentioned above, were used to determine the most suitable sites for electrical conductivity, temperature with the depth surveying measurements, which depend on the contrast between the saline Dead Sea water and the fresh groundwater which feed the Dead Sea along its shores. Accordingly four stations were chosen for measurements, depending on the geological findings and field survey. These measurements gave us an idea about the depths underneath the surface of the Dead Sea where the fresh groundwater discharrge into the Dead Sea as submarine springs or seepages.

The findings obtained from EC and T with the depth measurements were used to determine the most suitable depths and distance to collect samples for Radon-222 measurements. The compenation between the electrical conductivity-Temperature technique and the chemical tracer technique gave us an idea about the layring of the Dead Sea water.

Thermal infrared imagery results were used to determine the length of the shore where the water discharges occur and its extending from the shoreline. These results were used to calculate the quantity of discharges using radon-222 method.

4.   FIELDWORK

4.1.   Electrical Conductivity-Temperature with Depth

Different vertical profiles of the EC and T with depth measurements were taken at discrete stations by using small engine boat between July and August 2005 (summer months) after several drought winter seasons. The measurements were carried out at daytime between 11 a.m. and 16 p.m. That time was chosen because of the sea was calm or very low tide.

The first station (S_1) was located at the northern part of the Dead Sea in Sweimah (Hotel area) at the coordinate 1129 N and 205.5 E PG (Palestine grid coordinate system).

Five vertical water column profiles were carried out at these stations. The first profile (S_{1-1}) was carried out at 200 meter away from the shoreline of the Dead Sea. The EC and T with depth measurements were carried out for a depth from 1 m to total 55 m. Then the boat was moved farther to the west for about 300 m from the shoreline where, the second (S_{1-2}) vertical profile was located. The measurements were carried out from the depth 1 m to 45 m below Dead Sea surface then the measurements stopped due to the deviation in the sensor underneath this depth. The third (S_{1-3}) vertical profile at this station was located at a distance of 400 m from the shoreline to the west. The EC, T and depth measurements in this profile were carried out from 1 m to 94 m depth. The fourth (S_{1-4}) profile at this station was at distance of about 500 m from the shoreline. The measurements were carried out from a depth 1 m to 88 m below Dead Sea surface. The measurements at the fifth (S_{1-5}) vertical profile at the first station were carried out from 1 m to 93 m below Dead Sea level at the distance of 800 m away from the shoreline to the west.

The second station (S_2) was located in Zarka Ma'in area at the middle part of the Dead Sea to the south of the first station. It was located at a coordinate of 1114 N PG and 203 E PG.

The EC, T and depths were measured at this area at a different four vertical column profiles. These profiles also were located at a different distance away from the shoreline and at different depth from the Dead Sea water surface. The distance of the first vertical profile (S_{2-1}) was located at about 100 m away from the shoreline to the west direction. The measurements at this profile were carried from 1 m to 80 m depth. The measurements at the second profile (S_{2-2}), which was located about 200 m away from shoreline, were carried out from a depth 1 m to 91 m beneath the Dead Sea water surface. The third vertical profile (S_{2-3}) at the Zarka Ma'in area was located at about 400 m away from the shoreline to the west direction. The EC, T and depths measurements for this profile were carried out from a 1 m to 96 m

depth. The farthest EC, T and depth profile at this station is profile 4 which donated as (S_{2-4}). It located at about 800 m away from the shoreline to the west direction. The measurements were carried from a depth 1 m to 94 m beneath the Dead Sea surface.

The third station (S_3) was located in Zara area at the coordinate of 1111.8 N PG and 202.8 E PG. This area includes many hot springs discharging to the Dead Sea. The temperatures of these springs range from about 40°C to about 60°C at the source.

Four different EC, T and depths vertical profiles were carried out at this area relating to the distance from the shoreline. The first profile (S_{3-1}) was carried out at 100 m distance from the shoreline to the west direction. The depth of this profile was from 1 m to 84 m beneath the Dead Sea water surface. The second profile (S_{3-2}) was carried out about 300 m distance away from the shoreline to the west. The depth of this profile was from 1 m to 89 m. The EC, T and depths for the third profile (S_{3-3}) were carried out from a depth 1 m to 96 m. This profile located at about 400 m away from the shoreline to west direction. The last profile at this area (S_{3-4}) was located of about 800 m distance away from the shoreline and the measurements were carried out from a 1 m depth to 94 m beneath the Dead Sea water surface.

The last station (S_4) at the investigated area was located in Mujeb area at the south part of the Dead Sea. This station was located at the coordinate of 1097.178 N PG and 203 E PG. The EC, T and depths vertical profile were carried out at this station for one vertical profile (S_{4-1}). This profile located at about 400 m distance away from the shoreline to the west direction. The depth of this profile was from 1 m to 87 m beneath the surface of the Dead Sea water. The location of the main stations are shown in (Fig. 4-14)

Representative samples from the Dead Sea water in Mujeb station were collected from different depths for chemical analysis. The samples were transferred to the laboratory for chemical analysis.

As well a small pump was used for sampling the Dead Sea water from different depths and deffernet stations. The samples were pumped directly from the specific depth into 250 ml plastic bottles at the same time they contemporaneous of carrying out the measurements. All the samples (n=15 samples) were transported to the laboratory for determining the total dissolved solids (TDS) of the Dead Sea water using a traditional technique (Gravimetric Technique).

4.2. Chemical Tracer (Radon-222)

Radon-222 measurements were carried out on the same day of carrying out the EC, T and depth measurements between July and August 2005 using the same small engine boat and the small submersible water pump. Samples with a volume between 30 and 35 ml were collected from different depths and different distances away from the shoreline as well as from different stations along the Eastern shoreline of the Dead Sea. Stations were located almost at the same locations of the electrical EC, T and depth stations with differences in the distances from the shoreline. These stations were spread from the north to the south along the Eastern shoreline of the Dead Sea.

Four main stations were chosen for ^{222}Rn sampling. The first station (S_{rn1}) was located in Sweimah area (Hotels area) of about 20 m distance away from the coastline. Five samples were collected from this station at five different depths. The first sample was from a depth 2 m underneath the Dead Sea water surface. Then the pump was taken down to a 4 m depth for sampling a next sample, and then it was taken down to a depth 7 m for sampling the third sample. The fourth sample was collected from a depth of 12 m, and the last sample was collected from a depth of 20 m underneath DS surface by taking down the pump to that depth. These samples were used for calculating the ^{222}Rn inventory, radon-222 diffusion to the air, radon-222 in sediments and radon production from radium-226. As well some samples were collected to the west of this station at a distance of about 60 m away from the shoreline at depths of 12 m and 20 m. Three samples at 12 m depth were collected at a distances of about 200 m 300 m and 700 m away from the shoreline to the west of the main station (S_{rn1}). Three samples were collected at 2 m depth at the north of the main station with 5 km and with distances 50 m, 200 m and 700 m away from the shoreline. One sample was collected at about 5.5 km to the north of the main station and distance about 200 m away from the shoreline.

The second main station (S_{rn2}) for the radon-222 sampling was located in Zarka Ma'in area. The distance of this station was between 20-30 m away from the shoreline to the west direction. The samples from this station were collected also from different depths using the same procedures, which were used in the first station and as the same way of sampling. The first sample was collected from 2 m depth. The second sample was collected from a depth 4 m. The third, fourth and fifth samples were collected from depths 7, 12, and 24 m respectively using the same procedures and sampling techniques. These samples also were used for calculating the radon-222 inventory, diffusion from the sediment, and the radon-222 evasion to the atmosphere surrounding the station. In order to testing the radon-222 distribution at this station many other samples were collected from different distances away from the main station. Two samples were collected from 4 m depth at distances 10 m and 40 m away from the shoreline to the west direction at the same location of the main station. Two samples were collected at 4 m depth at distances 10 m and 40 m away from the shoreline to the west direction at 300 m

north of the main station. One sample was collected from a depth 4 m at distance about 10 m away from the shoreline at 800 m north of the main station.

As well radon-222 samples were collected from the third main station (S_{rn3}). This station was located in Zara (Hot springs) area. As in the other stations the radon-222 samples were collected from different depth and different distances away from the shoreline to the west and different distances toward north or south from the main station. The samples from this main station were used later for calculating the radon-222 inventory, diffusion from the sediments and atmospheric evasion. The depths of the samples at this main station were 2 m, 4 m, 7 m, 12 m, and 24 m underneath of the Dead Sea water surface and the distance of these samples nearly were 20 to 25 m. One sample was collected at depth of 12 m and distance 50 m away from the shoreline to the west of the main station. Two samples were collected at a depth 12 m of about 20 m and 30 m distances away from the shoreline and about 150 m to the north of the main station. Two samples were collected from a depth 12 m at the distances 20 m and 50 m away from the shoreline at a distance of about 500 m north of the main station. Six samples were collected at about 500 m distance to the south of the main station, two samples were collected at 12 m depth and a distances 20 m and 40 m away from the shoreline, and four samples were collected from 4 m depth at distances 20 m, 30 m, 40 m and 50 m away from the shoreline. As well three samples were collected from about 1000 m (1 Km) south of the main station at the depth of about 12 m and distances of about 20 m, 50 m and 200 m away from the shoreline to the west of the main station. One sample was collected at distance 3000 m (3 Km) to the south of the main station at a depth of 12 m and a distance of about 20 m away from the shoreline to the west.

The last main station for radon-222 sampling located in Mujeb area. This station was named (S_{rn4}). The radon-222 samples from this station were collected from the main station only because of the time of borrowing the boat was finished and could not extended. The samples were collected from this station at different depths. The first sample was collected from a depth 2 m, the second one was collected form a depth 4 m. The third, fourth and fifth samples were collected from depths of 7 m, 12 m, and 24 m respectively.

The number, the time of sampling, the depth, the station name, the distance from the shoreline and the distance from the main station and directions were written down in situ for each sample. The samples were transferred to the laboratory in order to analyze for radon-222 concentrations for each sample.

4.3. Thermal Infrared Imagery (TIR)

A thermal infrared survey was flown parallel over the study area at the eastern shoreline of the Dead Sea to circumscribe the groundwater discharge zones,. Four

flight lines (strips) were taken between Zarka Main area and south Mujeb for an area approximately 75 km^2 (Fig. 4-1).
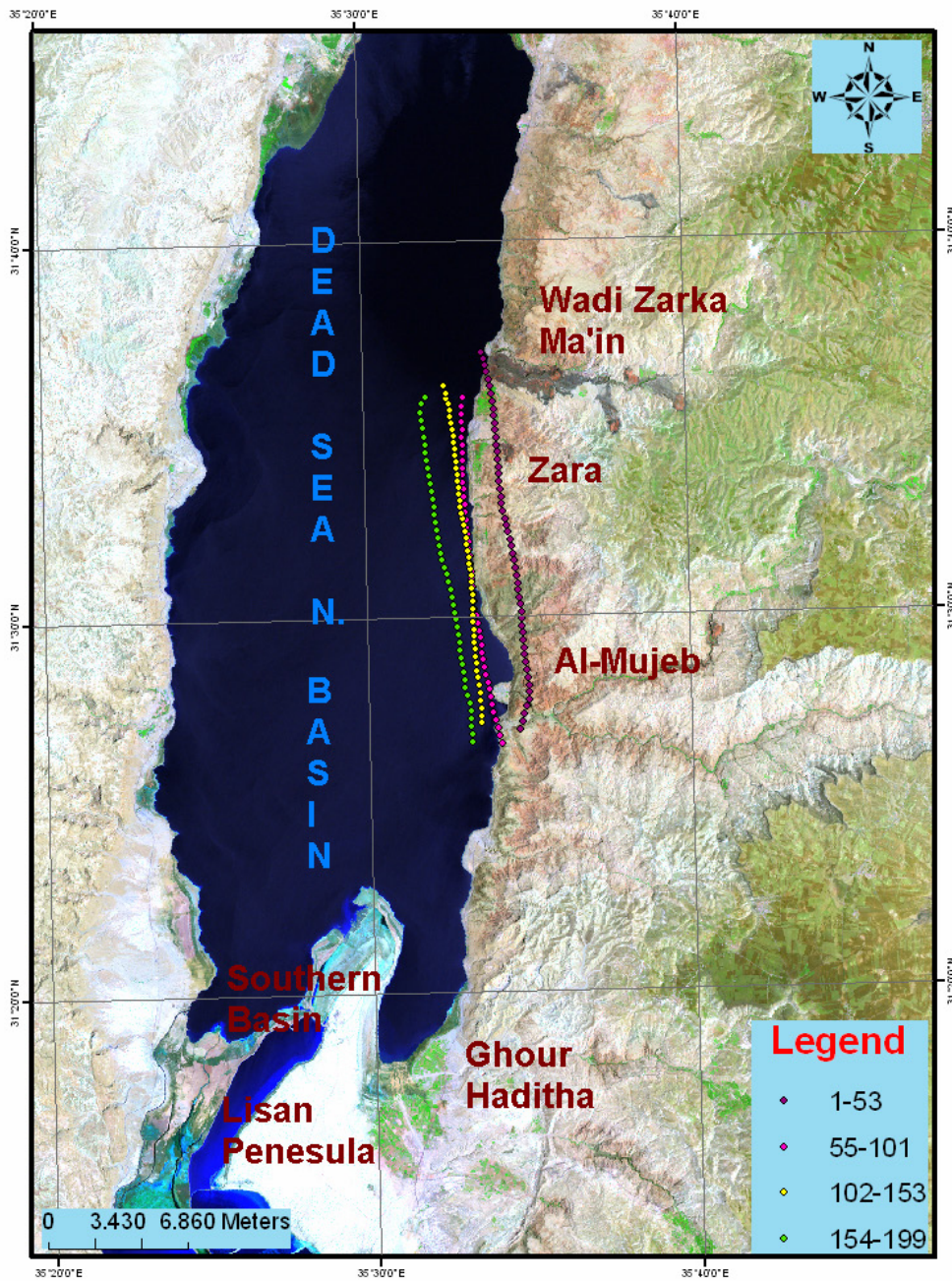
Figure (4-1): Thermal infrared flight strips over the Dead Sea

The thermal infrared imagery was performed using a thermal infrared camera that was fixed at the bottom of the small commercial plane. The survey was performing in December 2005 (winter season) and the time was between 19 and 20 P.M. This time and season were chosen to maximize temperature differentials between the

groundwater and sea surface temperatures at the same time to take an advantage of the lack of shadows cover, which can shield an anomaly from the TIR. The survey was performed at 1300-1600 m elevations. The TIR survey consisted high-resolution (4-8 m) imagery depending on the height of the plane. There was about 10-40 % TIR image footprint overlap between adjacent flight lines and about 25-40% also footprint overlap between the images along the same flight line. Survey conditions were good for identifying discharge zones: clear sky, ambient air Temperature 20-21°C, expected groundwater temperatures of 35°C in Zarka Ma'in, Zara and south Zara areas which have a hot springs, which expected about 26°C in Mujeb and adjacent areas. The coordinates of the images were obtained from a stationary GBS stations. One of these stations was fixed inside the plane top of the thermal camera, and the second GBS station was fixed on the ground at the airport. The coordinates were taken continuously from the starting point at the airport to the end point back to the airport.

4.4. Electromagnetic Radiation (EMR)

Four electromagnetic radiation profiles were carried out along the eastern coast of the Dead Sea. At the beginning the instrument was calibrated related to the number of beaks, amplification and frequency.

The first profile was carried out in Sweimah area. The beginning of the profile was at the coordinate 31° 43′ 62.7″ N and 35° 35′ 33.4″ E, and the end of the profile was at the coordinate 31° 45′ 45.07″ N and 35° 34′ 33.48″ E. The long of this profile was about 4 km.

One profile with a length about 3 km was carried out at south Sweimah area. This profile denoted as second profile. The starting point of this profile was located at the coordinate 31° 41′ 28.18″ N and 35° 34′ 38.87″ E, and the ending point was at the coordinate 31° 43′ 19.6″ N and 35° 35′ 08″ E.

The third profile was carried out in Zara area. The beginning of the profile was at coordinate 31° 34′ 43.83″ N and 35° 33′ 9.92″ E, and the end of the profile was at coordinate 31° 36′ 31.66 N and 35° 33′ 44.96″ E. The long of this profile was about 2.8 km.

The last profile was carried out in Mujeb area. This profile was numbered as profile four. It was located at the coordinate 31° 26′ 57.48″ N and 35° 33′ 55.74″ E at the starting point and at coordinate of 31° 28′ 39.92″ N and 35° 34′ 25.40″ E at the end of the profile. The long of this profile was about 3.7 km.

5.   RESULTS AND INTERPRETATION

5.1.   Electrical Conductivity-Temperature with Depth

- **Laboratory work results and discussion**

The laboratory experiments, which were used for calibrating the inductive electrical conductivity device and for testing the efficiency of this device for temperature compensation shows that the inductive device works properly for temperature compensation at 25°C. The experiments show also that the relationship between temperature and conductivity is a quadratic (R^2= 0.998) (Fig. 5-1). These experiments show that the electrical conductivity increases with temperature increase at constant TDS, while with the increase of the TDS at the same time of the increasing temperature to 40°C and coolling it back to 25°C the EC decreased.
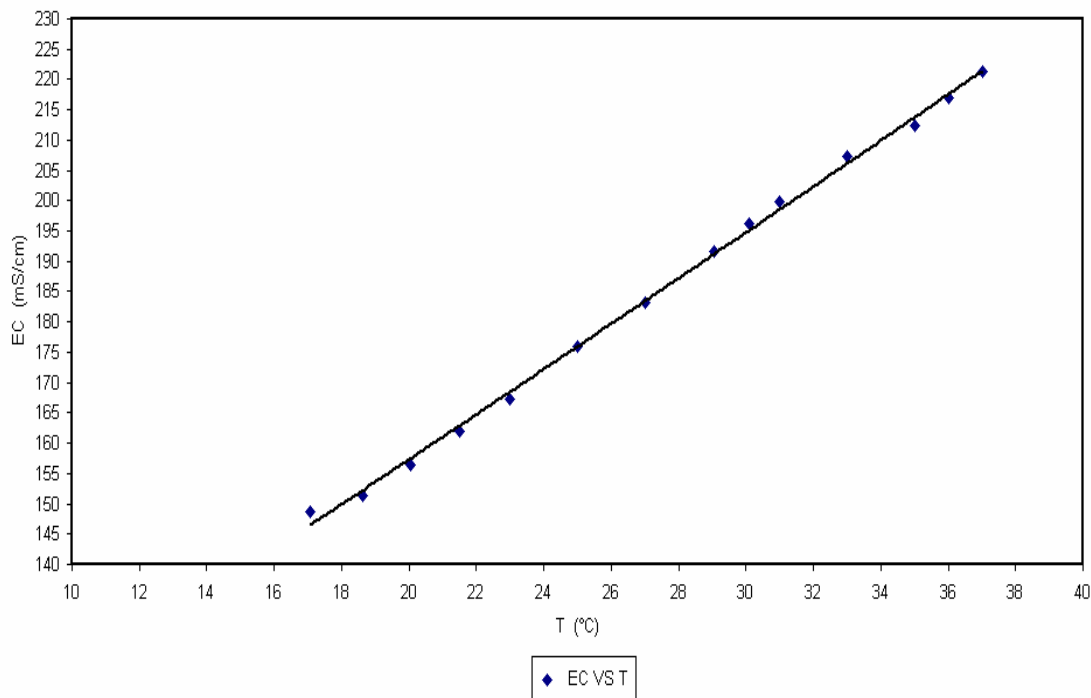
Figure (5-1): Relationship between EC and T for the inductive sensor.

Analyses of the representative samples from the Dead Sea water, which were collected in summer 2005, show that the TDS is 365 g/l. The concentration of $MgCl_2$ is 52.2 g/l, the concentration of sodium cations is 32.47 g/l and the chloride ions is 250 g/l. The concentrations of cations and anions of the Dead Sea water during summer 2005 are listed in table (5-1).

Table (5-1): Dead Sea water composition during summer 2005 (in g/l).

Na^+	K^+	Ca^{+2}	Mg^{+2}	Cl^-	Br^-	$HCO3^-$	$SO4^{-2}$	TDS
32.47	7.8	17.1	52.2	250	5.4	0.3	0.4	365.67

The realationship between the EC and the TDS was established in the laboratory. Laboratory experiments were carried out for calibrating the EC inductive device and for understanding the behaviour of the EC and the TDS for very high saline water as it as of the Dead Sea water. These experiments were done on standard salts. The salts were mixed with a distilled water to get 6 litters of solution with salinity of 380 g/l. This mixture was diluted gradually with 25 ml of distilled water for about one hundred and thirty times (R^2 = 0.9994). After that the relationship between the EC and the salinity was obtained as a quadratic relationship (Fig. 5-2). The right side of this quadratic curve was used later on for the interpretation of the field data results.

This quadratic curve (Fig. 5-2) shows that the relationship between the electrical conductivity and the salinity is indirect relationship for very high saline water (i.e. the electrical conductivity at a certain point of salt concentration begins to decrease with the increasing of salinity). The curve shows also that the maximum value of the electrical conductivity is reached about 202 mS/cm at a TDS of about 267 g/l. Then this value starts to decrease with the increasing of salinity and it reached about 176 mS/cm at a salinity of about 404 g/l. The electrical conductivity might also reach to 157 mS/cm at salinity about 460 g/l. This curve was used latter to calculate the TDS and to interpret the field data results.
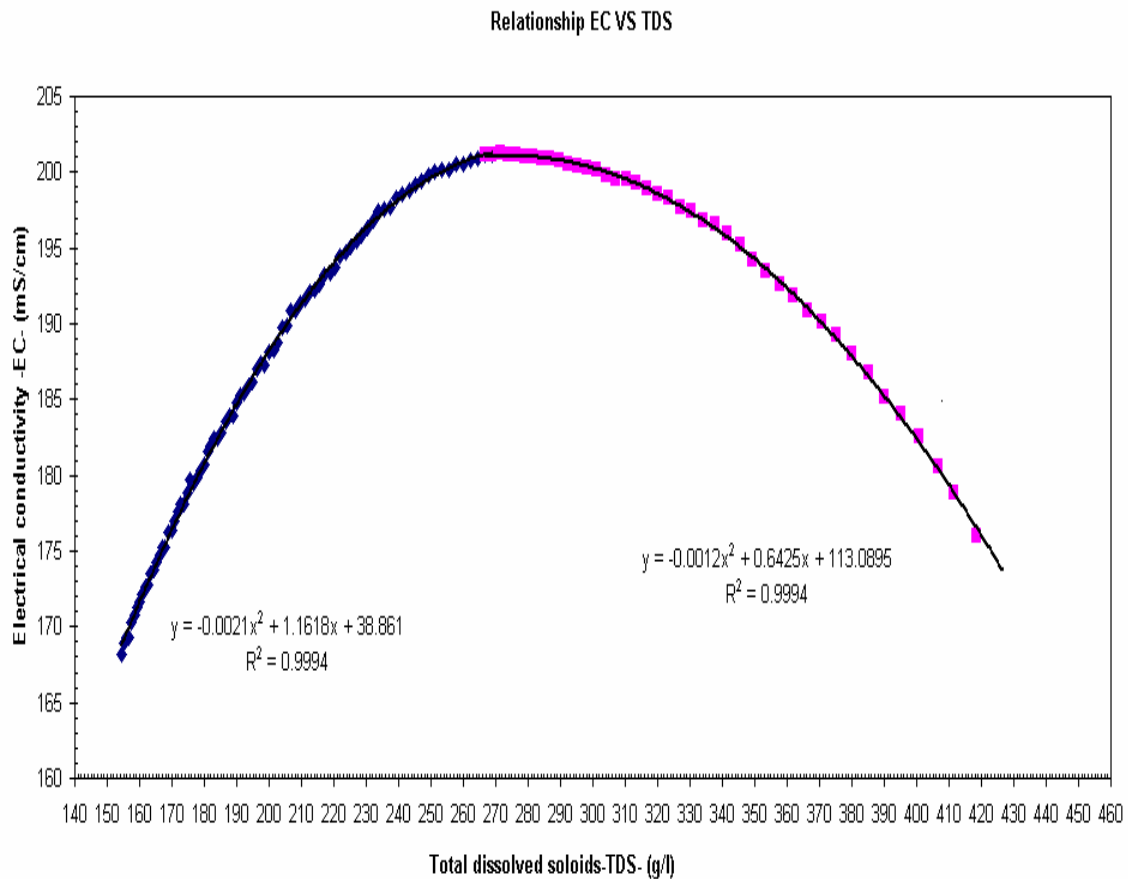
Figure (5-2): Relationship between TDS and EC

TDS measured in the laboratory by using the Gravimetric technique shows that the maximum TDS was 464 g/l in Mujeb area at a depth of 12 m, and in Zarka Main at a depth of 4 m at distance 100 m from the shoreline. The minimum TDS value was 356 g/l in Mujeb area at a depth of 15 m and in south Zara area at a depth of 4 m. The TDS was also calculated for the same samples by using the following equation:

Y= - 0.0012x^2 + 0.6425x +113.0895.

That was obtained from the EC versus TDS curve (Fig. 5-2), where y is the EC and x is the TDS. All the measured and calculated values of TDS are listed in table (4-2).

Table (5-2): Measured and calculated TDS at different depths

Area name	Depth (m)	TDS (g/l) measured	TDS (g/l) calculated
Zara	4	370	354
	7	372	362
	15	412	409
	24	410	412
South Zara	2	362	387
	4	356	379
	7	386	367
	15	396	363
	24	444	418
Zarka Ma'in	4	391	390
	4	416	425
	4	464	450
	4	440	438
Mujeb	2	412	408
	4	398	401
	7	388	390
	12	464	451
	15	356	355
	24	440	422

The maximum calculated value of TDS was 451 g/l in Mujeb area at a depth of 12 m and 450 g/l in Zarka Ma'in area at a depth of 4 m. The minimum TDS values were 355 and 354 in Mujeb at a depth of 15 m and in Zara at a depth of 4 m respectively. The differences between the measured TDS and the calculated TDS were ± 1-5 %. These differences may be presented because of some samples were not evaporated completely or are due to experimental errors. Generally, the measured and calculated TDS values are comparable with a significant corellations, which means that the curve and the equations used for calculating the TDS, are correct. The comparison between measured and calculated TDS values is shown in (Fig. 5-3).
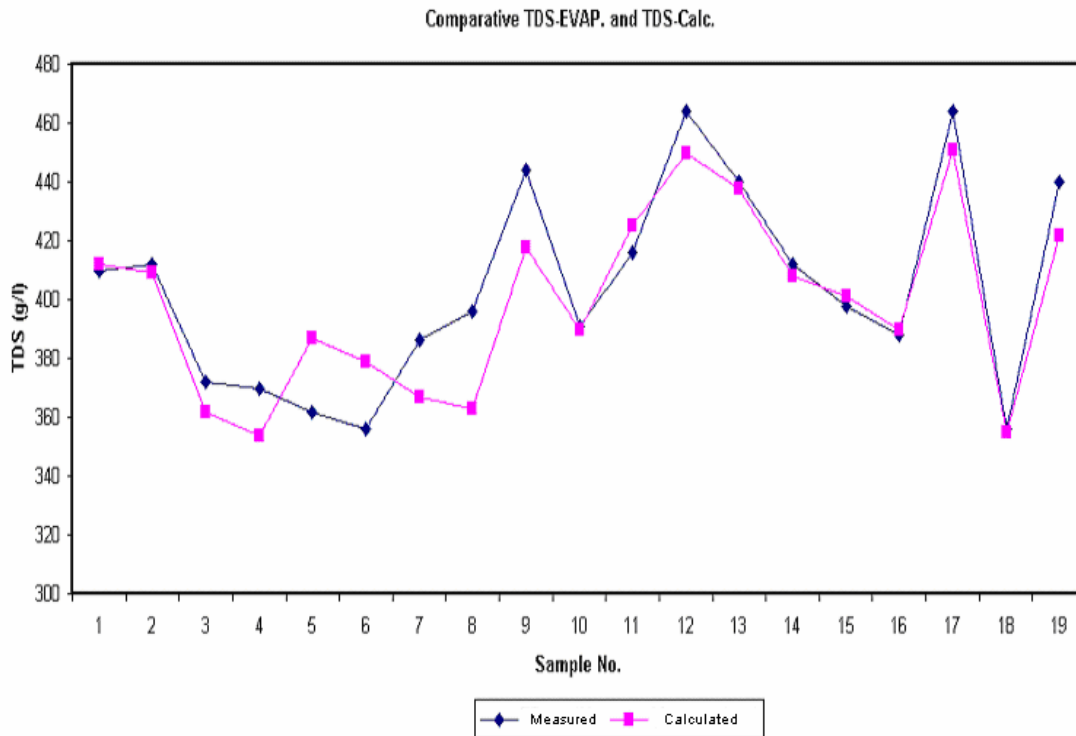
Figure (5-3): Comparison between measured and calculated TDS

Also the relationship between the EC and the TDS obtained in (Fig. 5-2) was approved by the laboratory's experiments by increasing the salinity gradually and measure the electrical conductivity after each salt adding. The salinity increases by adding known amounts of three different standard salts separately into the initial prepared standard solution (380 g/l) into separate beakers.

The expermants show that the EC decreases by adding different known amounts of $MgCl_2$ to the first beaker, which contained one litter of the initial standard solution. After adding 10 g of $MgCl_2$ to that solution the EC decreased from 181.03 mS/cm to 159.76 mS/cm. After adding 5 g more of this salt the EC decreased to 148.58 mS/cm. Adding 5 g more the EC decreased to 147.95 mS/cm and decreased to 146.47 mS/cm after adding the last 5 g of $MgCl_2$.

The same behaviour was observed after adding different known amounts of $CaCl_2.2H_2O$. The EC decreases from 181 mS/cm to about 169.88 mS/cm after adding the first 10 g of $CaCl_2.2H_2O$. After adding the second 10 g the EC decreased to 164.59 mS/cm. Then the EC continued decreasing by adding more and more of $CaCl_2.2H_2O$ until it reached an EC value of 148.89 mS/cm after the total adding become 60 g.

It was observed that the total amount of $CaCl_2.2H_2O$ dissolved completely when the solution was heated to 40°C and then a little amount of the salt started to precipitated when the solution was cooling down again to 25 °C.

The same behaviour was observed relating to the EC after adding NaCl salt to the solution. By adding the first 10 g of NaCl the EC decreased from 181 mS/cm to 166.89 mS/cm. After adding the second 5g the EC decreased to 159.55 mS/cm. Then after adding the last 5 g of NaCl when the total added amount reached to 20 g the EC decreased to 152.4 mS/cm. It was observed that NaCl dissolved completely at 40°C. After adding 15g of salt the solution starts to precipitate when cooling down to 25°C. But after adding 20g the salt did not dissolve completely in spite of heating to 40°C. The results of the adding salt amounts and the EC results with the T are listed in the table (5-3).

Table (5-3): The effect of the salt adding on the EC

Salt	Amount (g)	Electrical conductivity (mS/cm)	Temperature (°C)
MgCl₂	0	181.03	25
	10	159.76	25
	15	148.58	25
	20	147.95	25
	25	146.47	25
CaCl₂.2H₂O	0	181	25
	10	169.88	25
	20	164.59	25
	30	158.6	25
	40	157.0	25
	50	152.44	25
	60	148.89	25
NaCl	0	180.8	25
	10	166.89	25
	15	159.55	25
	20	152.4	25

By comparing the results of the added salts it was found that after adding 10 g of MgCl2, 10 g of $CaCl_2.2H_2O$ and 10 g of NaCl the EC decreased by about 21 mS/cm, about 12 mS/cm and about 14 mS/cm respectively. The results show that the highest salt effect on the EC is from MgCl2 then from NaCl and the lowest is from $CaCl_2.2H_2O$. On the other hand the results showed that the $CaCl_2.2H_2O$ has higher solubility than the other two salts.

Density was measured for the three solutions after the last adding and for the initial salt solution (380 g/l). The average density (n=5) for the initial solution (TDS 380 g/l) is 1.2472 g/cm^3. The average density (n=5) for the solution in the first beaker after adding 25 g of MgCl2 (TDS 405 g/l) is 1.25636 g/cm^3. The average density (n=5) for the solution in the second beaker after adding 60 g of $CaCl_2.2H_2O$ is 1.275 g/cm^3 and the average density (n=5) for the solution in the third beaker after adding 20 g of NaCl was 1.26383 g/cm^3. These results are used to interpret the field results (latter on). The results were summarized in table (5-4)

Table (5-4): Densities at different TDS values after adding different amounts of salts.

Type of Salt	Adding amount (g/l)	Final TDS (g/l)	Density (g/cm^3)
Initial solution	____	380	1.2472
$MgCl_2$	25	405	1.25636
$CaCl_2.2H_2O$	60	440	1.275
NaCl	20	400	1.26383

- **Combine the field and the laboratory results**

The results of EC and T with the depth profiles, which depend on the stations number, the distances away from the shoreline and the depths, are explaining as follows:

The Dead Sea water EC, depth, T and TDS results of all profiles of the first station, in Sweimah area at the northeastern corner of the Dead Sea, were plotted in (Figs 5-4 A, B, C, D and E). The TDS of all profiles were calculated using the formula obtained from the EC versus TDS curve (Fig. 4-2).

$Y = -0.0012 x^2 + 0.6425 x + 113.0895$

The T, EC and TDS for the first profile (S $_{1-1}$) at 200 m distance away from the shoreline (Fig. 5-4 A) show that:

The T at the surface of the Dead Sea water was 33.5°C, it increased gradually with the increase the water depth down to 10 m, and it reached 33.9°C. Then it started decreasing from a depth of 11 m gradually until it reached 30.44°C at a depth of 18 m. After that it decreased sharply at a depth of 19 m beneath the sea surface and it reached 29.77°C. From this depth it decreased gradually until a depth of 27 m and it reached 28.18°C and it increased to 28.21°C at a depth of 29 m. Finally it decreased gradually and it reached 25.59°C at a depth of 55 m.

The TDS in this profile was 348 g/l at the surface water. It increased gradually with the increase in the depth and it reached about 430 g/l at a depth of 10 m. After that it started decreasing and it reached about 413 g/l at a depth of 17 m and increased locally at a depth of 18 m and it reached 416 g/l. Then it decreased gradually and it reached about 411 g/l at a depth of 24 m. After this depth it started increasing again gradually and it reached about 435 g/l at a depth of 28 m. Then it decreased gradually to a depth of 55 m and it reached about 413 g/l.

The EC results for this profile showed that the EC at the surface of the seawater was about 190.35 mS/cm. It decreased gradually with the increasing in the depth and it reached about 166.11 mS/cm at a depth of 10 m underneath the sea surface. Then it started increasing and it reached about 172.44 mS/cm at a depth of 17 m. At a depth of 18 m it decreased locally and it reached about 171.5 mS/cm. After this depth it increased to about 173.34 mS/cm at a depth of 24 m. From this depth it decreased again gradually until a depth of 28 m and it reached about 164.38 mS/cm. Finally it increased again gradually until a depth of 55m and it reached about 172.75 mS/cm.
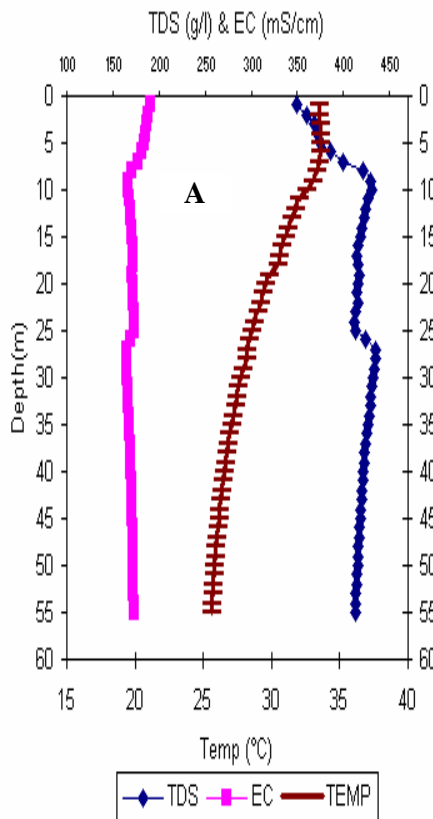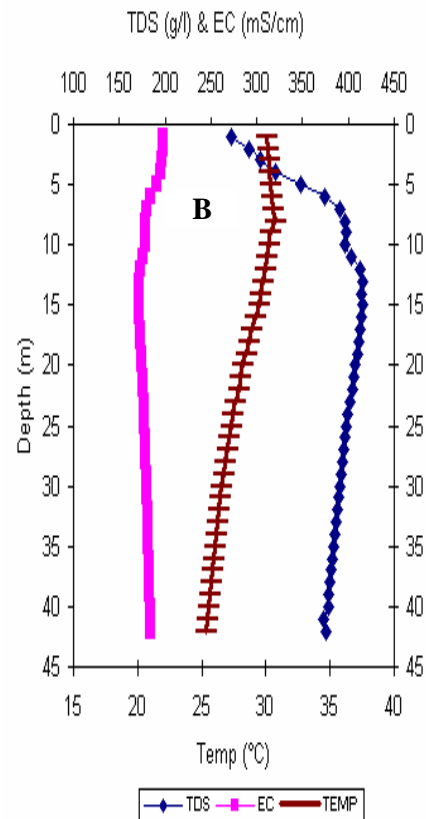
Figure (5-4A): EC, TDS and T Relationship with a depth in Sweimah area at a distance of 200 m from the shoreline. Figure (5-4B): EC, TDS and T relationship with a depth in Sweimah area at a distance of 300 m from the shoreline.

The second profile at this station (S_{1-2}) at 300 m distance away from the shoreline (Fig. 5-4 B) showed that:

The T was 30.1°C at the seawater surface. It increased gradually and it reached 30.7°C at a depth of 9 m underneath the Dead Sea surface. Then it started decreasing gradually and it reached about 25.23°C at a depth of 43 m.

The TDS measurements in this profile showed that the TDS at the surface water was about 272 g/l. After this depth it increased sharply and it reached about 397g/l at a depth of 9 m. Then it gradually increased down at a depth of 15 m and it reached about 415 g/l. It started decreasing gradually to about 375 g/l at a depth of 42 m.

The EC results for this profile showed that the EC at the surface water was 198.4 mS/cm. This value decreased gradually and it reached its minimum value of this profile of 171.7 mS/cm at a depth of 15 m below the sea surface. Then it started increasing slowly and it reached 184.29 mS/cm at a depth of 42 m.

Figure (5-4C): EC, TDS and T Relationship with a depth in Sweimah area at a distance of 400 m from the shoreline. Figure (5-4D): EC, TDS and T relationship with a depth in Sweimah area at a distance of 500 m from the shoreline.

The third profile (S_{1-3}) in the station 1 in Sweimah area at a distance of 400 m away from the shoreline (Fig. 5-4 C) displayed that the T at the surface was 30.54°C. This value of T started increasing slowly with the increase in the depth and it reached its maximum value 31.48°C at a depth of 10 m. then it decreased slowly until it reached about 24.07°C at a depth of 94 m below the Dead Sea surface.

The lowest TDS value of this profile was 271.94 g/l it was observed at the Dead Sea surface water. It started increasing until it reached its maximum value 422 g/l at a depth of 17 m. Then it reached about 394 g/l at a depth of 37 m underneath the seawater surface. Then it increased again for few meters to reach 405 g/l at a depth of 40 m. After this depth it started decreasing gradually down to 94 m and it reached 379 g/l.

The illustrating of the EC results of this profile (S_{1-3}) showed that the EC was 198.4 mS/cm at the surface seawater and it started decreasing with the increase in the depth and it reached its minimum value 169.5 mS/cm at a depth of 17 m. It started increasing gradually and it reached 176.64 mS/cm at a depth of 37 m. It increased slowly and it reached about 183 mS/cm at a depth of 94 m.

The T, TDS and EC were illustrated for the fourth profile (S_{1-4}) in the station 1 (Fig. 5-4 D). The figure showed that the T reading at the surface was 30.16°C then as of the other profiles it started decreasing and it reached its maximum value 32.01°C at a depth of 19 m. This value of T started deccreasing with the increase in the depth and it become less and less until it reached its minimum value 24°C of this profile at a depth of 88 m.

The illustrating of the TDS results showed that the minimum value was at the surface. This value was 272 g/l and it started increasing sharply until reached its maximum value in this profile 429 g/l at a depth of 25 m. Then it decreased slowly and it reached 372 g/l at a depth of 88 m.

The EC results for this profile showed that the maximum value of the EC 198.4 mS/cm was observed at the seawater surface. This EC value decreased gradually with the increase the depth and it reached 179.86 mS/cm at a depth of 19 m. It decreased sharply until reached 166.86 mS/cm at a depth of 25 m. After this depth it started increasing slowly down to a depth of 88 m and it reached 185.18 mS/cm.
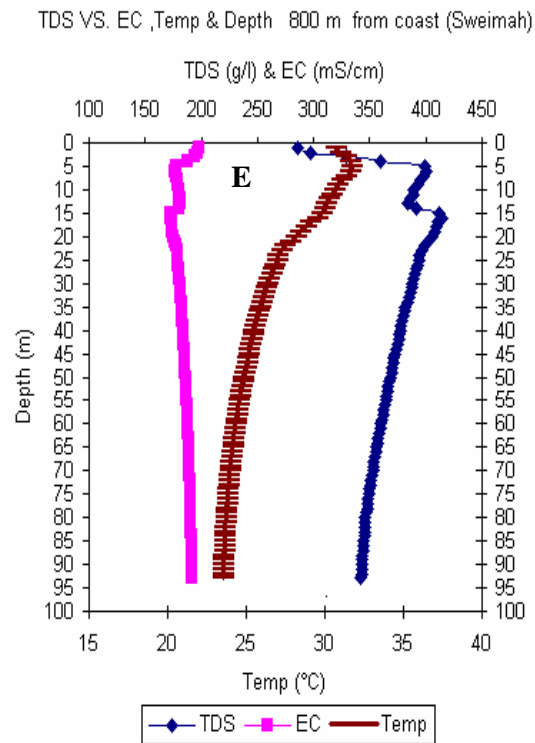
Figure (5-4E): EC, TDS and T Relationship with a depth in Sweimah area at a distance of 800 m from the shoreline.

The last profile (S_{1-5}) at this station located at 800 m distance away from the shoreline. It demonstrated the results of the T, TDS and EC measurements (Fig. 5-4 E). The T profile showed that the surface T of this profile was 30.7°C. Then it increased gradually and it reached its maximum value 31.71°C at a depth of 5 m underneath the sea surface. After this depth it decreased and it reached 29.98°C at a depth of 14 m. After that it increased slightly and it reached 30.2°C at a depth of 16 m. Finally it decreased gradually and it reached its minimum value of this profile 23.52°C at a depth of 93 m.

The TDS results showed that its value was 285 g/l at the Dead Sea surface. Then it increased sharply with the increase in the depth until reached 400 g/l at a depth of 5 m. After that it decreased slowly and it reached 384 g/l at a depth of 13 m. After that it increased sharply and it reached its maximum value of this profile 414 g/l at a depth of 16 m. Lastly it decreased gradually and it reached 342 g/l at a depth of 93m.

The EC profile in (Fig 5-4 E) showed that the maximum value was 198.1 mS/cm for the surface seawater. It started decreasing down to a depth of 5 m and it reached about 177.5 mS/cm. From this depth it increased gradually and it reached 179.92 mS/cm at a depth of 16 m. then it decreased sharply and it reached a value of 172.35 mS/cm at a depth of 16 m. Lastly it increased gradually dowm to a depth of 93 m until reached a value of 191.55 mS/cm.

The results of the EC, TDS and T with the depth for the profiles at station 2 located in Zarka Ma'in area are illustrating in (Fig. 5-5 F, G, H and J).

The T results of the profile (S_{2-1}), which located at 100 m distance from the shoreline, are summarized in (Fig. 5-5 F). The figure showed that the T of the Dead Sea water at the surface was 38.48°C. From the surface down to depth of 13 m underneath sea surface this value decreased gradually and it reached 36.24°C. It started decreasing sharply at the depth of 14 m and it reached 35.45°C that means the change was about 0.8°C within just one-meter change in the depth and this change conceder a significant. From this depth it decreased gradually to a depth of 24 m and it reached 33.19°C. Then it decreased sharply and it reached 31.93°C at a depth of 26 m. The changed was about 1.26°C which conceder also a significant change. Finally it decreased slowly to reach 24.4°C at the depth of 80 m underneath the sea surface.

The TDS results for the same profile showed that the TDS at the surface was 403 g/l because the T was very high at the surface and then the salts consists of the Dead Sea become more soluble. Then the suspension salt dissolved in the seawater. Then the TDS dropped to 385 g/l at a depth of 14 m at the same depth where the T dropped sharply. After that the TDS started increasing gradually and it reached its maximum value 430 g/l of this profile at a depth of 25 m one meter upper the T sharply changed. At last it decreased gradually and it reached 360 g/l at a depth of 80 m.

The EC profile showed that the EC was 176 mS/cm at the surface seawater. It started increasing slightly and it reached 181.47 mS/cm at a depth of 13 m where the TDS dropped down. Then it decreased slightly and it reached 178.9 mS/cm at a depth of 20 m then it decreased sharply to reach the lowest value 166.03 mS/cm of this profile at a depth of 25 m where the TDS was reached the highest value of this profile. Finally it increased slightly and it reached 188.8 mS/cm at a depth of 80 m.

The second profile (S_{2-2}) at the station 2 located at about 200 m distance from the shoreline (Fig. 5-5 G) showed that the T value at the sea surface was 33.74°C. It started decreasing gradually and it reached 31.8°C at a depth of 24 m underneath sea surface. Then it decreased sharply at a depth of 25 m and it reached 30.9°C. That mean the changed was about 0.9°C within only one meter depth. After this depth the T decreasing slowly and it reached its lowest value 24.08°C for this profile at a depth of 91 m.

The TDS value of this profile was 340 g/l at the surface, which is the lowest value of this profile. It increased gradually and it reached its maximum value 429 g/l in this profile at a depth of 24 m one meter above the sharply dropping in the T. Then it decreased slowly and it reached 362 g/l at a depth of 91 m.

On the other hand the EC profile showed that the EC at the surface was the highest value 192.03 mS/cm where the TDS was the lowest value of this profile. The EC started decreasing gradually with the increasing in the depth and it reached its lowest value 166.63 mS/cm at a depth of 24 m where the TDS was the highest value of this profile. At the last the EC increased slowly and it reached 187.46 mS/cm at a depth of 91 m the final depth of this profile.
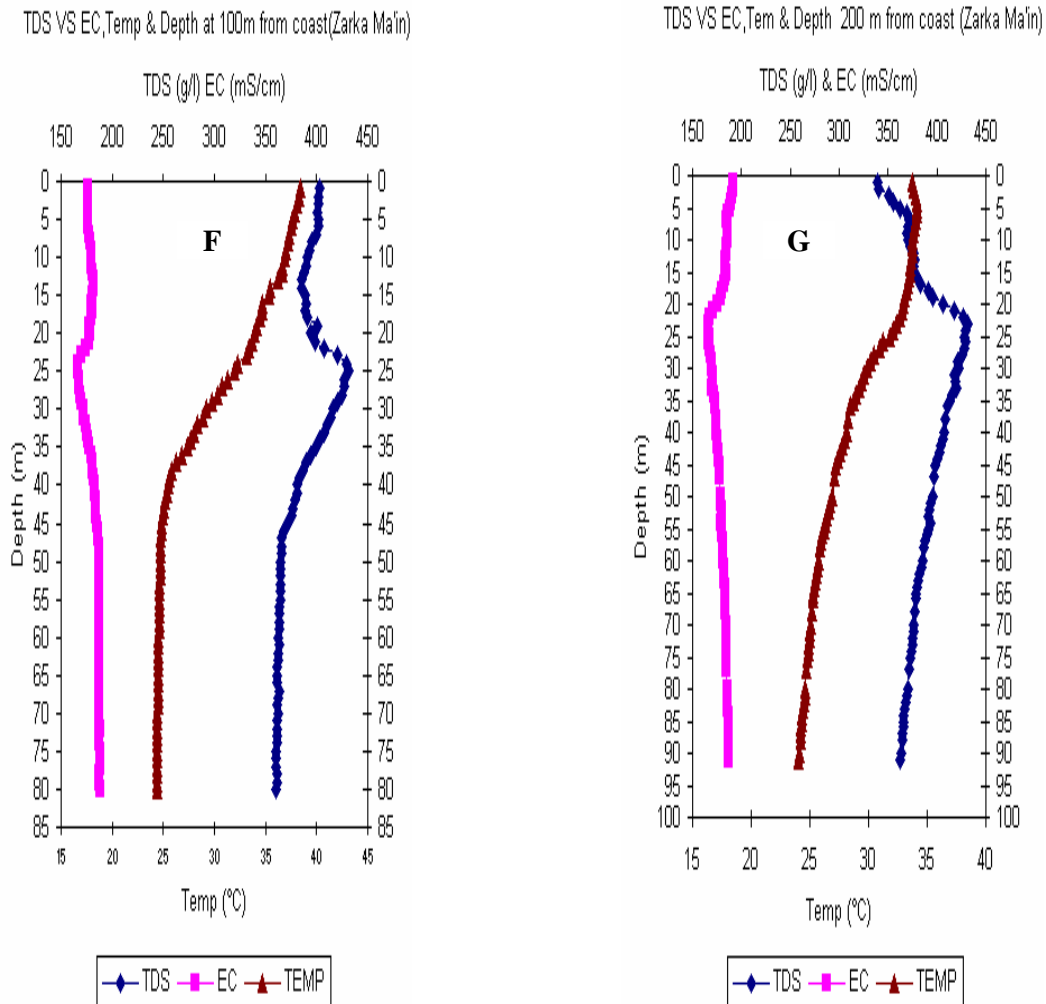
Figure (5-5F): EC, TDS and T relationship with a depth in Zarka Ma'in area at a distance of 100 m from the shoreline. Figure (5-5G): EC, TDS and T relationship with a depth in Zarka Ma'in area at a distance of 200 m from the shoreline.

The third vertical profile (S_{2-3}) in station2 (Fig. 5-5H) showed that the T at the surface was 34.04°C. This value decreased gradually and it reached 31.78°C at a depth of 25 m. Then it decreased sharply for about 1°C within 1 m only to reach 30.76°C at a depth of 26 m. This sharply changed was affected on the TDS value. After that the T started decreasing slowly with increasing the depth until the final depth of this profile and it reached its minimum value 24.44°C at a depth of 92 m underneath the sea surface.

The TDS results showed that the minimum value was 342 g/l at the surface. Then it increased sharply with increasing depth and it reached its maximum value 436 g/l at this profile at a depth of 25 m. This value located one meter above the dropping in the T at 26 m depth. The TDS values decreased gradually and it reached 360 g/l at a depth of 92 m the final depth of this profile.

89

The EC curve of this profile at this station showed that the highest value of EC was 191.48 mS/cm at the seawater surface. It decreased gradually and it reached about 179.46 mS/cm at a depth of 15 m below sea surface. Then it decreased distinctly and it reached 177.77 mS/cm at a depth of 16 m. It continued decreasing with the increase in the depth and it reached its minimum value 163.85 mS/cm at a depth of 25 m. This value was at the same depth where the maximum value of the TDS was observed. Then it increased constantly and it reached 187.78 mS/cm at the final depth of this profile at 92 m.
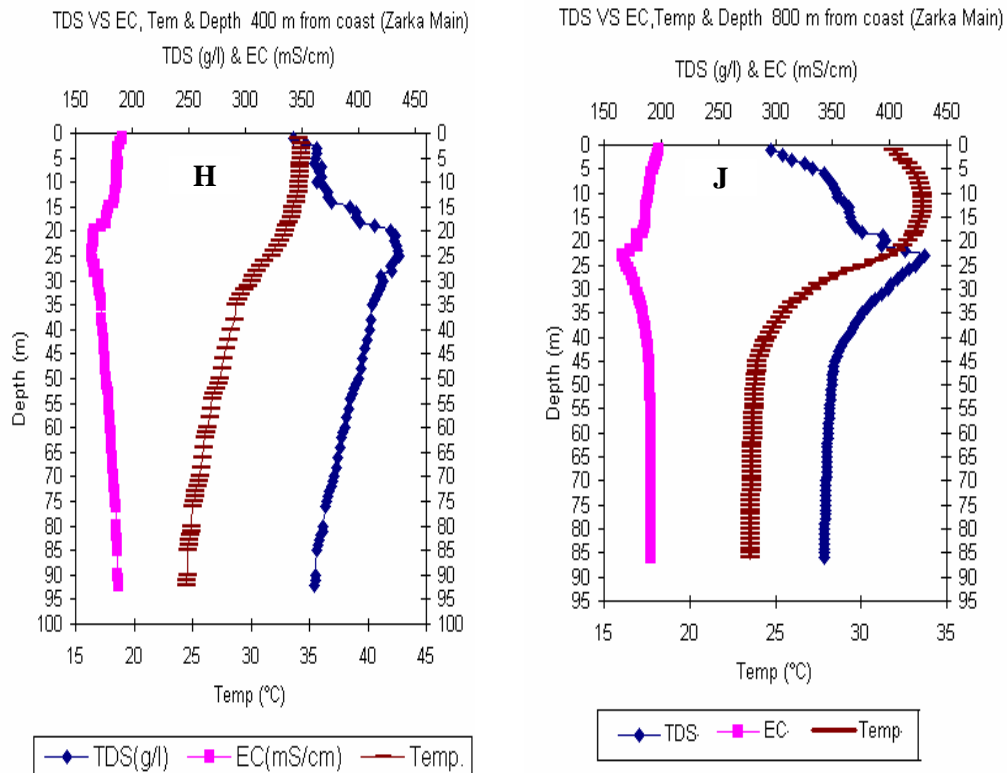
Figure (5-5H): EC, TDS and T relationship with a depth in Zarka Ma'in area at a distance of 400 m from the shoreline. Figure (5-5J): EC, TDS and T relationship with a depth in Zarka Ma'in area at a distance of 800 m from the shoreline.

Figure (5-5 J) illustrated the results of the T, EC and the TDS for the fourth profile (S_{2-4}) at the station 2 in Zarka Ma'in area. The surface T was 31.91°C. It started increasing gradually to reach its maximum value 33.59°C of this profile at a depth of 12 m below Dead Sea surface. After that it decreased apparently and it reached to 24.24°C at a depth of 42 m. From this depth it decreased very slightly to the final depth 86 m of this profile and reached to its minimum value 23.5°C.

The TDS results indicated that the surface seawater salinity was 295 g/l which is the lowest value of this profile. This value started increasing rapidly to reach its

maximum value of this profile 430 g/l at a depth of 23 m directly above the point of the T rapidly changed. Then it decreased apparently down to 48 m under sea surface and it reached 350 g/l. The deeper part of the TDS profile showed that the TDS decreased very slightly almost negligible changes from a depth of 48 m to the end of this profile at the depth of 86 m and it reached 342 g/l at this depth.

The profile, which illustrated the EC results, showed that the behaviour of the EC changing was in an opposite position of the TDS. The maximum value of the EC of this profile was 197.44 mS/cm at the surface of seawater that was against the minimum value of the TDS which was 295 g/l. Then the EC decreased sharply and it reached its minimum value 166.12 mS/cm of this profile at a depth of 23 m. This value was observed against the maximum value of the TDS of this profile, which was 430 g/l. After that the EC values started increasing and it reached 190.1 mS/cm at a depth of 48 m below the Dead Sea surface. Then it decreased very slightly with no noticeable changes to reach 191.5 mS/cm at a depth of 86 m below Dead Sea surface.

The results of the T, TDS and the EC were plotted related to the depth as in (Fig. 5-6 K, L, M and N) for all profiles at station 3, which located in Zara-Hot springs area. Figure (5-6 K) illustrated the results of the first profile (S_{3-1}). The T profile showed that the surface T was very high 43.44°C. It started decreasing sharply and it reached 38.53°C at a depth of 11 m, then it increased slightly between depths 12 m and 16 m. After that it decreased sharply again and it reached 26.89°C at a depth of 51 m. After this depth it decreased slightly to a depth of 84 m and it reached 24.47°C.

The TDS plot showed that the TDS at the surface seawater was 445 g/l. This value was opposite to the very high T value. Then this value started decreasing with a T decreasing, it reached 422 g/l at a depth of 11 m formerly it increased sharply and it reached its maximum value 464 g/l at a depth of 15 m. As the other profiles it started decreasing gradually and it reached its minimum value of this profile 367 g/l at a depth of 84 m.

The EC at the surface was 159.9 mS/cm then it reached 170.22 mS/cm at a depth of 9 m. It started decreasing and it reached its lowest value 151.66 mS/cm at the depth of 15 m. At the last it started increasing slowly and it reached 186.18 mS/cm at the end of this profile at a depth of 84 m.

Figure (5-6 L) illustrated the results of the T, TDS and EC with the depth for the second profile (S_{3-2}) in station 3. The T of this profile was 33.3°C at the surface, then it increased slowly, and it reached 33.47°C at adepth of 8 m. Then a shifting in the T values occurred at the depths of 12 m and 19 m. After that it started decreasing to reach its minimum value 24.12°C at a depth of 89 m.

The TDS at the surface was 353 g/l. It increased slightly from the surface to a depth of 8 m and it reached 362 g/l. Then it increased sharply at a depth of 12 m

where the shifting in T was occurred and it reached 411 g/l. After that it decreased again and it reached a value of 401 g/l at a depth of 19 m also at the same point where the shifting in T occurred. The TDS increased slightly again and it reached its maximum value 417 g/l of this profile at a depth of 25 m below Dead Sea level. Finally it decreased gradually and it reached 353 g/l at a depth of 89 m.

The results of the EC at this profile showed that the EC at the surface was 189.44 mS/cm. It decreased very slightly and it reached 187.11 mS/cm at a depth of 9 m. Then sharply decreasing occurred at a depth of 14 m and it reached 173.38 mS/cm. Then it increased slightly and it reached 176.56 mS/cm at a depth of 19 m. It decreased again to a depth of 25 m and it reached its minimum value 171.03 mS/cm at this profile. Finally it increased gradually and it reached 189.31 mS/cm at a depth of 89 m.

Figure (4-6 M) denoted to the third vertical profile (S_{3-3}) which is located at about 400 m distance away from the shoreline in station 3. The T results of this profile showed that the T at the surface was 31.08°C. This value increased gradually with the increase the depth and it reached its maximum value 32.33°C of this profile. Thereafter it decreased slightly and it reached 32.04°C at a depth of 16 m below Dead Sea level. Suddenly a shifting of the T value occurred and it decreased from 32.04°C at a depth of 16 m to 31.2°C at a depth of 20 m. Then it decreased gradually to a depth of 51 m and it reached value of 24.31°C. Finally it decreased very slightly almost negligible changes to a depth of 96 m and it reached its minimum value 23.42°C of this profile.
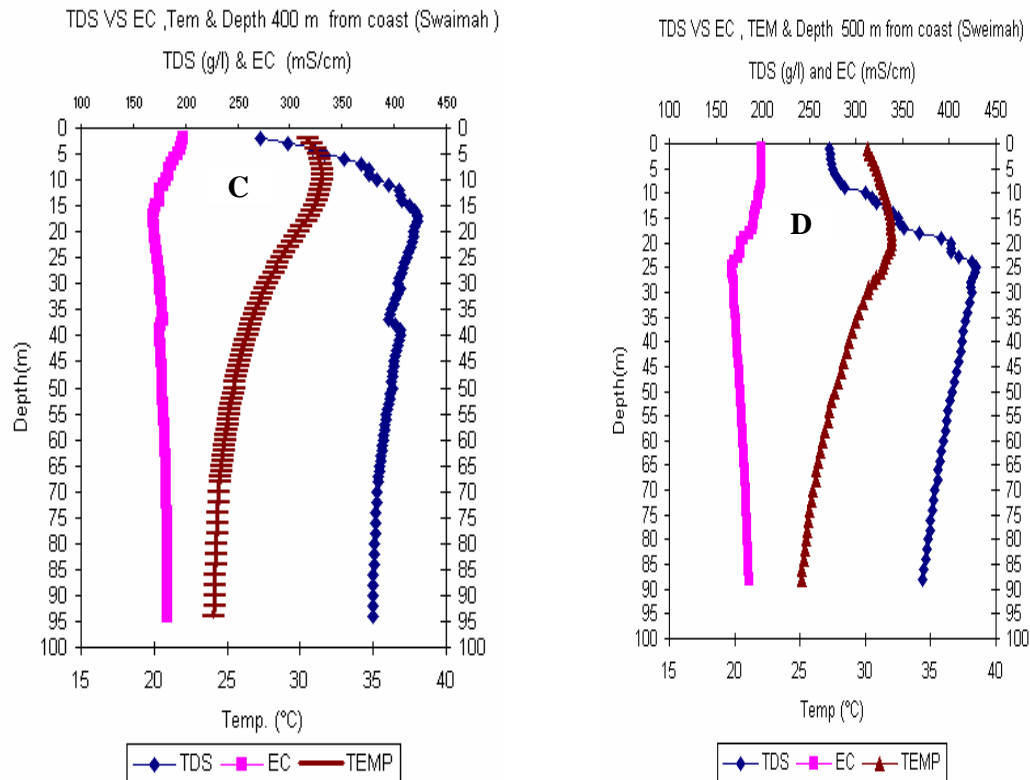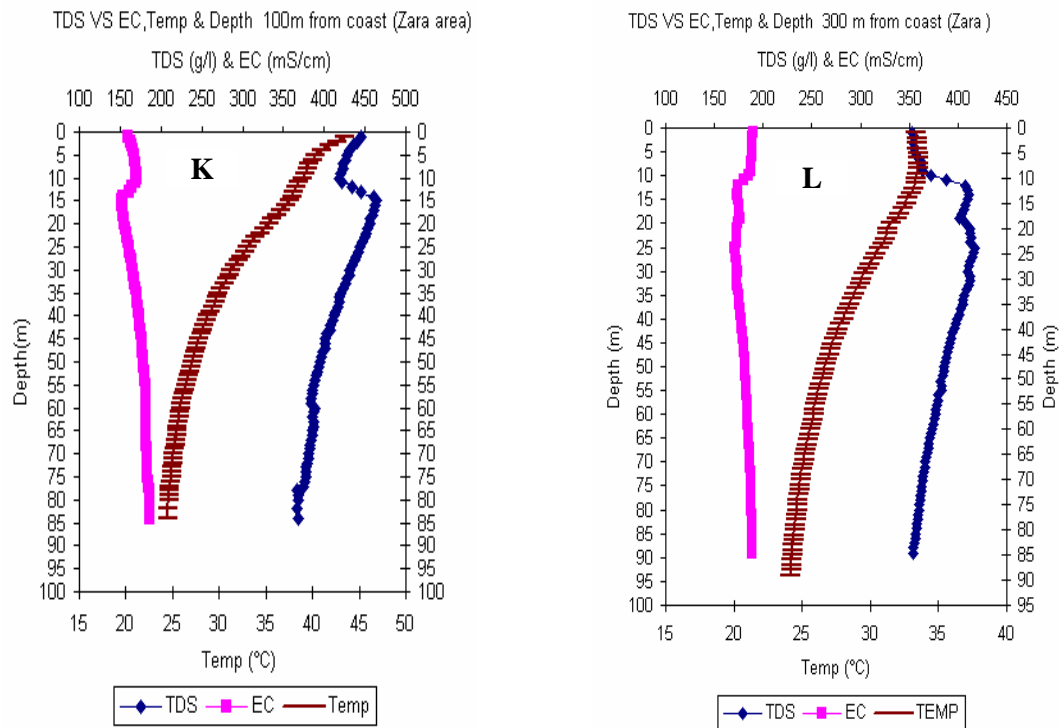
Figure (5-6K): EC, TDS and T relationship with the depth in Zara area at a distance 100 m from the shoreline. Figure (5-6L): EC, TDS and T with a depth in Zara area at a distance of 300 m from the shoreline.

The TDS graph in (Fig. 5-6 M) indicated that the TDS of the Dead Sea water at the surface of this profile was 272 g/l, then a sharply increasing was occurred from the surface to a depth of 13 m and it reached 396 g/l parallel with the increasing in the T values. Thereafter it increased gently and it reached its maximum value 430 g/l in this profile at a depth of 17 m below Dead Sea surface. Then it started decreasing gradually, it reached 358 g/l at a depth of 51 m. Lastly it decreased very gently with inconsiderable changes, and it reached a value of 338 g/l at a depth of 96 m.

The results of the EC for the same profile showed that the EC at the surface was 198.4 mS/cm. It decreased rapidly to a depth of 13 m and it reached 178.15 mS/cm. Thereafter a shifting occurred at this depth and started decreasing gently with increasing the depth, and it reached its minimum value 166.52 mS/cm at a depth of 17 m. Then it increased gradually until a depth of 51 m and it reached a value of 188.24 mS/cm. From this depth to the end of this profile the EC increased very slightly with unnoticeable changes and it reached a value of 192.22 at a depth of 96 m.
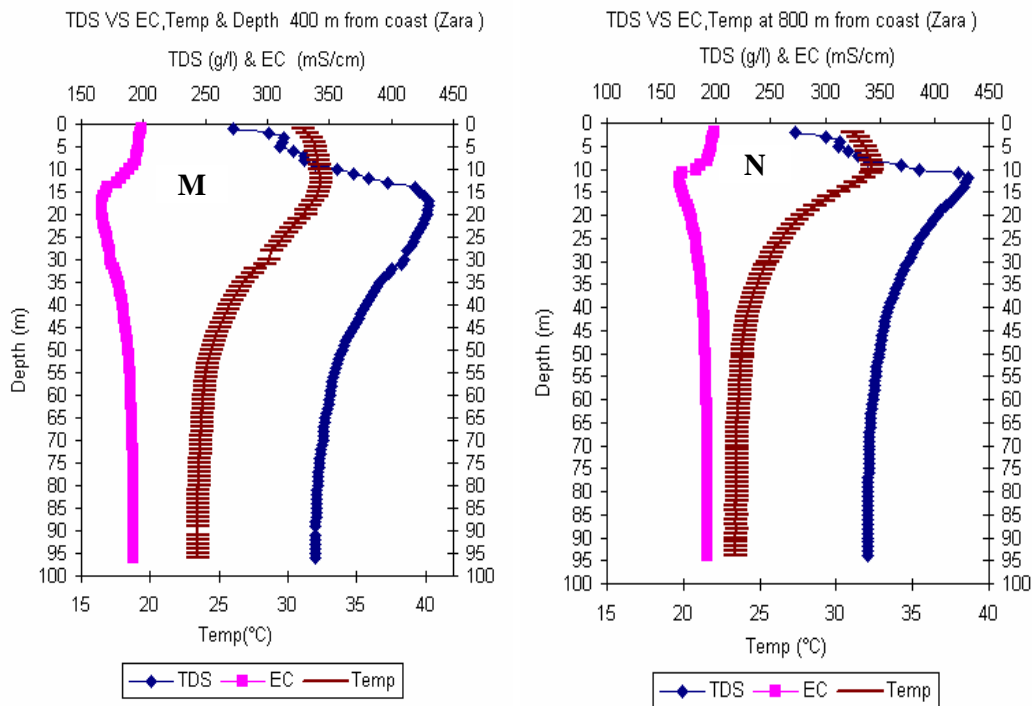
Figure (5-6M): EC, TDS and T relationship with the depth in Zara area at a distance 400 m from the shoreline. Figure (5-6L): EC, TDS and T with a depth in Zara area at a distance of 800 m from the shoreline.

The results of the T, TDS and the EC for the vertical profile (S_{3-4}), which is located at about 800 m distance away from the shoreline, were plotted into three graphs as shown in (Fig. 5-6 N). The T at the surface of this profile was 31.08°C. It increased sharply and it reached its maximum value at 32.37°C of this profile at a depth of 10 m, then it decreased gently until a depth of 12 m. At this depth the T was shifting and decreased sharply from a value of 32.2°C to reach 30.16°C at a depth of 15 m. Then it decreased gradually to a depth of 47 m and it reached a value of 23.91°C. Thereafter it decreased very slightly to the last depth of this profile at 94 m and it reached its minimum value 23.43°C.

The TDS at the surface of this profile was 272 g/l. This value increased sharply parallel with the increase of the T and it reached a value of 386 g/l at a depth of 10 m. Thereafter it increased gradually and it reached its maximum value 428 g/l at a depth of 12 m where the shifting of the T occurred. Then it decreased gradually to a depth of 47 m then it decreased very slightly with unnoticeable changes and it reached a value of 338 g/l at a depth of 94 m.

The results of EC showed that the EC at the surface was 198.4 mS/cm. It decreased gradually and it reached its minimum value 166.86 mS/cm of this profile at a depth of 13 m below sea surface. After that it increased slowly to a depth of 47 m. Then it increased very slightly with inconsiderable changes until a depth of 94 m and it reached a value of 192.18 mS/cm.
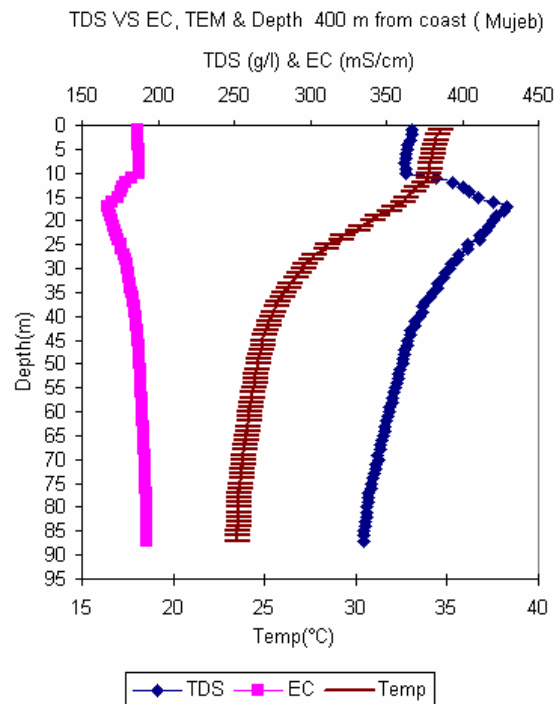
Figure (5-7): EC, TDS and T relationship with the depth in Mujeb area at a distanse of 400 m from the shoreline.

The results of T, TDS and EC for the vertical profiles at station 4, which located in Mujeb area, are shown in (Fig. 5-7). The T profile showed that the T at the Dead Sea water surface was 34.51°C. This value changed very slightly and conceder a negligible change to a depth of 10 m. At a depth of 12 m a shifting change occurred and it decreased sharply to a depth of 43 m and it reached 25.03°C. Finally it continued decreasing but very slightly to a depth of 87 m and it reached 23.51°C.

On the other hand the TDS profile showed that the surface salinity was 366 g/l. This value did not change or very slightly changed until the depth of 10 m, thereafter it increased rabidly after this depth. At 11 m it reached its maximum value at a depth of 18 m below the sea surface. Finally it decreased gradually to the final depth of this profile at 87 m and it reached to 335 g/l.

The EC profile showed that the EC at the surface was 186.4 mS/cm. This value did not change also as the T and TDS profiles or the changes were very slightly and unnoticeable until 10 m depth. From 11 m it changed rapidly and continued decreasing and it reached its minimum value 167.38 at a depth of 18 m. At the last it increased gradually and it reached 192.67 mS/cm at a depth of 87 m below the sea surface. The detailed results for all stations and all profiles are illustrated in (Appendix II).

The above results of T, TDS and EC with the depth can be inerpretated as follows:

The above results showed that the Dead Sea water divides into two layers in summer time and the border between the layers was observed. The upper layer was subdivided into two sub layers (members). The upper most member was different in its thickness related to the distance from the shore and the locations along the shoreline. This upper member characterized with a high temperature, low total dissolved solids and high electrical conductivity. The second member characterized by a very high TDS and the lowest in EC.

The thickness of the upper layer is different. It depends on the distance of the profile from the shoreline and the location. Generally the total thickness of this layer include both members was between 16 and 40 m. The lower layer located beneath the upper layer and it extends from 40 m in average to the final depth of the profiles. The lower layer characterizes with low T and moderate EC and TDS.

The upper layer of the Dead Sea is considered in this study with giving more pay attention to the upper member, because the submarine groundwater is discharged into the Dead Sea at this member as shown in the above results (Figs. 5-4, 5-5, 5-6 and 5-7). In station1 in Sweimah area the thickness of the upper member is 16 m in average and the groundwater discharged at the upper 16 m of the Dead Sea, while the upper member of the Dead Sea thickness in Zarka Ma'in area is 25 m in average and the groundwater discharged into the Dead Sea in the upper 25 m. On the other hand this upper member in station3 in Zara area is 15 m and the groundwater discharged into the Dead Sea in this area in the upper 15 m. Finally the thickness of the upper member in station4 in Mujeb area is 18 m. The groundwater discharged into the Dead Sea in this area in the upper 18 m.

Generally the vertical zones of the discharge into the Dead Sea indicated with a high EC and a low TDS. These results were supported by using the curve in (Fig. 5-2) above.

The T profiles in the (Fig. 5-5 to 5-7) showed that the surface temperatures for the profiles located near the shore was higher than that in the profiles located away from the shoreline, that is because of the thickness of the water layer for the profiles located close to the shores are less than that for the profiles located away from the shore then the solar heating is higher. So the TDS at the surface of all profiles is higher near the shore and lower for the profiles located away from the

shoreline because of the TDS increases with the increasing in temperature. In most of profiles the direct relationship between the TDS and the T is obvious. In other words the TDS is increasing with increasing in T and vice versa. Temperatures for the upper layer in summer are higher than that for the lower layer. The T of the lower layer decreases in the downward direction for all profiles.

On the other hand the inverse relationship between TDS and EC is clear for all the profiles in all stations. This means that in the Dead Sea the TDS are increases when EC decreases. These findings are supported with the findings from the laboratory experiments.

For Interpretation the reason of why the salinity of the second lower member is higher than that of the upper member and higher than that of the lower layer. The following interpretation was suggested:

Because the measurements were carried out during the summer at the end of July, there were no rain between March and July and the temperature was very high at the Dead Sea area at that time. So the evaporation during these four months was very high. As a result the salinity of the surface water of the Dead Sea becomes higher than that for the layer underneath where the fresh groundwater inflows into the Dead Sea. This water floats (upwellings) to the surface and the denser layer at the surface sinks to the depth beneath places where the groundwater discharge happening.

To support this suggestion the densities of the standard salts, which discussed above in this section (table 5-4) were used. The following calculations were done and then it was compared with the ratio between the regular seawater at 0°C and 4°C.

The following weights of salts were added for preparing the initial standard solution (380g/l):

203 g/l of $MgCl_2$, 83 g/l of NaCl and 62.24 g/l of $CaCl_2$ if these weights were transferred to percentages then these values equivalent to:

$MgCl_2$ = 203/380   = 0.53421

NaCl   = 83/380   = 0.21842

$CaCl_2$ = 62.24/380 = 0.1638

First the value of the maximum TDS was suggested to be 450 g/l then we need to add 70 g/l to the initial solution from these three salts to get this value of TDS. Then the weights needed from these salts were calculated as follows:

$MgCl_2$ (g/l) = 0.53421*70 = 37.39

NaCl   (g/l) = 0.21842*70 = 15.29

CaCl$_2$ (g/l) = 0.1638*70   = 11.47

The relationship between the TDS and the densities that discussed in the previous section was plotted as in (Fig. 4-8) and then these curves were used for estimating the density of each added salt.

Then the TDS values after adding each salt to the initial standard salt solution was calculated as follows:

MgCl$_2$ (g/l) = 380 + 37.39 = 417.39

The density was 1.2609 g/cm^3

NaCl   (g/l) = 380 + 15.29 = 395.29

The density was 1.2598 g/cm3

CaCl$_2$ (g/l) = 380 + 11.47 = 391.47

The density was 1.2522 g/cm^3

The density of the initial standard salts solution was 1.2472 g/cm^3

Then the differences of the densities between each salt and the density of the initial standard salt were calculated as follows:

For Mg Cl$_2$ = 1.2609 – 1.2472 = 0.0137 g/cm^3,

For NaCl   = 1.2598 – 1.2472 = 0.0126 g/cm^3,

For CaCl$_2$ = 1.2522 – 1.2472 = 0.005   g/cm^3.

The total of densities differences for the three salts was

0.0137 + 0.0126 + 0.005 = 0.0313 g/cm^3

Then the density of the solution with 450 g/l was

1.2472 + 0.0313 = 1.2785 g/cm^3

Finally the density of solution with TDS 450 g/l and the density of the intial solution with TDS 380 g/l ratio were:

1.2785/1.2472 = 1.0251

Then this ratio was compared with the ratio between the sea water at 0°C and 4°C which is equal

1.0001994/1.0000966 = 1.0001 where the density of the water at 0°C is 1.0000966 g/cm^3 and the density of water at 4°C is 1.0001994.

Then the results showed that the ratio between the density of the salt solution with TDS 450 g/l and density of the solution with TDS 380 g/l was larger than that ratio between the ocean water at the temperature 4°C and 0°C

As well the same procedure were done for the salt solution with TDS 420 g/l the ratio was found as 1.00922 and this ratio also larger than the ratio between the Ocean water at 4°C and 0°C then as a result because the water at 4°C sink beneath water at 0°C then the salt solution with TDS 450 g/l or 420 g/l will sink beneath a salt solution with TDS 380 g/l.
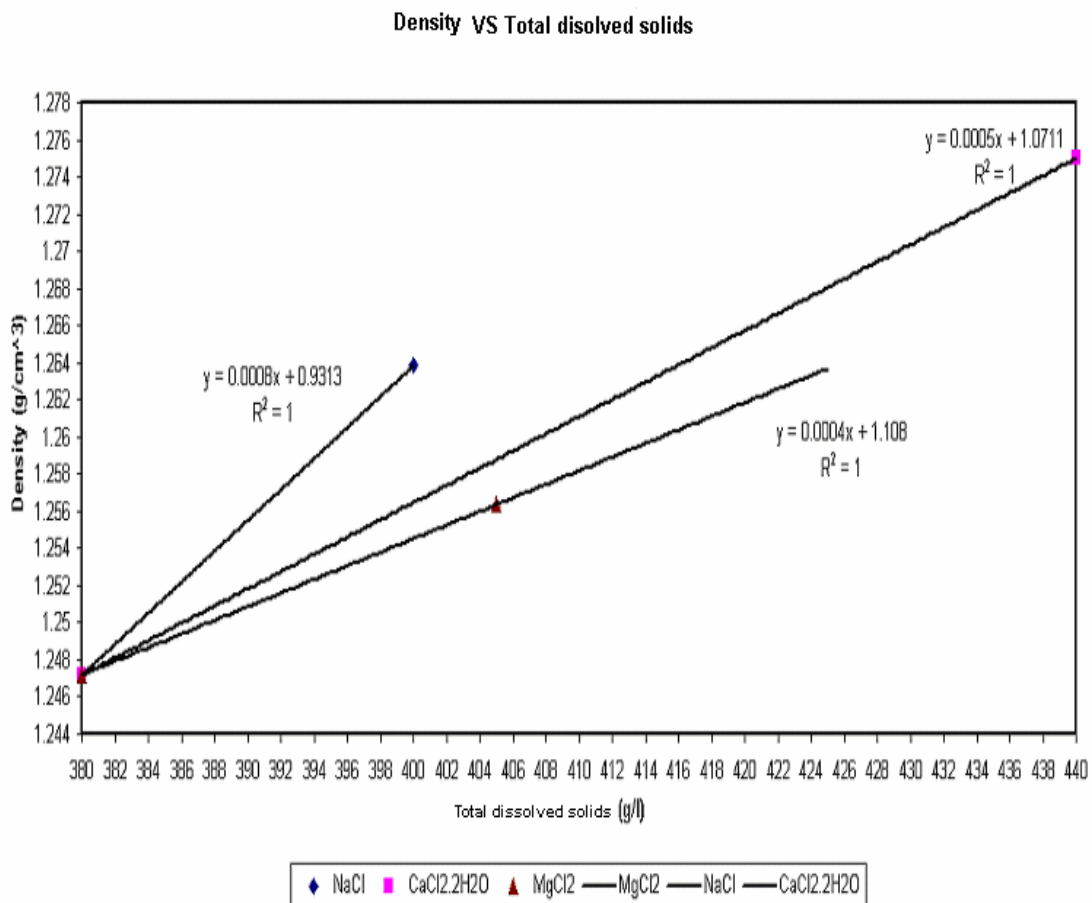
Figure (5-8): Relationship between TDS and densities of the standard salts solution

5.2. Chemical Tracer (Radon-222)

The long of zone of ground water discharge in Sweimah area (station1) is about 7 km, for Zarka Ma'in and Zara (station2 and station3) is about 5 km and in Mujeb area (station4) is about 5 km figure (5-9).
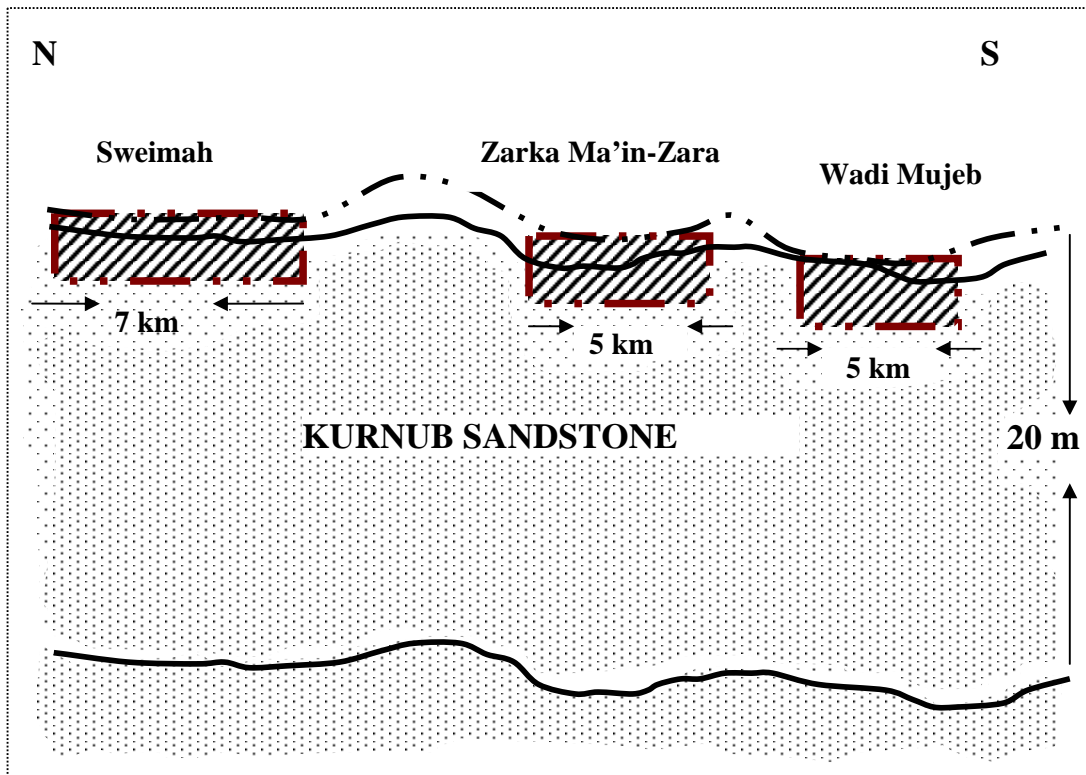
Fig. (5-9): Sketch diagram for the zones of discharge along the DS

In station 1 (S_{rn1}) located in Sweimah area at the northeastern corner of the Dead Sea, the total ^{222}Rn concentration at the depth profile in the water column at the distance 20 m away from the shoreline reached its maximum concentration 2520 Bq.m^{-3} (151200 dpm.m^{-3}) at depth 12 m underneath the sea surface. This concentration decreased up-ward and downward of this depth. It reached to about 1740 Bq.m^{-3} at depth of 20 m, 1580 Bq.m^{-3} at the depth of 7 m, 1890 Bq.m^{-3} at the depth of 4 m and it reached to 1140 Bq.m^{-3} at the depth of 2 m underneath of sea surface. These results will be used to calculate the ^{222}Rn decay, diffusion, and advection. The other samples results at this area around the main station showed that:

In the area located to the north of the main station with a distance about 800 m. The concentration was about 2190 at depth of 12 m and a distance about 50 m away from the shoreline, 1230 Bq.m^{-3} at the depth of 12 m and distance about 200 m from the shoreline, about 1950 Bq.m^{-3} at depth of 12 m and a distance of 300 m

away from the shoreline to the west. It concentration was about 2140 Bq.m^{-3} at the distance about 1000 m to the north of the main station and about 200 m away from the shoreline. At a location south of the main station with about 4500 m the results showed that the concentration was 2150 Bq.m^{-3} at the distance of about 60 m away from the shoreline at the depth 12 m underneath the sea water and about 1300 Bq.m^{-3} at depth of 20 m at the same distance away from the shoreline. At a depth of 12 m and distance of about 200 m away from the shoreline the concentration was 1440 Bq.m^{-3}. On the other hand the concentration was 1310 Bq.m^{-3} at the same location but the distance about 300 m away from the shoreline, and at about 700 m away from the shoreline the concentration was 1150 Bq.m^{-3}.

The results at the main station 2 (S_{rn2}) which located in Zarka Ma'in area at a distance of about 25 m away from the shoreline showed that the maximum ^{222}Rn concentration was 2180 Bq.m^{-3} (130800 dpm.m^{-3}) at depth of 7 m. It reached to about 1870 Bq.m^{-3} at a depth of 12 m, about 1310 Bq.m^{-3} at a depth of 24 m underneath the Dead Sea level, about 2080 Bq.m^{-3} at a depth of 4 m and about 870 Bq.m^{-3} at 2 m depth beneath the sea surface. These results also will be used calculate the radon-222 inventory (decay), diffusion and advection. As well the other samples analyzed at different distance from the main station and different distances away from the shoreline showed that the ^{222}Rn concentration at same location of the main station but at the distance of 10 m away from the shoreline and a depth of 4 m the ^{222}Rn concentration was 2140 Bq.m^{-3}. It was 2060 Bq.m^{-3} at distance about 40 m away from the shoreline. But at the location far away from the main station with about 300 m to the north the ^{222}Rn concentration was 1960 Bq.m^{-3} at the distance of about 10 m away from the shoreline and at a depth of about 4 m and about 680 Bq.m^{-3} at the distance of about 40 m away from the shoreline and at a depth of 4 m underneath the sea surface. On the other hand the concentration was about 2220 Bq.m^{-3} at the location about 800 m north of the main station, about 10 m away from the shoreline and depth of 4 m.

The maximum concentration of ^{222}Rn in the main station 3 (S_{rn3}) at distance of about 25 m away from the shoreline was 1780 Bq.m^{-3} (106800 dpm.m^{-3}) at a depth of 12 m. It decreased to 1000 Bq.m^{-3} at a depth of 24 m underneath the sea surface, and 1690 Bq.m^{-3} at the depth of 7 m. It was 1530 Bq.m^{-3} at a depth of 4 m and 1290 Bq.m^{-3} at a depth of 2 m below the sea surface. To the west of this main station the concentration was 1070 Bq.m^{-3} at depth of 12 m and at a distance of about 50 m away from the shoreline. As well the concentration at a location of 150 m north of the main station was 2520 Bq.m^{-3} at a depth 12 m and a distance about 15 m away from the shoreline and it was 1930 Bq.m^{-3} at a depth of 12 m and a distance about 30 m away from the shoreline. On the other hand at the location of about 500 m to the north of the main station the radon-222 concentration was 1560 Bq.m^{-3} at a depth of 12 m and at a distance of about 20 m away from the shoreline and it was 1230 Bq.m^{-3} at a depth 12 m and a distance of about 50 m away from the shoreline at this location. At the location about 500 m south of the main station3 the concentration was 2240 Bq.m^{-3} at the depth of 12 m and a distance of

about 20 m away from the shoreline. It was 1910 Bq.m^{-3} at a depth of 12 m and a distance of about 40 m away from the shoreline. At this location at a depth of 4 m and distance of about 20 m away from the shoreline the concentration was 2100 Bq.m^{-3}, at the distance of 30 m away from the shoreline the concentration was 1900 Bq.m^{-3} at 4 m depth and it was 1390 Bq.m^{-3} at a depth of 4 m and distance of about 40 m away from the shoreline. It was 710 Bq.m^{-3} at a distance of about 50 m away from the shoreline and depth of 4 m at this location. At a location of about 1000 m south of the main station the ^{222}Rn concentration at a depth of 12 m was 2700 Bq.m^{-3}, 2200 Bq.m^{-3} and 1440 Bq.m^{-3} at a distances of about 20 m, 50 m and 200 m away from the shoreline respectively. The concentration at a location about 2500 m south of the main station3 was 2790 Bq.m^{-3} at a depth of 12 m and a distance of about 20 m away from the shoreline.

In the station4 (S$_{rn4}$), which was located in Mujeb area, the ^{222}Rn concentration at a distance of about 25 m away from the shoreline was 640 Bq.m^{-3} (38400 dpm.m^{-3}) at depth of 2 m underneath the Dead Sea surface, 990 Bq.m^{-3} (59400 dpm.m^{-3}) at a depth of 4 m, 670 Bq.m^{-3} (40200 dpm.m^{-3}) at a depth of 7 m, the maximum concentration was 1780 Bq.m^{-3} (106800 dpm.m^{-3}) at a depth of 12 m and it was 820 Bq.m^{-3} (49200 dpm.m^{-3}) at the depth of 24 m underneath the sea surface. All the results of radon-222 concentrations are illustrated in (Appendix III).

The concentration values at the depth of 2 m and 7 m at station3, and Station 2 at 2 m depth were not representative because the internal humidity of RAD7 was higher than that required. It was about 35% but it must be equal or less than10%.

The radon-222 concentration results in the main four stations are plotted in (Fig. 5-10).
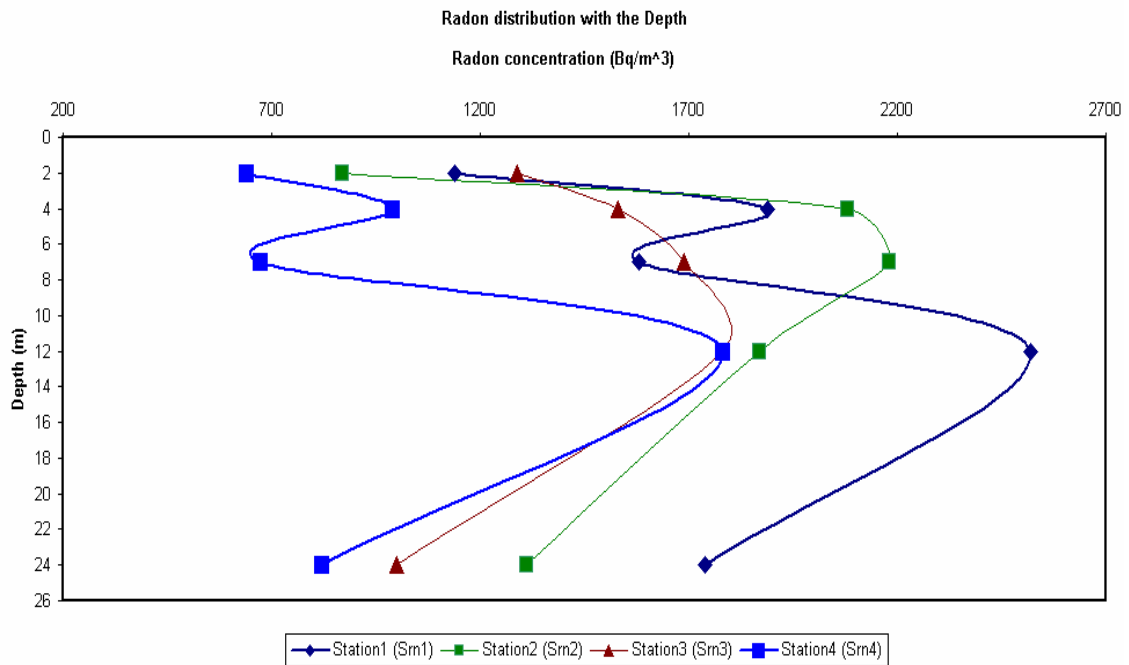
Figure (5-10): Radon-222 distribution with the depth in the main stations

Figure (5-10) showed that the radon-222 concentrated at the upper 20 m of the Dead Sea. The highest concentrations were at a depth of 12 m in Sweimah, Zara and Mujeb areas, while the highest concentration was at a depth of 7 m in Zarka Ma'in area. This means that there is groundwater discharged into the Dead Sea from the upper 20 m with maximum rates at a depth of 12 m below surface.

These findings coincide with the findings from the EC-T results for the four stations along the Dead Sea as shown in figures (5-11) to (5-14).
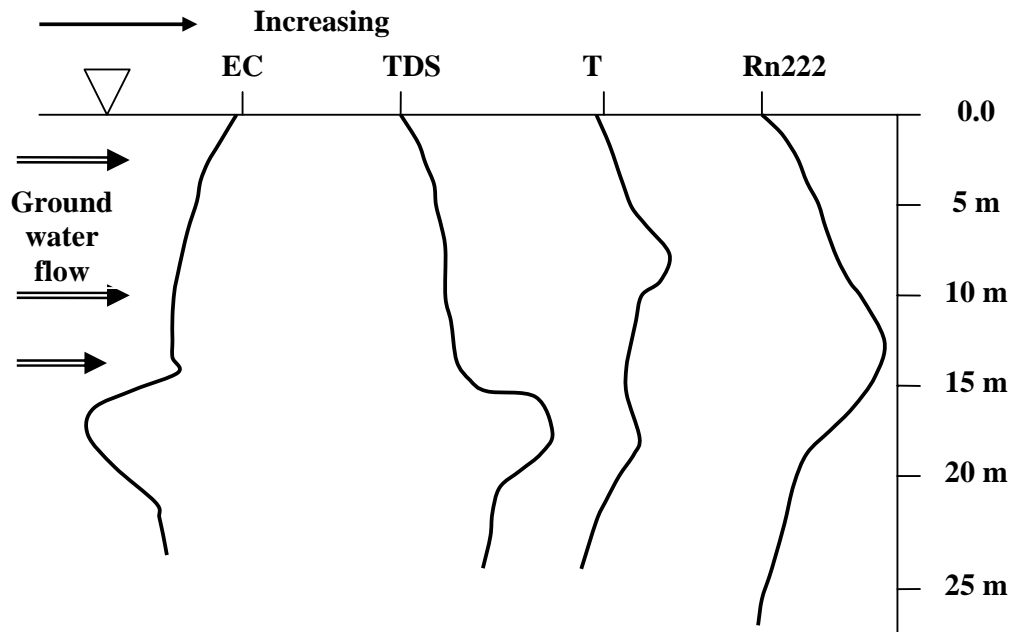
Figure (5-11): Schematic diagrams for EC, TDS, T and Rn222 showing the groundwater flow zone in Sweimah area.
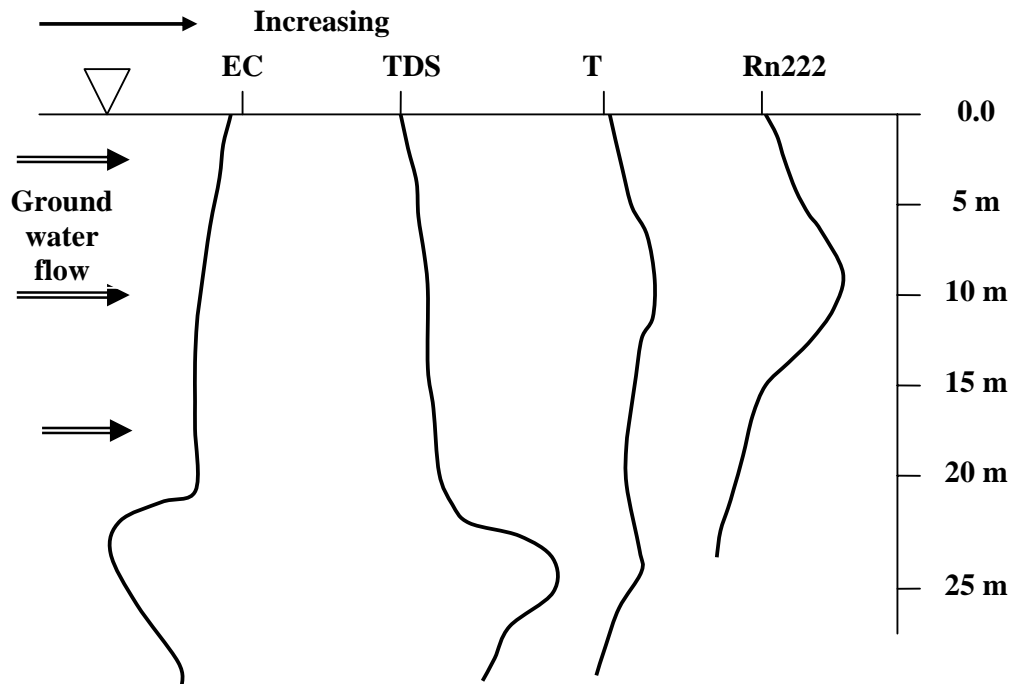
Figure (5-12): Schematic diagrams for EC, TDS, T and Rn222 showing the groundwater flow zone in Zarka Ma'in area.
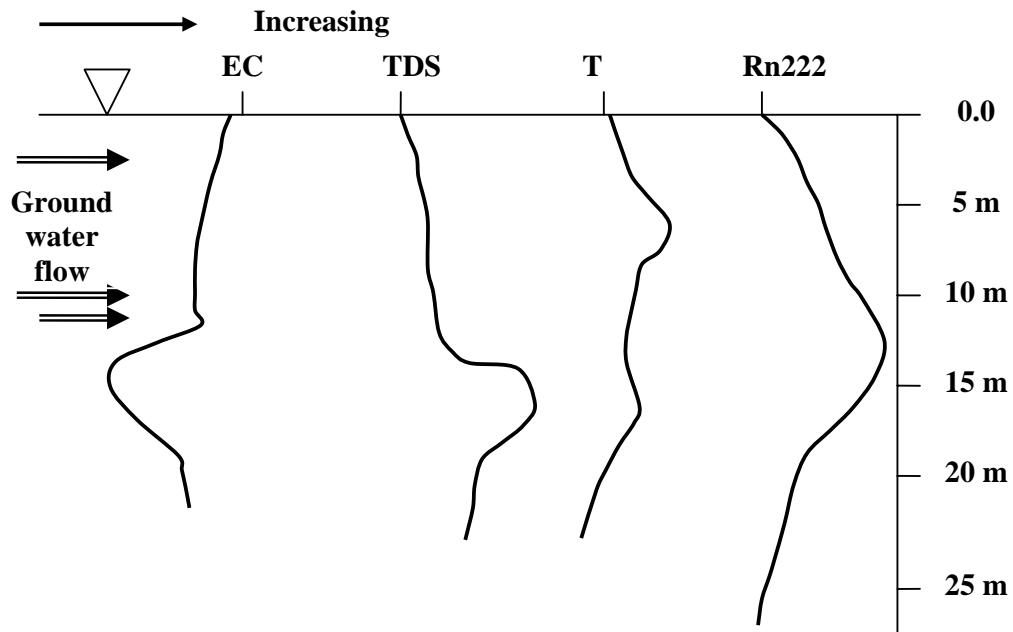
Figure (5-13): Schematic diagrams for EC, TDS, T and Rn222 showing the groundwater flow zone in Zara area.
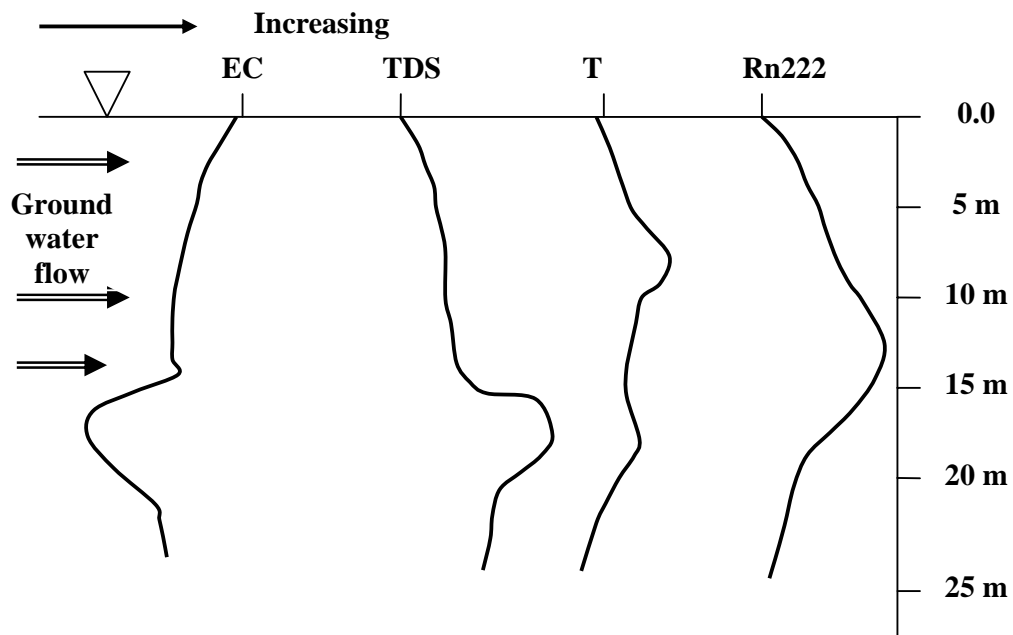
Figure (5-14): Schematic diagrams for EC, TDS, T and Rn222 showing the groundwater flow zone in Mujeb area.

The distributions of radon concentrations with the distance parallel to the shorte and with the depth were plotted using surfer (Fig. 5-15). This figure shows that highly concentrations are found in Station2 in Zarka Ma'in area and moderate concentrations in station3 in Zara and station1 in Sweimah area. The lowest concentrations are found in station4 in Mujeb, which might be the area with lowest groundwater discharge. The highest concentrations were found at a depth 12 m. Generally the maximum ^{222}Rn concentrations of the seawater were found close to the shoreline and it decreasing with increasing the distances away from the shoreline. This means that the maximum groundwater flow might be closed to the shores of the Dead Sea.
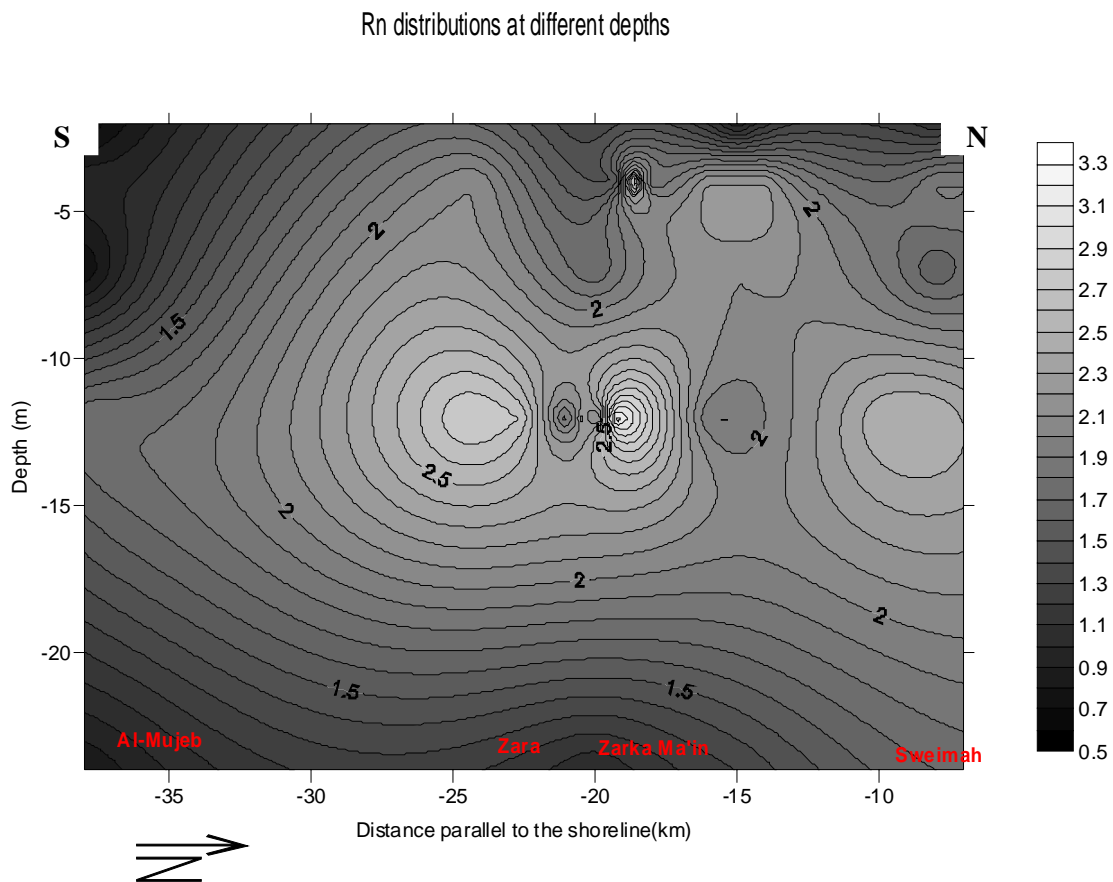
Figure (5-15): Radon-222 concentrations with the depth and distance N-S direction

The following general equation was used to calculate the radon budget:

$$J_{benthic} + J_{production} - J_{atm} - J_{decay} - J_{outflow} = 0 \qquad (1)$$

$J_{benthic}$: Flux of radon across the sediment-water interface consisting of a diffusion component of Rn from bottom sediments into overlying lake water ($J_{diffusion}$) and an advective component of Rn-rich groundwater through sediments ($J_{advective}$), $J_{production}$ is the production of ^{222}Rn in the water column by Ra^{226} decay, J_{atm} is the ^{222}Rn loss across the air-water interface, J_{decay} is the ^{222}Rn decay in the water column, $J_{outflow}$ is surface outflow of ^{222}Rn-rich water from the sea.

The approach was to assess all flux terms to estimate the total benthic flux required to support the ^{222}Rn inventory

$$J_{benethic} = J_{atm} + J_{decay} + J_{outflow} - J_{production} \qquad (2)$$

Equation (2) has been simplified to equation (3) because there is no outflow from the Dead Sea.

$$J_{benethic} = J_{atm} + J_{decay} - J_{production} \qquad (3)$$

If the total benthic flux exceeds the independently estimated diffusive flux from the bottom sediments, then the advective component can be calculated by the following equation.

$$J_{advective} = J_{benethic} - J_{diffussion} \qquad (4)$$

5.2.1. Radon Inventory and Radon Decay

Radon inventory is defined as the radon concentration at the water column gradient with the water depth column. After determining the concentration of ^{222}Rn the inventory was calculated by integrating the total radon concentrations over water depth.

$$C_{Rn} (I) (Bq.m^{-2}) = total\ ^{222}Rn (Bq.m^{-3}) * water\ depth (m) \qquad (5)$$

C_{Rn} is the radon inventory. The total radon is the concentration of supported and unsupported ^{222}Rn.

^{222}Rn inventories were calculated for each station separately follows:

The total radon-222 concentration at specific depth was multiplied by the difference of the depth between two succession samples. After that the results of each station were added to get the total inventory for the all samples for each station.

- The total inventory At station1 (S_{rn1}) was

1200 ($Bq.m^{-3}$) * 2 m (the difference of the depths between of this sample and the depth of the next sample) = 2400 ($Bq.m^{-2}$)

1900 (Bq.m^{-3}) * 4 m   = 5700 (Bq.m^{-2})

1600 (Bq.m^{-3}) * 5 m   = 8000 (Bq.m^{-2})

2500 (Bq.m^{-3}) * 12 m = 30,000 (Bq.m^{-2})

1700 (Bq.m^{-3}) * 2 m (The difference between the final depth -26 m- and the depth of the sample –24 m-) = 3400 (Bq.m^{-2}).

The total inventory for the first station was 49,500 (Bq.m^{-2}) (i.e. the total of the above values).

- The total inventory at station 2 (S$_{rn2}$) was calculated as that in the first station and it was 61,100 (Bq.m^{-2}).

- The total inventory at station 3 (S$_{rn3}$) was calculated as 39,200 (Bq.m^{-2}).

- The total inventory at station 4 (Srn4) was calculated as 30,900 (Bq.m^{-2}).

The Decay of ^{222}Rn not supported by the decay of ^{226}Ra in the water column is the most important term and must be considered in the ^{222}Rn balance. This term can be calculated by using the radon inventory for the whole water column multiplyed by the ^{222}Rn decay constant (λ) (expressed in day $^{-1}$ which is equal 0.181 day^{-1}) according to the following equation:

J $_{decay}$ = λ C$_{Rn}$ (6)

Then the decay of radon-222 in the station 1 (S$_{rn1}$) was calculated as follows:

J $_{decay}$ = 0.181 * 49,500 = 8959.5 Bq/m^{-2}.day

The decay in station 2 was calculated in the same way and gave 11059.1 Bq/m^{-2}.day

The decay in station 3 (S$_{rn3}$) was 7095.2 Bq/m^{-2}.day. Finally the decay in station 4 (S$_{rn4}$) was calculated as 5592.9 Bq/m^{-2}.day.

5.2.2. Radon Loss to the Atmosphere

One of the important loss terms especially in shallow water is loss to the atmosphere. Radon losses by atmospheric evasion were calculated for each measurements station. The radon gas flux across air-water interface depends on the molecular diffusion produced by the concentration gradient across this interface and turbulent transfer governed primarily by wind speed above the sea surface.

The gas exchange equations presented by Macintyre et al. (1995) were used to calculate the flux (J_{atm}) of radon across sea-air interface using the radon concentration gradient, the surface water temperature, and the wind speed above the sea surface.

$$J_{atm} = k (C_w - \alpha \, C_{atm}) \tag{7}$$

Where C_w and C_{atm} are the concentration of the gas of inters in surface water and Air respectively and the units are ($Bq.m^{-3}$); α is Ostwald's solubility coefficient which deafens the distribution of radon between the water and air phases (dimensionless); and k is the gas transfer coefficient dependent on the wind speed (Jahne et al. 1987, MacIntyre et al. 1995 and Corbett et al. 1997). It is a function of the physical processes at the air–sea boundary, especially the turbulence and kinematics viscosity of the water (v), and the Molecular diffusion coefficient of the gas D_m, where $D_m = 1.7317 *10^{-5}$ $cm^2.s^{-1}$ at 36°C for the radon. The Schmidt number (Sc) is the ratio of the kinematics viscosity to the molecular diffusion coefficient.

$Sc = v/D_m$ (dimensionless).

$D_m = 10^{(-((980/(273+T)) + 1,59)}$.

$K = ((0.45 * (\text{wind speed})^{1.6} * ((Sc/600)^{-0.667}))/100) / 60$

$\alpha = 0.105 + 0.405 \, e^{(-0.05027 * T)}$.

Both wind speed and temperature are very important in controlling the loss of radon across the sea surface while the concentration of radon in the air has less importance, especially when the radon activity in the water is relatively high at the wind speed above 5 $m.s^{-1}$, while it is much less important when the wind speed under 2 $m.s^{-1}$ (Burnett et al. 2003).

The radon in atmosphere was estimated as 7 Bq/m^3, the radon concentration at the surface was considered as the radon concentration at 2 m depth for all the stations. The wind speed was taken as 3m/s. water temperature was measured between 36 and 38°C.

The radon loss to the atmosphere at the station1 (S_{rn1}) was calculated by using equation 7 above:

J_{atm} = 0.000519 m/min (1200 Bq/m^{-3} − 0.17129849 * 7 Bq/m^{-3}) = 0.66217 Bq/m^2.min

This value was multiplied by (60 * 24) to transfer to unit of Bq/m^2.day. Then the radon loss to the surrounding atmosphere in station 1 was 895 Bq/m^2.day.

The same calculations were made for the other thee stations and the radon loss to atmosphere results were as the following:

The loss to atmosphere in station 2 (S_{rn2}) was 692.73 Bq/m^2 .day. While in station 3 (S_{rn3}) the result was 1001 Bq/m^2.day and in station 4 (S_{rn4}) the radon loss to the surrounding atmosphere was 596.69 Bq/m^2.day.

5.2.3. Radon Input via Diffusion from the Sediments

All sediments contain some amounts of uranium and daughter products including radon. Thus diffusion of ^{222}Rn from the bottom sediments into the overlying seawater may be it provides some unsupported radon into standing bodies of water and must be evaluated as part of an overall radon budget. These diffusive ^{222}Rn fluxes were obtained using a sediment equilibration technique, and radon flux was estimated using the following equation, which developed by (Martens et al. 1980).

$$J_{sedm} = (\lambda D_s)^{1/2} (C_{eq} - C_0) \tag{8}$$

D_s are the effective wet bulk sediments diffusion coefficient in the sediments (m^2 day^{-1}) corrected for temperature and sediment tortuosity.

C_{eq} is the radon concentration in pore fluids in equilibrium with radium in the sediments, determined by the sediment equilibration experiments (Bq.m^{-3}). C_0 is the radon concentration in the overlying water at the sediment-water interface. Ds is a wet sediment diffusion coefficient (m^2/day).

$D_s = \Phi D_0$ (Ullman and Aller 1981).

The expression for the temperature dependency of D_s is outlined in Peng et al. (1974). The ^{222}Rn molecular diffusivity coefficient (D_0) is 14.2*10 $^{-5}$ m^2/day at 36°C. Then to get the wet bulk sediments diffusion coefficient (D_s) this value was multiplied by the porosity of each soil. It equals 3.98 * 10^{-5} m^2/day at station 1, where the porosity was 0.45-0.48

The C_{eq} at the station1 was 0 .0016 Bq/g, the bulk density of the soil was 2.07 g/cm^{-3} then the C_{eq} for wet sediment was (0.0016*2.07) = 0.003312 Bq/cm^3 which is equal to 3312 Bq/m^3. Radon-222 concentration was 1700 Bq/m3 at the bottom sediments. The porosity of the sediments was 0.45-0.48. Then the C_0 was obtained by multiplying the radon concentration at the bottom sediments by the porosity. C_0 was equal to 476 Bq/m^3 at station1.

The radon input via sediments at the station 1 (S_{rn1}) was calculated as the following

J_{sedm} = (0.181* 3.98 * 10^{-5}) $^{1/2}$ (3312 – 476)   = 7.61 Bq/m^2.day in station1 (S_{rn1}). The diffusion via sediments at the station2 (S_{rn2}) was 7.74 Bq/m^2.day, at station 3 (S_{rn3}) it was 7.81 m^2.day and at station4 (S_{rn4}) was 5.73 Bq/m^2.day.

5.2.4. Radon Production

The additional inputs to the seawater are the Ingrowths (production) from Ra^{226} dissolved in the water column, which can be estimated by using the following equation:

$$J_{production} = C_{Ra} * h * \lambda \qquad\qquad (9)$$

C_{Ra} represents the average concentration of ^{226}Ra in the Dead Sea; h is the depth of the Dead Sea layer under investigation.

C_{Ra} was measured for some samples. Some samples were analyzed for radon activity, sealed for approximately 4 weeks, and then analyzed a second time for radon emanation. Radon emanation was considered to be equivalent to radium activity in these samples (Benoit et al. 1991). The depth was taken as 26 m for the investigated area, and λ is equal as before (0.181 day^{-1}). The average radon emanation was taken as the equivalent of ^{226}Ra at equilibrium with ^{222}Rn after 4 weeks storage. It was 1020 Bq.m^{-3} at the station 1 (S_{rn1}), in tation 2 (S_{rn2}) was 1050 Bq.m^{-3}, it was 1040 Bq.m^{-3} in station3 (S_{rn3}) and it was 640 Bq.m^{-3} in station 4 (S_{rn4}).

Then the radon-222 production for the first station (S_{rn1}) was calculated by applying equation 9 above:

$J_{production}$ (Bq.m^{-2}.day)= 1020 (Bq.m^3) * 26 (m) * 0.181 (day^{-1}) = 4800.12 Bq.m^{-2}.day.

The radon productions from ^{226}Ra in the other stations were as follows:

At station2 (S_{rn2}) it was 4941.3 Bq.m^{-2}.day, at station3 (S_{rn3}) was 4894.24 Bq.m^{-2}.day and at station4 (S_{rn4}) it was 3011.84 Bq.m^{-2}.day

5.2.5. Final Calculations

The $J_{benethic}$ were calculated for all the stations by using equation (3) above as the following:

The $J_{benethic}$ for station 1 (S_{rn1}) was

$J_{benethic}$ (Bq.m^{-2}.day) = 895.41 (Bq.m^{-2}.day) + 8959.5(Bq.m^{-2}.day) - 4800.12 ((Bq.m^{-2}.day) = 5054.79 (Bq.m^{-2}.day).

Then to calculate the $J_{advective}$ for all stations equation (4) was used. The advection at station 1 (S_{rn1}) was:

$J_{advective}$ (Bq.m^{-2}.day) = 5054.79 (Bq.m^{-2}.day) – 7.61(Bq.m^{-2}.day) = 5046.39 (Bq.m^{-2}.day).

The same calculations were done to the other stations. The $J_{benethic}$ for the station2 (S_{rn2}) was 6810.53 (Bq.m^{-2}.day), and $J_{advective}$ was 6802.79 (Bq.m^{-2}.day). The $J_{benethic}$ at station3 (S_{rn3}) was 3107.84 (Bq.m^{-2}.day) and $J_{advective}$ was 3147.09 (Bq.m^{-2}.day). The $J_{benethic}$ at the station4 (S_{rn4}) was 3177.7 (Bq.m^{-2}.day) and the $J_{advective}$ was 3171.97 (Bq.m^{-2}.day). All the results were summarized in the table (4-5).

Table (5-5): Radon-222 results of inventory, decay, advection, diffusion and production.

Station name	^{222}Rn Inv. (Bq.m^{-2})	J_{decay} (Bq.m^{-2}.day)	J_{atmos} (Bq.m^{-2}.day)	$J_{diffussion}$ (Bq.m^{-2}.day)	$J_{production}$ (Bq.m^{-2}.day)	$J_{benethic}$ (Bq.m^{-2}.day)	$J_{advective}$ (Bq.m^{-2}.day)
S_{rn1}	49500	8959.5	895.41	7.61	4800.12	5054.79	5046.39
S_{rn2}	61100	11059.1	692.73	7.74	4941.3	6810.53	6802.79
S_{rn3}	39200	7095.2	1001	7.81	4894.24	3107.84	3147.09
S_{rn4}	30900	5592.9	596.64	5.73	3011.84	3177.7	3171.97

5.2.6. Radon Concentration in the Groundwater and Advection Rate

^{222}Rn activities in the groundwater obtained from springs located around the Dead Sea shows a little variation. Activities ranged from 28100 Bq.m^{-3} to 69300 Bq.m^{-3} (1368 * 10^3 to 4158 *10^3 dpm.m^{-3}) (n=14). The maximum value in Sweimah area is 45900 Bq.m^{-3} the minimum value is 30100 Bq.m^{-3} and the range [(Maximum + minimum)/2] of the radon concentration in the groundwater in this area is 38000 Bq.m^{-3}. In Zarka Ma'in area the maximum, minimum and range values were 51400 Bq.m^{-3}. The maximum value of Rn-222 activity in groundwater in Zara area is 62600 Bq.m^{-3}, the minimum value is 32800 Bq.m^{-3} and the range is 47700 Bq.m^{-3}. The maximum Rn-222 concentration in the groundwater in Mujeb area is 69300 Bq.m^{-3}, the minimum value is 28100 Bq.m$^-$3 and the range is 48700 Bq.m$^-$3. Table (4-5) shows the ^{222}Rn concentrations and electrical conductivity for the springs and seepages surrounding the Dead Sea shores.

Table (5-6): Radon-222 concentrations and EC in the springs
and seepages surrounding the Dead Sea.

Springs Name	Rn-222 Bq/l	Station No.	EC (mS/cm)
Seepage-DS coast-N.Hotels	33.4	S_{rn1}	39
Seepage-DS coast-Hotels	45.9	S_{rn1}	22.1
Azrak-Sweimah	30.6	S_{rn1}	5.6
Hamdi Anis	30.1	S_{rn1}	6.1
Zarka Ma'in	51.4	S_{rn2}	2.7
Zara-Hotspring1	62.6	S_{rn3}	2.5
Zara-Hotspring22	53.9	S_{rn3}	2.2
Zara-Hotspring23	60.8	S_{rn3}	2.4
Zara-Hotspring24	32.8	S_{rn3}	2.54
Seepage-DS coast	38.2	S_{rn3}	4.2
Homrt Main-DS coast	53.7	S_{rn4}	4.8
Ein Skeen1-G.Mazra	30.6	S_{rn4}	1.3
Ein Skeen2-G.Mazra	28.1	S_{rn4}	1.1
Al-Moruaha-G. Hadithah	69.3	S_{rn4}	11.5
Al-Haditha-G. Haditha	48.8	S_{rn4}	0.9

The advection rates for all the stations were calculated as dividing the advection ($J_{advection}$) values, which calculated above over the range value of the radon-222 concentrations in the groundwater, where the advection rate is equivalent to the groundwater velocity. Then the total amount of the groundwater discharge (m3/day, year) is equal the advection rate multiplying by the area (m^2) of the discharge.

The advection rate in station1 (S_{rn1}) was = 5046.39 (Bq/m^2.day) / 38000 (Bq/m^3) = 0.1328 m/day

The advection rate in station2 (S_{rn2}) was = 6802.79 (Bq/m^2.day) / 51400 (Bq/m^3) = 0.1324 m/day

The advection rate in station3 (S_{rn3}) was = 3147.09 (Bq/m^2.day) / 47700 (Bq/m^3) = 0.066 m/day

The advection rate in station 4 (S_{rn4}) was = 3171.97 (Bq/m^2.day) / 48700 (Bq/m^3) = 0.0651 m/day

The areas of the groundwater discharges were estimated using the maps of the area and the thermal infrared images.

The area of groundwater discharge in Sweimah was estimated about 2,800,000 m^2, the area of discharge in Zarka Ma'in area, in Zara area and in Mujeb are 2,660,000 m^2, 1,400,000 m^2 and 2,000,000 m^2 respectively.

Then the total amount of groundwater discharge into the Dead Sea in station1 was 135.7 MCM/y, in station2 was 128.5 MCM/y, in station3 was equal 33.7 MCM/y and the amount of submarine groundwater discharge into the Dead Sea in station 4 was equal 90.3 MCM/y.

Finally the total amount of the submarine groundwater discharge into the eastern shoreline of Dead Sea is equal the sum of the discharges in all stations which equals 388.3 MCM/y. This value was compared with the amount of discharge was obtained from the water budget technique which was 480 MCM/y (million cubic meter per year). The difference is due to the amount of the discharge using the water budget was for the whole Dead Sea (the west and east sides) while the discharge estimated using radon technique was for the eastern shoreline.

5.3.   Estimating SGD by Using Mixing Technique for TDS

To estimate the groundwater discharge into the Dead Sea the schematic sketch in figure (5-16) was considered.
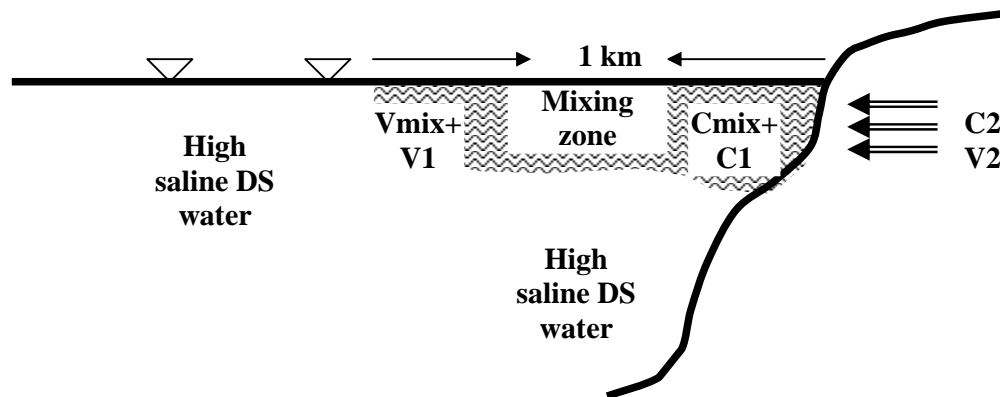
Figure (5-16): Schematic diagram of SGD and the mixing zones

To estimate the submarine groundwater discharge into the DS by using mixing technique depends on the TDS the following equations were used:

V1 * C1 + V2 * C2 = V$_{mix}$ * C$_{mix}$

V1 + V2 = V$_{mix}$

Where the V1 is the volume of the DS water at the mixing zone, Vmix is the total volume of the mixing zone, V2 is the volume of the submarine groundwater discharging into the DS at the mixing zone, C1 is the TDS of the DS water before mixing, C2 is the TDS of the submarine groundwater and Cmix is the TDS of the DS water after mixing with submarine groundwater.

V1 = V$_{mix}$ - V2

(Vmix – V2) C1 + V2 * C2 = Vmix * Cmix

V2 =[(Vmix * Cmix) – (Vmix * C1)] / (C2-C1)

The quantity of the submarine groundwater discharging (V2) into the DS in Sweimah area is:

V2 (in Sweimah) = [(112 MCM * 293 g/l) – (112 MCM * 405 g/l)] / (26 g/l – 405 g/l) = 33.1 MCM for the period from last winter on march until the time of carrying out the measurements on July (4 months) then this quantity of submarine groundwater discharge into the DS in Sweimah area is 33.1 MCM/4 months. Therefore the total amount of discharge into the DS in Sweimah area in the year is 33.1 MCM times 3 which is equal **100 MCM/y.**

The submarine groundwater discharge into the DS (V2) in Zarka Ma'in and Zara area is:

V2 (in Zarka Ma'in and Zara) = [(100 MCM * 311 g/l) – (100 MCM * 391 g/l)] / (18 g/l – 391 g/l) = 21.5 MCM/4 months and the total quantity in the year is 21.5 MCM times 3 which equals **65 MCM/y**

The discharge (V2) into the DS in Mujeb area is:

V2 (in Mujeb) = [(90 MCM* 366 g/l) – (90 * 388)] / (18 g/l – 388 g/l) = 5.4 MCM / 4 months. Therefore the total discharge into the DS in Mujeb area in the year is 5.4 MCM times 3 which is equal **16.2 MCM/y**

Then the total submarine groundwater discharge into the DS is:

100 + 65 + 16.2 = 181.2 MCM/y.

5.4.   Estimating SGD by Using Darcy's Law.

For estimating the groundwater discharge into the DS by using one-dimensional Darcy's law the following equation was used:

Q = A * K * (Δh/L)

Where,

Q is volumetric flow rate (m^3/s), A is flow area perpendicular to L (m^2), K is hydraulic conductivity (m/s), L is flow path length (m) and h is hydraulic head (m).

The average area of discharge was estimated as:

A   = 55000 m * 18 m = 990000 m

K   = 4.48 * 10^{-5} m/s (Salameh and Udluft, 1985)

Δh/L = 0.04 (Salameh and Udluft, 1985)

Q = 990000 * 4.48 * 10^{-5} * 0.04 = 1.8 m/s (which equals 57 MCM/y).

The quantities of the groundwater discharge estimating from radon222, mixing of TDS, and Darcy's' law in addition to water balance are listed in table 5-7

Table (5-7): The quantities of groundwater discharge estimating from the different methods

Method	Discharge (MCM/y)	Errors
Rn222	388	In measurements, in internal humidity of the RAD7 device, very low errors due to water density,
Mixing	181	Don't consider the horizontal mixing along the DS, don't consider the volume of dissolved salt from the salt layer at the coast.
Darcy	57	Don't consider the circulation, estimated as a steady state and homogeneity formation along the DS, lack of the information for the hydraulic conductivity and hydraulic gradient for lower aquifer in east of the DS area and no data for them at the distance less than 5 km to the east of the coast of the DS,
Water balance	480	Calculated for the whole DS (i.e. east and west shores), evaporation estimation, don't consider the water circulation.

The above results of the estimation of the SGD showed that the SGD might be between 200 and 300 MCM/y.

5.5. Thermal Infrared Imagery (TIR)

Field conditions for the imagery survey were ideal and the resolution of thermal signatures from upwelling groundwater was clear. The results of the thermal imagery survey indicate that there are groundwater discharge zones into the Dead Sea. These zones are characterized by high temperature compared to other zones where no discharges occur. In wintertime the temperature of the groundwater in the Dead Sea surrounding areas is higher than that of the surface water of the Dea Sea itself.

Figure (5-17) illustrates groundwater discharge zones in the areas of Zarka Ma'in, Zara and Mujeb and the coordinates for these zones. The thermal infrared images show that the highest groundwater discharges are found close to the Dead Sea

shorelines. These results are match well with the results obtained from the radon-222 technique. The images show also that the zones of the discharges in Zara, Zarka Ma'in and Mujeb areas are match with the results obtained by using the electromagnetic radiation technique (EMR) (section 5.4).

The main discharge zone obtained from the thermal infrared images in Zarka Ma'in area has coordinates 31.61080324 N and 35.56301848 E (Decimal coordinate), the other main zone in the same area has coordinate 31.59574664 N and 35.55765117 E. On the other hand the main discharge zones in Zara area lie between coordinates of 31.57230500 N, 35.55385840 E and 31.57050383 N, 35.55395937 E, while in Mujeb area it lie at 31.46635725 N and 35.56297085 E.

Some discharge zones and the coordinates are listed in table (5-8).

Table (5-8): Coordinates of some of the discharge zones along the eastern shoreline of the Dead Sea.

Area name	Coordinate (Geographic decimal)		Coordinate	
	N	E	N	E
Zarka Ma'in	31.60044167	35.56063333	31.59574664	35.55765117
	31.61080324	35.56301848	31.59305540	35.55727731
Zara	31.57615524	35.55411354	31.57230500	35.55385840
	31.57050383	35.55395937	31.56883709	35.55376381
	31.56421919	35.55333771	31.56344255	35.55361671
	31.56073928	35.55384319	31.55958030	35.55396167
	31.54414031	35.55489140		
Mujeb	31.46635725	35.56297085	31.45092313	35.56359963
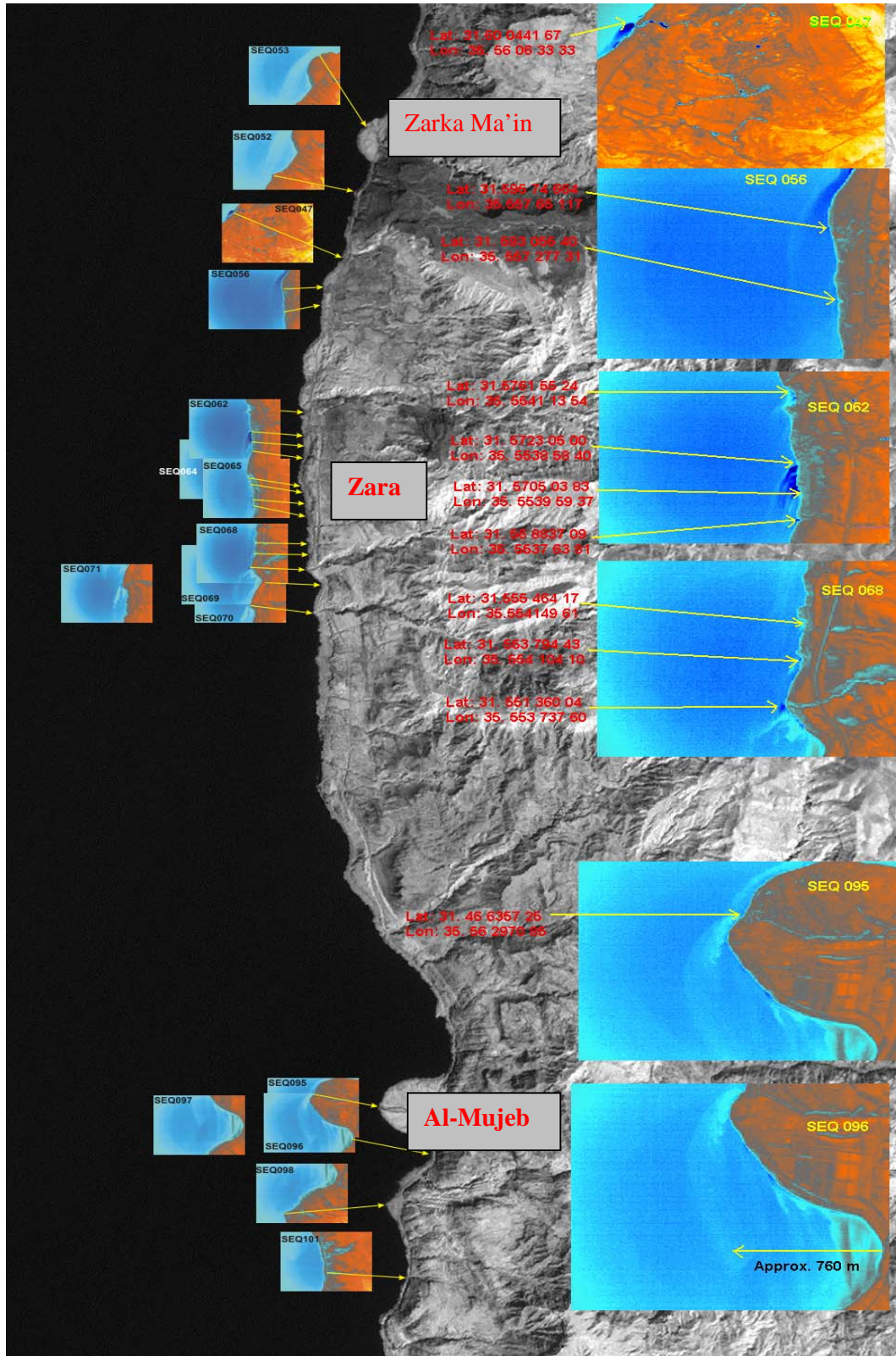
Figure (5-17): Discharges zones along the DS coast obtained by using TIR.

The dark blue color on the temperature scale indicates at a mixed groundwater flows to the Dead Sea. The light blue color on the temperature scale indicates at the Dead Sea water temperature without any mixing with groundwater. In Zara area the blue color is much darker than that in Mujeb area because the temperature of the groundwater (Thermal) in Zara area is warmer than that of Mujeb area (Fig. 5-18).
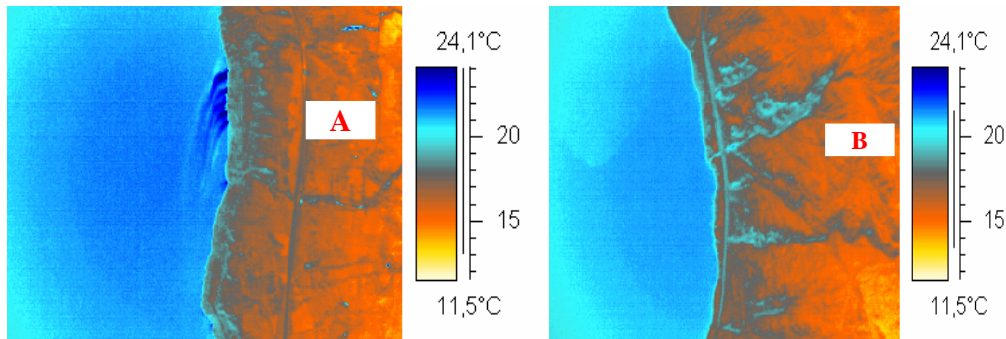
Figure (5- 18): TIR imagery with T scale in Zara (A) and in Mujeb (B).

The thermal infrared images show that the distribution of the groundwater discharges are concentrated at the shoreline and distributed to about between 360 m and more than 750 m away from the shoreline (Fig. 5-19 A-C). These results coincide with the results obtained from the electrical conductivity measurements (last section). Some springs were also indicated and their location difined by using thermal infrared images (Fig. 5-19).

(A) Zarka Ma'in area
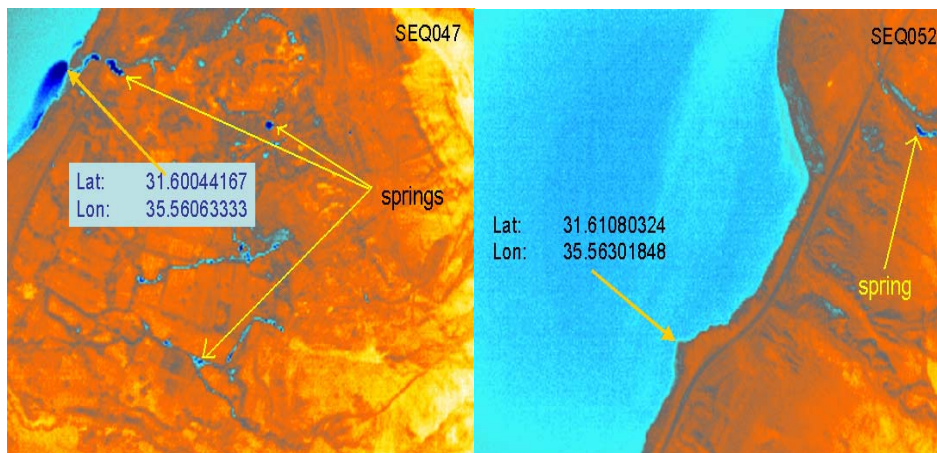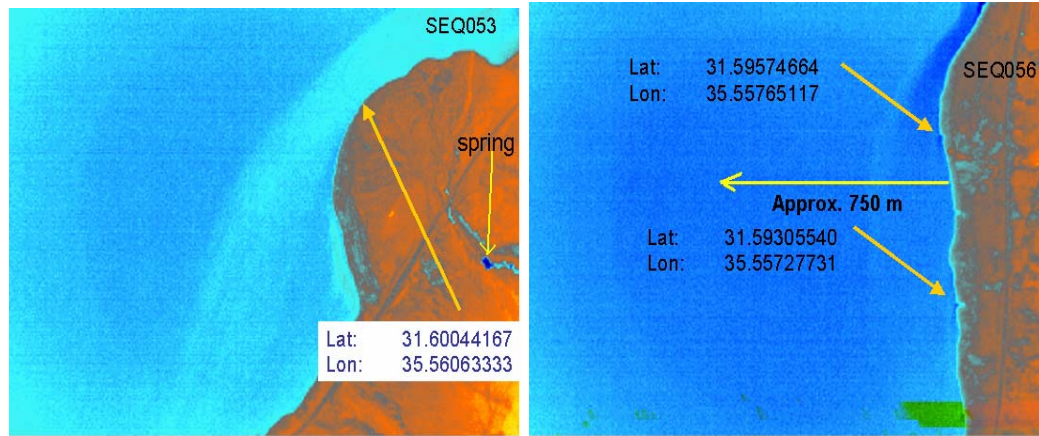
Figure (5-19 A): Groundwater flow distribution in Zarka Ma'in indicated by TIR images.

(B) Zara area
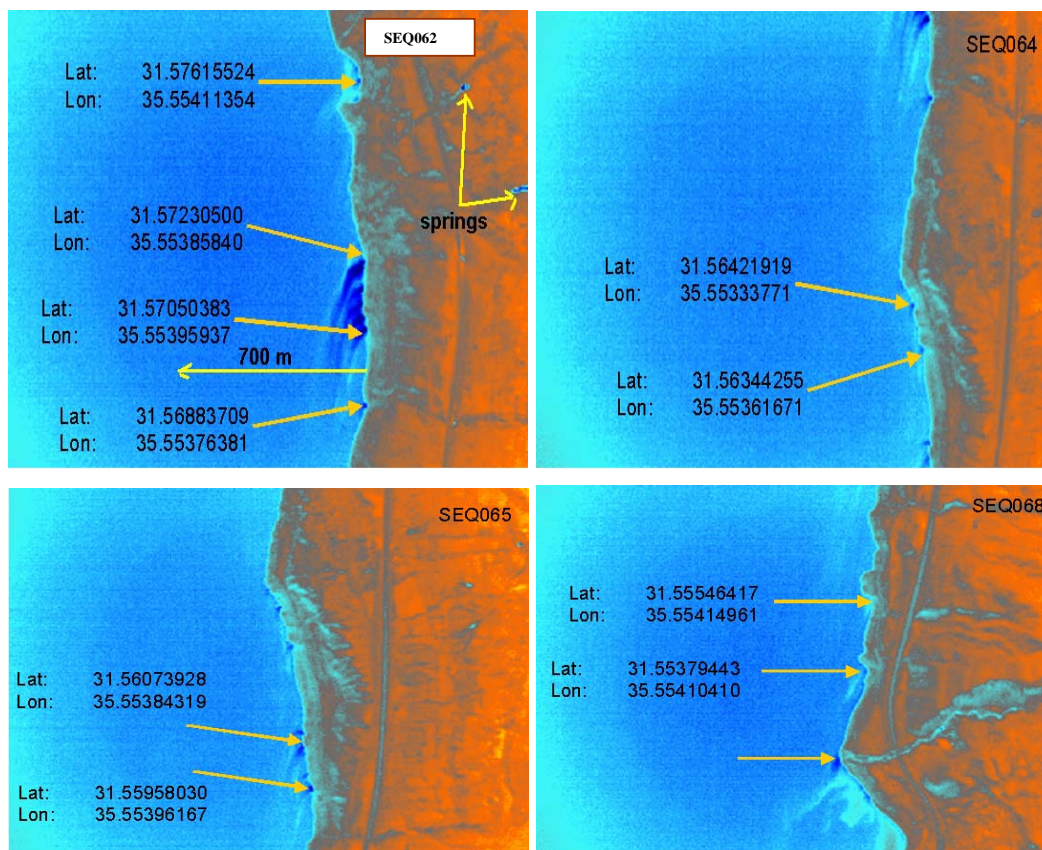
Figure (5-19 B): Groundwater flow distribution in Zara indicated by TIR images

(C) Mujeb area
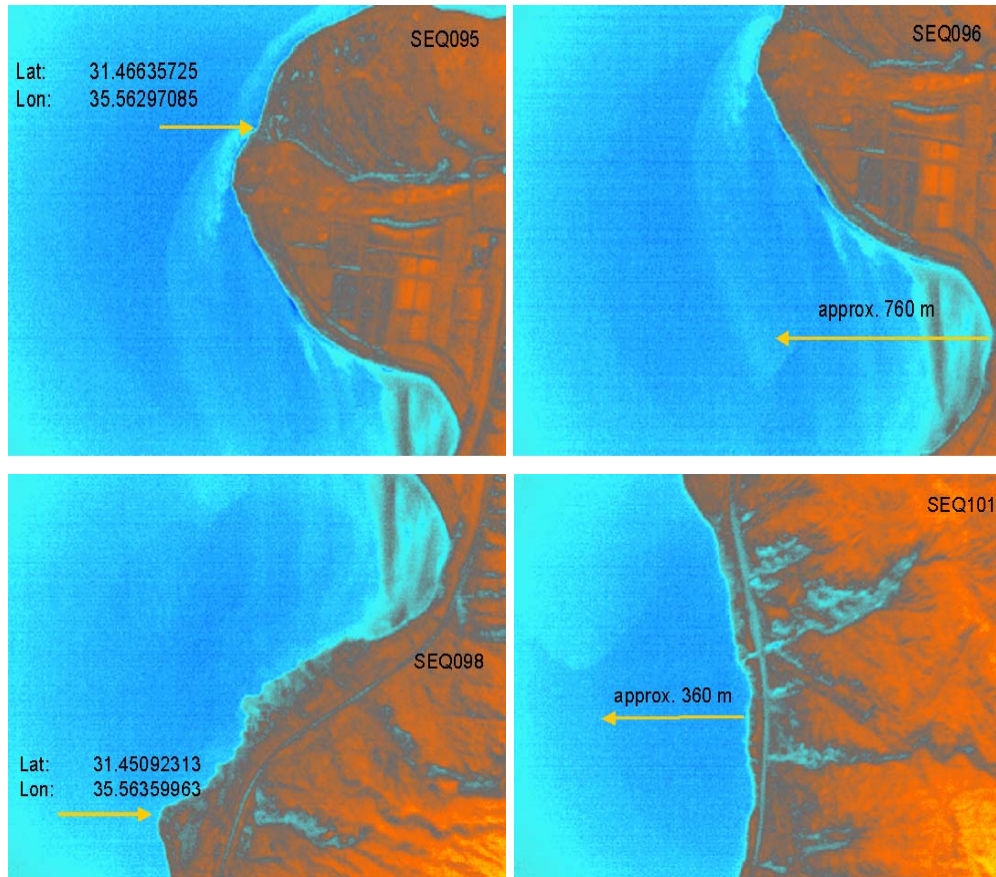
Figure (5-19 C): Groundwater flow distribution in Mujeb indicated by TIR images

5.6. Electromagnetic Radiation (EMR)

The results of the electromagnetic radiation (EMR) show that there are many active faults, farctures, joints and few of non-opened sinkholes along the coast of the Dead Sea extending from Sweimah in the north to Mujeb in the south. The zones are shown in (Fig. 5-20). Detailed results of the radiation anomalies illustrate in (Appendix IV).

In Sweimah area, the starting point of the profile has the coordinates of 31° 43 627 N and 35° 35 334 E. High energy was observed in a distance of about 300 m from that point. The sinkholes were found at distances of 2455 to 2460 m from the starting point and many of the active fault and joints were found along this profile at distances intervals of about 310-315 m, 660-665 m and from 695-700 m from the starting point. The main interesting areas were at the distance of 2440-2450, 2635-2643 m and the main fractured zones were found between 2490 and 2505 m and

from 2330 to the end of the profile at coordinates 31° 45′ 45.07″ N and 35° 34′ 33.48″ E with a distance of about 650 m. Figure (5-21) shows the results of the EMR in Sweimah area.
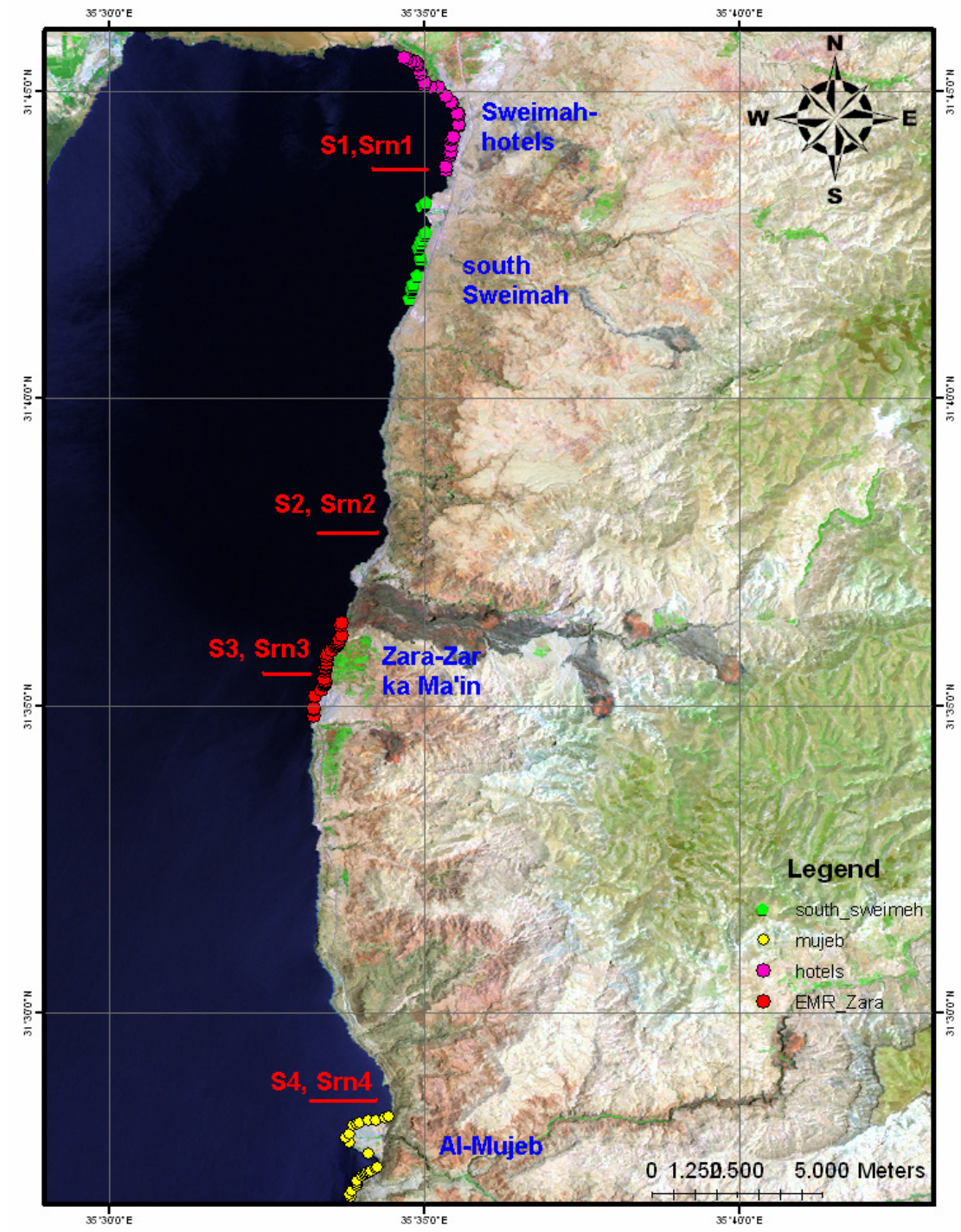
Figure (5-20): Locations of the EMR, EC and radon-222 stations
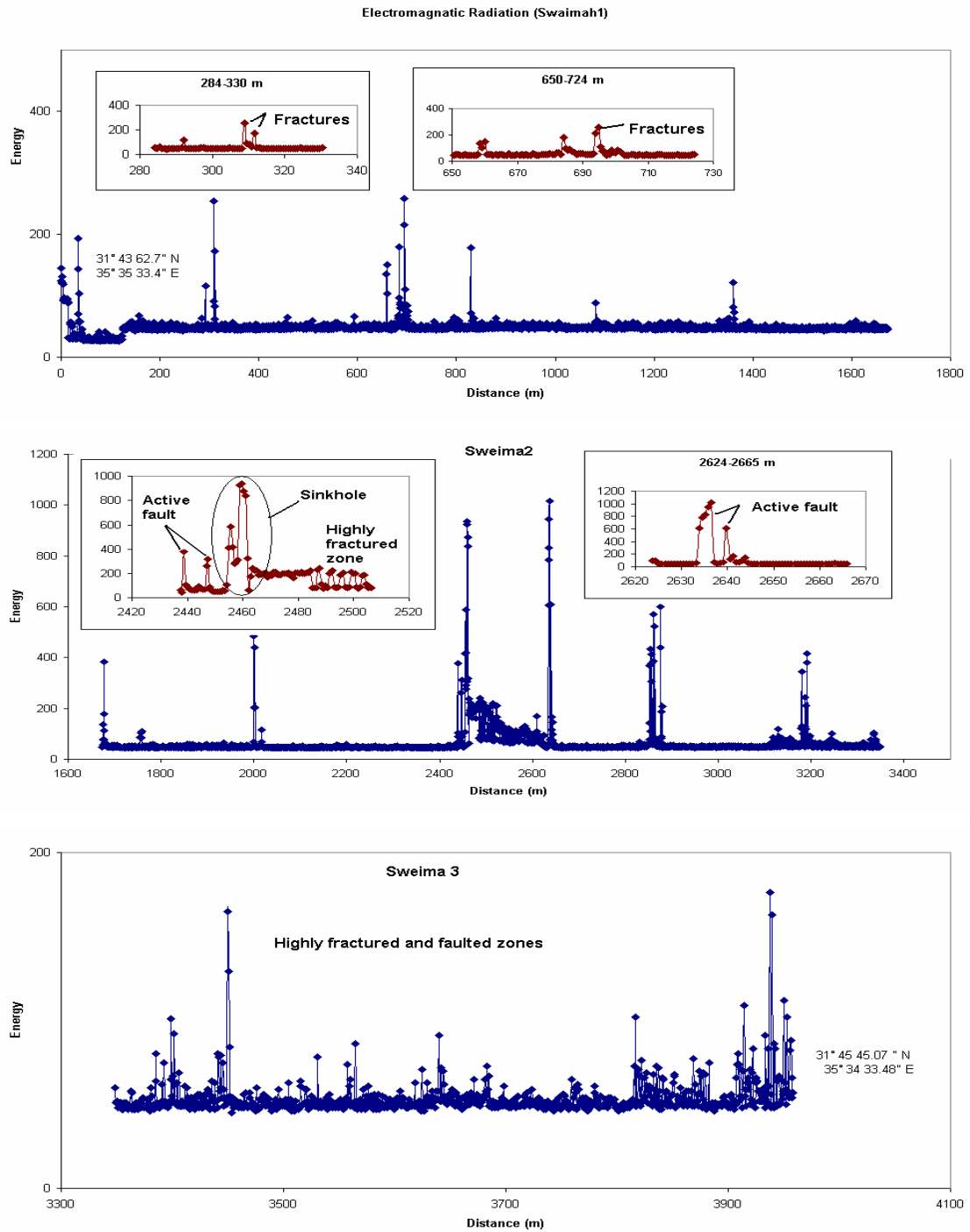
Figures (5-21): Magnitudes of EMR in Sweimah area.

South Sweimah profile started at coordinates 31° 41′ 28.18″ N and 35° 34′ 38.87″ E. Many fractured zones were observed along the profile. A main highly fractured zone was observed at a distance between 790 and 1500 m from the starting point

and another one between 880 and 1000 m. A few sinkholes were observed between distances of about 890 m and 1265 m from the starting point. A main sinkhole was recognised at a distance of 2718 to 2730 m from the starting point (Fig. 5-22).
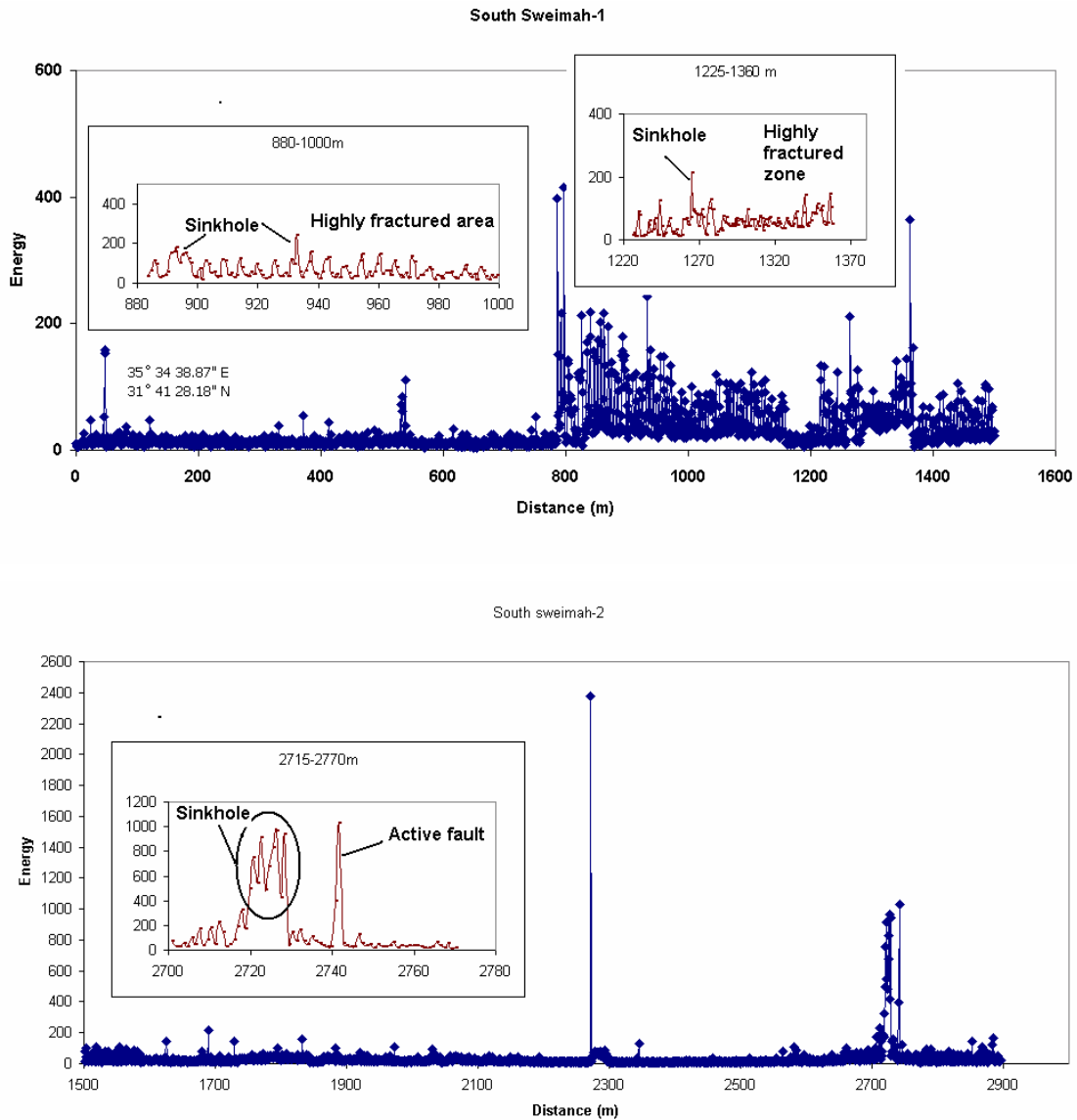
Figure (5-22): Magnitudes of EMR in south Sweimah area.

The EMR profile in Zara - Zarka Ma'in area is started at coordinate of 31° 34′ 43.83″ N and 35° 33′ 99.2″ E. The radiation start after about 50-60 m from the starting point where the active fault start and then after about 80 m from the starting point another active small faults were observed (Fig. 5-22). As well non-opened sinkhole was found at a distance of about 2305-2310 m from the starting

point. As well an active faults and fractured zone were recognised at the distance from about 2285 m to about 2320 m from the starting point.
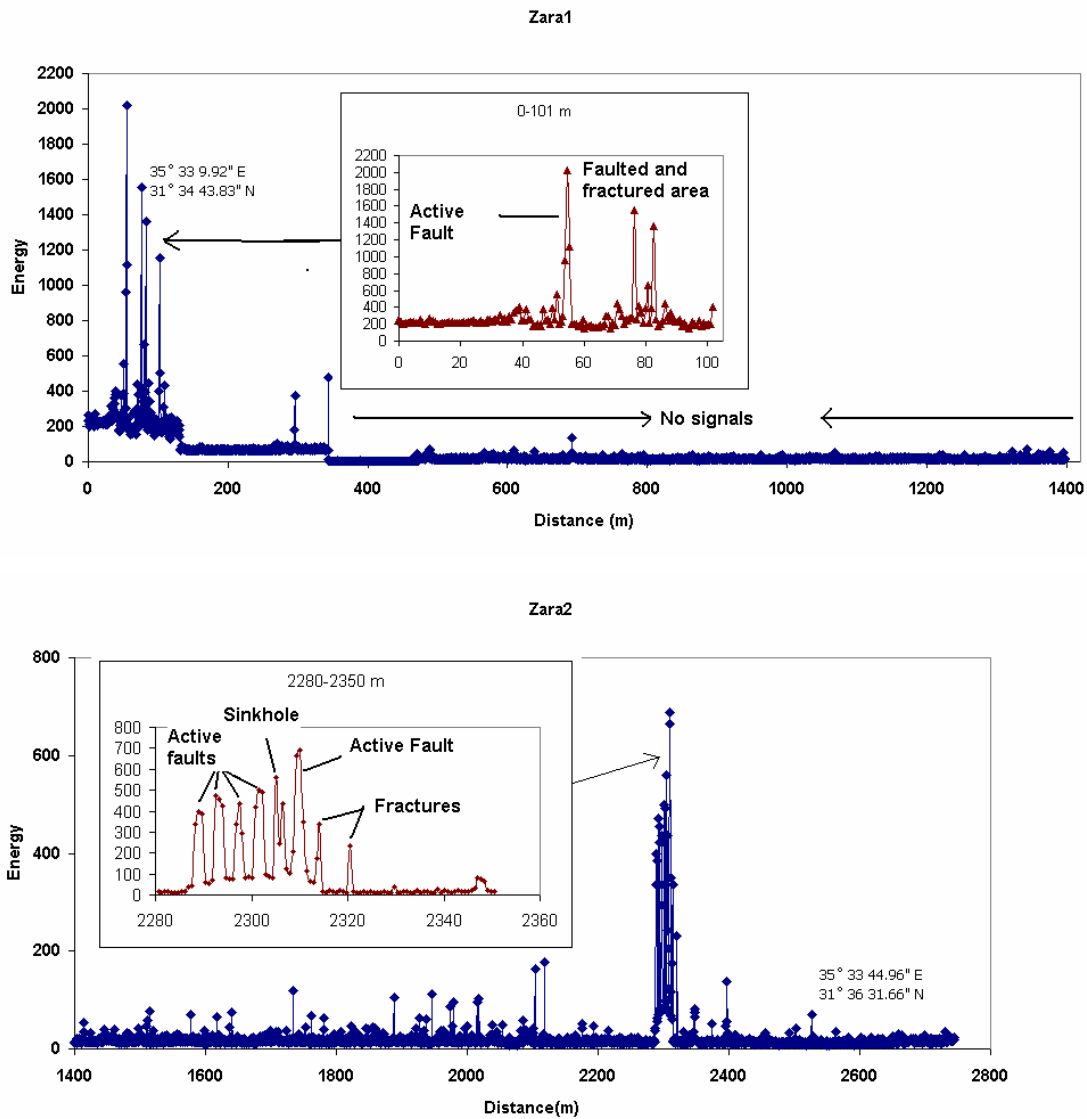
Figure (5-23): Magnitudes of EMR in Zara-Zarka Ma'in area

In Mujeb area the EMR results showed many fractured zones along the profile. The main features were at distances between 550 and 565 m and between 1148 and 1155 m from the starting point. A sinkhole was recognised at a distance between 140 and 150 m from the beginning point. As well a large fractured and faulted zone was observed between 1275 and 1380 m from that point (i.e at the end of the profile) at the coordinate of 31° 28′ 39.92″ N and 35° 34′ 25.40″ E. Figure (5-24) shows the results of EMR in Mujeb area.
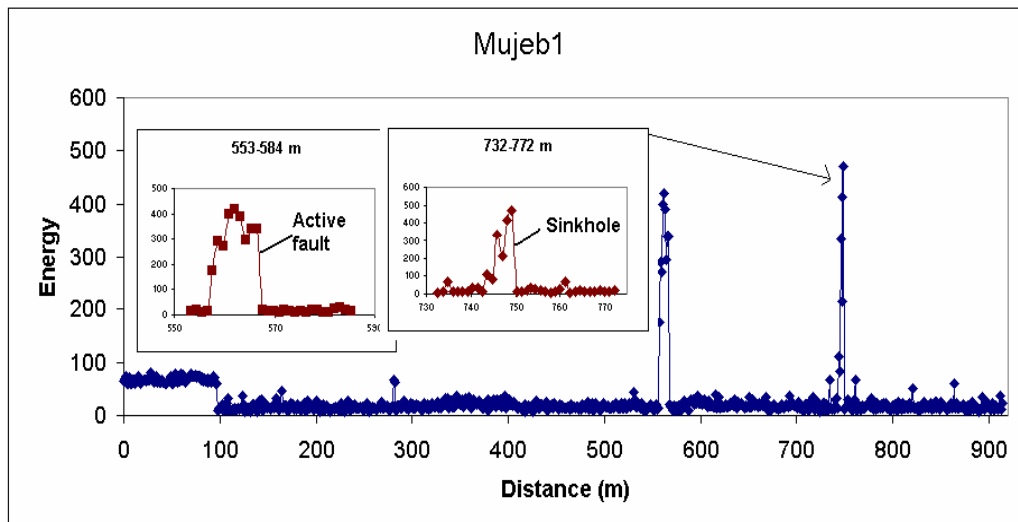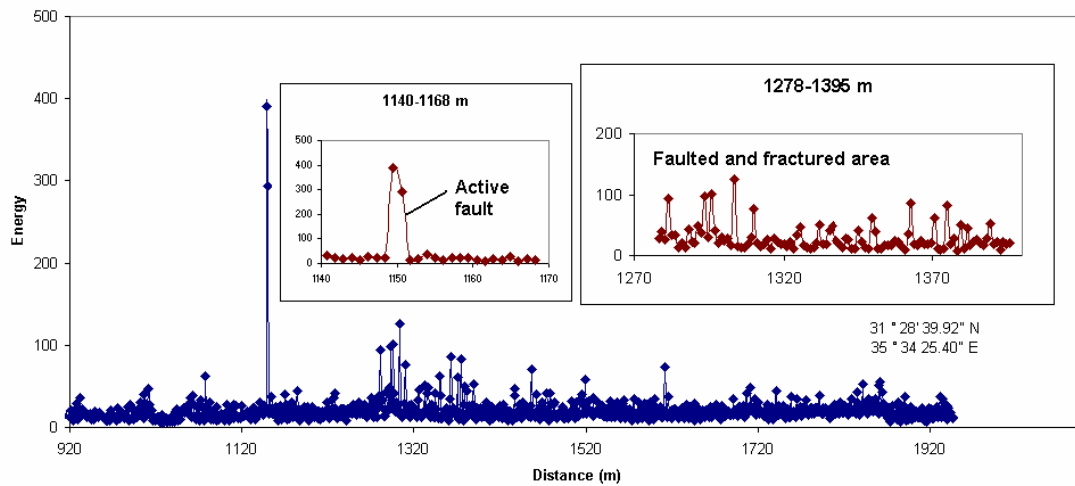
Figure (5-24): Magnitudes of EMR in Mujeb area.

The integration of the geology and the TIR and EMR results are explained as a spatial conception as shown in figure (5-25).
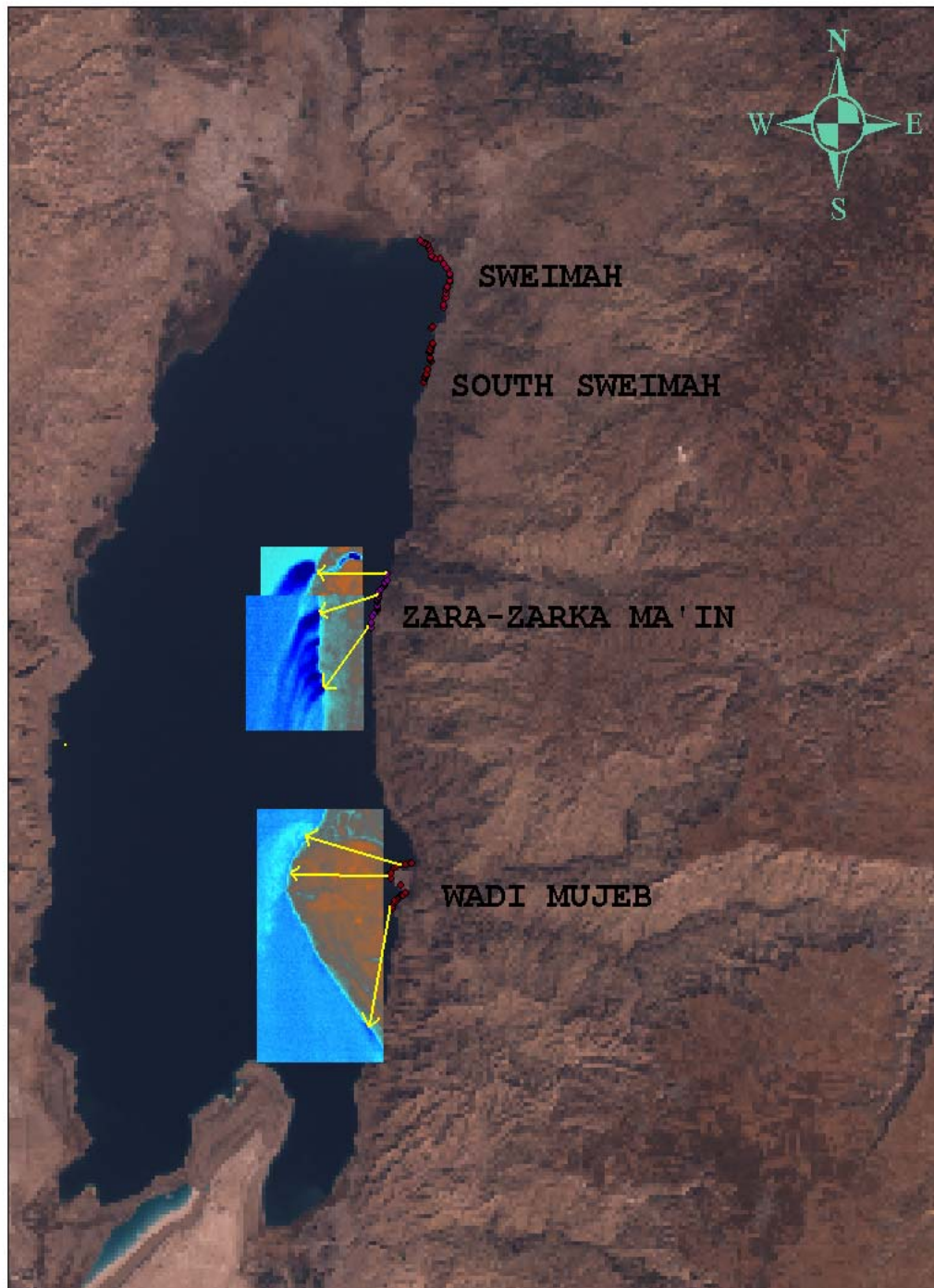
Figure (5-25): Spatial locations of the geological assessments, EMR and TIR

Figure (5-25) showed that the zones of discharge from TIR method coincide with results were getten from the EMR method

6.   HYDROGEOLOGICAL CONCEPTUAL MODEL

6.1. General Outlines

The geology of the Dead Sea area is quite complicated and includes both unconsolidated superficial lithology and bedrock outcrops. The area is characterized by a highly faulted with different trends and folded with a synclines extending from southeast to northwest along the Dead Sea. The faults at the area occurred due to a compression forces during the Late Cretaceous to Tertiary. These faults reactivated in Quaternary times and new faults, fractures and discontinuities created. These considered as a weakness zones for the discharge.

The bedrock is typically highly fractured at the surface and subsurface extending greater than 10s of meter deep. The fractures are often composed of two sets of vertical fractures at approximately right angles to each other, and a third, nearly horizontal, set. They may be observed directly in exposed bedrock. These fractures are widely distributed throughout the Dead Sea area.

These fractures are the principal sources of secondary permeability in many bedrock aquifers and then the recharge occurs chiefly through these faults and fractures. Then might be serving as paths for groundwater lateral and vertical movements.

Mountains, hills and Wadies characterize the topography of the Dead Sea area; the topography of the mountains commonly having steep slopes from east to west toward the Dead Sea coast**.**

As well the Dead Sea area is characterized by high differences in the hydraulic head, which provide the impetus for groundwater movement from the high head to the low head.

6.2. Aquifers

The main major aquifer systems within the Dead Sea basin are the upper aquifer Amman/ Al Hisa / Wadi Es-Sir (B_2-A_7) system and the lower aquifer system Kurnub and older age sandstone formations (Zarka, Ram, and Disi).

6.2.1. Amman Al Hisa Wadi Es-Sir Aquifer system (B_2-A_7)

This forms one of the most important and extensive aquifer systems in the study area. It consists of two formations: The Wadi Es-Sir (A_7), and Amman silicified limestone (B_2). The B_2 and the A_7 formations are hydraulically connected due to the

missing or limited lateral extent of the B_2, separating them elsewhere (Salameh and Bannayan 1993).

This aquifer crops out widely in the escarpment to the east of the Dead Sea in the high rainfall areas. The B_2/A_7 formations consist of limestone, intercalated with laminas of marl (Hunting and Macdonald, 1965). The upper part contains phosphatic limestone and silicified phosphate. The Wadi Ghudran (B_1) forms a thin aquiclude onsisting of marl and chalky marl in some places separting the B_2 from the A_7. The thickness of this system ranges between 170 and 325 m.

The B_2-A_7 aquifer system receives direct recharge from precipitation which infiltrates through the soil and rock covers (Salameh and Bannayan, 1993) and indirect recharge from the adjacent aquifer and from the surrounding areas. But the direct recharge is limited in some areas located farther to the east of the Dead Sea due to overlying by lower permeability strate the Muwaqqar Chalk Formation (B_3). According to Abu Ajameh (1980) the total direct and indirect recharges to this aquifer, in Zarka Ma'in sub-catchment is 6 MCM/y. About 88% of this amount leaks downward to feed the lower aquifer and the rest appears as base flow of springs in the upper reaches of Wadi Zarka Ma'in.

According to Khdeir (1997) the average rainfall in Wadi Waleh sub-catchment (part of Mujeb catchment area) is 144.8 MCM/y for the five years period (1980-1985). Only 11% of this amount enters the B_2-A_7 aquifer as a direct recharge. Also, the aquifer in Wadi Wala sub-catchment is feeding with 2.2 MCM/y as indirect recharge from the lower aquifer and 7.3 MCM/y as lateral recharge from the adjacent high recharge mounds for the same period.

The discharge occurs from the aquifer through the base flow of the Wadies, spring flows and subsurface outflow toward the Dead Sea. Some amounts leak downward to recharge the deep aquifer (Salameh and Udluft, 1985). This aquifer is unsaturated along the eastern shores of Dead Sea, because it crops out in this area and it is essentially an unconfined aquifer.

6.2.2. Lower Aquifer System

This aquifer system includes the sandstone formations of different ages. The formations are Kurnub Sandstone of Lower Cretaceous age, Zarka sandstone of Triassic age, and Ram sandstone of Camprian age. These aquifers are interconnected. The aquifer system crops out along the Dead Sea Shore and in the lower reaches of Wadi Zarqa Ma'in and Wadi Waleh-Heidan, with a thickness of more than 600 m along the northern part of the Dead Sea in Wadi Zarka Ma'in and Hidan.

The aquifer is mainly composed of sandstone. It becomes hydraulically extremely complex due to intercalation shale and clays. Because that the permeability is different in lateral and vertical directions. In some locations Lower Zarqa shale and

clays form an aquiclude confining the underlying saturated Cambrian sandstone (Umm Ishrin and Disi). But in most of the study area the Zarqa shale and clays are absent. Therefore, the whole sequence can be treated as one hydraulicly connected aquifer (Salameh and Udluft, 1985). This lower aquifer system underlies the study area with a total thickness of more than 600 m. The aquifer is exposed along the area of very low rainfall rates. Hence, direct recharge to this aquifer system is very low and negligible. The main recharge to this aquifer system takes place through the downward leakage from the upper aquifer and aquitards systems through the weakness zones of faults and fractures in the A_{1-6} (Salameh and Udluft, 1985). The main outflow from the aquifer takes place along the Dead Sea in the form of springs and seepages from Kurnub sandstone along the Dead Sea shorelines. The main spring discharge is in Zara and Zarqa Ma'in areas in the form of thermal hot springs. In addition, the main discharge takes place as subsurface outflows toward the Dead Sea (Salameh and Bannayan, 1993).

6.2.3. Minor Aquifers

There are two minor aquifers in the Dead Sea area. Na'ur aquifer (A $_{1-2}$) consists of limestones intercalated with thick sequences of marl. It crops out in the Dead Sea area. This aquifer becomes turns into an aquitard locally to the east of the Dead Sea. The second minor aquifer is Hummar (A_4). It consists of dolomitic limestones with a secondary permeability due to the presence of fractures and joints. Some springs issue from these aquifers to the east of the Dead Sea as Al Zarka spring in the upper of the Zarka Ma'in Wadi.

6.3. Aquitards

The formations of Fuheis (A_3) and Shueib (A_{5-6}) form a main aquitards in the area. In some places these include the minor aquifers mentioned above. They separate the lower main aquifer from the upper main aquifer. They crop out in the easteren shores of the Dead Sea.

6.4. Groundwater Movements

Based on the geological maps, (http://exact-me.org/overview/p17.htm) and the available data from (WAJ) the Dead Sea basin was constructed and modified as in (Fig. 6-1). The Dead Sea basin is bisected by Siwaqa fault into a northern and a southern part. The fault forms a permeable discontinuity (GTZ, 1995). The groundwater flows in a west north western direction and toward Wadi Wala. The figure shows that the upper aquifer (B2/A7) crops out in the Dead Sea basin area. On the other hand this aquifer absent on the north western part of the basin, while the minor aquifers and the aquitards crop out. The lower aquifers (Kurnub and

Umm Ishrin) crop out at the area adjacent to the Dead Sea shores. Figure (6-1) shows the groundwater flows toward the Dead Sea.
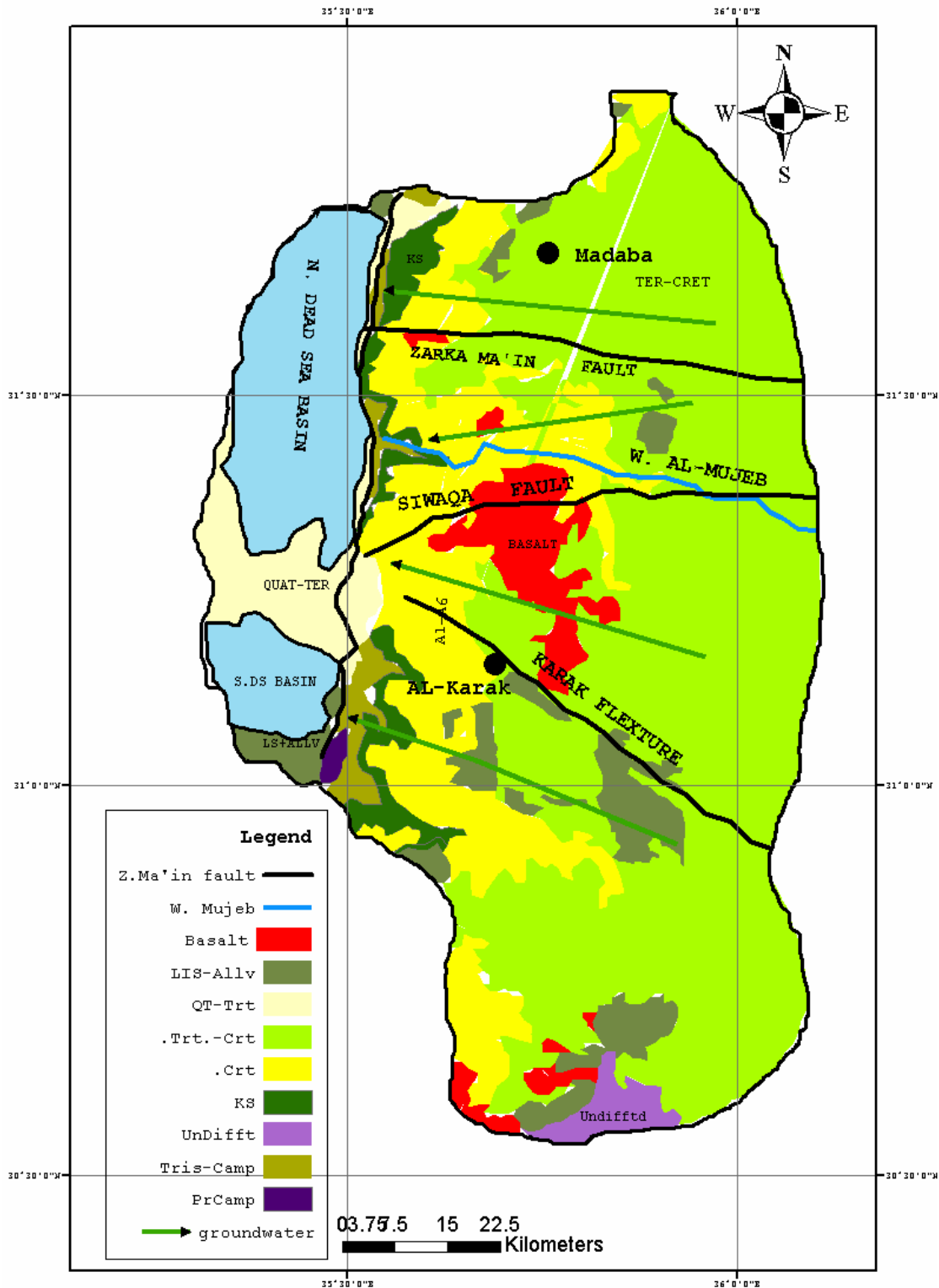
Figure (6-1): Dead Sea basin showing the outcropping rocks and the groundwater

directions (The arrows donate to GW directions)

Based on, the geological maps, the structural patterns, the geological model of the study area and the hydraulic model of central Jordan after (Salameh and Udluft, 1985) a conceptual hydrogeological model of the Dead Sea was produced along NE-SW direction (Fig. 6-2). The model shows the main upper aquifer (B_2/A_7) underlay with the minor aquifers, aquitard and lower aquifer (Kurnub-Zarka-Ram groups). It shows also that the groundwater flows from the east and northeast scarpments toward the Dead Sea. It shows saltwater intrusions from the Dead Sea toward the east direction and enters the lower aquifers. The precipitations infiltrate downward to feed the unsaturated (B_2/A_7) aquifer through the overlay soil and rocks. This water leaks downward to feed the lower aquifers through fractures and joints present in the aquitards which separate the upper aquifer from the lower aquifer. As well some of the groundwater flow upward direction from the minor aquifer and feed the upper unsaturated aquifers.
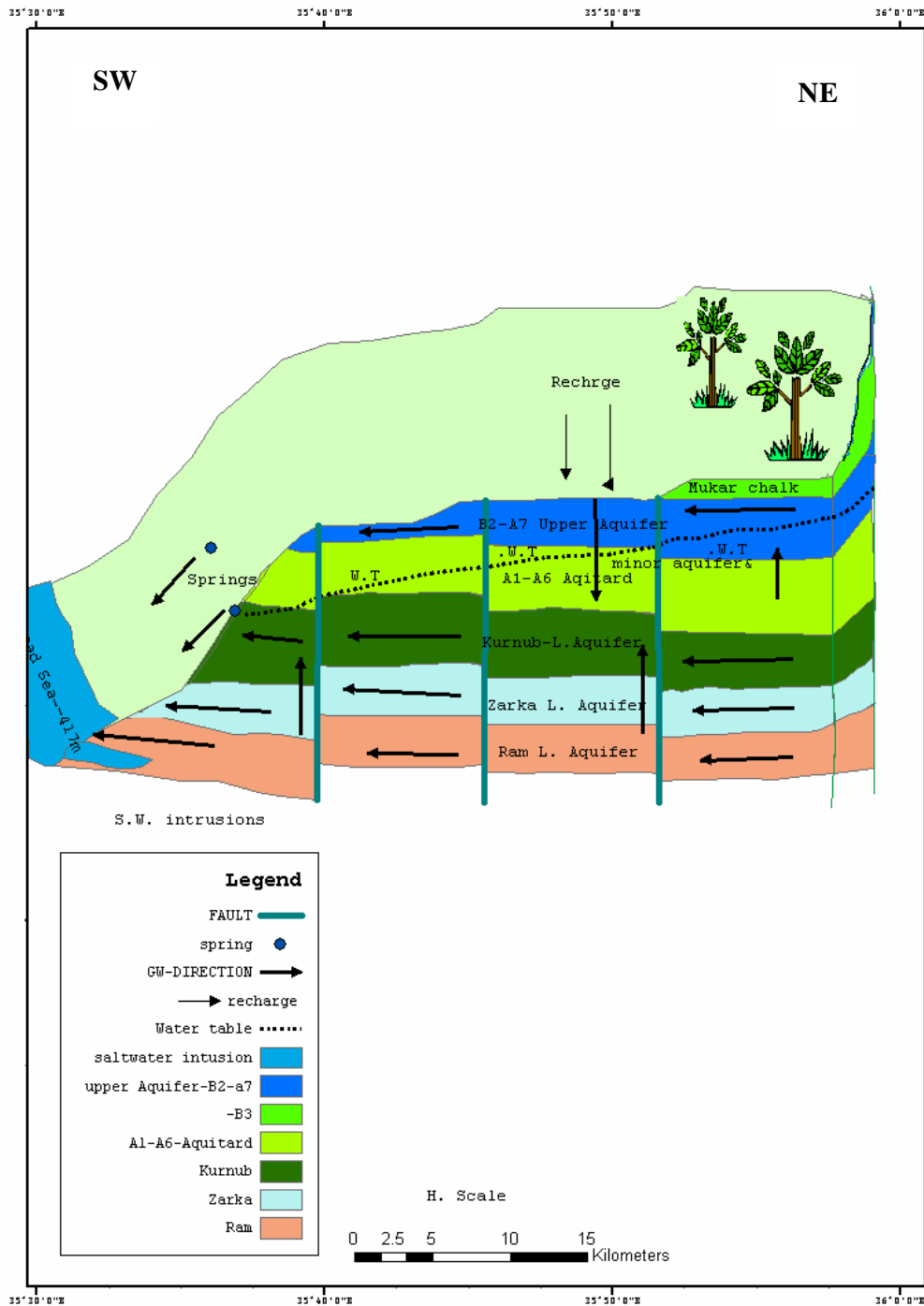
Figure (6-2): Conceptual groundwater model along E-W profile

7.   SUMMARY and FUTURE PROSPECTS

7.1.   Summary

The Dead Sea Rift zone is the main structural element governing the geomorphology, hydrology and hydrogeology of Jordan. Dead Sea located in the middle and forms an active part of the African-Syrian Rift, which extends from east Africa through the Red Sea, Wadi Araba, Dead Sea and Jordan Valley to southern Turkey.

The main purpose of this study is to locate the discharge zones and to estimate the quantity of groundwater that discharged along the eastern shores of the Dead Sea as submarine springs, in accordance to the electrical conductivity and temperature survey with the depth, chemical tracer (radon-222), thermal infrared imagery and electromagnetic radiation techniques. Using the results obtained from this study to determe the availability of exploitable water resources that can be abstracted to assist in the water supply along the shores of the Dead Sea. This might be provided the basis for future development for the area.

The geological model of the study area was developed. This model shows that the geological units dip to the west and southwest directions toward the Dead Sea. In the area adjacent to the shores of the Dead Sea the upper aquifers (B2/A7) were eroded and the lower aquifers (Kurnub sand stone, Zarka and Ram sandstone group) crop out. According to the geological model and based on the data obtained from different sources a conceptual hydrogeological model is constructed and the groundwater flow directions were expected. It shows that the groundwater flows from the east and northeast to the west and southwest toward the Dead Sea. At the east of the Dead Sea the upper aquifer is unsaturated because of it crops out. It gained its water from the direct recharge as infiltration from the precipitation and as indirect recharge as upward leakage from the lower aquifer through the fractures and joints presented in the minor aquifer and aquitard that separated the upper aquifer from the lower aquifer.

Laboratory experiments, which are used for calibrating the electrodless sensor and for checking the EC compensation with the T, show that the relationship between the EC and the T is a quadratic and the sensor works properly corresponding to T compensation at 25°C. As well the labratory experements show that the EC increases with the increase in the T when TDS is fixed, while with the increasing the TDS at 25°C the EC decrease.

The relationship between EC and TDS was obtained in the laboratory for high saline water as that as the Dead Sea. The relationship shows that the EC reached its maximum value at 202 mS/cm at a salinity of 267 g/l. This value decreases with the increasing salinity and it reached 176 mS/cm at a salinity of about 420 g/l. The

TDS was calculated using this relationship for all the EC values obtained from the field measurements. These values were compared with a TDS values were measured using gravimetric technique. A good comparison between the calculated values and the measured values was observed with a difference less than 5%.

Relating to the EC and T measurements with the depth the Dead Sea water divides into two layers. The first layer is from the Dead Sea surface down to a depth of approxmetly 40 m. The second layer extends from 40 m to the final depths of the profiles. The first layer subdivided into two members. The upper member extends from the Dead Sea surface down to 15–25 m and characterized by a low TDS and high in EC, while the second member extends from 15-25 to about 40 m and characterized by a higher salinity than that of the upper member and the lower layer. Submarine groundwater discharge into the Dead Sea was observed in the upper 16 m in average in Sweimah area in the north edge of the Dead Sea, while it was observed in the upper 25 m in average in Zarka Ma'in area and at the upper 15 m in average in Zara area in the middle part of the Dead Sea. Finally the submarine groundwater discharge was observed in the upper 18 m in Mujeb area in the southern part of the Dead Sea.

The reason for a very high TDS value in the lower member of the Dead Sea water is due to the high evaporation from the surface of the Dead Sea in the summer season. So the salinity become too high and its density increase. Then the dense saline water sinks down and the fresh groundwater, which flow into the Dead Sea from a depth of 15-25 m floats (upwelling) to the surface. As well the TDS values, at the surface, change with the change in the distances from the shoreline. It decreases with the increase of the distances away from the shoreline due to the decrease in temperature.

Radon-222 inventories and its activities in the groundwater are the two basic measurements needed to complete the radon model. Radon-222 advection to atmosphere and the radon productions were estimated to complete the radon budget calculations were estimated or measured. Four stations were considered according to the geology, hydrogeology and structure features of the area surrounding the Dead Sea area for carrying out the radon-222 measurements. The advection rates in these stations were calculated and the quantities of the groundwater discharge were computed by multiplying the advection rate with the area of discharge for each station.

The advection rate in Sweimah area is 0.1328 m/day and the quantity of submarine groundwater discharge is 135.7 MCM/y. The advection rate in Zarka Ma'in area is calculated as 0.1324 m/day and the discharge is 128.5 MCM/y. The advection rate in Zara area is 0.066 m/day and the discharge is 33.7 MCM/y and the advection rate in Mujeb area is 0.0651 m/day and the discharge is 90.3 MCM/y. The total quantity of the submarine groundwater discharge into the eastern shores of the Dead Sea in all stations is estimated as 388.2 MCM/y. This value was compared with the groundwater discharge quantity 480 MCM/y obtained by using the water

budget for the both sides (eastern side-Jordan, and the western side-Israel and Palestine). The amount of discharge using water budget for the period from 1957 to 1995 was calculated by (Salameh and El-Nasir, 1999). The reason for this difference in the two quatities obtained from the two methods is because of the water budget considered the whole Dead Sea in both sides, while the Rn-222 method considere only the eastern shoreline of the Dead Sea. Also the Rn-222 results show that the highest concentrations of radon are at the area close to the shoreline and decreases with the increase in the distances from the shoreline. These mean that the highest amount of submarine groundwater discharge is in the locations close to the shoreline. Also, the highest concentrations are at a depth of 12 m in Sweimah, Zara and Mujeb areas, while it is at a depth of 7 m in Zarka Ma'in area. Generally relating to radon-222 results the groundwater discharge occurs in the upper 20 m of the Dead Sea water. These results coincide with the results obtained by using EC and T results. As well the SGD is estimated about 181 MCM/y by using mixing of TDS, and it is estimated about 57 MCM/y by using Darcys' law. In conclusion the SGD into the eastern shores of the DS might be between 200 and 300 MCM/y

Thermal infrared imagery is the other method that used for locating the submarine groundwater discharge into the eastern shores of the Dead Sea. It is an effective method to assess to large-scale areas and to acquire information about specific locations of groundwater discharge. The contrast in temperatures between the warm groundwater and the cold surface water of Dead Sea was obvious. The warm water was considered as due to groundwater discharge in wintertime when the images were taken out. Many of groundwater discharge zones were found along the study area. The major zones were found in Zarka Ma'in, Zara and Mujeb areas. The length of the discharge zones were estimated by using the TIR about 3800 m and about 750 m wide in Zarka Ma'in area and in Zara area the length of the discharge zones was about 2000 m with 750 m wide. On the other hand the discharge zones length in Mujeb area was about 2400 m and its width extends between 360 and 760 m.

The results of the electromagnetic radiation measurements (EMR) showed that there are many small active faults and highly fractured rocks along the eastern shores of the Dead Sea. These faults and fractures consider as a zones of weaknesses for increasing the groundwater discharge. As well the results showed that there are some non-opened sinkholes in Sweimah area, in Zara Zarka Ma'in and Mujeb areas. The most active fault and fractured zones were found in Sweimah area in the northeren corner of the Dead Sea.

7.2. Zusammenfassung

Die Tote-Meer-Störungszone (Dead-Sea-Transform) ist das strukturelle Hauptelement, das die Geomorphologie, die Hydrologie und die Hydrogeologie von

Jordanien wesentlich beeinflußt. Jordanien liegt im nordwestlichen Teil der Arabischen Halbinsel. Das Tote Meer befindet sich in der Mitte dieser Störungszone, die einen aktiven Teil des Afrikanisch-Syrischen-Riftsystems darstellt. Dieses System läuft von Ostafrika durch das Rote Meer und den Wadi Araba, das Tote Meer und die Jordan-Tal - Senke bis in die Südtürkei.

Der Hauptzweck dieser Studie war es, die Grundwasser-Austrittszonen entlang der östlichen Uferlinie des Toten Meeres darzustellen und die Mengen quantitativ zu bestimmen.   Die Studie basiert auf der Anwendung folgender Techniken: Temperatur- und Tiefen-Abhängigkeit der elektrischen Leitfähigkeit; Verfolgung eines chemischen Tracers (Radon 222); thermische Abbildung durch Infrarot-Aufnahmen. Die Mengen des austretenden Grundwassers, die mit dem Radon-222-Indikator ermittelt wurden, wurden mit den Mengen verglichen, die mittels Wasserbilanztechniken bestimmbar sind. Die abschließenden Resultate dieser Studie sollen für die Bestimmung der verwertbaren Wasservorräte verwendet werden, die zur Wasserversorgung entlang den Ufern des Toten Meeres entnommen werden können.

Am Anfang der Studie wurde das geologische Modell des Untersuchungsgebietes entwickelt. Dieses Modell zeigt , daß die geologischen Schichten nach Westen und Südwesten in Richtung zum Toten Meer hin eintauchen. Die oberen Aquifere (B2-A7) fehlen im östlichen Uferbereich des Toten Meeres, aber die unteren Aquifere (Kurnub-Sandstein-Gruppe und Ram-Gruppe) streichen hier am Rand des Toten Meeres aus. Außerdem gab das Eintauchen der Schichten eine generelle Idee über die Fließrichtungen des Grundwassers. Es bewegt sich vom Osten und Nordosten von den Hochländern nach Westen und Südwesten in Richtung zum Toten Meer.

Die Laborexperimente zeigten, daß das Verhältnis zwischen der elektrischen Leitfähigkeit und der Temperatur für den Sensor, der in dieser Arbeit benutzt wurde, durch eine quadratische Funktion beschrieben wird. Zum Anderen wurde bei der Laborarbeit mit den Tote-Meer-Wasserproben gefunden, daß sich die elektrische Leitfähigkeit (EC) erhöht mit der Zunahme der Temperatur für den Fall eines konstanten unveränderten Gesamt-Lösungsinhalts (TDS). Wenn dagegen der TDS erhöht wird, dann sinkt die elektrische Leitfähigkeit bei vergleichbarer Temperatur. Dieser Befund wurde im Labor überprüft und er entspricht den Beobachtungen, die im Feld gewonnen wurden. Abhängig von den Bestimmungen der elektrischen Leitfähigkeit, Temperatur und Tiefe wurde der Wasserkörper des Toten Meeres in zwei Schichten geteilt. Die erste Schicht beginnt an der Oberfläche und reicht in eine Tiefe von 40 m. Die zweite beginnt bei 40 m und dehnt sich dann bis zur abschließenden Tiefe der Meßprofile aus. Die erste Schicht wurde in zwei Glieder unterteilt, von denen das obere sich von der See-Oberfläche bis in etwa 15 - 25 m Tiefe erstreckt, dessen Wasser sich wegen des Grundwasserzustroms durch eine relativ niedrige Salinität auszeichnet. Das zweite Glied von etwa 17- 25 m bis in eine Tiefe von ca. 40m hat dagegen eine höhere

Salinität nicht nur als das überlagernde sondern auch als das darunter folgende Seewasser. Dies wird erklärt durch einen Prozess, bei dem die hohe Verdampfung direkt an der Oberfläche des Toten Meeres die Salinität und damit die Dichte des Wassers so erhöht, daß eine Instabilität entsteht. Das hochsalinare Wasser sinkt ab unter das leichtere, durch den Grundwasserzustrom bis in eine Tiefe von 25 m geringer salinare Wasser, das im Austausch nach oben aufströmt.

Radonbilanzen und Aktivitäten von Radon-222 im Grundwasser das dem Toten Meer zufließt, sind die beiden grundlegenden Bestimmungsgrößen, die für die Radon-Modellabschätzungen notwendig sind. Andere notwendige Komponenten für die Komplettierung des Radon-Budgets wurden gemessen oder geschätzt. Advektion von Radon-222 in die Atmosphäre wurde geschätzt und die Radon-Produktion wurde gemessen und errechnet. Vier Stationen wurden für die Radon-222 Messungen berücksichtigt, abhängig von der Geologie und Hydrogeologie des Gebietes. Die Advektionsraten im Toten Meer wurden bestimmt und die Menge des Grundwasserzuflusses errechnet, indem die Advektionsrate mit der Fläche des Zuflusses an jeder Station multipliziert wurde. Die Advektion an Station 1 wurde bestimmt zu 0.1328 m/Tag, was einen Grundwasserzufluss von 135.7 MCM/Jahr ergab. Die Advektion an Station 2 wurde bestimmt mit 0.1324 m/Tag entsprechend 128.5 MCM/Jahr. An Station 3 war die Advektion 0.066 m/Tag woraus sich ein Zufluss von 33.7 MCM/Jahr ergab, und die Advektion an Station 4 wurde mit 0.0651 m/Tag bestimmt entsprechend einem Zufluss von 90,3 MCM/Jahr. Die Gesamtmenge des Grundwasserzuflusses aller Stationen am Ostufer des Toten Meeres wurde zu etwa 388.2 MCM/Jahr geschätzt. Dieser Wert wurde mit einem Zufluss von 480 MCM/Jahr verglichen, der erhalten wurde auf der Basis einer Wasserbilanz für das gesamte Tote Meer unter Einschluss aller Ufer (des Ost-Ufers in Jordanien und des West-Ufers in Israel und Palästina). Die Zuflussmengen wurden mittels einer Wasserbilanz berechnet, die Statistik bis zum Jahr 1995 benutzt. Aber der Zufluss dürfte heute viel höher sein, da der Spiegel des Toten Meeres beständig gesunken ist. Außerdem dürfte der Grund für den Unterschied der beiden Bilanzen sein, daß die Berechnung des Wasserbudgets für das ganze Tote Meer an beiden Seiten gilt, während die Bestimmung des Radon-222 Flusses nur die östliche Küste berücksichtigt. Weiterhin haben die Radon-Resultate gezeigt, daß die höchsten Konzentrationen im Gebiet zunächst der Küste gefunden werden und die Konzentrationen mit der Entfernung von der Küste abnehmen. Das bedeutet, daß der maximale Eintrag nahe der Strandlinie erfolgt. Zusaetzlich wurde der submarine Grundwasser-Zustrom zu 181 MCM/jahr abgeschaetzt, basierend auf der mischung der TDS- Gehatter, und mittels Darcy's Gesetz ist 57 MCM/jahr. Zusammenfassend liegt der submarine Grundwasser-Zustrom wohl zwischen 200 und 300 MCM/jahr.

Die Aufnahme thermischer Infrarot-Bilder war die dritte Methode, die für die Darstellung der Unterwasser-Grundwasseraustritte verwendet wurde. Es ist eine wirkungsvolle Methode um großräumige Bereiche schnell zu erfassen und um Informationen über spezifische Positionen des Grundwasseraustritts zu gewinnen. Der Kontrast in den Temperaturen zwischen dem Grundwasser , das höhertemperiert ist , und der niedrigen Temperatur des Oberflächenwassers des Toten Meeres war offensichtlich. Die beobachteten höheren

Oberflächentemperaturen während des Winters, als die Aufnahmen durchgeführt wurden, konnten daher als Grundwasser-Austritte interpretiert werden. Viele Grundwasseraustritte wurden entlang des untersuchten Küstenabschnitts erkannt. Die Hauptzonen wurden im Gebiet von Zarqa Ma 'in , Zara und Al-Mujeb gefunden. Die Länge der Austrittszone bei Zarqa Ma'in wurde zu 3800m , die Breite zu etwa 750 m geschätzt, und im Zara-Gebiet war die Austrittszone etwa 2000 m lang und 750 m weit. Andererseits waren die Austritte im Al-Mujeb -Gebiet ungefähr 2400 m lang und zwischen 360 und 760 m breit.

Die Resultate der elektromagnetischen Messungen (EMR) zeigen, daß es viele kleine aktive Störungen und stark geklüftete Gesteine an der Ostküste gibt. Diese Störungen und Brüche sind Wegsamkeiten für Grundwasser-Zutritte. Die Resultate lassen außerdem vermuten, daß es einige nicht durchgebrochene Lösungshohlräume im Sweimah - Gebiet gibt. Diese Beobachtung könnte eine Begründung für die höhere Radon-222-Advektion dort geben, wenn man diese mit den anderen Stationen vergleicht.

7.3. Future Prospects

Future work should focus on the following recommendations to obtain a complete concept on the groundwater discharge into the Dead Sea.

 - ➢ Using the direct physical measurements as seepage flux meters techniques in Sweimah area, in Zara and Zarka Main area, in Mujeb area and in Ghor Haditha area. In order to determine the wide of submarine groundwater discharge for assuring of this study.

 - ➢ Using the hydrochemistry methods to compare the Ions and Cations content of the spring surrounding the area and the Dead Sea water content to calculate the discharge using a mass balance technique.

 - ➢ Carry out the thermal infrared images along the Dead Sea shore with very high resolution less than 5 meters in order to locolize the discharge from the seepages at the shoreline.

 - ➢ For future study using the thermal infrared imagery. It is recommended to measure the water surface temperature at the same time of carrying out the images, and to match the GBS time with the thermal camera time in order to do correct mosaic for all images.

 - ➢ Carry out the thermal infrared Images for the area east of the Dead Sea to investigate new springs surrounding the Dead Sea.

➢ Studying the rock alterations and the gypsum sedimentions along the Dead Sea to determine the history of the discharge in the past time.

➢ Using Radium and CH4 isotopes to estimate the Discharge and compare the results with the result have getten from this study.

➢ Carry out a high-resolution aerial photography along the Dead Sea to merge the groundwater discharge and the sinkholes along the Dead Sea.

➢ Long-term monitoring of water quality of groundwater discharge surrounding the Dead Sea is recommended to identify the significance of land use impacts upon submarine groundwater discharge.

➢ Feed the Dead Sea with water from other sources to increase its level, then to decrease the groundwater discharge into it, and to increase the groundwater table thereafter increasing the depth of the seawater-fresh water interface.

➢ Doing and intensive geological, geotechnical and geophysical investigations before establishing and constructing buildings or farmers along the shoreline of the Dead Sea.

➢ Carry out a continuous simulation model, this model must be function properly for the steep topography of hillside watersheds, must be able to delineate Wadies and streams as it flows down slope, model have a possibility for dams simulation because dams are considered essential in water management in Jordan, and this model should have relatively low data requirements due to few data are available for the Dead Sea hillside watershed.

➢ Doing the radon-222 measurements and radium-223 at different months in the year at least two months in summer time and two months in wintertime to correlate the difference in radon-222 concentrations and to estimate the mixing rate of the Dead Sea layers.

➢ Drilling some production wells at the distance about 1 km to the east and along the Dead Sea in order to pump and use the fresh water before reaching the Dead Sea.

8.   REFERENCES

Abraham, D., Charette M., Allen M., Rago A. and Kroeger, K. (2003): Radiochemical estimates of submarine groundwater discharge to Waquoit Bay, Massachusetts, Biol. Bull. 205: pp. 246-247.

Abu-Jaber, N. and Wafa, N. (1996): Hydrochemistry of aquifers in the southern Dead Sea, Southern Jordan. Environmental Geology 28: pp. 213-222.

Abu Ajamieh, M. (1980): The Geothermal Resources of Zarka Mai'n and Zara. Natural Resources Authority (NRA)/ Amman-Jordan.

Anati D. (1998): Dead Sea water trajectories in the T-S space, Hydrobiologia **381**: pp. 43-49.

Anati, D. and Shasha S., (1989): Dead Sea surface-level changes. Israel J. Earth Sci. **38**: pp. 29-32.

Anati, D., Gavrieli, L. and Oren, A. (1995): The residual effect of the 1991-1993 rainy winters on the Dead Sea stratification. Isr. J. Eart Sci. **44**: pp. 63-70.

Arab Potash Company (APC): open files of the Arab Potash Company/Jordan-Amman.

Asmar, B., Ergenzinger, P., (1999): Estimation of evaporation from the Dead Sea, Hydrological processes **13**: pp. 2743-2750.

Atalla, M. (1981): Geology and Structure of the area east of the Dead Sea. Master thesis. University of Jordan.

Bahat, D., Rabinovitch A., Frid, V., (2005): Tensile Fracturing in Rocks – Tectonofractographic and Electromagnetic Radiation Methods.- Springer Berlin Heidelberg: pp. 569.

Ballestero, T., Roseen, R., Brannaka, L. (2004): Inflow and loadings from groundwater to the Great Bay Estuary, New Hampshire, Final Report Summitted to the NOAA/UNH cooperative Insittute for Coastal and Estuarine Environmental Technology (CICEET).

Bandel, K. And Khoury, H. (1981): Lithostratigraphy of the triasic in Jordan. Facies **4** : 1-26, Erlangen.

Barberi, G. and others, (1980): Recent basaltic volcanism of Jordan and its implications on the geodynamic history of the Dead Sea Shear Zone. Acc. Nat. DeiLicei, **47**: pp. 667-673.

Baskin, R., (1990): Determination of ground-water inflow locations in Great Salt Lake, Utah, using the thermal infrared multispectral scanner, Master Thesis, The University of Utah.

Bender, F. (1968): Geologie von Jordanien, Bieter. Regionalen geologie Erde, Vol.**7**: pp. 230, Berlin Gebruder Brontraeger.

Bender, F. (1974). Gology of Jordan. Berlin: Borntraeger.

Benoit, J., Torgersen, T., and O'Donnel, J., (1991): An advection/diffusion model for Rn-222 transport in near-shore sediments inhabited by sedentary polychaetes. Earth and Planetary Science Letters **105**: pp. 463-473.

Beyth, M., Gavrieli I., Anati D., Katz O. (1993): Effects of the December 1991- May 1992 floods on the Dead Sea vertical structure. Israel Journal of Earth Sciences **41**: pp. 45- 48.

Blake, G., (1936): The stratigraphy of Palestine and its building stones. Printing and stationary office, Jerusalem: pp. 133.

Bokuniewicz, H., Buddemeier, R., Maxwell, B., Smith, C., (2003): The typological approach to submarine groundwater discharge (SGD), Biogeochemistry 11, vol. **66** (1-2): pp.145-158.

Borisenko, L.S. (2001): Hydrogeological conditions of submarine groundwater discharge in the Crimea; Water resources **28** (1): pp. 15-21.

Broeker, W., Cromwell, J., and Li, Y., (1968): Earth Planet. Sci. Lett., **5**: pp. 101

Bugna, G. C., Chanton, J.P., Cacble, J. E., Burnett, W. C., and Cable, P. H., (1996): The importance of groundwater discharge to the methane budgets of nearshore and continental shelf waters of the northeastern Gulf of Mesico. Geochimical Cosmochim. Acta **60**: pp. 4735- 4746.

Burdon, D., (1959): Handbook of the geology of Jordan: to accompany and explain the three sheets of 1:250,000 geological map east of the rift, by A.M. Quennel Govt. Hashemite Kingdom of Jordan 82 pp. Benham, Colchester.

Burdon, D. and Papakis, N., (1961): Methods of investigating the groundwater resources of the parnassos- Ghiona Limestones. In: Groundwater in Arid Zones, 1- Symp. Int. Association Sciences Hydrol., Athens, 10-18 Sept. 1961, A.I.H.S., Gentbrugge, Publ. **56**: pp. 143-159.

Burnett, W. , Cable, J. , Corbett, D. & Chanton, J., (1996): Tracing groundwater flow into surface waters using natural Rn-222. Proc of Int. Symp. On Groundwater Discharge in the coastal Zone, Land-Ocean Interactions in the Coastal Zone (LOICZ), Moscow, July **6-10**: pp. 22-28.

Burnett, W., Cable, J., and Corbett, D., (2003): Radon Tracing of Submarine Groundwater Discharge in Coastal Environments. Land and Marine Hydrogeology Elsevier B.V., Edited by Taniguchi M., Wang K. and Gamo T.: pp. 25- 43.

Burnet, W., Chanton, J., Christoff, J., Kontar, E., Kruba, S., Lambert, M., Moore, W., O'Rourke, D., Paulsen, R., Smith, C., Smith, L., & Taniguchi, M., (2002): Assessing methodologies for measuring groundwater discharge to the ocean, EOC **83**: pp. 117-123.

Burnett, W., Henry, B., Huettel, M., Moore, W., and Taniguchi, M., (2003): Groundwater and pore water inputs to the coastal zone, Biogeochemistry **66**: pp. 3-33.

Burnett, W, and Dulaiova, H., (2003): Estimating the dynamics of groundwater input into the coastal zone via continuous radon-222 measurements, Journal of Environmental Radioactivity **69**: pp. 21-35.

Burnett, W.; Kim, G.; Lane-Smith, D. (2001): A continuous monitor for assessment of Rn-222 in the coastal ocean, Journal of Radio analytical and Nuclear Chemistry **249**(1): pp. 167-172.

Burnett, W., Taniguchi, M. & Oberdorfer, J, (2001): Measurement and significance of the direct discharge of groundwater into the coastal zone. Journal Sea Research **46**: pp. 109-116.

Cable, J., Bugna, G., Burnett, W. & Chanton, J. (1996a): Application of Rn-222 and CH4 for assessment of groundwater discharge to the coastal ocean. Limnology Oceanography **41**: pp. 1347-1353.

Cable, J., Burnett, W. and Chanton, J. (1997): Magnitude and variations of groundwater seepage along a Florida marine shoreline. Biogeochemistry **38**: pp. 189-205.

Cable, J, Burnett, W., Chanton, J., Weatherly, G., (1996b): Estimating groundwater discharge into the northern Gulf of Mexico using radon-222; Earth and planetry Science Letters **144**: pp. 591-604

Capaccioni, B., Vaselli, O, Moretti, E., Tassi, F., and Franchi, R. (2003): The origin of thermal waters from the eastern flank of the Dead Sea Rift Valley (western Jordan). Blackwell Publishing Ltd. Terra Nova **15**: pp. 145-154.

Capone, D. and Bautista, M. (1985): A groundwater source of nitrate in nearshore marine sediments. Nature **313**: pp. 214-216

Charette, M. and Buesseler, K. (2004): Submarine groundwater discharge of nutrients and copper to an urban subestuary of Chesapeake Bay (Elizabeth River), Limnol. Oceanogr. **49** (2): pp. 376-385.

Charette, M., Buesseler, K., Andrews, J. (2001): Utility of radium isotopes for evaluating the input and transport of groundwater- derived nitrogen to a Cape Cod Estuary. Limol. Oceanography **46**: pp. 465-470.

Charetta, M., Splivallo, R., Herbold, C., Bollinger, M., and Moore, W. (2003): Salt marsh submarine groundwater discharge as traced by radium isotopes; Marine Chemistry **84**: pp. 113 – 121.

Chanton, J.P., Burnett W.C., Dulaiova H., Corbett D.R., Taniguchi M., (2003), Seepage rate variability in Florida Bay driven by Atlantic tidal height, Biogeochemistry 11, **66** (1-2): pp. 187-202.

Church, TM. (1996): An underground route for the water cycle. Nature **380**: pp. 579-580.

Corbett, D.R., Burnett,W.C., Cable.H.P., Clark, B.S. (1997): Radon tracing of groundwater input into Par Pond, Savannah River Site, Journal of Hydrology **203**: pp. 209-227.

Corbett, D., Burnett, W., Cable, P. & Clark S. (1998): A multiple approach to the determination of radon fluxes from sediments. Journal Radioanaly. Nucl. Chem. **236:** pp. 247-252.

Corbet, D., Chanton, J., Burnett, W., Dillon, K., and Rutkowski, C. (1999): Patterns of groundwater discharge into Florida Bay, the American Society of Limonol. Oceanogr., **44**(4): pp. 1045-1055.

Corbett, D., Dillon, K., Burnett, W. & Chanton, J. (2000): Estimating the groundwater contribution into Florida Bay via natural tracers Rn-222 and CH4. Limonology Oceanography **45**: pp. 1546-1557

Closson, D. (2005): Structural control of sinkholes and subsidence hazards along the Jordanian Dead Sea Coast. Environmental Geology **47**: pp. 290-301.

Closson, D., Abou Karaki, N., Klinger, Y. and Hussein, M. (2005): Subsidence and Sinkholes Hazards Assessment in the southern Dead Sea Area, Jordan.Pure appl. Geophys **162**: pp. 221-248.

Crusius, J., Koopmans, D., Bratton, J., Charette, M., Kroeger, K., Henderson, P., Ryckman L., Halloran, K., and Colman, J. (2005): Submarine groundwater discharge to a small estuary estimated from radon and salinity measurements and box model. Biogeosciences **2**: pp. 141-157.

D'Elia, C. Webb, K. And Poter, J. (1981): Nitrate- rich groundwater inputs to discovery Bay, Jamaica: A significant source of N to local reefs, Bull. Mar. Sci. **31**: pp. 903-910.

Destouni, G., Prieto, C. (2003): On the possibility for generic modelling of submarine groundwater discharge, Biogeochemistry 11, vol. 66 (1-2): pp. 171-186.

Duffield, W., Edwin, A., McKee, H., Salem, F., and Teimeh, M. (1987): K-AR ages, chemical composition, and geothermal significance of Cenozoic Basalt near the Jordan Rift, technical report, NRA, Amman.

Dulaiova, H., Burnett, C., Chanton, J., Moore, W., Bokuniewicz, H., Charette, M., and Scholkovitz, E. (2004): Continental Shelf Research report-USA.

Elhatip, H. (2003): The use of hydrochemical techniques to estimate the discharge of Ovac1k submarine springs on the Mediterranean coast of Turkey. Environmental Geology **43**: pp. 714-719.

Erica, L., Hmmack R., Harbert W., Sams J., Veloski G. and Ackman T. (2005): Using airborne thermal infrared imagery and helicopter EM conductivity to locate mine pools and discharges in the Kettle Creek watershed, north-central Pennsylvania, Geophysics **70** (6): pp. 73-81.

Feruson, H., (1981). Water balance equations of lakes and reservoirs In ed. H.L. Ferguson and V.A. Znamensky, Methods of Computation of the water Balance of Large Lakes and Reservoirs, United Nations Educational, Scientific and Cultural Organization: pp. 19-24.

Freund, R., Goldberg, M., Weissbrod,T., Druckman,Y. and Drin, B. (1975): The Triassic-Jurassic structure of Israel and its relation to the origin of Eastern Mediterranean, Geology survey of Israel Bull. No. **65**: pp. 1-26, Jerusalem

Gavrieli, I. (1997): Halite deposition from the Dead Sea: 1960-1993, in the Dead Sea the lake and its setting, Edited by Niemi T., Avraham Zvi and Gat, J., Oxford University Press, Oxford an New York: pp. 145-170.

Gavrieli, I., Bein, A., Oren, A. (2005): The expected impact of the peace conduit project (The Red Sea – Dead Sea pipeline) on the Dead Sea. Mitigation and Adaptation strategies for Global Change **10:** pp. 3-22

Gavrieli, I. and Oren, A. (2004): The Dead Sea as a dying lake. Dying and Dead Seas, Earth and Environmental Sciences **36**: pp. 287-305.

Gavrieli, I., Starinsky, A., and Bein, A. (1989): The solubility of the halite as a function of Temperature in the highly saline Dead Sea brine system. Limnol. Oceanography **34**: pp. 1224-1232.

German Technical Assistant (GTZ), (1995): Groundwater modelling in Jordan- A Review and Ground Water Information System of Jordan, Amman, Jordan and Atlanta, USA.

Getman, I., Hecht, A. (2002): The Dead Sea hydrography from 1992 to 2000, Journal of Marine System **35**: pp. 169-181.

Hunting and Macdonald, M. and Partners, (1965) East bank water resources. Hydrogeological survey of the Madaba-Ma'in area. Vol. 1-3. Central Water Authority, Hashemite Kingdom of Jordan.

Itmar, A., and Reizmann, Y. (2000): Air photo survey of sinkholes in the Dead Sea area. Curr. Res. **12** : pp. 21-24.

Jahne, B. Munnich, K.O., Bosinger, R., Dutzi, A., Huber, W., Libner, P. (1987): On the parameters influencing air-water gas exchange. J. Geophysics Res. **92**: pp.1937-1950

Jiries, A. El-Alali, A. (1996): Groundwater effect on salt reef growth in the southern Basin of the Dead Sea. Mu'tah Journal for research and studied **11** (1): pp. 97-109.

Kay, J., Kampf, S., Handcock, R., Cherkauer K., Gillespie, A., and Burges J., (2005): Accuracy of lake and stream Temperatures estimated from thermal infrared Images.

Kelly, R. and Moran, S. (2002): Seasonal changes in groundwater input to a well-mixed estuary estimated using radium isotopes and implications for

coastal nutrient budgets. Limnology and Oceanography **47**(6): pp. 1796-1807.

Khdeir, K. (1997): An assessment of regional hydrogeological framework of the

  Mesozoic aquifer system of Jordan. PhD thesis, University of Birmingham, UK.

Kim, G. and Hwang, W. (2002): Tidal pumping of groundwater into the coastal ocean revealed from submarine Rn 222 and CH4 monitoring. Geophysical Research Letters **29**(14): pp. 23-27.

Klein, C. (1961): On the fluctuations of the level of the Dead Sea since the beginning of the 19th century. Hydrological paper no.7, Ministry of Agriculture, Hydrological Service of Israel.

Krest, J. and Harvey, J., (2003): Using natural distributions of short-lived radium isotopes to quantify groundwater discharge and recharge. Limnology and Oceanography **48**(1): pp. 290-298.

Krumgalz, B. (1997): Ion interaction approach to geochemical aspects of the Dead Sea. in the Dead Sea the lake and its setting, Edited by Niemi T., Avraham Zvi and Gat, J., Oxford University Press, Oxford an New York: pp. 145-160.

Krumgalz, B., Hecht, A., Starinsky, A.and Katz, A., (2000): Thermodynamic constraints on Dead Sea evaporation: how much can the Dead Sea evaporate? Chemical Geology **165**: pp. 1-11.

Lambert, M.J., Burnett, W.C., (2003): Submarine groundwater discharge estimates at a Florida coastal site based on continuous radon measurements, Biogeochemistry 11, vol. **66** (1-2): pp. 55-73.

Lee, D. (1977): A device for measuring seepage flux in lakes and estuaries. Limnology. Oceanography. **22**: pp.140-147.

Loaiciga, H., Zektser, I. (2003): Estimation of Submarine Groundwater Discharge, Water Resources, Vol.**30** (5): pp. 473-479.

Li, L., Bary, D., Stagnitti, F., Parlange, J. (1999): Submarine groundwater discharge and associated chemical input to a coastal sea. Water Resources Research **35**: pp. 3253-3259.

Lloyd, J. (1969): The hydrogeology of the southern desert of Jordan. UNDP/FAO project 212. Tech. Rep. 1.

Mac Donald, Sir M. and Partners, (1965): East Bank water resources. Hydrogeological survey of the Madaba-Ma'an area. Vols 1-3. Central water Authority. Hashemite Kingdom of Jordan.

Macintyre, S., Wanninkhof, R., and Chanton, J. (1995): Trace gas exchange across the air sea interface in fresh water and coastal marine environments. In: P.A. Matson, R.C. Harriss (eds.) Biogenic Trace Gases: Measuring Emissions from Soil and Water, Blackwell Sciences Ltd. 52-97

Manheim, F., Krantz, D., Snyder, D., Bratton, J., White, E., Madsen, J. (2001): Streaming resisitivity survey and core drilling define groundwater discharge into coastal bays of the Delmarva peninsula, The Geological Society of America (GSA).

Mathieu, G., Biscayne, P., Lupton, R. & Hammond, D. (1988): System for measurements of Rn-222 at low levels in natural waters. Health Physics **55**: pp. 989-992.

Martens, C. S., Kipphut, G.W., and Klump, J.V. (1980): Sediment-water chemical exchange in the coastal zone traced by in situ radon-222 flux measurements. Science, **208**: pp. 285-288.

McBride, M.S., Pfannkuch, H.O. (1975): The distribution of seepage within lakebeds. US Geol. Surv. J. Res. **3**: pp. 505-512.

Mckenna, T., Andres, A., Wang, L., and Deliberty, T. (2001): Mapping locations of ground-water discharge in rehoboth and Indian River bays, Delaware using thermal imagery, the geological society of America (GSA).

Ministry of Water and Irrigation (MWI) (1997): Open files. Amman, Jordan.

Mower, R. (1968): Groundwater discharge toward Great Salt Lake through valley fills in the Jordan Valley, Utah. Geol. Survey Res., U.S. Geological Survey Professional paper, **600-D**: pp. 71-74.

Moore, W.S. (1976): Sampling Radium-228 in Deep Ocean; Deep-Sea Res. **23**: pp. 647-651.

Moore, W.S. (1984): Radium Isotope Measurements Using Germanium Detectors, Nucl. Inst. Methods **223**: pp. 407-411.

Moore, W.S., (1996): Large groundwater inputs to coastal waters revealed by Ra226 enrichments, Nature **380**: pp. 612-614.

Moore, W.S. (1999): The subterranean estuary: a reaction zone of groundwater and sea water, Marine Chemistry 65: pp. 111-126.

Moore, W.S. (2000): Determining coastal mixing rates using radium isotopes. Continental Shelf Res. **20**: pp. 1995-2007.

Moore, W.S., Key, R.M. and Samiento, J.L. (1985): Techniques for precise Mapping of Ra-226 and Ra-228 in the Ocean, J.Geophys. Res. **90**: pp. 6983-6994.

Moore, W.S. (2003): Sources and fluxes of submarine groundwater discharge delineated by radium isotopes, Biogeochemistry11, vol. **66** (1-2): pp. 75-93.

Moore, W.S. and Shaw, T.J. (1998): Chemical signals from submarine fluid advection onto the continental shelf, J. Geophys. Res. **103**: pp. 21543-21552.

Mulligan, E. and Charette, M. (2006): Intercomparison of submarine groundwater discharge estimates from a sandy unconfined aquifer, Journal of Hydrology, in press.

Natural Resources Authority (NRA): Internal reports and geological maps sheets in Natural Resources Authority-Jordan/Amman.

Neev, D., Emery, K. (1967): The Dead Sea. Ministry of development, Geological survey, Israel Bulletin No. 41.

Neev, D. and Hall, J. (1976): The Dead Sea geophysical survey, 19 July-1August 1974-Final Report2: Geological survey of Israel, Marine Geology Division, Report No. 6/76: pp. 21.

Neev, D., Hall, J., (1979): Geophysical investigations in the Dead Sea. Sedimentary Geology **23**: pp. 209-238.

Niemi, T. and Ben-Avraham, Z. (1997): The Dead Sea, The Lake and its setting. New Yourk, Oxford University press: pp. 73.

Oberdorfer, J. (2003): Hydrogeological modeling of submarine groundwater discharge: comparison to other quantitative methods. Biogeochemistry **66**: pp. 159-169.

Obermeyer, H. (2005): Personal commencations, Gesellschaft fuer Erkundungortung, Karlsruhe-Germany.

Parker, D. H. (1970): The hydrogeology of the Mesozoic-Cainozoic aquifers of the wetern highlands and plateau of East Jordan. UNDP/FAO, AG2. SF/JOR9, Technical report No. 2, Rome.

Parnes, A. (1975): Middle Triassic ammonite biostratigraphy in Israel. Geological Survey of Israel Bulletin **66**: pp.1-35.

Peng, T., Takahashi, T. and Broecker, W. (1974). Surface radon measurements in the North Pacific station Pape. Journal of Geophysics Res. **79** (12): pp. 1772-1780.

Pluhowski, E. and Kantrowitz, I. (1964): Hydrology of the Babylon-slip area, Suffolk County, Long Island, New York. US Geological survey water-Supply, 1768: pp. 120.

Powell, J. (1988): The geology of the Karak area. Bull. 8, Geol. Mapping Div., Geol. Dir., Natural Resources Authority, Jordan.

Powel, J. (1989): Stratigraphy and Sedimention of Phanerozoic Rocks in Central and South Jordan. Part B Kurnub, Ajlun and Belqa Group. Bulletin 11B, NRA, Amman.

Quennell, A.M. (1951): The geology and mineral resources of former Transjordan. Colon. Geol. Min. Resources, 2.

Quennell, A.M. (1959): Tectonics of the Dead Sea rift. Inter. Geol. Cong. 20th, Assoc. African Geol. Surv.: pp. 385-405.

Rama, M. and Moore, W.S. (1996): Using the radium quartet for evaluating groundwater input and water exchange in salt marches, Geochim. Cosmochim acta **60**: pp. 4645-4652.

Rishmawi K., Eagleton N., Harimat N., and Isaac J. (2005): Using medium-high spatial resolution Sattellite data to monitor biomass changes in the Dead Sea Basin. International Conference on : promotion community-driven conservative and sustainable use of Dry land Argo biodiversity, Syria 18-21 April.

Rundquist, D., Murray, G., Queen, L. (1985): Airborne thermal mapping of a "flow-through" lake in the Nebraska Sand Hills, Water Resources Bulletin **216** (6): pp.989-994.

Salameh, E. (1996): Water quality in Jordan (impacts on environments and future generations resources base). Friedrich Ebert Stiftung, Royal Society for the conservation of nature.

Salameh, E., (1996): Water quality degradation in Jordan (impacts on environment, economy and future generations resources base). National library.

Salameh, E. and Bannayan, H. (1993): Water resources of Jordan present status and future potentials. Friedrich Ebert Stiftung- Amman.

Salameh, E. and El-Naser, H. (1999): Does the actual drop in Dead Sea level reflect the development of water sources within its drainage basin, Acta hydrochim. Hydrobiol. **27**: pp. 5-11.

Salameh, E. and El-Naser, H. (2000a): Changes in the Dead Sea level and their impact on the surrounding Groundwater bodies, Acta hydrochim. Hydrobiol. **28**: pp. 24-33.

Salameh, E. and El-Naser, H., (2000b): The interface configuration of the fresh -/Dead Sea water-Theory and measurements, Acta hydrochim. Hydrobiol. **28**: pp. 323-328.

Salameh, E., and Khawaj, M. (1984): The Mediterranean Dead Sea Canal and its environmental impacts, WRSC Bull, 2nd Issue, University of Jourdan, Amman.

Salameh, E. and Rimawi, O. (1988): The special features of the groundwater flow system in central Jordan. Dirasat **9**, University of Jordan, Amman: pp. 38-58.

Salameh, E., and Udluft, P. (1985): The hydrodynamic pattern of central Jordan, Geol. Jb, c38, Hannover.

Schneider, R. L., Negley, T.L., Wafer, C., (2005): Factors influencing groundwater seepage in a large, mesotrophic lake in New York, J. of Hydrology **310**: pp. 1-16.

Schwartz, (2003): Significant groundwater input to a coastal plain estuary: assessment from excess Radon; Eatuarine, Coastal and Shelf Science **56**: pp. 31-42.

Senior, L., Vogel, K., (1995): Radium and Radon in groundwater in the Chickies quartzite, southern eastern Pennsylvania. US Geological survey water-resources Investigation Report, 92-4088: pp. 15.

Shaban, A., Khawlie, M., Abdallah, C., Faour, G. (2005): Geologic controls of submarine groundwater discharge: application of remote sensing to north Lebanon. Environ. Geol. **47**, pp. 512-522.

Shawabekeh, K. (1998): The Geology of Mai'n Area, Map sheet No. (3153 III). Natural Resources Authority-Amman (Internal Report).

Smith A.J., Nield S.P, (2003): Groundwater discharge from the superficial aquifer into Cockburn Sound Western Australia, estimation by inshore water balance, Biogeochemistry 11, **66** (1-2): pp. 125-144.

Smith, L., Zawadzki W. (2003): A hydrogeological model of submarine groundwater discharge; Florida inter comparison experiment, Biogeochemistry 11, **66**, (1-2): pp. 95-110.

Steinhorn, I. (1983): In situ salt precipitation at the Dead Sea. Limnol. Oceanogr. **28**: pp. 580-583.

Steinhorn, I. and Gat, J. R. (1983): The Dead Sea, Scientific Am. **149**: pp. 102-109.

Steinhorn, I., (1985): The disappearance of the long-term meromictic stratification of the Dead Sea. Limnology and Oceanography **30**: pp. 451-472.

Stiller, M., Chung, Y. (1984): Radium in the Dead Sea: A possible tracer for the duration of meromixis. Limnology and Oceanography **29**(3): pp. 574-586.

Swarzenski W., Jonathan M., and Cable C. (2001): Submarine ground-water discharge in upper Indian River Lagoon, Florida, U.S. Geological Survey Karst Interest Group Proceedings, Water-Resources Investigations Report 01-4011: pp. 194-197.

Taniguchi, M., Burnett, W., Cable, E., Turner, J. (2002): Investigation of submarine groundwater discharge, Hydrological processes **16**: pp.2115-2129.

Taniguchi, M., Burnett W.C., Smith C.F., Paulsen R.J., O'Rourke D., Kruba S.L., Christoff J.L. (2003): Spatial and Toral distributions of submarine groundwater discharge rates obtained from various types of seepage meters at the site in the north eastern gulf of Mexico, Biogeochemistry 11, **66** (1-2): pp. 35-53.

Taqieddin, S., Abderahman, N. and Attalah, M. (2000): Sinkholes Hazards along the Eastern Dead Sea Shoreline Area, Jordan. A Geological and Geotechnical Consideration, Environ. Geology **39** (11): pp. 1237-1253.

Tcherepanov, E.N., and Zlotnik, V. (2002): Applications of remote sensing for hydrological studies in the Nebraska, Report for NE9B, in GSA Abstracts with program, Denver, Colorado: pp. 88.

Valiela, I., Costa J., Foreman, K., Teal, J., Howes, B., and Aubrey, D. (1990): Transport of groundwater borne nutrients from watersheds and their effects on coastal waters. Biogeochemistry **10**: pp. 177-198.

Valiela, I & D'Elia, C. (1990): Groundwater inputs to coastal waters. Special Issue Biogeochemistry **10**: pp. 328.

Vsevolozhskii, V. and Kochetkova, R. (2003): Groundwater runoff in Karelia, Water Resources **30** (4): pp. 351-360.

Ullman, W. and Aller, R. (1981): Diffusion coefficients in nearshore marine sediments. Limnology Oceanography **27**: pp. 552-556

US geological survey Bulletin (1971): pp. 195-225.

Water Authority of Jordan (WAJ): Open files of the Water Authority of Jordan/Amman.

Wanninkhof, R., (1992): Relationship between wind speed and gas exchange over the ocean. Journal Geophysics Research **97**: pp. 7373-7382.

Water Data Banks Project, Multilateral Working Group on Water Resources, Middle East Peace Process. http://exact-me.org/overview/p17.htm.

Wiesemann, G. (1969): Zur Tektonik des Gebietes Ostlich des Grabeabschnittes Totes Meer-Jordantal. Beih. Geol. Jb., 81 Hannover.

Yechieli, Y., Ronen, D., Kaufman, A. (1996): The source and age of groundwater brines in the Dead Sea area as deduced from Cl 36 and C14. Geochimica et cosmochimica Acta, **60** (11): pp. 1909-1916.

Zektser, I., Dzhamalov, R., Safronova, T. (1983): Role of submarine groundwater discharge in the water balance of Australia. IAHS-AISH publication, No. 142 ' Groundwater in Resources Planning': pp. 209-219.

<u>APPENDICES</u>

<u>APPENDIX I</u>

**Photos for The Thermal Infrared Camera and The Plane which
Used for Carring out TIR Imagery**
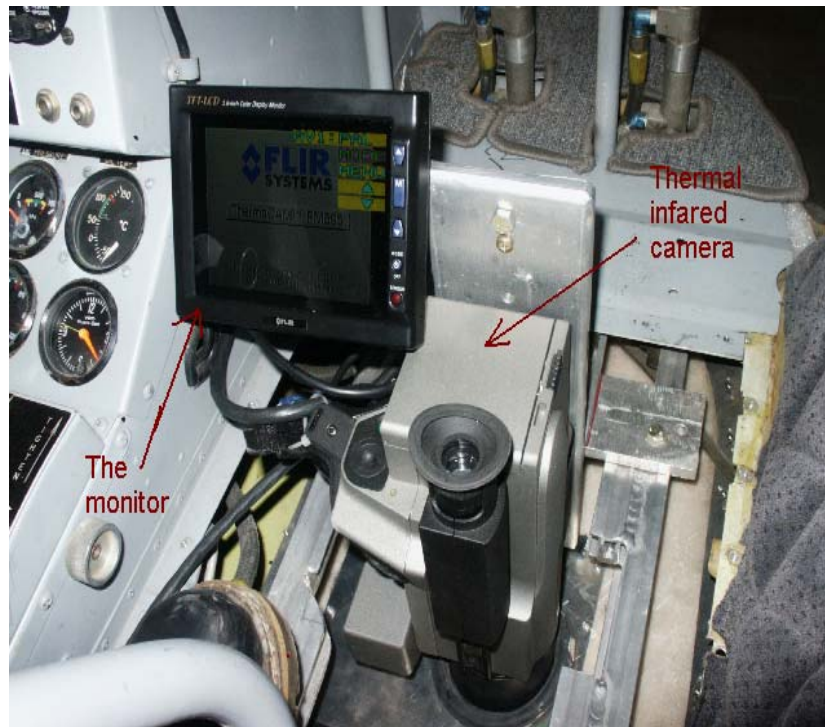
Photo1: the thermal infrared camera fixed inside the plane.

Photo 2: commercial plane which was used for TIR imagery

APPENDIX II

The Electrical Conductivity, Temperature, Total Dissolved Solids and The Depth Data for Sweimeh area, Zarka Ma'in, Zara and Mujeb Area.

Zarka ma'in 100m away from the shoreline

Depth [m]	E.C. [mS/cm]	T. [C°]	TDS [g/l]	Depth [m]	E.C. [mS/cm]	T. [C°]	TDS [g/l]
1	176.05	38.48	403.241839	47	186.56	24.79	366.137489
2	176.53	38.27	401.769508	48	186.73	24.75	365.42282
3	176.6	38.07	401.55345	49	186.79	24.73	365.169346
4	176.69	37.88	401.275152	50	186.87	24.71	364.830362
5	176.47	37.7	401.954426	51	186.88	24.7	364.787907
6	176.46	37.53	401.985221	52	186.93	24.69	364.575354
7	177.3	37.36	399.373528	53	186.99	24.68	364.319681
8	178.46	37.19	395.680017	54	186.99	24.67	364.319681
9	179.14	37.02	393.464844	55	187.05	24.65	364.063336
10	179.88	36.86	391.009383	56	187.13	24.64	363.720489
11	180.1	36.71	390.269975	57	187.18	24.63	363.505594
12	180.88	36.64	387.612017	58	187.21	24.61	363.376427
13	181.47	36.24	385.562046	59	187.29	24.59	363.031137
14	181.47	35.45	385.562046	60	187.38	24.58	362.6412
15	180.41	35.39	389.22051	61	187.27	24.58	363.117575
16	180.1	34.75	390.269975	62	187.48	24.55	362.206071
17	180.71	34.69	388.19627	63	187.46	24.54	362.293255
18	180.08	34.44	390.337376	64	187.57	24.53	361.812753
19	176.99	34.19	400.343308	65	187.56	24.52	361.856535
20	178.9	33.99	394.251061	66	187.61	24.51	361.637422
21	177.49	33.7	398.775628	67	187.2	24.5	363.419502
22	174.52	33.42	407.832448	68	187.4	24.49	362.554332
23	169.99	33.19	420.623731	69	187.7	24.48	361.24174
24	166.53	32.32	429.719146	70	187.4	24.47	362.554332
25	166.03	31.93	430.991886	71	187.7	24.46	361.24174
26	167.44	31.35	427.376896	72	187.8	24.46	360.800142
27	167.59	30.77	426.987526	73	187.7	24.45	361.24174
28	168.51	30.34	424.578386	74	187.7	24.44	361.24174
29	170.14	29.76	420.217237	75	187.9	24.43	360.356462
30	171.61	29.23	416.175121	76	187.9	24.42	360.356462
31	172.32	28.87	414.183144	77	187.9	24.42	360.356462
32	173.7	28.41	410.23237	78	187.7	24.41	361.24174
33	174.85	28.08	406.855032	79	187.6	24.41	361.681285
34	176.17	27.68	402.875249	80	188	24.4	359.910672
35	177.36	27.33	399.185009				
36	179.06	26.78	393.727457				
37	180.11	26.29	390.23626				
38	181.15	25.87	386.67824				
39	181.99	25.67	383.725531				
40	182.62	25.49	381.461169				
41	182.89	25.38	380.476938				
42	183.48	25.22	378.296014				
43	183.96	25.09	376.489757				
44	184.2	25	375.575395				
45	185.39	24.9	370.923294				
46	186.23	24.83	367.51033				

Zarka Ma'in 200 m away from the shoreline

Depth [m]	E.C. [mS/cm]	T. [C°]	TDS [g/l]	Depth [m]	E.C. [mS/cm]	T. [C°]	TDS [g/l]
1	192.03	33.74	339.715357	51	179.14	26.75	393.464844
2	191.9	33.8	340.453145	52	179.66	26.6	391.74442
3	190	34.03	350.498509	53	179.91	26.45	390.908814
4	188.98	34.13	355.423513	54	179.19	26.37	393.300434
5	187.52	34.14	362.031463	55	179.69	26.22	391.644442
6	185.77	34.1	369.393381	56	180.22	26.08	389.864791
7	185.18	34.03	371.759218	57	180.75	25.95	388.059052
8	185.64	33.9	369.919323	58	181.2	25.83	386.50452
9	185.78	33.81	369.352812	60	181.47	25.77	385.562046
				61	181.92	25.66	383.974429
10	185.42	33.79	370.803329	62	182.38	25.56	382.32901
11	184.97	33.75	372.588546	63	182.73	25.47	381.061208
12	184.05	33.71	376.147766	64	183.07	25.38	379.816027
13	183.78	33.67	377.170563	65	183.35	25.3	378.7802
14	183.97	33.58	376.45181	66	183.49	25.27	378.258682
15	184.06	33.52	376.109701				
16	183.19	33.46	379.373267	68	183.8	25.19	377.095125
17	182.02	33.4	383.618699	70	184.09	25.11	375.995427
18	179.84	33.25	391.143349	71	184.07	25.04	376.071623
19	178.4	33.1	395.87365	72	184.23	24.97	375.460559
20	175.13	32.99	406.020333	73	184.35	24.94	375
21	171.15	32.86	417.45165	74	184.58	24.88	374.111743
22	167.77	32.7	426.519029	75	184.86	24.81	373.020374
23	165.87	32.38	431.397086	77	185.13	24.75	371.95727
24	166.63	32.12	429.463404	80	185.54	24.65	370.322079
25	167.1	31.83	428.255995	81	185.88	24.57	368.94624
26	166.58	31.24	429.591325	82	186.11	24.48	368.004934
27	167.15	30.94	428.127016	83	186.27	24.41	367.344922
28	168.24	30.47	425.28921	84	186.53	24.34	366.263074
29	169.73	30.17	421.32579	85	186.67	24.31	365.675645
30	169.27	29.89	422.560149	86	186.77	24.27	365.253909
31	171.24	29.61	417.202746	87	186.84	24.24	364.957618
32	170.59	29.47	418.991247	88	187.04	24.19	364.106107
33	170.04	29.22	420.488353	90	187.24	24.14	363.247088
34	171.78	28.97	415.700593	91	187.46	24.08	362.293255
35	172.86	28.73	412.649923				
36	173.52	28.5	410.753832				
38	174.27	28.28	408.568432				
40	174.61	28.16	407.566552				
41	175.2	27.95	405.810876				
42	175.78	27.75	404.063092				
43	176.41	27.56	402.139091				
44	177.09	27.37	400.031246				
45	177.69	27.18	398.143323				
47	177.96	27.09	397.284855				
50	178.52	26.93	395.486092				

Zarka Ma'in 400 m away from the shoreline

Depth [m]	E.C. [mS/cm]	T. [C°]	TDS [g/l]	Depth [m]	E.C. [mS/cm]	T. [C°]	TDS [g/l]
1	191.48	34.04	342.787915				
2	189.43	34.25	353.285243	56	179.73	26.58	391.511014
3	187.32	34.29	362.901334	58	180.27	26.44	389.69557
4	187.27	34.28	363.117575	60	180.79	26.29	387.921678
5	187.44	34.24	362.38036	61	181.32	26.14	386.086561
6	187.8	34.2	360.800142	62	181.79	26.01	384.435272
7	186.26	34.17	367.3863	64	182.03	25.94	383.583066
8	186.64	34.14	365.801816	66	182.47	25.82	382.004335
9	186.3	34.12	367.220688	68	182.89	25.7	380.476938
10	187.28	34.06	363.074366	70	183.33	25.59	378.854505
11	185.59	34.04	370.120897	71	183.74	25.48	377.321284
12	184.85	34	373.059544	72	183.97	25.42	376.45181
13	184.79	33.83	373.294264	73	184.56	25.26	374.189274
14	184.15	33.8	375.766519	74	184.74	25.21	373.489469
15	179.46	33.57	392.408907	75	185.14	25.11	371.917689
16	177.77	33.5	397.889547	76	185.55	25	370.281874
17	177.73	33.41	398.016496	80	185.89	24.92	368.905494
18	176.81	33.16	400.903191	81	186.06	24.88	368.210308
19	172.46	33.02	413.787177	82	186.41	24.79	366.763842
20	166.82	32.94	428.976384	83	186.66	24.72	365.71772
21	165.37	32.76	432.656961	84	186.9	24.65	364.702941
22	165.91	32.51	431.29588	85	187.17	24.58	363.548611
23	164.77	32.23	434.156302	90	187.42	24.53	362.467386
24	164.23	31.93	435.494324	91	187.57	24.49	361.812753
25	163.85	31.78	436.429573	92	187.78	24.44	360.888627
26	165.54	31.1	432.229679				
27	167	30.76	428.513645				
28	166.6	30.45	429.540169				
29	170.43	30.15	419.428282				
30	169.38	30	422.265867				
31	170.47	29.71	419.319141				
32	170.77	29.43	418.498079				
33	171.46	29.15	416.592574				
34	172.3	28.89	414.239624				
35	173	28.65	412.249785				
38	173.32	28.53	411.331029				
40	173.93	28.31	409.563288				
42	174.68	28.08	407.359397				
44	175.4	27.86	405.210683				
46	176.07	27.65	403.180809				
48	176.38	27.55	402.231329				
50	177.02	27.36	400.249766				
51	177.63	27.18	398.333333				
52	178.28	27	396.260048				
53	178.9	26.82	394.251061				
54	179.47	26.66	392.375766				

Zarka Ma'in 800 m away from the shoreline

Depth [m]	E.C. [mS/cm]	T. [C°]	TDS [g/l]	Depth [m]	E.C. [mS/cm]	T. [C°]	TDS [g/l]
1	197.44	31.91	295.437794				
2	196.57	32.17	306.071968	47	189.97	23.87	350.647485
3	195.76	32.41	313.866008	48	190.09	23.84	350.049985
4	194.19	32.7	326.131876	49	190.16	23.82	349.699458
5	193.27	32.96	332.262229	50	190.28	23.8	349.095087
6	191.48	33.16	342.787915	51	190.35	23.78	348.740482
7	190.92	33.31	345.79385	52	190.43	23.76	348.333333
8	190.13	33.41	349.849865	53	190.5	23.75	347.975406
9	189.61	33.47	352.415006	54	190.61	23.72	347.409743
10	189.34	33.53	353.717099	55	190.63	23.71	347.306469
11	189.21	33.56	354.337136	56	190.7	23.7	346.943964
12	188.07	33.59	359.597346	57	190.73	23.69	346.788102
13	186.91	33.55	364.660431	58	190.82	23.67	346.318688
14	186.84	33.52	364.957618	59	190.85	23.66	346.1616
15	186.57	33.45	366.095592	60	190.88	23.66	346.004202
16	186.37	33.3	366.930208	61	190.94	23.65	345.688464
17	185.72	33.24	369.595984	62	190.96	23.63	345.582937
18	184.18	33.13	375.651885	63	190.99	23.62	345.424382
19	178.81	33.01	394.544647	64	190.99	23.62	345.424382
20	178.29	32.7	396.227892	65	191.03	23.61	345.212478
21	179.21	32.38	393.234611	66	191.07	23.6	345
22	172.62	32.01	413.333333	67	191.13	23.59	344.680198
23	166.12	31.57	430.763522	68	191.14	23.59	344.62677
24	168.09	30.74	425.682739	69	191.16	23.58	344.519805
25	169.41	30.03	422.185512	70	191.18	23.57	344.412692
26	171.21	29.35	417.285759	71	191.22	23.56	344.198022
27	173.48	28.62	410.869456	72	191.21	23.56	344.251745
28	174.94	28.07	406.587279	73	191.3	23.55	343.76689
29	176.89	27.49	400.654643	74	191.3	23.55	343.76689
30	177.4	27.08	399.059181	75	191.32	23.54	343.65873
31	179.35	26.63	392.772883	76	191.29	23.54	343.820913
32	180.82	26.3	387.818546	77	191.35	23.53	343.496204
33	182.11	25.95	383.297614	78	191.35	23.53	343.496204
34	183	25.7	380.073506	79	191.42	23.51	343.115633
35	183.98	25.43	376.413851	80	191.42	23.51	343.115633
36	184.76	25.23	373.41143	81	191.43	23.51	343.061111
37	185.49	25.02	370.522871	82	191.44	23.51	343.00655
38	186.06	24.84	368.210308	83	191.46	23.5	342.897311
39	186.77	24.65	365.253909	84	191.44	23.51	343.00655
40	187.36	24.51	362.72799	85	191.46	23.5	342.897311
41	188	24.37	359.910672	86	191.5	23.5	342.678362
42	188.48	24.24	357.740507				
43	188.95	24.12	355.564236				
44	189.35	24.02	353.669221				
45	189.72	23.93	351.87882				
46	189.86	23.91	351.191482				

160

Sweimah 200 m away from the shoreline

Depth [m]	E.C. [mS/cm]	T. [C]	TDS [g/l]	Depth [m]	E.C. [mS/cm]	T. [C]	TDS [g/l]
1	190.35	33.52	348.74	48	171.63	25.94	416.119
2	187.92	33.54	360.267	49	171.84	25.88	415.533
3	186.09	33.58	368.087	50	171.95	25.84	415.225
4	184.91	33.6	372.824	51	172.09	25.79	414.831
5	184.17	33.59	375.69	52	172.29	25.74	414.268
6	181.38	33.56	385.877	53	172.48	25.68	413.731
7	177.34	33.51	399.248	54	172.61	25.64	413.362
8	169.83	33.29	421.056	55	172.75	25.59	412.964
9	166.49	33	429.821				
10	166.11	32.58	430.789				
11	167.74	32.07	426.597				
12	168.62	31.79	424.288				
13	169.44	31.51	422.105				
14	170.24	31.25	419.946				
15	170.95	31.01	418.003				
16	171.73	30.77	415.84				
17	172.44	30.56	413.844				
18	171.54	30.44	416.37				
19	171.08	29.79	417.645				
20	171.61	29.56	416.175				
21	172	29.34	415.084				
22	171.96	29.22	415.196				
23	172.63	29	413.305				
24	173.34	28.7	411.273				
25	172.69	28.58	413.134				
26	168.89	28.38	423.573				
27	164.78	28.18	434.131				
28	164.38	28.21	435.124				
29	164.94	27.9	433.733				
30	165.5	27.73	432.33				
31	166.07	27.56	430.89				
32	166.62	27.42	429.489				
33	166.94	27.33	428.668				
34	167.32	27.2	427.688				
35	167.77	27.07	426.519				
36	168.19	26.94	425.42				
37	168.61	26.84	424.314				
38	169.03	26.73	423.2				
39	169.21	26.67	422.72				
40	169.59	26.56	421.703				
41	169.91	26.46	420.84				
42	170.19	26.38	420.082				
43	170.48	26.29	419.292				
44	170.76	26.2	418.526				
45	170.92	26.16	418.086				
46	171.18	26.08	417.369				
47	171.47	26	416.565				

Sweimah 300 away from the shoreline

Depth (m)	E.C. [mS]	T. [C]	TDS [g/l]
1	198.4	30.1	271.937
2	197.71	30.18	291.218
3	196.76	30.23	304.009
4	194.91	30.3	320.853
5	190.43	30.36	348.333
6	184.45	30.41	374.615
7	179.84	30.51	391.143
8	178.3	30.7	396.196
9	178.02	30.33	397.093
10	178.12	30.23	396.773
11	175.95	30.05	403.547
12	172.75	29.92	412.964
13	171.75	29.75	415.784
14	172.09	29.56	414.831
15	171.97	29.44	415.168
16	172.23	29.13	414.437
17	172.64	28.9	413.277
18	173.26	28.68	411.504
19	173.9	28.44	409.651
20	174.54	28.23	407.773
21	175.32	28.01	405.451
22	175.76	27.9	404.124
23	176.65	27.62	401.399
24	177.28	27.44	399.436
25	177.77	27.26	397.89
26	178.23	27.09	396.421
27	178.51	27.01	395.518
28	179.07	26.85	393.695
29	179.64	26.69	391.811
30	180.15	26.55	390.101
31	180.56	26.43	388.709
32	180.77	26.36	387.99
33	181.17	26.24	386.609
34	181.55	26.12	385.281
35	181.96	26	383.832
36	182.38	25.89	382.329
37	182.74	25.79	381.025
38	182.95	25.72	380.257
39	183.33	25.62	378.855
40	183.45	25.51	378.408
41	184.74	25.41	373.489
42	184.29	25.32	375.231

Sweimah 400 m away from the shoreline

Depth (m)	E.C. [mS]	T. [C]	TDS [g/l]	Depth (m)	E.C. [mS]	T. [C]	TDS [g/l]
1	198.43	30.28	268.333	48	177.68	25.6	398.175
2	198.4	30.54	271.937	49	177.81	25.51	397.762
3	197.2	30.77	298.726	50	177.72	25.48	398.048
4	194.83	31.07	321.464	51	178.28	25.39	396.26
5	193.07	31.22	333.521	52	178.36	25.31	396.003
6	189.55	31.33	352.706	53	178.9	25.24	394.251
7	185.97	31.43	368.579	54	179.22	25.17	393.202
8	184.15	31.47	375.767	55	179.44	25.11	392.475
9	183.93	31.48	376.604	56	179.62	25.07	391.878
10	182.03	31.47	383.583	57	179.83	25.01	391.177
11	178.66	31.41	395.032	58	180.03	24.96	390.506
12	175.66	31.35	404.427	59	180.23	24.9	389.831
13	174.95	31.25	406.557	60	180.35	24.87	389.424
14	174.76	31.12	407.122	61	180.53	24.81	388.812
15	171.96	30.96	415.196	62	180.79	24.75	387.922
16	170.48	30.79	419.292	63	180.99	24.7	387.232
17	169.22	30.59	422.694	64	181.15	24.66	386.678
18	169.5	30.37	421.944	65	181.31	24.62	386.121
19	170.14	30.01	420.217	66	181.42	24.58	385.737
20	170.51	29.89	419.21	67	181.57	24.54	385.211
21	170.8	29.64	418.416	68	181.75	24.49	384.577
22	171.22	29.4	417.258	70	181.88	24.44	384.116
23	171.79	29.16	415.673	72	182.11	24.4	383.298
24	172.39	28.93	413.985	74	182.27	24.35	382.725
25	173.15	28.69	411.82	76	182.37	24.33	382.365
26	173.85	28.46	409.796	78	182.47	24.29	382.004
27	174.2	28.35	408.774	80	182.61	24.25	381.497
28	174.84	28.13	406.885	82	182.73	24.22	381.061
29	175.51	27.93	404.879	84	182.85	24.19	380.623
30	176.12	27.74	403.028	86	182.93	24.17	380.33
31	174.92	27.55	406.647	88	182.98	24.15	380.147
32	176.11	27.36	403.059	90	183.13	24.12	379.595
33	176.63	27.26	401.461	92	183.16	24.1	379.484
34	177.29	27.09	399.405	94	183.23	24.07	379.225
35	177.93	26.94	397.381				
36	178.33	26.8	396.099				
37	178.87	26.67	394.349				
38	176.64	26.54	401.43				
39	175	26.47	406.408				
40	175.23	26.35	405.721				
41	175.67	26.23	404.396				
42	176.05	26.12	403.242				
43	176.43	26.01	402.078				
44	176.63	25.95	401.461				
45	176.97	25.86	400.406				
46	177.27	25.77	399.468				
47	177.48	25.68	398.807				

Sweimah 500 m away from the shoreline

Depth (m)	E.C. [mS]	T. [C]	TDS [g/l]	Depth (m)	E.C. [mS]	T. [C]	TDS [g/l]
1	198.4	30.16	271.937	64	180.19	26.43	389.966
2	198.39	30.29	272.676	66	180.73	26.28	388.128
3	198.39	30.5	272.676	68	180.97	26.22	387.302
4	198.38	30.68	273.333	70	181.72	26.02	384.683
5	198.35	30.84	275	72	182.09	25.92	383.369
6	198.3	30.99	277.208	74	182.65	25.77	381.352
7	198.2	31.14	280.611	76	183.06	25.66	379.853
8	198.1	31.22	283.333	78	183.26	25.61	379.114
9	197.89	31.37	287.945	80	183.66	25.5	377.622
10	196.1	31.42	310.763	82	184.09	25.4	375.995
11	195.3	31.62	317.766	84	184.5	25.28	374.422
12	194.78	31.72	321.843	86	184.86	25.19	373.02
13	193.16	31.79	332.957	88	185.18	25.11	371.759
14	191.97	31.84	340.057				
15	190.88	31.91	346.004				
16	190.65	31.95	347.203				
17	189.79	31.98	351.536				
18	186.3	32	367.221				
19	179.86	32.01	391.076				
20	176.51	32.01	401.831				
21	176.36	31.92	402.293				
22	176.68	31.78	401.306				
23	173.6	31.64	410.522				
24	168.83	31.48	423.732				
25	166.86	31.38	428.874				
26	167.29	31.15	427.765				
27	168.15	30.87	425.525				
28	169	30.57	423.28				
29	169.12	30.31	422.961				
30	168.88	30.15	423.599				
32	169.54	29.86	421.837				
34	170.49	29.55	419.265				
36	171.23	29.26	417.23				
38	171.93	28.99	415.281				
40	172.73	28.73	413.02				
42	173.11	28.61	411.935				
44	173.84	28.37	409.825				
46	174.6	28.13	407.596				
48	175.41	27.88	405.181				
50	176.09	27.67	403.12				
52	176.85	27.45	400.779				
54	177.49	27.25	398.776				
56	177.83	27.15	397.699				
58	178.54	26.92	395.421				
60	179.05	26.77	393.76				
62	179.69	26.58	391.644				

Sweimah 800 m away from the shoreline.

Depth (m)	E.C. [mS]	T. [C]	TDS [g/l]	Depth (m)	E.C. [mS]	T. [C]	TDS [g/l]
1	198	30.71	285.67	47	185.41	25.05	370.843
2	197.33	31	296.989	48	185.66	24.98	369.839
3	193.7	31.37	329.471	49	185.79	24.92	369.312
4	188.03	31.61	359.777	50	186.05	24.85	368.251
5	177.5	31.71	398.744	51	186.28	24.79	367.304
6	176.89	31.6	400.655	52	186.48	24.73	366.472
7	177.85	31.36	397.635	53	186.67	24.67	365.676
8	178.71	31.09	394.87	54	186.8	24.64	365.127
9	179.29	30.86	392.971	55	187.02	24.58	364.192
10	180.5	30.65	388.914	56	187.22	24.53	363.333
11	180.65	30.45	388.402	57	187.41	24.47	362.511
12	181.2	30.28	386.505	58	187.59	24.44	361.725
13	181.85	30.11	384.223	59	187.83	24.38	360.667
14	179.92	29.98	390.875	60	187.98	24.34	360
15	173.06	29.82	412.078	61	188.17	24.3	359.148
16	172.35	29.56	414.098	62	188.32	24.26	358.47
17	173.67	29.1	410.319	63	188.55	24.21	357.42
18	173.84	28.81	409.825	64	188.64	24.19	357.006
19	174.36	28.43	408.304	65	188.78	24.15	356.357
20	175.21	28.14	405.781	66	188.96	24.12	355.517
21	176.38	27.79	402.231	67	189.15	24.07	354.622
22	177.52	27.46	398.681	68	189.31	24.03	353.861
23	178.28	27.24	396.26	69	189.44	24	353.237
24	178.93	27.04	394.153	70	189.54	23.98	352.754
25	179.13	26.98	393.498	71	189.7	23.95	351.977
26	179.44	26.85	392.475	72	189.86	23.9	351.191
27	179.71	26.73	391.578	73	190.02	23.87	350.399
28	180.04	26.61	390.472	74	190.11	23.85	349.95
29	180.47	26.48	389.016	75	190.29	23.82	349.045
30	180.84	26.37	387.75	76	190.35	23.79	348.74
31	180.96	26.31	387.336	77	190.43	23.79	348.333
32	181.3	26.2	386.156	78	190.55	23.76	347.719
33	181.69	26.1	384.789	79	190.68	23.72	347.048
34	182.11	25.99	383.298	80	190.83	23.7	346.266
35	182.51	25.88	381.86	81	190.87	23.69	346.057
36	182.84	25.79	380.66	82	190.94	23.67	345.688
37	183.05	25.74	379.89	83	190.99	23.65	345.424
38	183.36	25.65	378.743	84	191.06	23.63	345.053
39	183.65	25.57	377.66	85	191.11	23.62	344.787
40	183.82	25.49	377.02	86	191.21	23.6	344.252
41	183.95	25.45	376.528	87	191.24	23.6	344.09
42	184.2	25.37	375.575	88	191.33	23.57	343.605
43	184.49	25.29	374.46	89	191.37	23.56	343.388
44	184.83	25.21	373.138	90	191.38	23.55	343.333
45	185.1	25.14	372.076	91	191.49	23.54	342.733
46	185.31	25.08	371.243	92	191.51	23.53	342.624
				93	191.55	23.52	342.404

Zara 100 m away from the shoreline

Depth [m]	E.C. [mS/cm]	T. [C°]	TDS [g/l]	Depth [m]	E.C. [mS/cm]	T. [C°]	TDS [g/l]
1	159.9	43.44	445.8624007	47	176.85	27.46	400.7789745
2	162.01	42.61	440.8871528	48	177.53	27.37	398.6494096
3	164.26	41.76	435.4202675	49	178.22	27.2	396.4528156
4	165.99	40.98	431.0932798	50	178.78	27.04	394.6423588
5	167.34	40.27	427.6359529	51	179.2	26.89	393.2675268
6	168.16	39.93	425.499213	52	179.7	26.74	391.6110988
7	168.9	39.59	423.545955	53	180.15	26.6	390.1013097
8	169.34	39.43	422.3729429	54	180.41	26.54	389.2205097
9	170.22	39.13	420	55	180.87	26.4	387.646463
10	170.88	38.82	418.1959084	56	181.35	26.27	385.9818422
11	169.44	38.53	422.1051146	57	181.47	26.15	385.5620455
12	164.69	38.26	434.3552007	58	182.06	26.02	383.4761031
13	160.56	37.98	444.3211378	59	181.91	25.9	384.0099428
14	153.32	37.82	460.5595351	60	180.79	25.85	387.921678
15	151.66	37.47	464.0945719	61	181.07	25.75	386.9556705
16	152.33	37.06	462.6754533	62	181.47	25.65	385.5620455
17	153.13	36.58	460.9674072	63	180.87	25.57	387.646463
18	154.03	36.08	459.0277276	64	180.93	25.48	387.4396401
19	155.16	35.57	456.5642999	65	181.49	25.41	385.4919352
20	155.55	35.31	455.7066389	66	181.7	25.37	384.7532639
21	156.64	34.81	453.2886851	67	182	25.3	383.6899312
22	157.59	34.33	451.1554498	68	182.25	25.23	382.7963834
23	158.41	33.87	449.2940955	69	182.43	25.17	382.148748
24	159.54	33.42	446.6975282	70	182.77	25.07	380.9154206
25	160.76	32.98	443.8514415	71	182.98	25.02	380.1469635
26	161.35	32.77	442.4585259	72	183.27	24.96	379.0771249
27	162.56	32.36	439.5667663	73	183.46	24.91	378.3706405
28	163.67	31.98	436.8707925	74	183.69	24.86	377.5093981
29	164.77	31.61	434.1563015	75	183.84	24.82	376.9440946
30	165.82	31.26	431.5235069	76	184	24.7	376.3378925
31	166.24	31.09	430.45854	77	184.51	24.66	374.3828575
32	167.19	30.77	428.0237586	78	186.32	24.61	367.1377792
33	168.16	30.46	425.499213	79	186.14	24.58	367.8815097
34	169.04	30.16	423.1736775	80	186.13	24.56	367.9226679
35	169.94	29.89	420.7589911	82	186.33	24.51	367.0962993
36	170.7	29.63	418.6900567	84	186.18	24.47	367.7167093
37	170.92	29.5	418.0858787				
38	171.64	29.26	416.0914898				
39	172.33	29.01	414.154896				
40	173	28.79	412.2497853				
41	173.76	28.55	410.0581277				
42	174.49	28.33	407.9209685				
43	174.72	28.23	407.2408859				
44	175.99	28.02	403.4247662				
45	176.5	27.82	401.8619986				
46	176.5	27.64	401.8619986				

166

Zara 300 m away from the shoreline

Depth [m]	E.C. [mS/cm]	T. [C°]	TDS [g/l]	Depth [m]	E.C. [mS/cm]	T. [C°]	TDS [g/l]
1	189.44	33.3	353.2371261	47	180.47	26.71	389.0163477
2	189.09	33.36	354.9056099	48	180.84	26.59	387.7497419
3	189.22	33.4	354.2895962	49	181.02	26.54	387.12874
4	189.11	33.43	354.8111188	50	181.29	26.42	386.1911876
5	188.92	33.46	355.7047359	51	181.47	26.32	385.5620455
6	188.45	33.47	357.8776553	52	181.69	26.22	384.7885435
7	187.41	33.47	362.5108689	53	182.36	26.13	382.4010369
8	187.36	33.45	362.7279897	54	182.18	26.03	383.0472683
9	187.11	33.36	363.8063141	55	182.3	25.98	382.6168475
10	185.05	33.34	372.2733794	56	183.06	25.89	379.8528456
11	180.79	33.32	387.921678	57	183.31	25.81	378.9287608
12	174.49	33.11	407.9209685	58	183.37	25.73	378.7058463
13	173.63	32.97	410.4353853	59	183.76	25.64	377.2459494
14	173.38	32.71	411.158112	60	183.86	25.57	376.8685017
15	174	32.63	409.359032	61	184.01	25.52	376.2998936
16	174.8	32.34	407.0035629	62	184.4	25.45	374.8075213
17	175.19	32.14	405.8408182	63	184.68	25.37	373.7232457
18	175.83	31.97	403.9113792	64	185.13	25.25	371.9572698
19	176.56	31.45	401.6769543	65	185.42	25.18	370.803329
20	174.53	31.2	407.8029286	66	185.55	25.14	370.2818736
21	173.14	31.21	411.8485449	67	185.76	25.08	369.4339334
22	172.84	31.04	412.706996	68	185.95	25.02	368.6606752
23	172.61	30.85	413.3617397	69	186.33	24.91	367.0962993
24	172.81	30.66	412.7925637	70	186.45	24.88	366.5971981
25	171.03	30.36	417.7828839	71	186.69	24.82	365.5914417
26	171.55	30.15	416.3422418	72	186.9	24.77	364.7029411
27	172.23	29.93	414.4371343	73	187.05	24.71	364.0633356
28	172.92	29.72	412.4785699	74	187.22	24.66	363.3333333
29	173.42	29.5	411.0427189	75	187.38	24.62	362.6412003
30	173.63	29.3	410.4353853	76	187.49	24.6	362.162449
31	173.11	29.21	411.9346183	77	187.66	24.55	361.4178027
32	173.13	29.01	411.8772417	78	187.75	24.51	361.021199
33	173.47	28.81	410.8983476	79	187.89	24.46	360.4009246
34	174.34	28.62	408.362742	80	188.09	24.42	359.5076298
35	174.9	28.43	406.7063436	81	188.24	24.38	358.8319771
36	175.32	28.24	405.4510718	82	188.28	24.36	358.6509648
37	175.58	28.15	404.668277	83	188.43	24.32	357.9689728
38	176.16	27.98	402.9058355	84	188.6	24.29	357.1898374
39	176.79	27.79	400.9652561	85	188.69	24.25	356.7746266
40	177.28	27.63	399.4363084	86	188.82	24.22	356.1714772
41	177.77	27.47	397.8895475	87	188.96	24.19	355.5173529
42	178.34	27.32	396.066993	88	189.17	24.16	354.5270357
43	178.89	27.17	394.2837153	89	189.31	24.12	353.8605757
44	179.15	27.1	393.4319791				
45	179.64	26.96	391.8110278				
46	180.06	26.83	390.4047413				

167

Zara 400 m away from the shoreline

Depth [m]	E.C. [mS/cm]	T. [C°]	TDS [g/l]	Depth [m]	E.C. [mS/cm]	T. [C°]	TDS [g/l]
1	198.4	31.08	271.9371294	49	187.51	24.52	362.0751452
2	197.04	31.4	300.7417472	50	187.86	24.41	360.5341856
3	195.83	31.65	313.243962	51	188.24	24.31	358.8319771
4	195.96	31.85	312.0661282	52	188.54	24.24	357.4655898
5	196.15	31.93	310.2875078	53	188.82	24.16	356.1714772
6	194.9	32.01	320.929402	54	189.04	24.12	355.1413963
7	193.71	32.15	329.4051007	55	189.24	24.06	354.19444
8	193.59	32.22	330.1970618	56	189.45	24.01	353.1889823
9	192.18	32.25	338.8546928	57	189.63	23.96	352.3177677
10	188.69	32.29	356.7746266	58	189.73	23.93	351.8299086
11	185.65	32.34	369.8789614	59	189.88	23.9	351.0928343
12	182.45	32.35	382.0765642	60	190.02	23.86	350.3990446
13	178.15	32.33	396.67735	61	190.11	23.84	349.949985
14	170.53	32.29	419.1552819	62	190.23	23.82	349.347445
15	169.31	32.2	422.4532015	63	190.32	23.8	348.8926426
16	167.82	32.04	426.3886473	64	190.63	23.78	347.3064694
17	166.21	31.8	430.5348386	65	190.74	23.76	346.736081
18	166.52	31.53	429.7446984	66	190.85	23.73	346.1616001
19	166.86	31.25	428.8736675	67	190.93	23.71	345.7411744
20	166.98	31.23	428.5651259	68	190.95	23.7	345.6357183
21	167.58	30.78	427.0135129	69	191.03	23.68	345.2124778
22	168.14	30.47	425.5516705	70	191.12	23.67	344.7335895
23	168.92	30.16	423.4928266	71	191.22	23.65	344.1980223
24	169.8	29.85	421.1370881	72	191.4	23.62	343.2245605
25	170.61	29.55	418.9365294	73	191.48	23.59	342.787915
26	170.98	29.4	417.9206841	74	191.64	23.56	341.9070223
27	171.92	29.11	415.3086676	75	191.66	23.55	341.7961845
28	172.81	28.84	412.7925637	76	191.72	23.54	341.4626856
30	173.63	28.58	410.4353853	77	191.8	23.52	341.0156934
31	174.44	28.34	408.0683797	78	191.83	23.51	340.8473769
32	176.92	27.59	400.5613185	79	191.89	23.5	340.5095931
33	177.52	27.42	398.6809757	80	191.93	23.49	340.2835428
34	178.91	27.01	394.2183991	81	191.94	23.48	340.2269216
35	179.89	26.72	390.975869	82	191.95	23.48	340.1702569
36	180.8	26.47	387.8873103	83	191.96	23.47	340.1135485
37	181.27	26.3	386.260888	84	192.06	23.45	339.544037
38	181.98	26.08	383.7611205	85	192.03	23.46	339.7153567
39	182.63	25.89	381.4248666	86	192.04	23.46	339.6582948
40	183.15	25.75	379.5210468	87	192.12	23.45	339.2001838
41	183.71	25.58	377.434191	88	192.17	23.42	338.9123893
42	184.32	25.41	375.1153232	89	192.22	23.42	338.6234438
43	184.73	25.28	373.5284673	91	192.2	23.42	338.739161
44	185.32	25.12	371.2026785	92	192.17	23.42	338.9123893
45	185.83	24.98	369.1497276	93	192.17	23.42	338.9123893
46	186.21	24.87	367.5929324	94	192.19	23.42	338.79695
47	186.69	24.74	365.5914417	95	192.18	23.42	338.8546928
48	187.21	24.6	363.3764272	96	192.22	23.42	338.6234438

Zara 800 m away from the shoreline

Depth [m]	E.C. [mS/cm]	T. [C°]	TDS [g/l]	Depth [m]	E.C. [mS/cm]	T. [C°]	TDS [g/l]
1	198.4	30.72	271.9371294	48	189.93	23.88	350.8457087
2	198.4	31.08	271.9371294	49	190.05	23.85	350.2496261
3	197.04	31.4	300.7417472	50	190.16	23.84	349.699458
4	195.83	31.65	313.243962	51	190.24	23.81	349.297035
5	195.96	31.85	312.0661282	52	190.58	23.79	347.5644073
6	194.9	32.01	320.929402	53	190.69	23.77	346.9958505
7	193.71	32.15	329.4051007	54	190.79	23.75	346.475466
8	192.18	32.25	338.8546928	55	190.88	23.72	346.0042016
9	185.65	32.34	369.8789614	56	190.96	23.71	345.5829373
10	181.15	32.37	386.6782402	57	190.93	23.7	345.7411744
11	169.31	32.2	422.4532015	58	191.07	23.68	345
12	166.21	31.8	430.5348386	59	191.18	23.66	344.4126919
13	166.86	31.25	428.8736675	60	191.3	23.63	343.76689
14	167.58	30.78	427.0135129	61	191.43	23.6	343.0611109
15	168.92	30.16	423.4928266	62	191.56	23.58	342.3487503
16	170.61	29.55	418.9365294	63	191.63	23.56	341.96238
17	171.92	29.11	415.3086676	64	191.67	23.55	341.7407042
18	173.63	28.58	410.4353853	65	191.81	23.52	340.9596303
19	175.18	28.11	405.8707535	66	191.82	23.51	340.9035248
20	176.29	27.79	402.5076685	67	191.9	23.5	340.4531454
21	177.52	27.42	398.6809757	68	191.93	23.49	340.2835428
22	178.38	27.16	395.9381295	69	191.97	23.49	340.0567962
23	179.42	26.85	392.5413839	70	191.98	23.48	340
24	180.35	26.59	389.4243322	71	191.98	23.47	340
25	181.13	26.36	386.7476579	72	192	23.47	339.8862755
26	181.62	26.2	385.035206	73	192.01	23.46	339.8293469
27	182.37	25.98	382.3650293	74	192.04	23.46	339.6582948
28	182.99	25.8	380.1102405	75	192.03	23.46	339.7153567
29	183.39	25.67	378.6314429	76	192.06	23.45	339.544037
30	184.01	25.5	376.2998936	77	192.1	23.45	339.3149824
31	184.62	25.33	373.9565129	78	192.09	23.44	339.3723137
32	184.96	25.2	372.6278755	79	192.12	23.44	339.2001838
33	185.58	25.05	370.1611646	80	192.11	23.44	339.2576058
34	185.97	24.94	368.5789383	81	192.14	23.44	339.0852033
35	186.44	24.81	366.638885	82	192.16	23.44	338.9700399
36	186.94	24.67	364.5327884	83	192.16	23.43	338.9700399
37	187.32	24.57	362.9013336	84	192.15	23.43	339.0276445
38	187.66	24.47	361.4178027	85	192.14	23.44	339.0852033
39	188.05	24.36	359.6869751	86	192.14	23.43	339.0852033
40	188.34	24.29	358.3787766	87	192.16	23.43	338.9700399
41	188.7	24.2	356.7283739	88	192.17	23.44	338.9123893
42	188.98	24.14	355.423513	89	192.15	23.43	339.0276445
43	189.14	24.08	354.6691919	90	192.16	23.43	338.9700399
44	189.33	24.03	353.7649509	91	192.17	23.42	338.9123893
45	189.55	23.99	352.7060633	92	192.17	23.42	338.9123893
46	189.68	23.95	352.0741865	93	192.17	23.43	338.9123893
47	189.84	23.91	351.2900152	94	192.18	23.43	338.8546928

Wadi Mujeb 400 m away from the shoreline

Depth [m]	E.C. [mS/cm]	T. [C°]	TDS [g/l]	Depth [m]	E.C. [mS/cm]	T. [C°]	TDS [g/l]
1	186.4	34.6	366.81	44	186.66	25.02	365.72
2	186.37	34.51	366.93	45	187.09	24.9	363.89
3	186.74	34.39	365.38	46	187.21	24.87	363.38
4	187.02	34.29	364.19	47	187.49	24.8	362.16
5	187.14	34.24	363.68	48	187.57	24.77	361.81
6	187.29	34.19	363.03	49	187.87	24.68	360.49
7	187.35	34.14	362.77	50	187.89	24.68	360.4
8	187.61	34.09	361.64	51	188.19	24.59	359.06
9	187.41	34.04	362.51	52	188.42	24.52	358.01
10	187.36	34	362.73	53	188.53	24.49	357.51
11	182.31	33.94	382.58	54	188.65	24.46	356.96
12	178.98	33.72	393.99	55	188.95	24.39	355.56
13	176.82	33.29	400.87	56	189.05	24.36	355.09
14	175.58	33.16	404.67	57	189.31	24.3	353.86
15	173.57	32.71	410.61	58	189.37	24.28	353.57
16	169.94	32.55	420.76	59	189.62	24.22	352.37
17	166.76	32.06	429.13	60	189.71	24.19	351.93
18	167.38	31.8	427.53	61	189.93	24.14	350.85
19	169.23	31.15	422.67	62	190.02	24.12	350.4
20	169.93	30.89	420.79	63	190.28	24.06	349.1
21	171.25	30.29	417.18	64	190.32	24.04	348.89
22	171.81	30.07	415.62	65	190.48	24.01	348.08
23	173.18	29.25	411.73	66	190.59	23.98	347.51
24	173.41	29.16	411.07	67	190.8	23.93	346.42
25	175.83	28.41	403.91	68	190.88	23.91	346
26	175.99	28.33	403.42	69	191.18	23.84	344.41
27	177.79	27.72	397.83	70	191.13	23.85	344.68
28	178.34	27.57	396.07	71	191.45	23.79	342.95
29	179.44	27.25	392.48	72	191.49	23.78	342.73
30	179.82	27.12	391.21	73	191.66	23.75	341.8
31	180.48	26.85	388.98	74	191.74	23.73	341.35
32	180.78	26.75	387.96	75	191.95	23.69	340.17
33	181.98	26.35	383.76	76	192.01	23.67	339.83
34	182.04	26.32	383.55	77	192.26	23.62	338.39
35	182.94	26.05	380.29	78	192.32	23.61	338.04
36	183.24	25.96	379.19	79	192.35	23.6	337.87
37	184.06	25.7	376.11	80	192.4	23.59	337.57
38	184.61	25.61	374	81	192.44	23.58	337.34
39	184.78	25.47	373.33	82	192.51	23.57	336.92
40	185.15	25.41	371.88	83	192.58	23.55	336.51
41	185.83	25.24	369.15	84	192.61	23.55	336.33
42	185.89	25.22	368.91	85	192.74	23.52	335.55
43	186.62	25.03	365.89	86	192.77	23.51	335.36
				87	192.76	23.51	335.43

APPENDIX III

RADON RESULTS IN ALL THE STATIONS

Radon –222 measurements

Area Name	Rn-222 (Bq/l)	Sample direction	Day	Sample location
Mujeb-2m	0.64	Virtical	Jul-05	S_{rn4}- 20m from the shoreline
Mujeb-4m	0.99	Virtical	Jul-05	S_{rn4}- 20m from the shoreline
Mujeb-7m	0.67	Virtical	Jul-05	S_{rn4}- 20m from the shoreline
Mujeb-12m	1.78	Virtical	Jul-05	S_{rn4}- 20m from the shoreline
Mujeb-24m	0.82	Virtical	Jul-05	S_{rn4}- 20m from the shoreline
Zara-2m	1.29	Virtical	Jul-05	S_{rn3}- 25m from the shoreline
Zara-4m	1.53	Virtical	Jul-05	S_{rn3}- 25m from the shoreline
Zara-7m	1.69	Virtical	Jul-05	S_{rn3}- 25m from the shoreline
Zara-12	1.78	Virtical	Jul-05	S_{rn3}- 25m from the shoreline
Zara-24m	1.00	Virtical	Jul-05	S_{rn3}- 25m from the shoreline
NAVI-4m	1.39	Perbendicular	Jul-05	500 m south S_{rn3}- 40m from SH
NAVI-4m	2.10	Perbendicular	Jul-05	500 m south S_{rn3}- 20 m from SH
NAVI-4m	1.90	Perbendicular	Jul-05	500 m south S_{rn3}- 30m from SH
Zara-12m	1.07	Parallel	Jul-05	S_{rn3}- 50 m from SH
Zara-12m	2.52	Parallel	Jul-05	150 m north S_{rn3}-15-20 m from SH
Zara-12m	1.93	Parallel	Jul-05	150m north S_{rn3}- 30 m from SH
Zara-12m	1.56	Parallel	Jul-05	500 m north S_{rn3}- 15-20 m from SH
Zara-12m	1.23	Parallel	Jul-05	500 m north S_{rn3}- 50 m from SH
Navi-2m	2.24	Perbindicular	Jul-05	500 m south S_{rn3}- 20m from SH
Navi-12m	1.91	Perbindicular	Jul-05	500 m south S_{rn3}- 40m from SH
south-navi-12m	2.70	Perbendicular	Jul-05	1000 south S_{rn3}- 20m from SH
south-navi-12m	2.20	Perbendicular	Jul-05	1000 south S_{rn3}- 50m from SH
south-navi-12m	1.44	Perbendicular	Jul-05	1000 south S_{rn3}- 200 from SH
south-navi-12m	2.79	Perbendicular	Jul-05	2500 m south S_{rn3}- 20m fom SH
Z.Ma'in-2m	0.87	Virtical	Jul-05	S_{rn2}- 25m from the shoreline
Z.Ma'in-4m	2.08	Virtical	Jul-05	S_{rn2}- 25m from the shoreline
Z.Ma'in-7m	2.18	Virtical	Jul-05	S_{rn2}- 25m from the shoreline
Z. Ma'in-12m	1.87	Virtical	Jul-05	S_{rn2}- 25m from the shoreline
Z. Ma'in-25m	1.31	Virtical	Jul-05	S_{rn2}- 25m from the shoreline
Zma'in-4m	2.14	PARALLEL	Jul-05	S_{rn2}-10m from the shoreline
Zma'in-4m	2.06	PARALLEL	Jul-05	S_{rn2}-40m from the shoreline
Zma'in-4m	1.96	PARALLEL	Jul-05	300 m north S_{rn2}-10m from the SH
Zma'in-4m	0.68	PARALLEL	Jul-05	300 m north S_{rn2}-40m from the SH
Zma'in-4m	2.22	PARALLEL	Jul-05	800 m north S_{rn2}-10m from the SH
North area-2m	1.14	vertical	Jul-05	S_{rn1} -15-20m from SH
North area-4m	1.89	vertical	Jul-05	S_{rn1} -15-20m from SH
North area-7m	1.58	vertical	Jul-05	S_{rn1} -15-20m from SH
North area-12m	2.52	vertical	Jul-05	S_{rn1} -15-20m from SH
North area-20m	1.74	vertical	Jul-05	S_{rn1} -20m from SH
North area-12m	2.15	Perbendicular	Jul-05	4500 m south S_{rn1} -60m from SH
North area-20m	1.30	Perbendicular	Jul-05	4500m south S_{rn1} -60m from SH

North area-12m	**1.44**	Perbendicular	Jul-05	**4500 m south S$_{rn1}$ -200m from SH**
North area-12m	**1.31**	Perbendicular	Jul-05	**4500 m south S$_{rn1}$ -300m from SH**
North area-12m	**1.15**	Perbendicular	Jul-05	**4500 m south S$_{rn1}$ -700m from SH**
conference palace-12m	**2.19**	Perbendicular	Jul-05	**800m north S$_{rn1}$. -50m from SH**
conference palace-20m	**1.23**	Perbendicular	Jul-05	**800 north S$_{rn1}$-200m from SH**
conference palace-12m	**1.95**	Perbendicular	Jul-05	**800m north S$_{rn1}$- 300m from SH**
conference palace-12m	**2.14**	Perbendicular	Jul-05	**1000m north S$_{rn1}$-200m from SH**

APPENDIX IV

ANOMALIES OF THE ELECTRICAL RADIATION (EMR**)**

North	East	Date	Elevation (m)
31.727131	35.588908	29-dec-05	-418
31.728626	35.589044	29-dec-05	-421
31.729329	35.589092	29-dec-05	-420
31.729364	35.589134	29-dec-05	-417
31.732338	35.590058	29-dec-05	-417
31.733003	35.590334	29-dec-05	-420
31.733337	35.590427	29-dec-05	-414
31.735135	35.590440	29-dec-05	-417
31.736960	35.590535	29-dec-05	-418
31.737092	35.590832	29-dec-05	-416
31.737600	35.591111	29-dec-05	-419
31.740407	35.592425	29-dec-05	-415
31.740717	35.592546	29-dec-05	-414
31.743493	35.592405	29-dec-05	-409
31.743914	35.592292	29-dec-05	-413
31.746417	35.590838	29-dec-05	-411
31.746986	35.590599	29-dec-05	-412
31.748608	35.589117	29-dec-05	-412
31.748607	35.589117	29-dec-05	-412
31.750979	35.587228	29-dec-05	-410
31.750789	35.585118	29-dec-05	-412
31.751724	35.583490	29-dec-05	-417
31.752436	35.583384	29-dec-05	-418
31.754745	35.582497	29-dec-05	-420
31.755484	35.582021	29-dec-05	-415
31.756997	35.581641	29-dec-05	-409
31.757293	35.581570	29-dec-05	-411
31.757426	35.581484	29-dec-05	-412
31.757945	35.580675	29-dec-05	-415
31.758040	35.579938	29-dec-05	-414
31.758805	35.578721	29-dec-05	-417
31.759028	35.578277	29-dec-05	-418
31.761104	35.576475	29-dec-05	-419
31.579778	35.554578	01/05/2006	-418
31.580321	35.554602	01/05/2006	-418
31.580346	35.554542	01/05/2006	-420
31.580464	35.554339	01/05/2006	-420
31.580468	35.554270	01/05/2006	-418
31.580619	35.554391	01/05/2006	-418
31.580833	35.554541	01/05/2006	-419
31.580876	35.554577	01/05/2006	-418
31.580873	35.554632	01/05/2006	-418
31.580989	35.554686	01/05/2006	-418
31.580972	35.554589	01/05/2006	-416
31.581114	35.554622	01/05/2006	-417
31.581293	35.554567	01/05/2006	-415
31.581328	35.554560	01/05/2006	-415
31.581298	35.554715	01/05/2006	-412
31.581422	35.554584	01/05/2006	-413
31.581450	35.554549	01/05/2006	-415
31.581656	35.554437	01/05/2006	-415
31.581725	35.554441	01/05/2006	-415
31.582203	35.554392	01/05/2006	-416
31.582204	35.554393	01/05/2006	-416
31.582109	35.554256	01/05/2006	-414

North	East	Date	Elevation (m)
31.582152	35.554220	01/05/2006	-415
31.582248	35.554192	01/05/2006	-415
31.582283	35.554202	01/05/2006	-415
31.582284	35.554209	01/05/2006	-414
31.582518	35.554136	01/05/2006	-415
31.582557	35.554138	01/05/2006	-416
31.582580	35.554136	01/05/2006	-416
31.582866	35.554010	01/05/2006	-417
31.582879	35.553995	01/05/2006	-417
31.583362	35.554118	01/05/2006	-420
31.583243	35.554114	01/05/2006	-417
31.583674	35.554244	01/05/2006	-417
31.584061	35.554303	01/05/2006	-417
31.584253	35.554228	01/05/2006	-417
31.584539	35.554194	01/05/2006	-417
31.584629	35.554402	01/05/2006	-394
31.584678	35.554373	01/05/2006	-410
31.584813	35.554338	01/05/2006	-413
31.584734	35.554330	01/05/2006	-419
31.584835	35.554219	01/05/2006	-415
31.584810	35.554319	01/05/2006	-414
31.584884	35.554295	01/05/2006	-415
31.584767	35.554335	01/05/2006	-414
31.584820	35.554334	01/05/2006	-413
31.585025	35.554323	01/05/2006	-414
31.585315	35.554464	01/05/2006	-412
31.585591	35.554763	01/05/2006	-412
31.585431	35.554665	01/05/2006	-405
31.585578	35.554815	01/05/2006	-405
31.585610	35.554697	01/05/2006	-405
31.585783	35.554768	01/05/2006	-406
31.585906	35.554781	01/05/2006	-409
31.586002	35.554870	01/05/2006	-413
31.586167	35.555015	01/05/2006	-414
31.586228	35.555064	01/05/2006	-414
31.586429	35.555200	01/05/2006	-415
31.586833	35.555460	01/05/2006	-414
31.586927	35.555584	01/05/2006	-416
31.586992	35.555630	01/05/2006	-419
31.587248	35.555925	01/05/2006	-419
31.587300	35.555965	01/05/2006	-420
31.587421	35.556049	01/05/2006	-420
31.587524	35.556189	01/05/2006	-420
31.587581	35.556231	01/05/2006	-420
31.587612	35.556278	01/05/2006	-420
31.587702	35.556372	01/05/2006	-420
31.587811	35.556470	01/05/2006	-420
31.587854	35.556520	01/05/2006	-420
31.587867	35.556570	01/05/2006	-420
31.587953	35.556692	01/05/2006	-418
31.588014	35.556766	01/05/2006	-418
31.588130	35.556860	01/05/2006	-419
31.588839	35.557204	01/05/2006	-419
31.588817	35.557129	01/05/2006	-420
31.588790	35.557126	01/05/2006	-420
31.588847	35.557145	01/05/2006	-420
31.588962	35.557184	01/05/2006	-420

North	East	Date	Elevation (m)
31.589057	35.557161	01/05/2006	-420
31.589311	35.557163	01/05/2006	-420
31.589478	35.557132	01/05/2006	-420
31.589500	35.557131	01/05/2006	-420
31.589706	35.557149	01/05/2006	-420
31.589866	35.557152	01/05/2006	-420
31.589965	35.557132	01/05/2006	-420
31.590231	35.557092	01/05/2006	-420
31.590282	35.557087	01/05/2006	-420
31.590607	35.556920	01/05/2006	-420
31.590693	35.556975	01/05/2006	-420
31.590996	35.557024	01/05/2006	-420
31.591417	35.557233	01/05/2006	-408
31.591667	35.557360	01/05/2006	-405
31.591982	35.557375	01/05/2006	-410
31.592323	35.557387	01/05/2006	-409
31.592416	35.557368	01/05/2006	-410
31.592522	35.557359	01/05/2006	-413
31.592861	35.557336	01/05/2006	-416
31.592969	35.557375	01/05/2006	-417
31.593020	35.557387	01/05/2006	-417
31.593138	35.557392	01/05/2006	-417
31.593209	35.557401	01/05/2006	-417
31.593460	35.557373	01/05/2006	-415
31.593496	35.557367	01/05/2006	-415
31.593661	35.557445	01/05/2006	-416
31.593676	35.557441	01/05/2006	-417
31.593819	35.557547	01/05/2006	-416
31.593883	35.557558	01/05/2006	-416
31.594172	35.557667	01/05/2006	-416
31.594329	35.557684	01/05/2006	-417
31.594528	35.557705	01/05/2006	-418
31.594737	35.557721	01/05/2006	-419
31.595422	35.557736	01/05/2006	-417
31.595448	35.557735	01/05/2006	-417
31.595721	35.557739	01/05/2006	-413
31.595755	35.557728	01/05/2006	-416
31.595953	35.557668	01/05/2006	-415
31.596225	35.557588	01/05/2006	-415
31.596447	35.557562	01/05/2006	-420
31.596603	35.557664	01/05/2006	-417
31.596794	35.557722	01/05/2006	-417
31.596970	35.557809	01/05/2006	-416
31.597226	35.557929	01/05/2006	-417
31.597117	35.557935	01/05/2006	-420
31.597275	35.558001	01/05/2006	-420
31.598063	35.558760	01/05/2006	-420
31.598127	35.558863	01/05/2006	-413
31.598142	35.558870	01/05/2006	-417
31.598792	35.559631	01/05/2006	-417
31.598940	35.559778	01/05/2006	-417
31.599328	35.560042	01/05/2006	-417
31.599356	35.560058	01/05/2006	-418
31.599369	35.560063	01/05/2006	-417
31.599408	35.560088	01/05/2006	-417
31.599600	35.560240	01/05/2006	-416
31.599764	35.560466	01/05/2006	-416

North	East	Date	Elevation (m)
31.599770	35.560479	01/05/2006	-414
31.599776	35.560465	01/05/2006	-417
31.599942	35.560618	01/05/2006	-417
31.599997	35.560673	01/05/2006	-421
31.600011	35.560661	01/05/2006	-416
31.599960	35.560473	01/05/2006	-416
31.599942	35.560423	01/05/2006	-416
31.600221	35.560786	01/05/2006	-416
31.600266	35.560798	01/05/2006	-415
31.600344	35.560808	01/05/2006	-415
31.600560	35.560869	01/05/2006	-415
31.600561	35.560914	01/05/2006	-413
31.600556	35.561004	01/05/2006	-415
31.600538	35.561064	01/05/2006	-415
31.600486	35.561195	01/05/2006	-416
31.600610	35.561173	01/05/2006	-416
31.600613	35.560966	01/05/2006	-409
31.600611	35.560974	01/05/2006	-410
31.600660	35.560953	01/05/2006	-409
31.600757	35.560917	01/05/2006	-415
31.600787	35.560882	01/05/2006	-413
31.600821	35.560867	01/05/2006	-414
31.601188	35.561018	01/05/2006	-420
31.601164	35.561044	01/05/2006	-421
31.601180	35.561045	01/05/2006	-420
31.601417	35.561168	01/05/2006	-418
31.601566	35.561262	01/05/2006	-418
31.601665	35.561317	01/05/2006	-419
31.601835	35.561488	01/05/2006	-416
31.602009	35.561545	01/05/2006	-414
31.602029	35.561546	01/05/2006	-415
31.602162	35.561599	01/05/2006	-417
31.602259	35.561640	01/05/2006	-416
31.602285	35.561681	01/05/2006	-415
31.602328	35.561739	01/05/2006	-416
31.602767	35.561733	01/05/2006	-406
31.602834	35.561682	01/05/2006	-416
31.602939	35.561667	01/05/2006	-415
31.603173	35.561571	01/05/2006	-412
31.603441	35.561490	01/05/2006	-409
31.603521	35.561417	01/05/2006	-410
31.603720	35.561330	01/05/2006	-413
31.603835	35.561337	01/05/2006	-411
31.603936	35.561352	01/05/2006	-413
31.604033	35.561366	01/05/2006	-413
31.604253	35.561321	01/05/2006	-413
31.604384	35.561320	01/05/2006	-411
31.604620	35.561379	01/05/2006	-411
31.604797	35.561473	01/05/2006	-411
31.604873	35.561527	01/05/2006	-410
31.604899	35.561557	01/05/2006	-412
31.605019	35.561618	01/05/2006	-413
31.605284	35.561705	01/05/2006	-414
31.605458	35.561752	01/05/2006	-410
31.605491	35.561765	01/05/2006	-413
31.605567	35.561790	01/05/2006	-410
31.605616	35.561794	01/05/2006	-414

North	East	Date	Elevation (m)
31.605756	35.561949	01/05/2006	-415
31.605735	35.562040	01/05/2006	-400
31.605799	35.561968	01/05/2006	-417
31.605556	35.562099	01/05/2006	-415
31.605788	35.561907	01/05/2006	-415
31.605541	35.561818	01/05/2006	-409
31.605455	35.561759	01/05/2006	-409
31.605185	35.561722	01/05/2006	-409
31.605270	35.561758	01/05/2006	-416
31.460011	35.571362	01/07/2006	-402
31.459997	35.571324	01/07/2006	-414
31.460003	35.571328	01/07/2006	-411
31.460006	35.571361	01/07/2006	-413
31.460033	35.571440	01/07/2006	-417
31.460159	35.571238	01/07/2006	-405
31.460278	35.571184	01/07/2006	-404
31.460407	35.571090	01/07/2006	-405
31.460566	35.571000	01/07/2006	-410
31.460791	35.570771	01/07/2006	-409
31.461149	35.570362	01/07/2006	-410
31.461425	35.569946	01/07/2006	-406
31.461599	35.569457	01/07/2006	-407
31.461603	35.569432	01/07/2006	-408
31.461673	35.568822	01/07/2006	-406
31.461703	35.568641	01/07/2006	-406
31.461740	35.568358	01/07/2006	-408
31.461854	35.567972	01/07/2006	-406
31.462008	35.567326	01/07/2006	-405
31.462130	35.567004	01/07/2006	-406
31.462352	35.566473	01/07/2006	-407
31.462432	35.566379	01/07/2006	-414
31.462523	35.566218	01/07/2006	-414
31.462611	35.565977	01/07/2006	-413
31.462746	35.565685	01/07/2006	-412
31.462858	35.565507	01/07/2006	-410
31.462892	35.565460	01/07/2006	-410
31.462998	35.565299	01/07/2006	-413
31.463397	35.564814	01/07/2006	-411
31.463618	35.564624	01/07/2006	-413
31.463769	35.564486	01/07/2006	-412
31.464073	35.564189	01/07/2006	-412
31.464390	35.563874	01/07/2006	-413
31.464650	35.563603	01/07/2006	-411
31.464655	35.563590	01/07/2006	-411
31.464821	35.563593	01/07/2006	-413
31.465324	35.563228	01/07/2006	-409
31.465691	35.562979	01/07/2006	-411
31.466106	35.562742	01/07/2006	-402
31.466232	35.562794	01/07/2006	-413
31.466385	35.562818	01/07/2006	-412
31.467003	35.563270	01/07/2006	-412
31.467031	35.563288	01/07/2006	-412
31.467137	35.563397	01/07/2006	-415
31.467098	35.563440	01/07/2006	-417
31.467096	35.563504	01/07/2006	-418

North	East	Date	Elevation (m)
31.467221	35.563612	01/07/2006	-417
31.467517	35.563738	01/07/2006	-417
31.468053	35.563852	01/07/2006	-417
31.468622	35.564010	01/07/2006	-418
31.468770	35.564128	01/07/2006	-418
31.468930	35.564330	01/07/2006	-418
31.469100	35.564505	01/07/2006	-418
31.469362	35.564714	01/07/2006	-416
31.469472	35.564861	01/07/2006	-416
31.469502	35.564896	01/07/2006	-416
31.469626	35.565078	01/07/2006	-417
31.469719	35.565296	01/07/2006	-417
31.469741	35.565335	01/07/2006	-417
31.469776	35.565494	01/07/2006	-418
31.469835	35.565656	01/07/2006	-417
31.469860	35.565792	01/07/2006	-415
31.470045	35.566219	01/07/2006	-415
31.470163	35.566419	01/07/2006	-415
31.470186	35.566452	01/07/2006	-416
31.470260	35.566602	01/07/2006	-416
31.470386	35.566862	01/07/2006	-416
31.470557	35.567308	01/07/2006	-416
31.470659	35.567578	01/07/2006	-415
31.470673	35.567788	01/07/2006	-416
31.470667	35.567976	01/07/2006	-418
31.470669	35.568292	01/07/2006	-418
31.470679	35.568427	01/07/2006	-419
31.470752	35.568718	01/07/2006	-419
31.470785	35.568912	01/07/2006	-419
31.470834	35.569241	01/07/2006	-419
31.470747	35.569615	01/07/2006	-421
31.470734	35.569947	01/07/2006	-422
31.470790	35.570305	01/07/2006	-420
31.470804	35.570601	01/07/2006	-419
31.470829	35.570658	01/07/2006	-419
31.470828	35.570786	01/07/2006	-416
31.470820	35.571202	01/07/2006	-414
31.470784	35.571630	01/07/2006	-416
31.470777	35.571856	01/07/2006	-418
31.470860	35.572145	01/07/2006	-418
31.470971	35.572521	01/07/2006	-417
31.471204	35.573030	01/07/2006	-417
31.471298	35.573231	01/07/2006	-416
31.471425	35.573441	01/07/2006	-415
31.471528	35.573624	01/07/2006	-415
31.471623	35.573784	01/07/2006	-415
31.471737	35.574013	01/07/2006	-413
31.471695	35.574111	01/07/2006	-402
31.471702	35.574028	01/07/2006	-415
31.448243	35.565469	01/07/2006	-420
31.448111	35.565496	01/07/2006	-420
31.448091	35.565506	01/07/2006	-410
31.448172	35.565468	01/07/2006	-420
31.448384	35.565265	01/07/2006	-420
31.448428	35.565203	01/07/2006	-420
31.448510	35.565108	01/07/2006	-420
31.448637	35.564966	01/07/2006	-420

North	East	Date	Elevation(m)
31.448721	35.564902	01/07/2006	-420
31.448748	35.564885	01/07/2006	-420
31.449018	35.564640	01/07/2006	-420
31.449212	35.564466	01/07/2006	-420
31.449450	35.564313	01/07/2006	-420
31.449745	35.564229	01/07/2006	-420
31.450075	35.564092	01/07/2006	-420
31.450173	35.564002	01/07/2006	-420
31.450353	35.563888	01/07/2006	-420
31.450357	35.563884	01/07/2006	-420
31.450730	35.563689	01/07/2006	-420
31.450742	35.563711	01/07/2006	-420
31.450925	35.563644	01/07/2006	-419
31.451086	35.563659	01/07/2006	-418
31.451353	35.563827	01/07/2006	-419
31.451393	35.563885	01/07/2006	-419
31.451555	35.564196	01/07/2006	-419
31.451561	35.564207	01/07/2006	-415
31.451709	35.564348	01/07/2006	-416
31.451950	35.564686	01/07/2006	-416
31.452037	35.564917	01/07/2006	-417
31.452248	35.565140	01/07/2006	-419
31.452533	35.565362	01/07/2006	-420
31.452734	35.565491	01/07/2006	-420
31.452890	35.565585	01/07/2006	-420
31.453098	35.565656	01/07/2006	-420
31.453263	35.565731	01/07/2006	-420
31.453530	35.565841	01/07/2006	-420
31.453691	35.565856	01/07/2006	-420
31.453733	35.565902	01/07/2006	-420
31.454165	35.565941	01/07/2006	-420
31.454404	35.565746	01/07/2006	-420
31.454427	35.565693	01/07/2006	-420
31.454544	35.565697	01/07/2006	-420
31.454767	35.565957	01/07/2006	-420
31.454945	35.566070	01/07/2006	-420
31.454989	35.566134	01/07/2006	-420
31.455087	35.566294	01/07/2006	-420
31.455179	35.566486	01/07/2006	-418
31.455325	35.566739	01/07/2006	-419
31.455430	35.566963	01/07/2006	-419
31.455504	35.567070	01/07/2006	-420
31.455636	35.567226	01/07/2006	-419
31.455721	35.567307	01/07/2006	-420
31.455743	35.567437	01/07/2006	-419
31.455979	35.567692	01/07/2006	-420
31.456072	35.567767	01/07/2006	-420
31.456151	35.567855	01/07/2006	-420
31.456295	35.568024	01/07/2006	-420
31.456375	35.568177	01/07/2006	-420
31.456512	35.568266	01/07/2006	-420
31.456627	35.568467	01/07/2006	-420
31.456639	35.568549	01/07/2006	-420
31.456700	35.568796	01/07/2006	-420
31.456786	35.569036	01/07/2006	-420
31.456825	35.569203	01/07/2006	-420
31.456834	35.569280	01/07/2006	-420

North	East	Date	Elevation(m)
31.456837	35.569360	01/07/2006	-420
31.456868	35.569432	01/07/2006	-420
31.457027	35.569652	01/07/2006	-420
31.457058	35.569695	01/07/2006	-420
31.457329	35.570068	01/07/2006	-420
31.457462	35.570245	01/07/2006	-420
31.457488	35.570263	01/07/2006	-420
31.457563	35.570368	01/07/2006	-420
31.457719	35.570658	01/07/2006	-420
31.457754	35.570715	01/07/2006	-417
31.457937	35.570871	01/07/2006	-415
31.457961	35.570936	01/07/2006	-418
31.458012	35.570979	01/07/2006	-417
31.458230	35.571077	01/07/2006	-417
31.458433	35.571136	01/07/2006	-417
31.458488	35.571166	01/07/2006	-416
31.458476	35.571200	01/07/2006	-420
31.816396	35.647351	01/13/2006	-418
31.816315	35.647422	01/13/2006	-418
31.693579	35.579533	01/13/2006	-416
31.693504	35.579647	01/13/2006	-416
31.693501	35.579712	01/13/2006	-420
31.693471	35.579783	01/13/2006	-420
31.693457	35.579804	01/13/2006	-420
31.693475	35.579893	01/13/2006	-420
31.693475	35.579910	01/13/2006	-420
31.693613	35.579946	01/13/2006	-420
31.693646	35.579954	01/13/2006	-420
31.693747	35.579981	01/13/2006	-416
31.693925	35.580017	01/13/2006	-417
31.694147	35.580056	01/13/2006	-418
31.694330	35.580145	01/13/2006	-418
31.694602	35.580243	01/13/2006	-418
31.694774	35.580307	01/13/2006	-417
31.694985	35.580381	01/13/2006	-418
31.695296	35.580472	01/13/2006	-417
31.695443	35.580484	01/13/2006	-417
31.695633	35.580452	01/13/2006	-418
31.695856	35.580489	01/13/2006	-418
31.696097	35.580553	01/13/2006	-417
31.696140	35.580571	01/13/2006	-417
31.696352	35.580651	01/13/2006	-416
31.696522	35.580677	01/13/2006	-414
31.696513	35.580663	01/13/2006	-416
31.696644	35.580653	01/13/2006	-416
31.696840	35.580692	01/13/2006	-414
31.697022	35.580698	01/13/2006	-416
31.697500	35.580781	01/13/2006	-418
31.697704	35.580885	01/13/2006	-418
31.697717	35.580896	01/13/2006	-416
31.697895	35.580956	01/13/2006	-418
31.698418	35.580992	01/13/2006	-419
31.698892	35.581024	01/13/2006	-421
31.699298	35.581100	01/13/2006	-420

North	East	Date	Elevation (m)
31.699623	35.581330	01/13/2006	-419
31.699838	35.581492	01/13/2006	-417
31.700033	35.581628	01/13/2006	-417
31.700150	35.581724	01/13/2006	-416
31.700224	35.581845	01/13/2006	-417
31.700315	35.581954	01/13/2006	-417
31.700330	35.582006	01/13/2006	-417
31.700260	35.582037	01/13/2006	-418
31.700363	35.582169	01/13/2006	-417
31.700371	35.582174	01/13/2006	-416
31.700094	35.582214	01/13/2006	-412
31.700104	35.582214	01/13/2006	-412
31.700432	35.582256	01/13/2006	-418
31.700527	35.582204	01/13/2006	-419
31.700534	35.582104	01/13/2006	-421
31.700558	35.582115	01/13/2006	-421
31.700883	35.582370	01/13/2006	-417
31.700973	35.582452	01/13/2006	-417
31.701235	35.582629	01/13/2006	-416
31.701622	35.582960	01/13/2006	-413
31.701928	35.583147	01/13/2006	-413
31.702141	35.583288	01/13/2006	-415
31.702375	35.583385	01/13/2006	-414
31.702437	35.583383	01/13/2006	-414
31.702514	35.583367	01/13/2006	-414
31.702929	35.583407	01/13/2006	-415
31.703206	35.583343	01/13/2006	-417
31.703493	35.583200	01/13/2006	-418
31.703561	35.583100	01/13/2006	-418
31.703879	35.582897	01/13/2006	-417
31.703971	35.582878	01/13/2006	-418
31.704087	35.582935	01/13/2006	-421
31.704230	35.582863	01/13/2006	-421
31.704326	35.582875	01/13/2006	-420
31.704390	35.582934	01/13/2006	-420
31.704547	35.582954	01/13/2006	-420
31.704895	35.582865	01/13/2006	-420
31.705144	35.582794	01/13/2006	-420
31.705286	35.582742	01/13/2006	-420
31.705491	35.582680	01/13/2006	-420
31.705843	35.582618	01/13/2006	-420
31.706150	35.582557	01/13/2006	-420
31.706321	35.582443	01/13/2006	-420
31.706582	35.582324	01/13/2006	-420
31.706925	35.582216	01/13/2006	-420
31.707207	35.582201	01/13/2006	-418
31.707348	35.582197	01/13/2006	-420
31.707520	35.582270	01/13/2006	-420
31.707670	35.582420	01/13/2006	-420
31.707723	35.582492	01/13/2006	-420
31.707764	35.582533	01/13/2006	-420
31.708117	35.582770	01/13/2006	-420
31.708327	35.582818	01/13/2006	-420
31.708517	35.582879	01/13/2006	-420
31.708672	35.582901	01/13/2006	-419
31.708855	35.582926	01/13/2006	-419
31.709130	35.582936	01/13/2006	-420

North	East	Date	Elevation (m)
31.709266	35.582973	01/13/2006	-420
31.709430	35.583039	01/13/2006	-420
31.709736	35.583181	01/13/2006	-420
31.709798	35.583220	01/13/2006	-420
31.709957	35.583313	01/13/2006	-420
31.710096	35.583384	01/13/2006	-420
31.710184	35.583451	01/13/2006	-420
31.710285	35.583486	01/13/2006	-420
31.710601	35.583658	01/13/2006	-420
31.710639	35.583682	01/13/2006	-420
31.711041	35.583746	01/13/2006	-420
31.711048	35.583731	01/13/2006	-420
31.711188	35.583776	01/13/2006	-419
31.711371	35.583907	01/13/2006	-418
31.711586	35.584048	01/13/2006	-416
31.711753	35.584134	01/13/2006	-418
31.712005	35.584325	01/13/2006	-419
31.712282	35.584433	01/13/2006	-420
31.712519	35.584644	01/13/2006	-420
31.712804	35.584754	01/13/2006	-420
31.713149	35.584666	01/13/2006	-419
31.713568	35.584568	01/13/2006	-420
31.713837	35.584537	01/13/2006	-420
31.713861	35.584552	01/13/2006	-420
31.714005	35.584538	01/13/2006	-420
31.714073	35.584533	01/13/2006	-420
31.714172	35.584459	01/13/2006	-419
31.714425	35.584282	01/13/2006	-420
31.714848	35.584005	01/13/2006	-419
31.715344	35.583883	01/13/2006	-420
31.715888	35.583716	01/13/2006	-420
31.716273	35.583616	01/13/2006	-420
31.716280	35.583611	01/13/2006	-420
31.716308	35.583533	01/13/2006	-420
31.716459	35.583395	01/13/2006	-420
31.716612	35.583343	01/13/2006	-420
31.716959	35.583282	01/13/2006	-420
31.717240	35.583268	01/13/2006	-420
31.717293	35.583235	01/13/2006	-420
31.717536	35.583293	01/13/2006	-420
31.717858	35.583315	01/13/2006	-420
31.717982	35.583283	01/13/2006	-420
31.718254	35.583225	01/13/2006	-420
31.718560	35.583241	01/13/2006	-420
31.718586	35.583251	01/13/2006	-420
31.718701	35.583375	01/13/2006	-420
31.718897	35.583603	01/13/2006	-420
31.719099	35.583785	01/13/2006	-420
31.719222	35.583878	01/13/2006	-419
31.719295	35.583925	01/13/2006	-420
31.719457	35.584015	01/13/2006	-420
31.719464	35.584059	01/13/2006	-420
31.719619	35.584075	01/13/2006	-420
31.719725	35.584170	01/13/2006	-420
31.719819	35.584238	01/13/2006	-420
31.719920	35.584364	01/13/2006	-420
31.720122	35.584540	01/13/2006	-420

North	East	Date	Elevation (m)
31.720424	35.584696	01/13/2006	-420
31.720521	35.584750	01/13/2006	-420
31.720751	35.584871	01/13/2006	-420
31.720918	35.585056	01/13/2006	-420
31.721152	35.585244	01/13/2006	-420
31.721454	35.585227	01/13/2006	-420
31.721678	35.585271	01/13/2006	-420
31.721827	35.585252	01/13/2006	-420
31.721906	35.585311	01/13/2006	-419
31.722093	35.585481	01/13/2006	-420
31.722179	35.585546	01/13/2006	-418
31.721952	35.585505	01/13/2006	-420
31.722078	35.585549	01/13/2006	-420

Curriculum Vitae of the Author

Emad Akawwi was born on February 02, 1966 in Al Fuhais, in Jordan. He was obtained his General Secondary Certificate (Tawjihi)-Scientific Stream in 1984 from Al Fuhais secondary school. In this year he began to attend the Earth and Environmental Department-Al Yarmouk University-Irbid, Jordan and he was awarded a B.Sc. Degree in 1988.

He has working at Natural Resources Authority from 1989 until now. During these years he got a study leave on Oct.1997 and he attend the Faculty of Graduate Studies-Cardiff University-Wales, UK. He was awarded a Master of Science in Geotechnical Engineering in March 2000.

From 2003 to 2006 he was a Ph.D. student at the University of Goettingen, Germany, Department of Applied Geology.

The addresses of the author are:

Postal address: Al Fuhais- P. O. Box 27
                        Postal code 19152/ Jordan.
E-mail: ejeakawwi@hotmail.com.